UNIVERSITÀ DEGLI STUDI DI SALERNO
Dipartimento di Farmacia

PhD Program

in **Drug Discovery and Development**

XXXV Cycle — Academic Year 2022/2023

# *PhD Thesis in*

# *Design, synthesis and pharmacological evaluation of new enzyme inhibitors*

Candidate

*Gerardina Smaldone*

Tutor

Prof. *Alessia Bertamino*

PhD Program Coordinator: Prof. Dr. *Gianluca Sbardella*

**INDEX**

## Abstract

*My PhD research plan relates to the exploration of the structural requirements for the modulation of enzymes involved in the pathogenesis of viral infections and inflammatory disorders. The first part of my doctoral project focused on the study of viral targets, particularly the main protease (Mpro) of SARS-CoV-2, the etiologic agent of COVID-19 that caused not only the biggest health crisis in the last century but also an unrecoverable socio-economic collapse. Despite all the efforts, addressed to build an efficient vaccine campaign, the virus spread is still ongoing and the challenge is still open. So, in the first chapter of this PhD thesis I report a step-by-step in silico design of a library of peptidomimetic compounds able to inhibit Mpro: the synthesized derivatives were screened by enzymatic assays, conducted on different viral targets, and, then, cellular activity was evaluated using Vero cells based viral infection model, leading to the identification of a dual inhibitor (**29**) of the two proteases of SARS-CoV-2, the main protease (Mpro) and the papain-like protease (PLpro). Subsequently, in vitro studies of a second series of molecules, designed from the most potent derivative of the first series, led to the identification of a new hit compound (**51**) characterized by high inhibitory potency against Mpro, as well as remarkable antiviral activity against several variants of SARS-CoV-2.*

*Metabolic pathways involving arachidonic acid (AA) play key roles in cardiovascular physiology, carcinogenesis, and in many inflammatory diseases such as asthma or arthritis, so the second chapter of this PhD thesis focuses on the study of two enzymatic targets involved in the metabolism of arachidonic acid: the 5-lipoxigenase and the soluble epoxide hydrolase (sEH). In vitro and in vivo*

*characterization of a first series of indoline scaffold derivatives led to the identification of a dual inhibitor of the two enzymes (**73**), while additional assays conducted on successive series of compounds designed as selective inhibitors of the enzyme sEH, led to the identification of an indole derivative (**110**) as a selective inhibitor of epoxide hydrolase, paving the way for further investigation as well as optimization of a new series of analogues.*

# CHAPTER 1

# Design, synthesis and biological evaluation of new anti-SARS-CoV-2 agents

## 1.1 The novel coronavirus Sars-CoV-2

### *1.1.1 Identification of the new coronavirus SARS-CoV-2*

On December 31, 2019, Chinese health authorities reported to the World Health Organization (WHO) an epidemic outbreak of pneumonia of unknown etiology in the city of Wuhan, a transportation hub for goods and people with a population of 11 million, in Hubei Province (east-central China) (Lu *et al*., 2020). The first cases were recorded in December 2019 (Du Toit, 2020) and epidemiological investigations suggested that they were linked to the Wuhan fish market (Lu *et al*., 2020). Subsequently, the crucial role occupied by humans in the spread and transmission of the disease was recognized (Li *et al*., 2020). Clinical manifestations consisted of high fever, severe respiratory illness, and high mortality (Huang *et al*., 2020).

The first confirmation that a coronavirus was present in the clinical specimens of people with this new disease was obtained by a Reverse Transcriptase-Polymerase Chain Reaction (RT-PCR) assay employing pan-coronavirus primers (Cheng *et al*., 2007; Zhou *et al*., 2020).

This novel coronavirus was tentatively named *Wuhan coronavirus* or *2019 novel coronavirus* (2019-nCoV) by Chinese researchers. Subsequently, the ICTV

(International Committee on Taxonomy of Viruses) renamed it new SARS-CoV-2 (Severe Acute Respiratory Syndrome Coronavirus 2), given its high homology (about 80%) with the previous and already known SARS-CoV (Gorbalenya *et al.*, 2020); in fact, by aligning the coronavirus sequences with the genome of SARS-CoV-2, it was possible to confirm that the new coronavirus has similar genomic organization to known CoVs and that the virus belongs to the genus *Betacoronavirus*, subgenus *Sabercovirus* (Huang *et al*., 2020; Cheng *et al*., 2007; Chan *et al*., 2020; Wu *et al*., 2020).

### *1.1.2 COVID-19: diagnosis and symptoms*

The disease caused by SARS-CoV-2 has been named COVID-19 (Coronavirus disease), and due the exponential increase in cases of infection, the World Health Organization declared a pandemic status on March 11, 2020. WHO itself has provided a definition of a "confirmed COVID-19 case" as a patient who tests positive on the RT-PCR test for SARS-CoV-2, regardless of clinical symptoms. The RT-PCR test should be performed on respiratory material obtained (a) from an upper airway specimen taken by nasopharyngeal and oropharyngeal swab or lavage in outpatients; (b) from a lower airway specimen, saliva and/or endotracheal aspirate or bronchoalveolar lavage in the case of patients with more severe respiratory disease.

Symptoms of infection appear after an incubation period of about 5.2 days (Li *et al*., 2020) and in the early stage of the disease the most common ones include fever, cough, fatigue or myalgia; less recurrent are sputum production, headache, hemoptysis and diarrhea (Huang *et al*., 2020). Other clinical manifestations frequently seen in

patients with COVID-19 are anorexia, chest oppression, shortness of breath, and dyspnea (Zhu *et al*., 2020).

Alterations in taste (hypogeusia or ageusia) and sense of smell (hyposmia or anosmia) are also frequently observed in patients with SARS-CoV-2 infection (Agyeman *et al*., 2020).

Complications include Acute Respiratory Distress Syndrome (ARDS), RNAemia, acute cardiac injury, and secondary infections (Huang *et al*., 2020).

Many of the COVID-19 positive cases have normal leukocyte count, lymphocytopenia, elevated C-reactive protein (CRP) and erythrocyte sedimentation rate (ESR) levels and decreased oxygen saturation level (Zhu *et al*., 2020). Increased plasma levels of pro-inflammatory chemokines and cytokines, including IL1, IL1RA, IL7, IL8, IL9, IL10, basic FGF2, GCSF, GMCSF, IFNγ, IP10, MCP1, MIP1α, MIP1β, PDGFB, TNFα, and VEGFA, were also found.

Some of the severe cases, which required transfer to the intensive care unit, showed high levels of pro-inflammatory cytokines including IL2, IL7, IL10, GCSF, IP10, MCP1, MIP1α, and TNFα that are believed to increase the severity of the disease (Huang *et al*., 2020).

It is important to note the similarities between COVID-19-induced symptoms and cases of infection with other beta-coronaviruses such as pyrexia, dry cough, dyspnea, and bilateral ground-glass opacities in computed tomography (CT) of the chest (Huang *et al*., 2020).

Nevertheless, infections caused by the new coronavirus show peculiar clinical features affecting the upper respiratory tract, such as rhinorrhea, sneezing, and

inflamed throat. It should be added that while COVID-19 patients manifest gastrointestinal symptoms such as diarrhea, only a low percentage of cases of MERS-CoV and SARS-CoV positive patients report such complications (Assiri *et al*., 2013; Lee *et al*., 1994).

### 1.2 SARS-CoV-2 life cycle

Under the electron microscope, coronavirus particles appear to be carpeted on the outer surface by the spike protein, which is extruded from the virus envelope, giving it the appearance of a crown (hence the name); they are roughly spherical in shape and range in size from 118 to 140 nm. Inside the envelope is the nucleocapsid, which consists of genomic RNA associated with the nucleocapsid protein (N). SARS-CoV-2 has got a genome of 29.881 nitrogenous bases that is divided into genes for structural proteins, which code for spike protein (S), pericapsid protein (E), membrane protein (M) and nucleocapsid protein (N), and genes for non-structural proteins that code instead for those proteins that can regulate the processes of virus replication and assembly, such as 3-chymotrypsin-like protease also referred to as Main Protease (MPro), Papain-like protease (PLpro) or RNA-dependent RNA polymerase (RdRp) (Payne, 2017). The process of infection by SARS-CoV-2 begins with the entry of the virus into the host cell following the interaction between the spike and the human ACE2 receptor and the cleavage of the S protein by a protease called TMPRSS2 (transmembrane serine protease 2) (**Figure 1**) (Hoffmann *et al*., 2020).

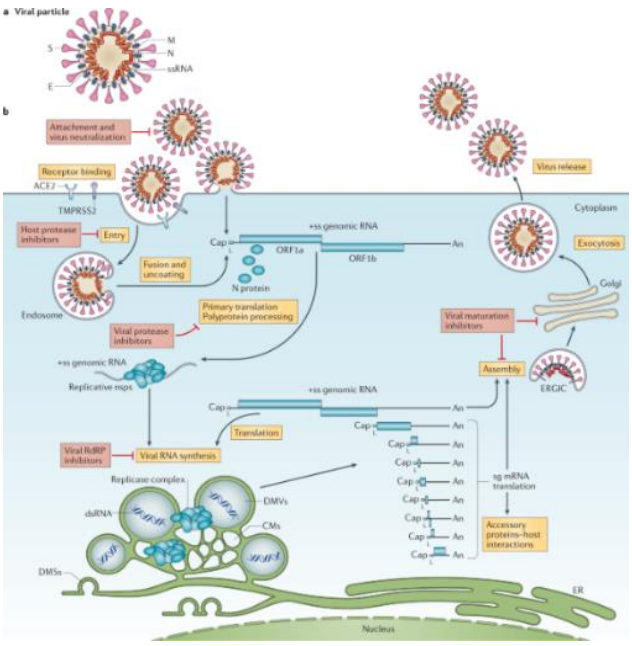


**Figure 1.** *The coronavirus virion and its life cycle. (Adapted from V'kovski et al., 2021).*

Shortly after the SARS outbreak in 2002-2003, ACE2 was identified as the receptor that mediated the entry of SARS-CoV into the human cells (Li *et al*., 2003); the high genomic and structural homology between the S proteins of SARS-CoV and SARS-CoV-2 supported the recognition of ACE2 as a receptor for the new coronavirus as well (Letko *et al*., 2020). The S protein is a class I homotrimeric fusion glycoprotein, and each of its three monomers is divided into two functional parts: the S1 subunit, which is responsible for host recognition, and the S2 subunit, which drives the fusion of the virus membrane with that of the host cell: the exposed S1 portion in fact contains the RBD, which determines the tropism of the virus and its pathogenicity, while the transmembrane S2 subunit contains, in addition to repeated regions, the fusion peptide (**Figure 2**) (Tortotici *et al*., 2019).

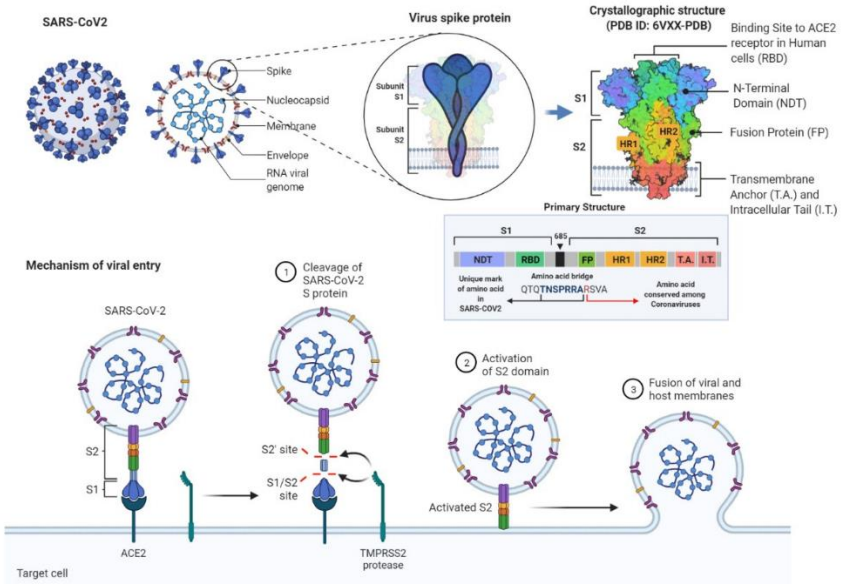


**Figure 2.** *Schematic representation of the SARS-CoV-2 and its surface spike protein structure with their structural descriptions and detailed mechanisms of the viral entry to cells during infection. (Adapted from Petrovszki et al., 2022).*

ACE2 is a carboxypeptidase located on the cell surface that can bind zinc, which is essential for the regulation of cardiac function and blood pressure. This enzyme is part of the renin-angiotensin-aldosterone system and is involved in the conversion of angiotensin I to angiotensin 1-9 and angiotensin II to angiotensin 1-7. It is the latter that, through the MAS receptor, promotes the release of vasoactive substances such as nitric oxide (NO), bradykinin and PGE2 with vasodilatory, anti-inflammatory and organ-protective effects. This enzyme is expressed by epithelial cells of lung, small intestine, as well as other organs. Once the virus has penetrated inside the cell, it is disassembled to release the nucleocapsid and viral RNA. The host cell ribosomes are responsible for the translation of the largest open reading frame (ORF) of the virus, ORF1ab, which encodes for two overlapping polyproteins, pp1a and pp1ab, that are cleaved into 16 non-structural proteins (nsp 1-16); the remaining ORFs lead to the formation of structural and accessory proteins.

The two main cysteine proteases involved in polyprotein cleavage are the main protease Mpro (also called 3CLpro, 3C-like protease) and the papain-like protease PLpro, located in nsp5 and nsp3, respectively. This cleavage process leads to the production of nsp2-16 involved in the replication-transcription complex (RTC) (V'kovski *et al*., 2019), which includes various proteins such as RNA-dependent RNA polymerase (RdRp, nsp12) and helicase (nsp13).

### 1.3 SARS-CoV-2 variants

Adaptive mutations in the viral genome can cause an alteration in the pathogenicity of the virus, going to affect even drastically the ability of the virus to evade the immune system and complicating the ability of vaccines to act against the virus (Aleem *et al*., 2022). The accumulation of these mutations leads to the emergence of multiple variants that may have different characteristics from the original strain (**Figure 3**); however, new genetic variants of the virus can be detected by periodic genomic sequencing of viral samples.

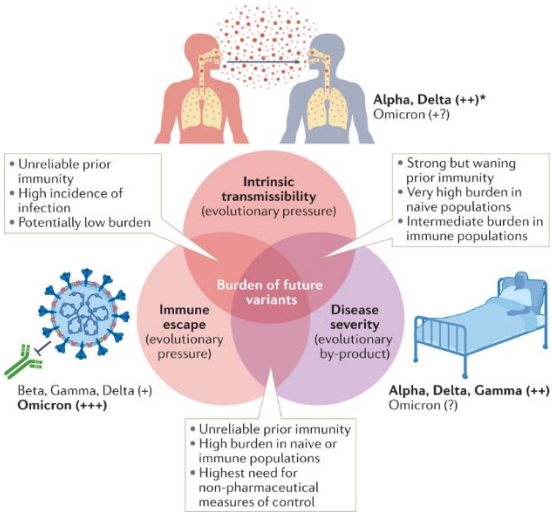


**Figure 3.** *Effects of the interactions between transmissibility, disease severity and immune escape of variants of concern on SARS-CoV-2 population burden. (Adapted from Markov et al., 2022).*

The first evidence of SARS-CoV-2 genetic evolution emerged in early 2020 with the appearance of a new variant of the virus, characterized by a mutation in the spike protein named at first D614G, which in June 2020 reached 100% prevalence (Hou *et al*., 2020). Later, particularly between 2020 and 2021, additional variants characterized by recurrent mutations (in addition to D614G) were identified, occurring in particular, but not exclusively, in the spike protein. Then, in December 2020, a rapidly growing variant named B.1.1.7 associated with an unexpectedly high number of genetic mutations was reported (Giles *et al*., 2021) the first clinical sample of this variant was obtained in the UK in late September 2020. Within a short time, two more rapidly spreading variants characterized by a high number of genetic mutations were identified, one from South Africa (B.1.351) (Planas *et al*., 2021) and the other one (P.1) from Brazil (Da Silva *et al*., 2021). In February 2021, an additional new variant (B.1.617.2) spread widely, increasing from a prevalence rate of 2% to 87%, particularly in Maharashtra, India, leading to a sharp surge in COVID-19 cases and

then spreading to several countries, proving to have a higher rate of diffusivity than the previous variant and causing significantly more severe symptomatology than the variants discussed so far (Zhan *et al*., 2022).

Thus, since 2020, several variants of SARS-CoV-2 have been identified and studied, and many of them are classified as VOCs (variants of concern) because of their serious impact on human health; these are associated with high virulence, ability to resist antibody attack or evade detection by common laboratory techniques, and reduction in therapeutics or vaccine efficacy. According to WHO epidemiological update, five SARS-CoV-2 VOCs have been identified since the beginning of the pandemic; all five variants, *Alpha* (B.1.1.7); *Beta* (B.1.351); *Gamma* (P.1); *Delta* (B.1.617.2); and *Omicron* (B.1.1.529) reported mutations affecting RBD and NTD: the N501Y mutation, common to all variants except Delta, leads to a greater affinity by the spike protein for the ACE2 receptor and so to a greater capacity for the virus entry into the host cell (Salehi-Vaziri *et al*., 2022). Currently, the Omicron variant is the dominant one globally, accounting for more than 98% of the viral sequences shared on GISAID after February 2022. As transmission of these VOCs has been sustained, this has led to significant intra-VOC evolution. Since its designation as a VOC by WHO on 26 November 2021, viruses part of the Omicron complex have continued to evolve, leading to descendent lineages with different genetic constellations of mutations. Given the wide transmissibility of the omicron variant worldwide and the resulting increase in viral diversity, WHO has added a new category to its variant tracking system, named “Omicron subvariants under monitoring", with the aim of facilitating the reporting to public health authorities of VOCs that may require priority attention and monitoring.

Another class of variants are VOIs (variants of interest), defined as variants characterized by specific genetic markers associated with changes that may cause increased transmissibility or virulence, decreased neutralization by antibodies obtained through natural infection or vaccination, ability to evade detection, or decreased efficacy of therapies or vaccinations. So far, since the beginning of the pandemic, WHO has described eight variants of interest, namely *Epsilon* (B.1.427 and B.1.429); *Zeta* (P.2); *Eta* (B.1.525); *Theta* (P.3); *Iota* (B.1.526); *Kappa* (B.1.617.1); *Lambda* (C.37) and *Mu* (B.1.621).

### 1.4 Management of SARS-CoV-2: therapeutic options

Since the beginning of the pandemic, significant progress has been made in the management of the health emergency, thanks largely to the immense efforts of global clinical research that have led to the development of effective vaccines and promising new therapies (https://www.covid19treatmentguidelines.nih.gov/).

Several therapeutic options (**Figure 4**) are currently available for the treatment of COVID-19, which include antiviral drugs (molnupiravir, ritonavir in combination with nirmatrelvir, remdesivir) (Singh *et al*., 2021; Mahase, 2021; Beigel *et al*., 2020), anti-SARS-CoV-2 monoclonal antibodies (sotrovimab) (Chavda *et al*., 2022), anti-inflammatory drugs (dexamethasone) (Horby *et al*., 2021) and immunomodulatory agents (aricitinib, tocilizumab) (Burrage *et al*., 2020).

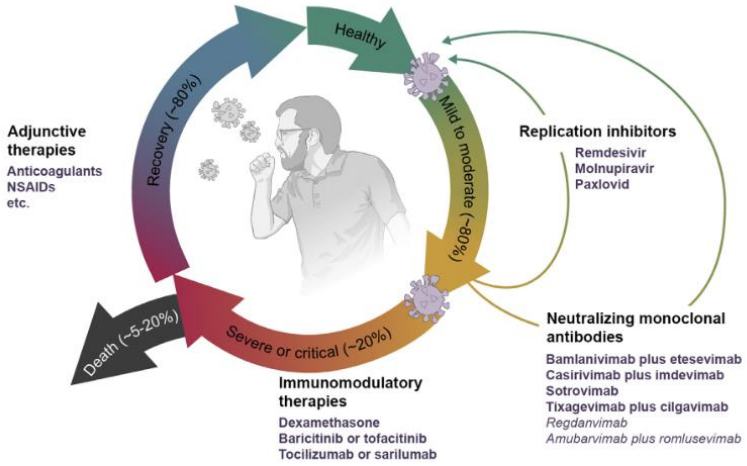


**Figure 4.** *Overview of antiviral therapies currently available for the treatment of COVID-19. (Adapted from Singh et al., 2022).*

However, not all patients respond in the same way to treatment with each of these drugs; in fact, the success of drug therapy depends on several factors such as the severity of the disease state or determined risk factors. In addition, the type of treatment also depends on the stage of the disease. The clinical course of COVID-19 is divided into two phases. An early one, in which the virus is at its peak replicative stage, usually before or soon after the onset of symptoms: in this case, the most effective therapy is antiviral drugs and antibody treatments. The next phase of the disease is characterized by a hyperinflammatory state due to the release of proinflammatory cytokines and activation of the coagulation system that induces a prothrombotic state: in this case, therapy with anti-inflammatory drugs such as corticosteroids, immunomodulatory therapies, or a combination thereof is preferred.

### *1.4.1 Antiviral agents*

Among SARS-CoV-2 proteins particular regard has the RNA-dependent RNA polymerase (RdRp). As this enzyme is necessary for the synthesis of new genetic

material its inhibition goes to impair the entire process of production of new viral particles. Since RdRp of SARS-CoV and that of SARS-CoV-2 exhibit 96% homology (Morse *et al*., 2020), some of the molecules active on the former, including remdesivir, favipiravir, ribavirin, (**Figure 5**) have shown to inhibit the new coronavirus *in vitro* as well. Remdesivir, an adenosine analogue prodrug with broad spectrum against RNA viruses, was developed for the treatment of infection caused by Ebola virus. This drug acts as a substrate for RdRp and competes with ATP; in particular, remdesivir acts as a chain terminator, but unlike other nucleoside analogues that lead directly to the synthesis reaction block after incorporation, RdRp adds three additional nucleotides after the addition of remdesivir.

This molecule has been shown to effectively reduce the replication of SARS-CoV-2 (Wang *et al*., 2020); it has been approved by the FDA for intravenous injection for the emergency treatment of hospitalized COVID-19 patients with severe disease.

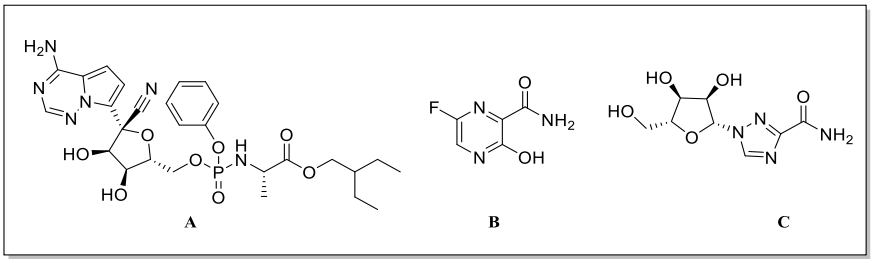


**Figure 5.** *Structures of remdesivir (A), favipiravir (B) and ribavirin (C).*

Molnupiravir (**Figure 6**) (also known as MK 4482) is an antiviral active agent developed by the pharmaceutical company MSD (Merck Sharp & Dohme) in collaboration with Ridgeback Biotherapeutics, whose trade name is Lagevrio. The Italian Medicines Agency announced that its Technical Scientific Committee (STC), on December 22, 2021, authorized the use of molnupiravir for the treatment of patients not hospitalized for COVID-19 with mild to moderate disease of recent onset and

having concomitant clinical conditions that represent specific risk factors for the development of severe SARS-CoV-2 disease.

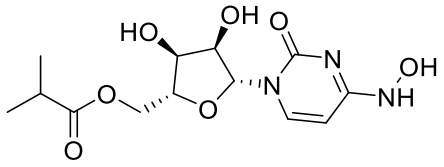


**Figure 6.** *Structure of molnupiravir*.

It is a broad-spectrum, direct-acting oral antiviral agent that targets the RdRp enzyme and was initially developed as a possible antiviral treatment for influenza, alfa-viruses, including eastern, western, and Venezuelan equine encephalitis viruses. Based on a meta-analysis of available phase 1-3 studies, molnupiravir was observed to demonstrate a significant reduction in hospitalization and death in mild COVID-19 disease (Singh *et al*., 2021). Results of a randomized double-blind placebo-controlled phase 3 study reported that early treatment with molnupiravir reduced the risk of hospitalization or death in unvaccinated at-risk adults with laboratory-confirmed mild-to-moderate COVID-19.

Chloroquine and hydroxychloroquine (**Figure 7**), which belong to the class of 4-aminoquinolines, can be included in this group, even if they act on endocellular structures rather than proteins.

Beyond their antimalarial action, chloroquine and hydroxychloroquine have proven to be broad-spectrum antiviral agents with potent activity toward both RNA and DNA viruses. Regarding their mechanism of action, they appear to interfere with the acidification process of endosomes and lysosomes by accumulating within these vesicles characterized by an acidic environment and within organelles, such as the Golgi apparatus, where they are ionized and increase pH causing inactivation of

proteolytic enzymes. This appears to inhibit the entry and replicative process of the virus (Hammond, 2017). However, a study published in Nature in 2021 that aimed to estimate the effects of hydroxychloroquine and chloroquine on survival in COVID-19 from all currently available published and unpublished RCTs showed that treatment with hydroxychloroquine is associated with increased mortality in COVID-19 patients and there is no benefit of chloroquine (Axfors *et al*., 2021).

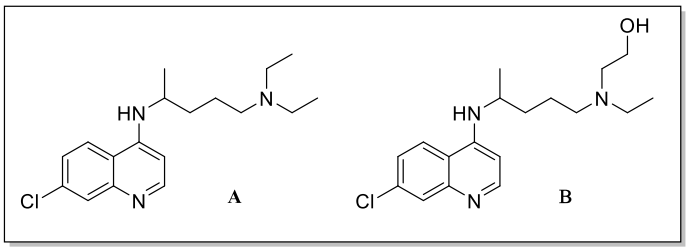


**Figure 7.** *Structures of chloroquine (A) and hydroxychloroquine (B).*

Ritonavir-boosted nirmatrelvir (Paxlovid) (**Figure 8**) is an oral combination pill of two antiviral agents that, based on data from phase 2 and 3 studies that included 1219 patients, found that following administration within three days of symptom onset, the risk of hospitalization or COVID-19-related mortality was 89 percent lower (Mahase, 2021). On December 22, 2021, the FDA issued an approval for the use of nirmatrelvir boosted with ritonavir for patients with mild to moderate COVID-19.

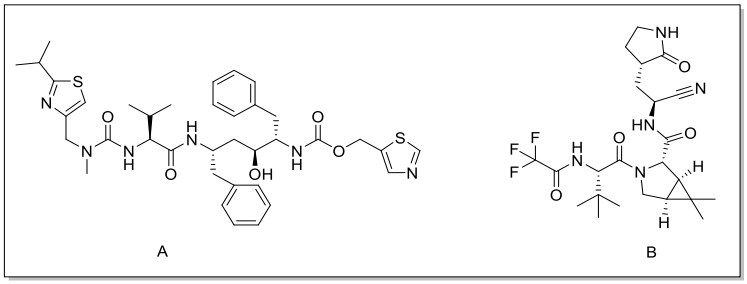


**Figure 8.** *Structures of ritonavir (A) and nirmatrelvir (B).*

Nirmatrelvir is a covalent 3C-like protease (3CLpro) of SARS-CoV-2 inhibitor binding to the catalytic cysteine 145 (Leister-Tebbe *et al*., 2022). This cysteine is responsible for the activity of the 3CLpro of SARS-CoV-2 and potentially other members of the coronavirus family. The 3CLpro, also known as the main protease or non-structural protein 5, is responsible for cleaving polyproteins 1a and 1ab (Mody *et al*., 2021). These polyproteins contain the 3CLpro itself, a papain-like (PL) cysteine protease, and 14 other non-structural proteins. Without the activity of the 3CLpro, non-structural proteins (including proteases) cannot be released to perform their functions, inhibiting viral replication.

Lopinavir and ritonavir are anti-retroviral drugs belonging to the protease inhibitor classis: the combo therapy of these two drugs has been approved by FDA for treating HIV and was proposed as antiviral therapy against COVID-19 during the early onset of the pandemic.

Given its crucial role in the life cycle of the virus, Mpro is one of the most appealing targets for drug discovery. Through a high-throughput screening of FDA-approved drugs and drugs involved in clinical trials, several molecules were identified as main protease inhibitors of SARS-CoV-2. The most potent was found to be ebselen, a synthetic organoselenic compound with anti-inflammatory, antioxidant and cytoprotective actions.

Although ebselen has been shown to act as a covalent inhibitor of Mpro of the new coronavirus, it can also interact with the target non-covalently; this may explain the low $IC_{50}$ value observed (0.67 μM). Carmofur, a 5-fluorouracil analogue, also reported an interesting $IC_{50}$ value of 1.82 μM. Both these compounds covalently bind to Cys145 in the Mpro active site of SARS-CoV-2 (**Figure 9**) (Jin *et al*., 2020).

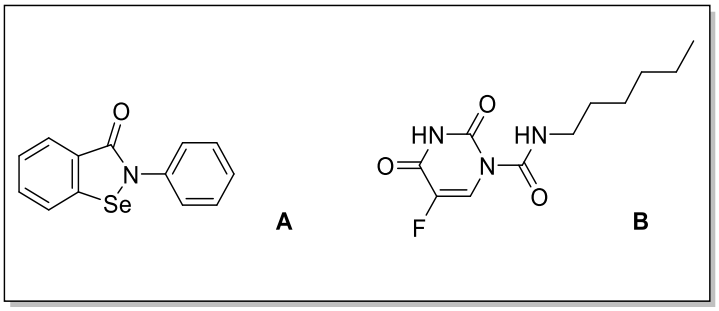


**Figure 9.** *Structures of ebselen (A) and carmofur (B).*

### *1.4.2 Indolic core-based antiviral agents*

The concept of privileged structure was introduced by Evans in the late 1980s to define scaffolds useful to obtain ligands able to modulate a wide range of receptors. A prime example is the indolic core, which forms the scaffold of several molecules that have been shown to inhibit PLpro and Mpro proteases.

**11a** and **11b** (**Figure 10**) are among the most potent known Mpro inhibitors of SARS-CoV-2. They are peptidomimetic compounds characterized by an aldehyde function that irreversibly blocks Cys145, an amino acid involved in the mechanism of catalysis.

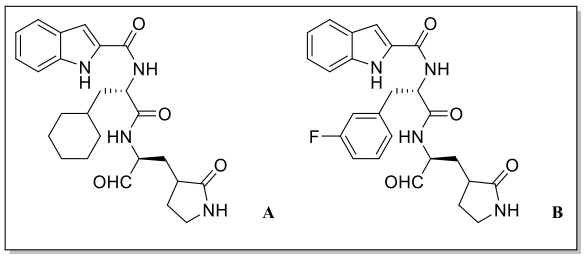


**Figure 10.** *Structures of **11a** (A) and **11b** (B).*

Both molecules contain the indolic core chosen both to increase useful interactions with the target through additional hydrogen bonds and to improve their druglikeness (Dai *et al*., 2020).

Natural compounds have also shown effective as Mpro inhibitors. *Isatis indigotica* was one of the first medicinal plants reported to have potential anti-SARS action. It is a Chinese medicinal herb belonging to the *Cruciferae* family, which has been widely used for the prevention of SARS. Further investigation of its metabolites led to the characterization of several isatin-derived alkaloids, among which we can include indica, indirubin, and indigo (**Figure 11**) (Gilbert *et al*., 2004).

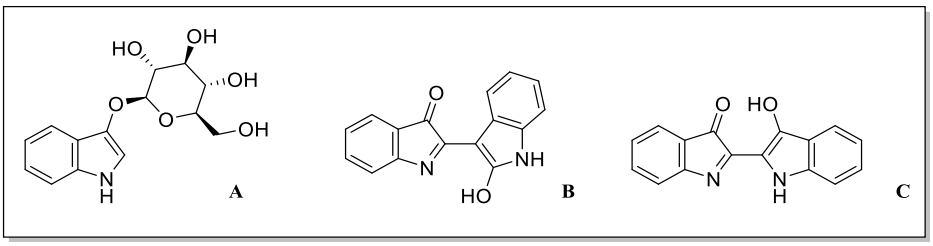


**Figure 11.** *Structures of indica (A), indirubin (B) and indigo (C).*

An additional molecule extracted from *Isatis indigotica* yielded interesting results: triptantrine (**Figure 12**), an indolquinazoline alkaloid, reported to have anti-inflammatory, antioxidant activities, was shown to inhibit the proteolytic activity of PLpro with an $IC_{50}$ of 1.52 μM (Tsai *et al*., 2020).

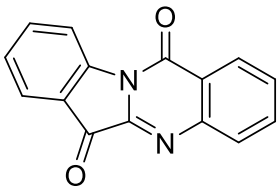


**Figure 12.** *Structure of triptantrine.*

Molecular docking studies on other molecules of natural origin, such as flavonoids, and in particular on a subset of them composed of synthetic molecules, namely indole-core chalcones, have demonstrated their efficacy in various diseases (Lee *et al*., 2015).

These compounds have also been studied for their anti-SARS-CoV-2 properties, and their action has been highlighted especially at the level of Mpro protease and S-glycoprotein.

### 1.5 SARS-CoV-2 protease Mpro: scientific background

SARS-CoV-2 proteases Mpro and PLpro are promising targets for antiviral drug development (Narayanan *et al*., 2022).

The Mpro of SARS-CoV-2 is a homodimeric protease: it consists of two protomers, which, upon dimerization and activation, are oriented into a conformation that is functional for catalytic activity. Similarly to other proteases, each protomer is subdivided into 3 domains: domains I (residues 8-101) and II (residues 102-184) are formed by antiparallel barrels; domain III (residues 201-306), which is mainly formed by helices, is responsible for the catalytic process. The catalytic site of the enzyme consists of 4 pockets, denoted S1', S1, S2, S4, with S1' containingthe catalytic dyad. The latter is composed of Cys145 and His41 and is inserted into the cavity between domains I and II (**Figure 13**).

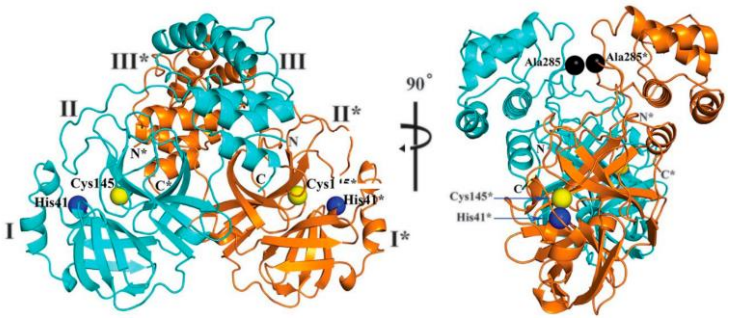


**Figure 13.** *3D structure of the main protease of SARS-CoV-2. (Adapted from Zhang et al., 2020).*

Analyzing its catalytic mechanism, after Cys145 is deprotonated by the imidazole of His41, the thiolate ion formed performs nucleophilic attack on the carbonyl carbon of the substrate amide bond. The peptide product with free N-terminal is released following the deprotonation carried out by His41, before the thioester is hydrolyzed by releasing the C-terminal portion and restoring the catalytic dyad (Ulrich *et al*., 2020).

As Mpro has a specific cleavage action in the vicinity of a glutamine residue, a feature not found in any human protease and suggesting the absence of off-target effects, a wide range of covalent and non-covalent inhibitors was developed.

Whether peptidomimetics or small molecules, covalent-type inhibitors are characterized by the presence of a particularly reactive electrophilic function, called warhead, required for protease inactivation (Citarella *et al*., 2021).

Although the use of covalent inhibitors represents the most widely pursued approach, it is characterized by a number of inconvenient aspects, including the propensity to interact with off-targets thus causing side effects and toxicity, which is why the development of noncovalent type inhibitors is essential (Lipiński *et al*., 2021).

The excellent inhibitory activity of ebselen, which goes on to covalently bind Cys145 with the formation of a stable selenyl sulfide, has been previously highlighted. For this reason, ebselen has been considered a lead compound for the development of a series of benzisoselenazolone core analogues and diselenide analogues. The ebselen-like compounds have been shown to be more potent than the diselenides confirming that the electrophilic nature of the Se atom is a key feature in the reaction with cysteine.

In fact, in ebselen-like derivatives, the N-Se bond reduces the electron density of selenium; in contrast, this reduction is much less pronounced in the diselenides. Among the benzisoselenazolones, the isoleucine and valine derivatives, named **5** and **7**, respectively (**Figure 14**), gave the best results in terms of $IC_{50}$.

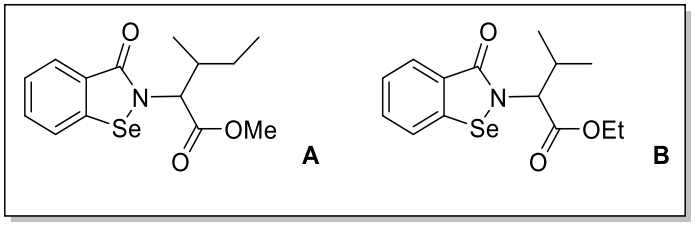


**Figure 14.** *Structure of analogues **5** (A) and **7** (B).*

Jin *et al*. (2020) identified an interesting peptidomimetic inhibitor called N3 (**Figure 15**). It is a pseudo-tetrapeptide belonging to the Michael class of acceptors, which can irreversibly block the enzyme due to the presence of an activated double bond.

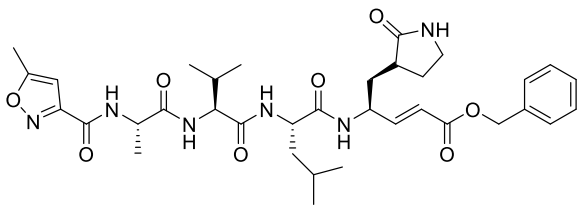


**Figure 15.** *Structure of N3.*

Noncovalent inhibitors of Mpro include flavonoids. Baicalein (**Figure 16**), a flavone extracted from the root of *Scruitellaria baicalensis*, a plant used in traditional Chinese medicine for prophylaxis and treatment of numerous viral infections, significantly reduced virus growth in Vero E6 cells infected with SARS-CoV-2 (Liu *et al*., 2021).

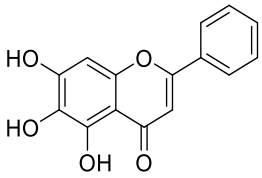


**Figure 16.** *Structure of Baicalein.*

## 2.1 Mpro inhibitors: series I in silico design

Based on the numerous scientific evidence reported in the literature and considering the crucial role of Mpro in the replicative cycle of the virus, our research group decided to contribute to the health emergency by synthesizing a small library of potential modulators of SARS-CoV-2 Mpro. Therefore, in the first part of my PhD, I focused on the design and synthesis of a new series of compounds as both covalent and noncovalent SARS-CoV-2 Mpro inhibitors (**Figure 17**). The synthesized peptidomimetic derivatives (**7**, **22**-**29**) derive from the combination of *L*-tryptophan and *L*-leucine as natural amino acids, while *L*-propargylglycine and *L*-allylglycine were used to provide the electrophilic moiety required to bind Cys145; note that, within this group, derivative **29** exhibits as many as two electrophilic groups.

Derivatives **34** and **35**, on the other hand, don't derive from the combination of amino acids; however, the peptidomimetic nature of these compounds was

nevertheless maintained by using substituents capable of mimicking lipophilic amino acids, such as a benzylamine group and, again, *L*-propargylglycine, which obviously serves as an electrophilic substituent. The choice of the indolic core was dictated by its nature as a preferred structure given its ability to be an easily derivatizable core and to provide several useful bonds for interaction with numerous targets: this means that it can be used extensively as a scaffold in the synthesis of pharmacologically active molecules.

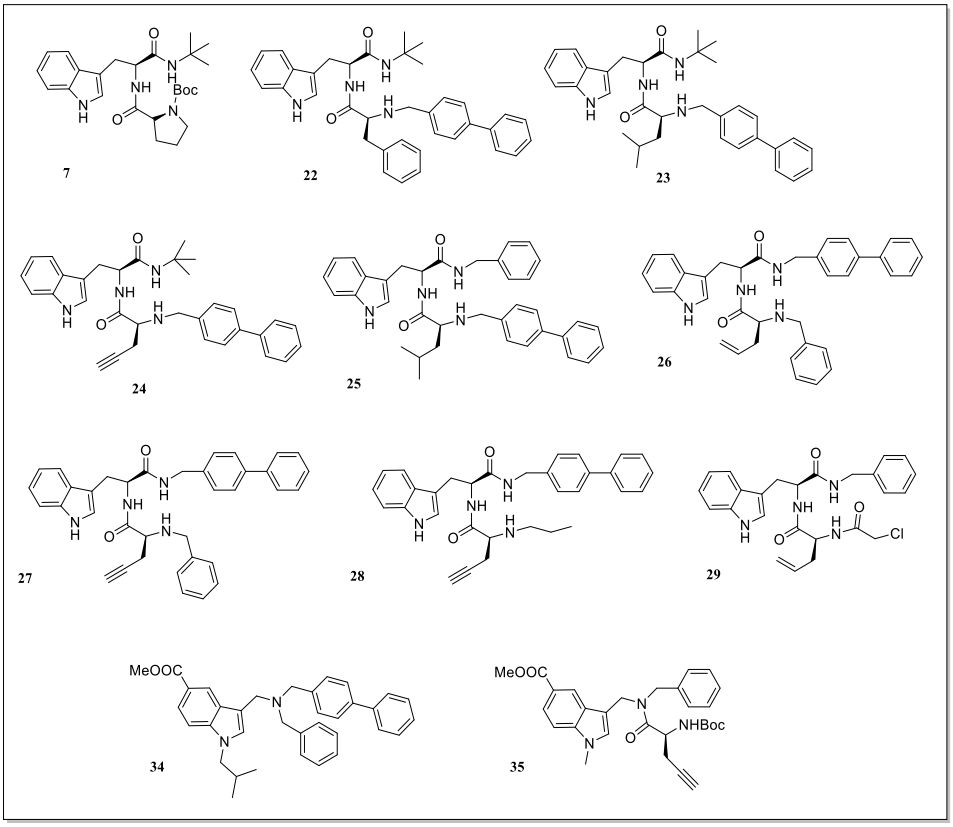


**Figure 17.** *Series I: synthesized derivatives.*

The design was carried out with the aid of molecular modelling (via molecular docking, through the Glide software (Friesner *et al*., 2004)) with the aim of better explore the extent and structuring of the pocket at the active site level to maximize the number and extent of possible interactions with the synthesized derivatives. In this

regard, also considering the docking studies previously carried out on inhibitors reported in the literature (Dai *et al*., 2020), the indole core was derivatized at position 3 with more or less lipophilic substituents with some steric bulk to better understand the size of the binding pocket so that structure-activity relationships could be derived.

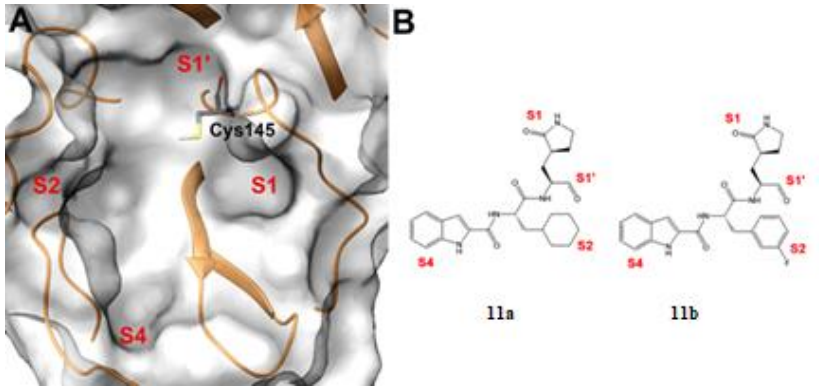


**Figure 18.** *A) SARS-CoV-2 Mpro binding site; S1', S1, S2, and S4 sites and Cys145 key residue are highlighted. B) Chemical structures of compounds* ***11a*** *and* ***11b****, with specified the chemical moieties interacting with the S1', S1, S2, and S4 Mpro sites.*

Specifically, it was evaluated whether the initial fragment of *L*-tryptophan could preserve, at least in part, the interaction network established by reference compounds **11a** and **11b**, particularly with regard to the positioning of the indole function in the binding site (**Figure 18**).

Unfortunately, preliminary molecular docking calculations showed that the *L*-Trp-methylated (mtrp) structure is positioned at the S2 site instead of S4 (**Figure 19A**). In order to force the 1H-indol-3-yl moiety in the S4 site, the *L*-Trp starting fragment was decorated introducing voluminous substituents at both the amino (N-) and carboxyl (C-) termini. After different attempts, satisfactory outcomes were obtained by linking the *L*-Leu at the *L*-Trp N-terminus and an N-benzyl moiety at the *L*-Trp C-function

terminus. The introduction of a ([1,10 -biphenyl]-4- yl)-substituent at the *L*-Leu N-terminus led to compound **25**, showing a good accommodation in the Mpro binding site (**Figure 19B**). This compound was indeed able to fit S1', S1, S2, and S4 sites while also establishing a set of interactions with His41 and Cys145 (belonging to the catalytic dyad), Phe140, Glu166, and Gln189. Also, the careful analysis of the sampled binding poses of **25** disclosed that the terminal benzyl moiety could be replaced by a shorter and bulky substituent, finally leading to compound **23** (**Figure 19C**) featuring a tert-butyl moiety. Starting from compound **23**, we then wondered whether the introduction of a reactive chemical function able to covalently bind the Cys145 could lead to an improved biological activity. With this aim, the isobutyl moiety from *L*-Leu residue in **23** was replaced with a propyn-2-yl function (compound **24**), thus considering the reactivity of alkyne group with cysteine residues, as widely reported (Kim *et al*., 2021; Mons *et al*., 2019; Sommer *et al*., 2013). On the other hand, the analysis of the covalent complex revealed the loss of a series of key interactions with the key residues belonging to S1', S1, S2, and S4 sites as previously detected for **23** (**Figure 19F**). Starting from compound **24**, we introduced the ([1,10 -biphenyl]-4- yl) substituent at the C-terminus while using a smaller benzyl moiety at the N-terminus (compound **27**). Covalent docking calculations showed a binding mode compatible with that previously observed for **23** (**Figure 19G**). In derivative **28**, the substitution of benzyl with an alkyl function on the N-terminal resulted in the loss of a number of key interactions with the protein counterpart (**Figure 19I**), so the chemical structure was further modified by introducing a second covalent attachment point (α-chlorochetone, derivative **29**): in this case, a promising covalent complex-related binding mode was obtained (**Figure 19J**).

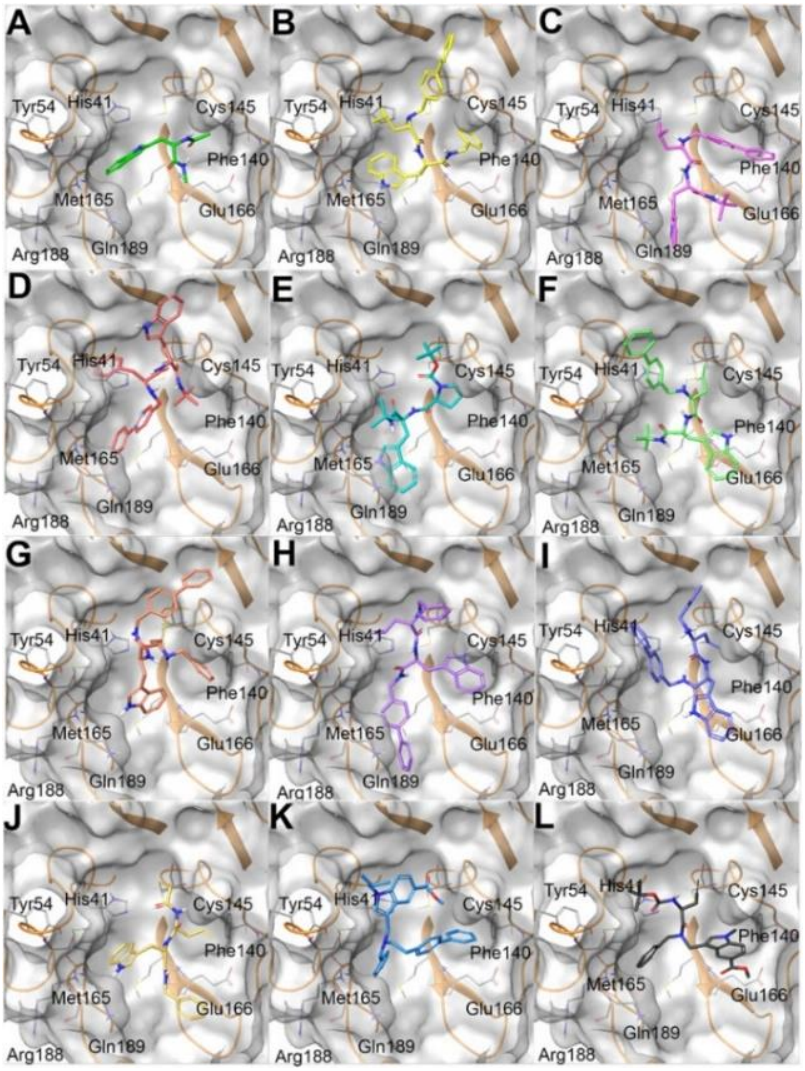


**Figure 19.** *A) mtrp; B)* ***25****; C)* ***23****; D)* ***22****; E)* ***7****; F)* ***24****; G)* ***27****; H)* ***26****; I)* ***28****; J)* ***29****; K)* ***34****; L)* ***35*** *in docking with SARS-CoV-2 Mpro.*

Eventually, two small molecules (compounds **34** and **35**), obtained according to the synthetic route reported in the chemistry section, were evaluated. Specifically, the indole function was modified introducing alkyl substituents on the basic nitrogen while also showing an ester function at C-5 position. As expected, molecular docking calculations highlighted that such modifications led to a poor predicted binding with the protein counterpart, especially for what concerned the interaction network in the

S4 site, since the modified indole moiety pointed in a region between the S2 and S1' site (**Figure 19K**).

### *2.1.1. Synthesis of series I*

Final compounds **7** and **22-29** were synthesized as summarized in **Figure 20**. *L*-Boc-Trp-OH was coupled with tert-butyl amine, 4-phenylbenzylamine or benzylamine using HOBt and HBTU as coupling agents and DIPEA as base. Amides **1**-**3** were thus obtained in 65-80% yields. Removal of the Boc protecting group by DCM:TFA (3:1 v:v), gave intermediates **4**-**6** in almost quantitative yields. The intermediates were coupled, without further purification, with different *L*-aminoacids (*L*-Boc-Pro-OH, *L*-Boc-Phe-OH, *L*-Boc-LeuOH, *L*-Boc-Pra-OH or *L*-Boc-allylgly-OH) using the same coupling protocol described above. In this way, final compound **7** (59% of yield) and pseudo-peptides intermediates **8**-**14** (74-82% of yields) were obtained. Removal of the Boc protection from derivatives **8**-**14**, led to compounds **15**-**21**, that were further derivatized by reductive amination with 4-phenylbenzaldehyde, benzaldehyde or propionaldehyde to give final derivatives **22**-**28** in 55-66% yields. Alternatively, acylation of **20** with chloroacetyl chloride led to compound **29** in 62% yield.

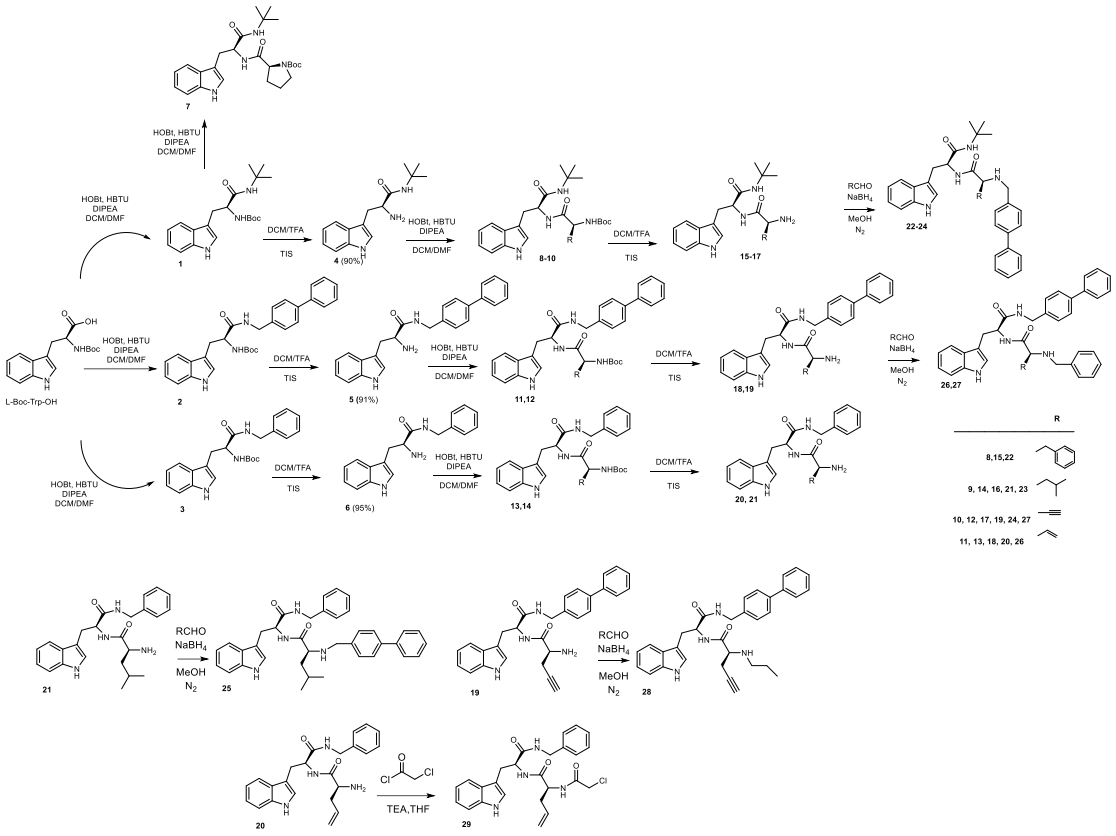


**Figure 20.** *Synthesis of compounds **7**, **22-29**.*

The synthetic route to obtain small molecules **34** and **35** is illustrated in **Figure 21**.

Using methyl 1H-indole-5-carboxylate as starting material, N-1 alkylation was performed by reaction with isobutyl iodide or methyl iodide using sodium hydride as base. In this way, intermediates **30** and **31** were synthesized in 80% and 82% yields, respectively. Starting from these compounds, Mannich reaction was carried out leading to intermediates **32** and **33** in 70% and 75% yields, respectively. Upon alkylation with benzyl bromide, final compound **34** was obtained in 78% yield, while compound **35** resulted from a coupling reaction of **33** with *L*-propargyl glycine as described above and was isolated in 80% yield.

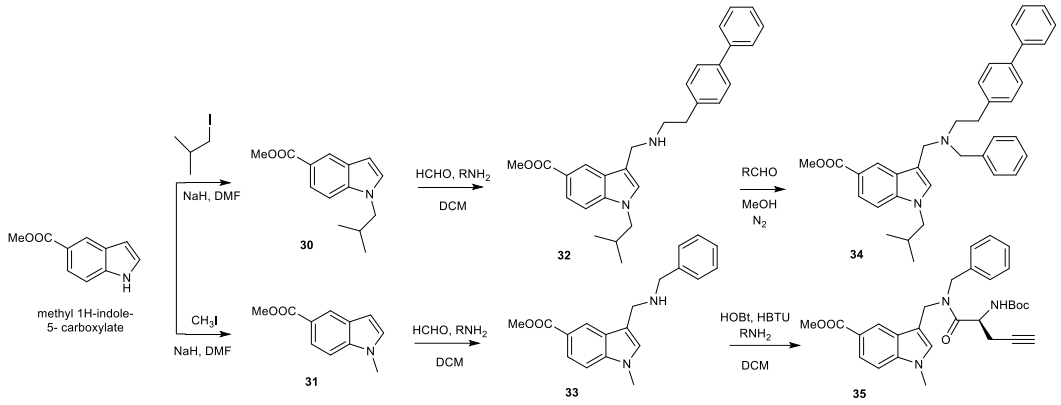


**Figure 21.** *Synthesis of compounds **34** and **35**.*

### *2.1.2. Biological evaluation*

To preliminarily evaluate the interaction of the synthesized small molecules against the main protease, an enzymatic assay conducted by 3CL Protease, MBP-tagged (SARS-CoV-2) Assay Kit (Bioscience) was performed: the binding ability of the synthesized compounds to Mpro was determined by co-administration of a fluorescent substrate that competes with the molecules for binding to the active site of that enzyme. GC-376, a known inhibitor of Mpro, was used as a positive control, and protease alone in assay buffer was used as a negative control.

As shown in **Table 1**, derivatives **7**, **23**, **27** and **29** showed the most interesting results, with $IC_{50}$ values of 5.01, 1.73, 2.86 and 1.72 μM, respectively, in accordance with previously discussed docking studies.

**Table 1.** *3CL Protease, MBP-tagged (SARS-CoV-2) Assay.*

| ***Compounds*** | ***Mpro $IC_{50}$ (μM)*** |
|---|---|
| ***GC-376*** | 0.57 ± 0.15 |
| ***GRL-0617*** | - |
| ***7*** | **5.01 ± 2.31** |
| ***22*** | >25 |
| ***23*** | **1.73 ± 0.89** |
| ***24*** | >25 |
| ***25*** | 23.61 ± 8.72 |
| ***26*** | >25 |
| ***27*** | **2.86 ± 1.42** |
| ***28*** | 22.65 ± 9.82 |
| ***29*** | **1.72 ± 0.75** |
| ***34*** | >25 |
| ***35*** | >25 |

Given the promising data from the enzymatic assay, especially regarding derivative **29**, cell experiments were carried out at the Rega Institute (Belgium), in collaboration with Prof. Graciela Andrei. Vero cells derived from African green monkey kidneys transfected with two different strains of SARS-CoV-2: UC-1074 and UC-1075, from human nasopharyngeal samples, were used for the assays. The viral cythopathic effect (CPE) is measured microscopically 5 days after incubation with the compounds and expressed as $EC_{50}$. All data were compared with those of the reference compound remdesivir. In parallel, the cytotoxic activity of the compounds on mock-infected lines was also evaluated (**Table 2**).

**Table 2**. *Cellular assays results.*

| Compounds | Antiviral activity $EC_{50}$[a] UC-1074 #1 strain Vero cells | Antiviral activity $EC_{50}$[a] UC-1075 #1 strain Vero cells | Cytotoxicity | Cytostaticity |
|---|---|---|---|---|
| | | | Cell morphology (MCC)[b] | Cell growth ($CC_{50}$)[c] |
| **Remdesivir** | 0.87 µM | 0. 61µM | >40 µM | >40 µM |
| **7** | >100 µM | >100 µM | >100 µM | >100 µM |
| **22** | **2.19 µM** | **2.01 µM** | **>100 µM** | **1.49 µM** |
| **23** | >4 µM | >4 µM | 20 µM | 10.61 µM |
| **24** | >4 µM | >4 µM | 20 µM | 4.67 µM |
| **25** | >4 µM | >20 µM | ≥20 µM | 34.70 µM |
| **26** | 63.14 µM | >20 µM | ≥100 µM | 78.37 µM |
| **27** | **8.94 µM** | **10.94 µM** | **≥100 µM** | **51.52 µM** |
| **28** | >20 µM | >20 µM | >100 µM | 42.35 µM |
| **29** | **0.32 µM** | **1.37 µM** | **100 µM** | **38.67 µM** |
| **34** | **5.98 µM** | **0.44 µM** | **100 µM** | **31.53 µM** |
| **35** | 4 µM | 20 µM | 100 µM | 8.09 µM |

[a] Effective concentration required to reduce virus plaque formation by 50%. Virus input was 100 CCID50.
[b] Minimum cytotoxic concentration that causes a microscopically detectable alteration of cell morphology.
[c] Cytostatic concentration required to reduce cell growth by 50%.

Despite the remarkable activity showed in enzymatic assays, compounds **7** and **23** largely failed to inhibit viral plaque formation with compound **23** showing high cytotoxicity. These data could be probably justified on the basis of the predominant lipophilic character of the two compounds, determining unfavourable pharmacokinetic properties as well as precipitation and/or aggregation in the cellular medium (Locatelli *et al*., 2008; Liao *et al*., 2014). On the other hand, compounds **27** and **29** confirmed the antiviral activity showed *in vitro*. In particular, compound **29** potency was comparable to remdesivir and 28-fold higher than compound **27** over two different SARS-CoV-2 strains, with negligible cytotoxicity. Moreover, derivatives **22** and **34**, that were unable to antagonize Mpro *in vitro*, showed cellular antiviral activity. Besides results for derivative **22** were largely affected by high cytotoxicity (**Table 2**), compound **34** antiviral activity was worth of further investigations.

Therefore, based on the results obtained from the enzyme inhibition experiments conducted on Mpro and subsequently from the in-cell antiviral assays, we questioned whether the synthesized compounds were also able to bind other SARS-CoV-2 proteins, namely Papain-like Protease (PLpro) and Spike protein (SP). Additional enzymatic assays were then carried out: for PLpro the assay was conducted using the Papain-like Protease Assay Kit: Deubiquitinase Activity (Bioscience), going to measure the deubiquitination activity of this protease.

**Table 3.** *Papain-like Protease Assay: Deubiquitinase Activity* and *SP-SPR binding assay.*

| ***Compounds*** | ***PLpro $IC_{50}$ (μM)*** | ***SP KD (μM)*** |
|---|---|---|
| ***GC-376*** | - | - |
| ***GRL-0617*** | 1.67 ± 0.63 | - |
| ***7*** | >25 | >25 |
| ***22*** | >25 | 19.05 ± 0.41 |
| ***23*** | >25 | >25 |
| ***24*** | >25 | >25 |
| ***25*** | >25 | - |
| ***26*** | >25 | >25 |
| ***27*** | >25 | - |
| ***28*** | >25 | - |
| ***29*** | 0.67 ± 0.59 | >25 |
| ***34*** | >25 | 3.26 ± 0.11 |
| ***35*** | >25 | 11.41 ± 0.36 |

As reported in **Table 3**, compound **29** showed remarkable affinity for PLpro with lower $EC_{50}$ than the reference compound GRL-0617, while compound **34** showed good affinity for the spike protein. The dual inhibitory effect of compound **29** is likely

responsible for its higher cellular antiviral activity, when compared to **23**, highlighting the potential of dual Mpro and PLpro inhibitors as anti-SARS-CoV-2 therapeutics. As for compounds **22** and **35**, which showed good antiviral activity in in-cell assays and some affinity for the spike protein, they nevertheless exhibited considerable levels of cytotoxicity, which is why their potential activity towards new targets was not investigated further.

### *2.1.3. Molecular docking studies: PLpro and SP*

Starting from these data, molecular docking calculations were performed for derivative **29** on PLpro; specifically, two different models were generated, related to noncovalent and covalent binding. In the noncovalent ligand/protein complex (PDB: 7JIW), compound **29** docks to the protein binding site by establishing a large and diverse number of interactions, such as π-π bonds with Tyr268, cation-π interaction with Arg166, hydrogen bonds with Gln269 and Thr301 (**Figure 22A**). Moreover, comparison of the binding modes of the tested compound and the VBY compound, which was originally co-crystallized in the protein structure, showed similar binding interaction (Osipiuk *et al.*, 2021), thus confirming the promising interaction of **29** with PLpro. On the other hand, in order to shed light on the hypothesized covalent binding, PLpro was evaluated co-complexed covalently with a peptide inhibitor (PDB: 6WX4) through the reactive residue Cys111 (Rut *et al*., 2020). In this case, the covalent docking calculations for compound **29** showed a different binding mode and, in particular, the indole and benzyl portions result oriented toward the outer part of the protein, while establishing hydrogen bonds with Gly271 and His272 (belonging to the catalytic triad of this enzyme) and π-π interactions with Trp106 (**Figure 22B**).

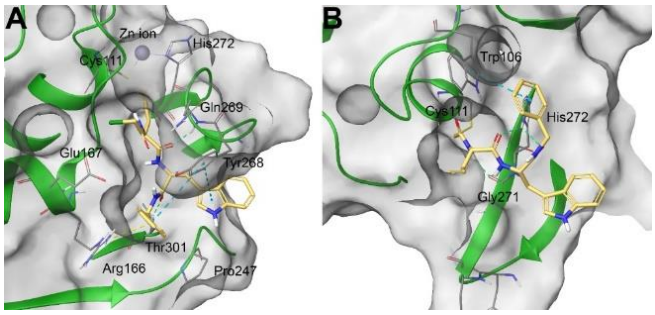


**Figure 22.** *A) non-covalent and B) covalent molecular docking complexes between **29** and SARS-CoV-2 PLpro.*

Interestingly, we found that the cellular inhibitory effects of compound **34**, is due to its ability to selectively inhibit SARS-CoV-2 spike protein in the low micromolar range (**Table 3**).

The small molecule **34** could be thus considered an interesting chemotype for the development of a new class of anti-SARS-CoV-2 agents, selectively inhibiting SP. Molecular docking calculations were performed targeting the SP receptor-binding domain structure released by Wang et al. (PDB code: 6LZG) originally co-complexed with ACE2 (Wang *et al*., 2020). *In silico* experiments highlighted the accommodation of **34** featuring a good shape complementarity with the external surface of SP and a large network of contacts with some residues responsible for the SP-ACE2 protein-protein interaction (**Figure 23**). Specifically, **34** made π-π stacking with Phe459 and Tyr348 and H-bond with Glu484 as well as a large set of hydrophobic and polar contacts with Tyr449, Leu455, Phe486, Gln493, and Ser494.

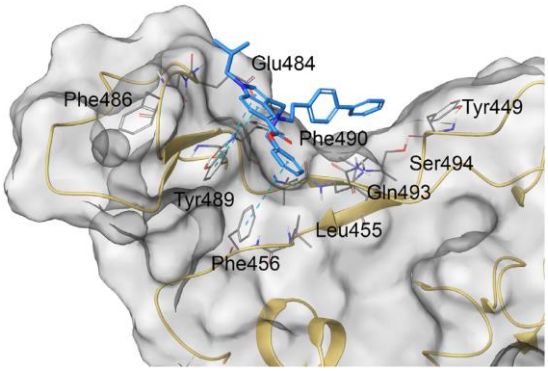


**Figure 23.** *Molecular docking complex between **34** and SARS-CoV-2 SP.*

## 2.2. Mpro inhibitors: series II

Mutations are a direct consequence of each pandemic because they reflect the intrinsic ability of the viruses to adapt themselves to the surrounding habitat and to escape host defences perpetuating their infectious cycle. As consequence of SARS-CoV-2 long term permanence, mutations are closely related to the recent opinion that COVID19 is moving toward an endemic infection (Biancolella *et al*., 2022). This new collocation of the illness, even if it doesn't make it less dangerous, will completely change the global scenario. It will result in a readjustment of all the measures currently fielded, from social behaviour to therapeutic intervention. In fact, the endemization of SARS-CoV-2 will require, besides the achievement of "herd immunity", an appropriate therapy, which must be based on a safer, homely administrated and readily accessible drug arsenal. This prospective enliven the research endeavour headed for the discovery of potent and selective anti-SARS-CoV-2 agents.

Therefore, based on the promising results obtained from the previous series of compounds, it was decided to design a second library of molecules aiming to increase the antiviral activity. Based on the SAR studies carried out on the most powerful

compound in the first series (**29**), a second library of molecules was designed; the novel molecules retained the central peptidomimetic scaffold of the first series most potent compound **29** (**Figure 24**).

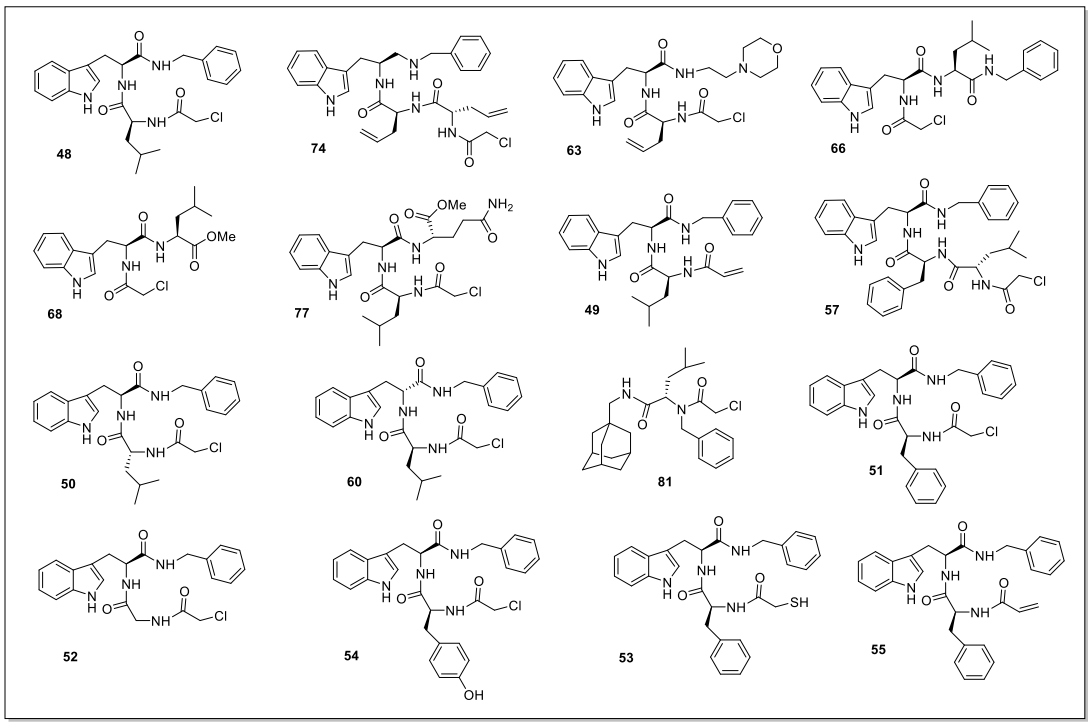


**Figure 24.** *Series II: synthesized derivatives.*

It was previously observed that the indolic core is crucial for interaction with the S4 pocket.

For this reason, it was decided to retain the indole scaffold for most of the molecules in the new series except for derivative **81**, for which we decided to replace the tryptophan indole with a methylamine adamantan group, in order to explore new possible binding interactions with the enzyme pocket. Furthermore, with the aim of investigating the importance of the benzyl substituent, whose presence is necessary to establish hydrophobic interactions in the binding pockets of both proteases, it was decided to replace it with aliphatic groups with a certain polarity (**63** and **77**). Finally,

all the designed compounds are characterised by the presence of one or more electrophilic groups, given their importance in establishing covalent bonds with Cys145 in the catalytic site of Mpro.

### *2.2.1. Synthesis of series II*

Final pseudo-peptides **48**-**55**, **57** and **60** were synthesized according to scheme reported in **Figure 25**.

Boc-L-Tryptophane was treated with benzylamine in classic coupling conditions, using HOBt, HBTU and DIPEA in DCM leading to intermediate **36** in 80% yield. After Boc protecting group removal with TFA in DCM (1:3 as ratio) and using TIS as scavenger, the α-amino group of compound **37** was coupled with Boc-*L*-Leu-OH, or Boc-D-Leu-OH, or Boc-*L*-Phe-OH or Boc-Gly-OH, or Boc-*L*-Tyr-OH in the same conditions discussed above. Pseudo-dipeptides **38**-**42** were obtained in a range of 65-82% of yields. Amino group deprotection of intermediates **38**-**42** in the same conditions described before, almost quantitatively, led to derivatives **43**-**47** that were treated with the proper acyl chloride to furnish final compounds **48**-**55** (48-68% yields).

Intermediate **45** was also coupled with Boc-*L*-Leu-OH in the previously described conditions, giving, after Boc removal, compound **56** (78% yield), which was reacted with cloroacethyl chloride in DCM using TEA as base, yielding final derivative **57** in 52% yield.

Starting from Boc-*D*-Trp-OH, following the same pathway and the same reaction conditions described for the synthesis of **48**, final compound **60** was obtained in 36% of overall yield.

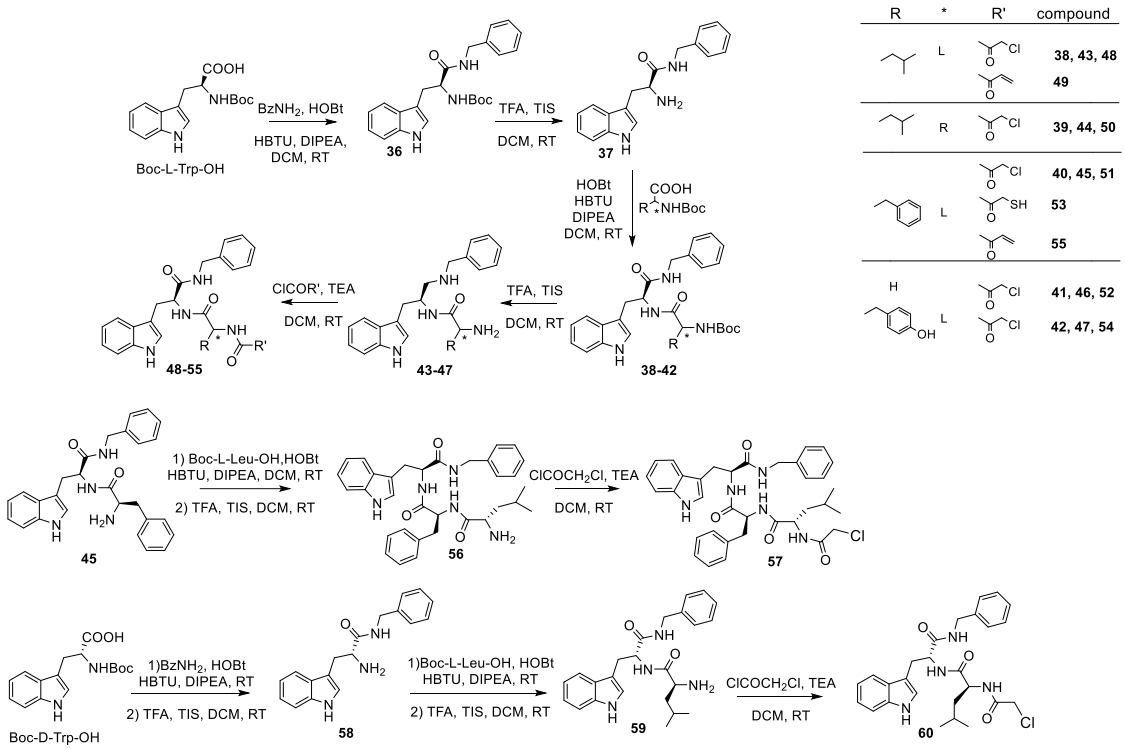


**Figure 25.** *Synthesis of derivatives **48**-**55**, **57** and **60**.*

Compounds **63**, **66** and **68** were obtained as depicted in **Figure 26**.

Using Boc-*L*-Trp-OH as starting material, coupling reaction with 4-(2-aminoethyl)morpholine employing HOBt and HBTU as coupling agents and DIPEA as base, compound **61** was obtained in 74% yield. A cycle of Boc deprotection in DCM/TFA (3:1 as ratio) in presence of TIS, and a further coupling with Boc-*L*-Allyl-Gly-OH in the same reaction conditions described above, afforded intermediate **62** (58% yield).

Compound **63** was obtained in 52% yield, after a classical Boc removal and subsequent reaction with chloroacetyl chloride in DCM and TEA.

Derivative **66** was synthesized starting from Boc-*L*-Trp-OH, which was coupled with L-Leu-OMe, using the previously described reaction conditions to yield intermediate **64**.

Hydrolysis of methyl ester in aqueous NaOH and subsequent coupling with benzylamine, employing HOBt, HBTU and DIPEA afforded **65**. The last reaction steps consisted in Boc removal and acyl substitution with chloroacetyl chloride leading to final compound **66** in 21% overall yield.

Starting from methyl (tert-butoxycarbonyl)-*L*-tryptophyl-*L*-leucinate (**64**), deprotection with TFA/DCM (1:3 v:v) and TIS led to **67**, which was subsequently treated with chloroacetyl chloride in DCM and TEA, affording final compound **68** in 45% overall yield.

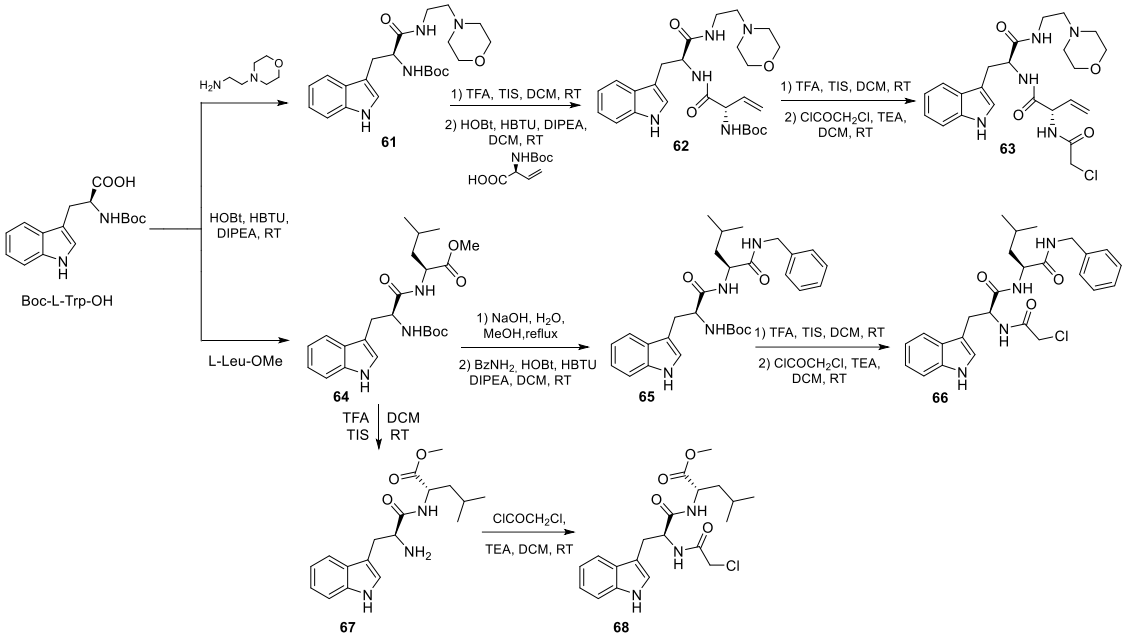


**Figure 26**. *Synthesis of derivatives **63**, **66** and **68**.*

Compounds **74**, **77** and **81** were obtained in accordance with scheme reported in **Figure 27**.

Commercially available Cbz-*L*-Trp-OH was subjected to Weinreb amidation with N,O-dimethyl hydroxylamine, HOBt, HBTU and DIPEA, to furnish the carbamoyl intermediate **69**, in 85% yield. Weinreb amide was reduced to the corresponding aldehyde using $LiAlH_4$ and then, subjected to reductive amination with benzylamine, affording compound **70** in 52% yield.

The introduction of Boc protecting group using Boc anhydride in DCM, and Cbz removal under hydrogenation conditions gave **71** in 88% yield. Intermediate **71** was coupled with Fmoc-*L*-allyl-Gly-OH using HOBt, HBTU and DIPEA in DCM and then subjected to Fmoc removal in a mixture of diethylamine/DCM (1:3 v:v) leading to compound **72** (78% yield). Another cycle of coupling and Fmoc-deprotection, using the same reagents and conditions described above, afforded pseudo-tripeptide **73** in 72% yield. Finally, compound **74** was obtained in 78% yield by free amino-group

reaction with chloroacetyl chloride and TEA in DCM and subsequent Boc deprotection in TFA/DCM (1:3 v:v) using TIS as scavenger.

Coupling reaction between Cbz-*L*-Trp-OH and *L*-Gln(Trt)-OMe using HOBt, HBTU and DIPEA generated dipeptide **75** (72% yield), that was deprotected from Cbz group under reduction conditions and coupled with Fmoc-*L*-Leu-OH as described above to afford compound **76** in 68% yield. After Fmoc removal in DEA/DCM (1:3 v:v), $NH_2$ acylation with chloroacetyl chloride and, in the end, Boc deprotection in a mixture of TFA/DCM (1:3 v:v), final derivative **77** was obtained in 38% yield.

Compound **81** was obtained starting from *L*-Leu-OMe, which was treated with benzaldehyde to form the corresponding imine derivative that, in turn, was reduced with $NaBH_4$ leading to compound **78** in 72% yield. Boc protecting group was introduced on the secondary amine, using Boc anhydride and TEA in DCM, then the methyl ester function was hydrolysed by aqueous NaOH to furnish intermediate **79** (38% yield). Coupling reaction with 1-adamantanemethylamine in the same usual conditions gave intermediate **80** in 68% yield; Boc removal in standard conditions and NH-acylation with chloroacetyl chloride, finally led to compound **81** in 38% yield.

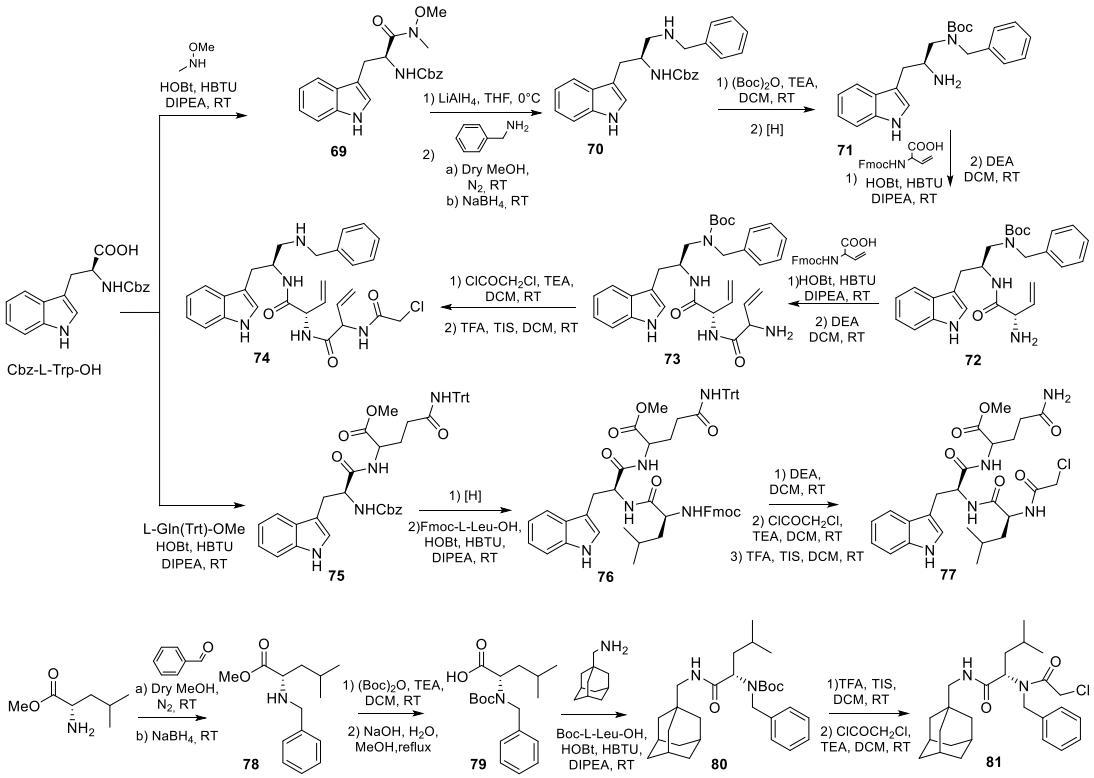


**Figure 27.** *Synthesis of derivatives **74**, **77** and **81**.*

### *2.2.2. Biological evaluation*

All synthesized compounds were tested for their enzyme inhibition capacity against Mpro using the enzyme assay reported for the previous series of derivatives (3CL Protease, MBP-tagged (SARS-CoV-2) Assay Kit (Bioscience)) (**Table 4**). The binding ability of the synthesized compounds to Mpro was determined by co-administration of a fluorescent substrate that competes with the molecules for binding to the active site of that enzyme; derivative **29**, was used as reference compound, and protease alone in assay buffer was used as a negative control.

**Table 4.** *3CL Protease, MBP-tagged (SARS-CoV-2) Assay.*

| ***Compounds*** | ***$IC_{50}$ Mpro (μM)*** |
|---|---|
| ***29*** | 1.72 ± 0.44 |
| ***48*** | 2.81 ± 0.52 |
| ***49*** | >30 |
| ***50*** | >30 |
| ***51*** | 0.73 ± 0.32 |
| ***52*** | >30 |
| ***53*** | >30 |
| ***54*** | 8.35 ± 1.85 |
| ***55*** | >30 |
| ***57*** | >30 |
| ***60*** | 14.61 ± 2.12 |
| ***63*** | >30 |
| ***66*** | 8.32 ± 0.89 |
| ***68*** | >30 |
| ***74*** | >30 |
| ***77*** | >30 |
| ***81*** | >30 |

As shown in **Table 4**, only derivative **51** showed a good inhibitory activity against the enzyme of interest, with an $IC_{50}$ value (0.73 ± 0.32 μM) even lower than the starting analogue **29** (1.72 ± 0.44 μM).

Cell experiments were then conducted on this second set of molecules as well, in collaboration with Prof. Graciela Andrei's research group, at the Rega Institute (Belgium).

Thus, given the encouraging results from the enzymatic assay performed on Mpro, especially for derivative **51**, it was decided to evaluate the antiviral activity of the synthesised derivatives on different virus variants. Vero cells derived from African

green monkey kidneys transfected with five different strains of SARS-CoV-2 from human nasopharyngeal samples, were used for the assays. The viral cythopathic effect (CPE) is measured microscopically 5 days after incubation with the compounds and expressed as $EC_{50}$. All data were compared with those of the reference compounds remdesivir, molnupiravir and derivative **29** (**Table 5**). In parallel, the cytotoxic activity of the compounds on mock-infected lines was also evaluated (**Table 6**).

**Table 5.** *Cellular assays results.*

| *Compounds* | *Antiviral activity EC50[a] 1074#2 (µM) (Wuhan) Vero cells* | *Antiviral activity EC50[a] RG-2674#2 (µM) (South Africian) Vero cells* | *Antiviral activity EC50[a] NVDBB-2220#3 (µM) (UK) Vero cells* | *Antiviral activity EC50[a] 860-J1#2 (µM) (Delta) Vero cells* | *Antiviral activity EC50[a] B1.1529BA.1#3 (µM) (Omicron) Vero cells* |
|---|---|---|---|---|---|
| ***Remdesivir*** | 0.93 ± 0.23 | 1.89 ± 0.99 | 0.51 ± 0.16 | 3.36 ± 1.22 | 1.23 ± 0.36 |
| ***Molnupiravir*** | 1.55 ± 0.69 | 2.88 ± 2.03 | 1.12 ± 0.39 | 3.55 ± 2.00 | 1.00 ± 0.45 |
| ***29*** | 1.29 ± 1.39 | 1.16 ± 1.13 | 0.46 ± 0.32 | 2.12 ± 0.82 | 5.89 ± 8.18 |
| ***48*** | 0.27 ± 0.18 | 0.32 ± 0.034 | 0.44 ± 0.15 | 1.47 ± 0.46 | 1.28 ± 0.41 |
| ***49*** | >100 | >100 | >100 | >100 | >100 |
| ***50*** | 0.10 ± 0.04 | 0.47 ± 0.25 | 0.09 ± 0.01 | 1.08 ± 0.81 | 1.37 ± 0.93 |
| ***51*** | 0.12 ± 0.08 | 0.81 ± 0.74 | 0.08 ± 0.05 | 1.30 ± 1.02 | 1.33 ± 1.41 |
| ***52*** | 0.16 ± 0.09 | 0.29 ± 0.07 | 0.16 ± 0.16 | 0.54 ± 0.20 | 0.81 ± 0.80 |
| ***53*** | >100 µM | >100 µM | >100 µM | >100 µM | >100 µM |
| ***54*** | 2.37 ± 0.47 | 3.46 ± 2.18 | 3.32 ± 2.31 | 12.28 ± 3.18 | 5.04 ± 3.49 |
| ***55*** | >20 µM | >20 µM | >20 µM | >20 µM | >20 µM |
| ***57*** | 4.81 ± 3.96 | >20 | >20 | >20 | >20 |
| ***60*** | 8.71 ± 6.00 | >20 | 8.93 ± 5.23 | >20 | >20 |
| ***63*** | 10.33 ± 0.52 | 17.12 ± 11.07 | 5.89 ± 2.19 | 29.24 ± 12.79 | 13.49 ± 2.53 |
| ***66*** | 0.25 ± 0.08 | 0.41 ± 0.02 | 0.26 ± 0.12 | 1.25 ± 0.71 | 0.40 ± 0.01 |
| ***68*** | >20 | >20 | >20 | >20 | >20 |
| ***74*** | 4.29 ± 1.56 | 2.53 ± 0.05 | 2.16 ± 0.45 | 18.05 ± 12.97 | 15.15 ± 12.97 |
| ***77*** | >100 | >100 | >100 | >100 | >100 |
| ***81*** | >4 | >4 | >4 | >4 | >4 |

[a] Effective concentration required to reduce virus plaque formation by 50%. Virus input was 100 CCID50.

The antiviral activity of derivative **51**, evidenced by the enzymatic assay conducted on Mpro, was also confirmed by cellular experiments, where derivative **51** showed excellent antiviral activity on all the virus variants considered. However, derivatives

**48**, **66**, **50** and **52**, which have previously shown no inhibitory activity against Mpro, also appear to possess considerable antiviral activity in cellular assays, with negligible cytotoxicity. For this reason, further investigations are still underway to assess their direct interference with further targets.

**Table 6.** *Evaluation of cytotoxicity on mock-infected lines.*

| ***Compounds*** | ***Cytotoxicity Cell morphology (MCC)[b] (μM)*** | ***Cytostaticity Cell growth ($CC_{50}$)[c] (μM)*** |
|---|---|---|
| ***Remdesivir*** | >40 | >40 |
| ***Molnupiravir*** | >100 | >40 |
| ***29*** | >40 | >40 |
| ***48*** | >40 | >40 |
| ***49*** | 100 | ND |
| ***50*** | 100 | >40 |
| ***51*** | >20 | >20 |
| ***52*** | 100 | >40 |
| ***53*** | >100 | >100 |
| ***54*** | 100 | >40 |
| ***55*** | 100 | >40 |
| ***57*** | >20 | ND |
| ***60*** | 100 | >40 |
| ***63*** | >100 | >100 |
| ***66*** | 20 | 13.77 ± 9.34 |
| ***68*** | 20 | ND |
| ***74*** | >100 | >100 |
| ***77*** | 100 | ND |
| ***81*** | 20 | 12.34 ± 7.97 |

[b] Minimum cytotoxic concentration that causes a microscopically detectable alteration of cell morphology.
[c] Cytostatic concentration required to reduce cell growth by 50%.

## 3.1. Conclusions

Given the pandemic emergency caused by COVID-19 and the need to identify new pharmacological approaches, part of my PhD project focused on design, synthesis and pharmacological evaluation of novel indole scaffold peptidomimetic derivatives

designed as potential inhibitors of Mpro. Specifically, this chapter described a step-by-step *in silico* design of a small library of compounds as main protease (Mpro) inhibitors. All the synthesized derivatives of series I were screened by an enzymatic assay on Mpro and, then, cellular activity was evaluated using Vero cells viral infection model. The cellular screening disclosed compounds **29** and **34** as *in vitro* SARS-CoV-2 replication inhibitors at non-toxic concentrations ($0.32 < EC_{50} < 5.98$ μM). To rationalize these results, additional *in vitro* assays were performed, focusing on Papain like protease (PLpro) and spike protein (SP) as potential targets for the synthesized molecules. This workflow led to the identification of compound **29**, as a dual inhibitor of the two proteases of SARS-CoV-2, with micromolar inhibitory potency against Mpro ($IC_{50} = 1.72$ μM) and submicromolar inhibitory potency against PLpro ($IC_{50} = 0.67$ μM), guiding the rational design of a second series of analogues: the novel molecules retained the central peptidomimetic scaffold of the first series most potent compound **29** and the electrophilic moieties required for covalent interaction with the main protease. *In vitro* assays revealed the high potency of derivative **51**, which showed good antiviral activity against all virus variants considered as well as significantly higher inhibitory activity against Mpro ($IC_{50} = 0.73 \pm 0.32$ μM) than the reference compound **29**. Further assays are still being conducted to evaluate the interaction with other SARS-CoV-2 targets.

### 4.1. Experimental section

All reagents and solvents used were purchased from Sigma-Aldrich (Milan, Italy). Reactions were performed under magnetic stirring in round-bottomed flasks unless otherwise noted. Moisture sensitive reactions were conducted in oven-dried glassware

under nitrogen stream, using distilled solvents. Purifications were conducted on the Biotage Isolera One flash purification system, using prepacked KP-sil columns, (Biotage, Uppsala, Sweden). TLC analyses were performed on precoated glass silica gel plates 60 (F254, 0.25 mm, VWR International). 1D-NMR spectra were recorded with Bruker Avance (400 MHz) spectrometer, at room temperature. Chemical shifts were reported in δ values (ppm) relative to internal $Me_4Si$ for 1H and 13C NMR. J values were reported in hertz (Hz). The following abbreviations are used to describe peaks: s (singlet), d (doublet), dd (doublet of doublets), t (triplet), q (quartet), and m (multiplet). HR-MS experiments were performed using an LTQ-Orbitrap-XL-ETD mass spectrometer (Thermo Scientific, Bremen, Germany), using electrospray ionization. Elemental analysis was carried on using a Perkin Elmer 2400 Series II CHNS/O analyzer. Results obtained were within ±0.4% of theoretical values.

**General Procedure A**: **Coupling Reactions**.

1 mmol of various N-*L*-Boc aminoacids was dissolved in dichloromethane and HOBt (1.2 eq), HBTU (1.2 eq), DIPEA (2.4 eq) and the corresponding amine (1.2 eq) were added and stirred at room temperature for 12 hours. Then, the solvent was evaporated in vacuum, and the residue was dissolved in dichloromethane and washed with water (3 x 200 mL), a saturated solution of $NaHCO_3$ (3 x 200 mL), and a solution of citric acid (10% w:w, 3 x 200 mL). The organic phase was extracted, dried over $Na_2SO_4$, filtered, and concentrated under vacuum. The crude products were purified by flash chromatography using mixtures of n-hexane/ethyl acetate as mobile phase.

**General Procedure B: Boc Removal**.

The N-Boc protected intermediate (0.2 mmol) was dissolved in a mixture of TFA/DCM (1/3, v/v), and added with triisopropylsilane (0.25 eq). Reaction was stirred

at room temperature for 2h. Then, a solution of NaOH (2 N) was added until pH 7. The mixture was diluted with water and dichloromethane, and the organic phase was extracted, dried over $Na_2SO_4$, filtered, and concentrated under vacuum. The intermediates obtained were not further purified.

**General Procedure C: Reductive amination**.

The proper intermediate (1 mmol) was dissolved in MeOH dry and 1.2 equivalents of the proper aldehyde was added. The mixture was allowed to react for 12h under nitrogen stream, at room temperature. Then, 3 equivalents of $NaBH_4$ were added portion wise and the mixture was stirred for further 3h. The reaction was quenched by 10% aqueous solution of citric acid, the solvent was evaporated in vacuum, and the residue was dissolved in dichloromethane and washed with water (3 x 200 mL). Organic layer was separated, dried over anhydrous $Na_2SO_4$, filtered, and evaporated in vacuo. The crude products were purified by column chromatography using mixtures of ethyl acetate/n-hexane as eluent.

**General Procedure D: N-alkylation**.

Methyl indole-5-carboxylate (1.0 mmol) was dissolved in anhydrous DMF under magnetic stirring at 0 °C. To this solution, 1.5 equivalents of NaH and 1.5 equivalents of iodomethane or 1-iodo-2-methylpropane in DMF were added dropwise and the reaction was warmed to room temperature and maintained under stirring overnight. The reaction was quenched by 10% aqueous solution of citric acid and washed with brine. Organic layer was separated, dried over anhydrous $Na_2SO_4$, filtered, and evaporated in vacuo. Crude products were purified by column chromatography.

**General Procedure E: Mannich reaction**.

A solution of formaldehyde (2.0 eq), trifluoroacetic acid (2.0 eq) and amine (2.0 eq) in dichloromethane was stirred at room temperature for 30 min. Then, a solution of the proper 1,5-disubstituted indole (1 mmol) in dichloromethane was added and the mixture was stirred for 12h. The reaction was quenched by 10% aqueous solution of sodium bicarbonate and washed with brine, dried over anhydrous $Na_2SO_4$ and filtered. Organic phase was evaporated in vacuum and 3-aminomethyl indole derivatives were obtained after purification by flash chromatography.

**General Procedure F: Acylation reaction.**

The proper intermediate (0.1 mmol) was dissolved in dichloromethane and added with 1.2 eq of TEA and 1.2 eq of chloroacetyl chloride or di-tert-butyl dicarbonate. The reaction mixtures were stirred at room temperature for 1 hour. After the completion of the reaction, monitored by TLC, the organic phases were washed with a saturated solution of $NaHCO_3$ (3 x 100 mL) and a solution of citric acid (10% w:w, 3 x 100 mL). The organic layers were extracted, dried over $Na_2SO_4$, filtered, and concentrated under vacuum. The crude mixtures were purified by flash chromatography using ethyl acetate/methanol as eluent.

**General procedure G: Hydrolysis.**

1.0 mmol of proper intermediate was dissolved in a solution of MeOH and NaOH 2M and stirred at reflux for 3 hours. The reaction was quenched by a 2M aqueous solution of HCl, and the mixture was extracted three times with ethyl acetate (3 x 50 mL), dried over sodium sulfate, and concentrated under vacuum. The obtained intermediates were used in the next step without further purification.

**General procedure H: Cbz removal.**

Removal of Cbz protecting group was achieved by continuous flow hydrogenation using the H-Cube hydrogenator and commercially available Pd/C 10% cartridges as catalyst. The proper intermediate was dissolved in a mixture of THF/$CH_3OH$ (1:1, v:v) at a final concentration of 0.1M and was pumped at a flow rate of 1.0 mL/min. Temperature was set at 30 °C, while the hydrogen inlet pressure was set at 10 bar. After completion, the reaction mixture was evaporated under vacuum and the obtained products used in the following step without further purification.

**General procedure I: Fmoc removal.**

The proper intermediate was dissolved in a mixture of dichloromethane/diethylamine (3:1 v:v) and stirred at room temperature for 3 hours. The organic mixture was added with a saturated solution of $NaHCO_3$, diluted with ethyl acetate, extracted, dried over sodium sulfate and concentrated under vacuum. The obtained reaction mixture was treated with n-hexane to precipitate the desired compound as a white powder, without further purification step.

***tert-butyl (1-(tert-butylamino)-3-(1H-indol-3-yl)-1-oxopropan-2-yl)carbamate (1)***

Synthesized according to the general procedure **A**, using Boc-*L*-Trp-OH and *tert*-butylamine as starting materials, FC in n-hexane/ethyl acetate 3/1, Rf = 0.35. Yellowish oil (65% yield). $^1$H NMR (400 MHz, $CDCl_3$): δ: 1.14 (s, 9H, C$H_3$); 1.46 (s, 9H, C$H_3$); 3.07-3.12 (m, 1H, C$H_{2a}$); 3.30-3.35 (m, 1H, C$H_{2b}$); 4.36 (bs, 1H, C*H*); 5.37 (bs, 1H, N*H*); 7.06 (s, 1H aryl); 7.15 (t, 1H, aryl, *J* = 7.2 Hz); 7.22 (t, 1H, aryl, *J* = 7.4

Hz); 7.39 (d, 1H, aryl, *J* = 8.2 Hz); 7.72 (d, 1H, aryl, *J* = 6.8 Hz); 8.43 (bs, 1H, N*H*). HR-MS m/z calcd for $C_{20}H_{30}N_3O_3$ $[(M + H)]^+$: 360.2282; found 360.2277.

***(S)-tert-butyl (1-(([1,1'-biphenyl]-4-ylmethyl)amino)-3-(1H-indol-3-yl)-1-oxopropan-2-yl)carbamate (2)***

Intermediate **2** was obtained according to the general procedure **A**, starting from Boc-*L*-Trp-OH and 4-phenyl benzylamine, FC in n-hexane/ethyl acetate 3/1, Rf = 0.4. Yellowish oil (82% yield). $^1$H NMR (400 MHz, $CDCl_3$): δ: 1.44 (s, 9H, C$H_3$); 3.22 (dd, 1H, C$H_{2a}$, *J'*= 7.7, *J''*= 14.4 Hz); 3.38 (dd, 1H, C$H_{2b}$, *J'*= 5.3, *J''*= 14.4 Hz); 4.30-4.36 (m, 2H, C$H_2$); 4.49 (bs, 1H, C*H*); 5.20 (bs, 1H, N*H*); 6.05 (bs, 1H, N*H*); 7.02 (s, 1H aryl); 7.17 (d, 1H, aryl, *J* = 7.6 Hz); 7.19 (t, 1H, aryl, *J* = 7.8 Hz); 7.24 (t, 1H, aryl, *J* = 7.8 Hz); 7.35-7.40 (m, 2H, aryl); 7.44-7.48 (m, 5H, aryl); 7.56 (d, 2H, aryl, *J* = 8.5 Hz); 7.71 (d, 1H, aryl, *J* = 7.8 Hz); 8.07 (bs, 1H, N*H*). HR-MS m/z calcd for $C_{29}H_{32}N_3O_3$ $[(M + H)]^+$: 470.2438; found 470.2445.

***(S)-tert-butyl (1-(benzylamino)-3-(1H-indol-3-yl)-1-oxopropan-2-yl)carbamate (3)***

Synthesized according to the general procedure A, starting from Boc-*L*-Trp-OH and benzylamine.

FC in n-hexane/ethyl acetate 3/1, Rf = 0.4. Yellowish oil (80% yield). $^1$H NMR (400 MHz, $CD_3OD$): δ: 1.40 (s, 9H, C$H_3$); 3.10 (dd, 1H, C$H_{2a}$, *J'*= 6.6, *J''* = 13.8 Hz); 3.25 (dd, 1H, C$H_{2b}$, *J'*= 6.9, *J''* = 14.4 Hz); 4.19-4.23 (m, 1H, C*H*); 4.34-4.41 (m, 2H, C$H_2$); 7.02-7.06 (m ,5H, aryl); 7.12 (t, 1H, aryl, *J* = 7.1 Hz); 7.20-7.25 (m, 2H, aryl); 7.37 (d, 1H, aryl, *J* = 8.1 Hz); 7.62 (d, 1H, aryl, *J* = 7.8 Hz). HR-MS m/z calcd for $C_{23}H_{28}N_3O_3$ $[(M + H)]^+$: 394.2125; found 394.2114.

***tert-butyl (1-(tert-butylamino)-3-(1H-indol-3-yl)-1-oxopropan-2-yl)carbamate (4)***

Intermediate **4** was synthesized according to the general procedure **B**, starting from **1**. White powder (90% yield). $^1$H NMR (400 MHz, $CDCl_3$): δ: 1.22 (s, 9H, C$H_3$); 3.10 (dd, 1H, C$H_{2a}$ *J'*= 7.8, *J''*= 14.5 Hz); 3.30 (dd, 1H, C$H_{2b}$ *J'*= 5.9, *J''*= 14.5 Hz); 3.86 (t, 1H, C*H*, *J* = 6.7 Hz); 5.09 (bs, 2H, N$H_2$); 6.78 (s, 1H aryl); 7.10-7.17 (m, 2H, aryl); 7.36 (d, 1H, aryl, *J* = 8.1 Hz); 7.64 (d, 1H, aryl, *J* = 7.8 Hz); 8.92 (bs, 1H, N*H*). HR-MS m/z calcd for $C_{15}H_{22}N_3O$ $[(M + H)]^+$: 260.1757; found 260.1750.

***(S)-N-([1,1'-biphenyl]-4-ylmethyl)-2-amino-3-(1H-indol-3-yl)propanamide (5)***

Intermediate **5** was synthesized according to the general procedure **B**, starting from **2**. White powder (91% yield). $^1$H NMR (400 MHz, $CD_3OD$): δ: 3.27-3.35 (m, 1H, C$H_{2a}$); 3.42 (dd, 1H, C$H_{2b}$, *J'*= 7.6, *J''*= 14.4 Hz); 4.16 (t, 1H, CH, *J* = 7.4 Hz); 4.31 (d, 1H, C$H_{2a}$, *J* = 14.8 Hz); 4.40 (d, 1H, C$H_{2b}$, *J* = 14.8 Hz); 7.07-7.19 (m, 6H aryl); 7.41-7.45 (m, 3H, aryl); 7.50 (d, 2H, aryl, *J* = 8.2 Hz); 7.58 (d, 2H, aryl, *J* = 7.2 Hz); 7.66 (d, 1H, aryl, *J* = 7.9 Hz). HR-MS m/z calcd for $C_{24}H_{24}N_3O$ $[(M + H)]^+$: 370.1914; found 370.1907.

***(S)-2-amino-N-benzyl-3-(1H-indol-3-yl)propanamide (6)***

Intermediate **6** was synthesized according to the general procedure **B**, starting from **3**. White powder (95% yield). 1H NMR (400 MHz, $CD_3OD$): δ: 3.05 (dd, 1H, C$H_{2a}$, *J'*= 5.8, *J''*= 10.4 Hz); 3.20 (dd, 1H, C$H_{2b}$, *J'*= 6.0, *J''*= 10.4 Hz ); 3.69 (t, 1H, C*H*, J = 5.2 Hz); 4.25 (d, 1H, C$H_{2a}$, J = 12.6 Hz); 4.35 (d, 1H, C$H_{2b,}$ J = 12.6 Hz); 7.02-7.07 (m, 5H, aryl); 7.12 (t, 1H, aryl, *J* = 7.2 Hz); 7.20-7.26 (m, 2H, aryl); 7.39 (d, 1H, aryl,

*J* = 8.2 Hz); 7.64 (d, 1H, aryl, *J* = 8.0 Hz). HR-MS m/z calcd for $C_{18}H_{20}N_3O$ [(M + H)]$^+$: 294.1601; found 294.1610.

***tert-butyl 2-((1-(tert-butylamino)-3-(1H-indol-3-yl)-1-oxopropan-2-yl)carbamoyl)pyrrolidine-1-carboxylate (7)***

Final product **7** was synthesized starting from **1** and *L*-Boc-Pro-OH, following the procedure **A**. FC dichloromethane/methanol 4.8/0.2, Rf = 0.40. Yellow oil (59% yield). (**A**) $^1$H NMR (400 MHz, $CD_3OD$): δ: 1.27 (s, 9H, C*H*$_3$); 1.29 (s, 9H, C*H*$_3$); 1.64-1.89 (m, 2H, C*H*$_2$); 2.11-2.20 (m, 2H, C*H*$_2$); 3.03-3.39 (m, 4H, C*H*$_2$); 4.08-4.10 (m, 1H, C*H*); 4.54-4.57 (m, 1H, C*H*); 7.05-7.17 (m, 3H, aryl); 7.33-7.40 (m, 1H, aryl); 7.60-7.69 (m, 1H, aryl). (**B**) $^1$H NMR (400 MHz, $CD_3OD$): δ: 1.21 (s, 9H, C*H*$_3$); 1.34 (s, 9H, C*H*$_3$); 1.64-1.89 (m, 4H, C*H*$_2$); 3.03-3.39 (m, 4H, C*H*$_2$); 4.14-4.16 (m, 1H, C*H*); 4.63-4.65 (m, 1H, C*H*); 7.05-7.17 (m, 3H, aryl); 7.33-7.40 (m, 1H, aryl); 7.60-7.69 (m, 1H, aryl).$^{13}$C NMR (100 MHz, $CD_3OD$) δ 22.3, 23.0, 23.9, 26.2, 27.1, 27.4, 28.0, 29.5, 29.7, 30.9, 54.4, 60.4, 60.7, 80.1, 108.4, 109.4, 110.8, 111.2, 117.7, 118.1, 118.4, 118.8, 121.1, 121.3, 123.3, 123.5, 124.7, 127.6, 136.6, 154.6, 155.2, 171.3, 173.2, 173.8. HR-MS m/z calcd for $C_{25}H_{37}N_4O_4$ [(M + H)]$^+$: 457.2809; found 457.2801.

***tert-butyl (1-((1-(tert-butylamino)-3-(1H-indol-3-yl)-1-oxopropan-2-yl)amino)-1-oxo-3-phenylpropan-2-yl)carbamate (8)***

Obtained from **4** and *L*-Boc-Phe-OH following the general procedure **A**. FC in n-hexane/ethyl acetate 3/1, Rf = 0.44. Yellowish oil (78% yield). $^1$H NMR (400 MHz, DMSO): δ: 1.18 (s, 9H, C*H*$_3$); 1.29 (s, 9H, C*H*$_3$); 2.67-2.73 (m, 1H, C*H*$_{2a}$); 2.89 (dd, 1H, C*H*$_{2b}$ *J'*= 4.2, *J''*= 13.8 Hz); 2.95-3.07 (m, 2H, C*H*$_2$); 4.08-4.13 (m, 1H, C*H*); 4.48-4.53 (m, 1H, C*H*); 6.92-6.99 (m, 2H aryl); 7.06 (t, 1H, aryl, *J* = 7.9 Hz); 7.14-7.26 (m, 3H, aryl); 7.31 (d, 1H, aryl, *J* = 8.0 Hz); 7.43 (s, 1H, aryl); 7.58 (d, 1H, aryl, *J* = 8.0

Hz); 7.80 (d, 1H, aryl, *J* = 7.8 Hz); 10.81 (bs, 1H, N*H*). HR-MS m/z calcd for $C_{29}H_{39}N_4O_4$ $[(M + H)]^+$: 507.2966; found 507.2974.

***tert-butyl (1-((1-(tert-butylamino)-3-(1H-indol-3-yl)-1-oxopropan-2-yl)amino)-4-methyl-1-oxopentan-2-yl)carbamate (9)***

Obtained from **4** and *L*-Boc-Leu-OH following the general procedure **A**. FC in n-hexane/ethyl acetate 2/1, Rf = 0.35. Yellowish oil (74% yield). $^1$H NMR (400 MHz, $CDCl_3$): δ: 0.92-0.95 (m, 6H, C$H_3$); 1.17 (s, 9H, C$H_3$); 1.35 (s, 9H, C$H_3$); 1.64-1.67 (m, 1H, C*H*); 1.79-1.87 (m, 2H, C$H_2$); 3.08 (dd, 1H, C$H_{2a}$ *J'*= 8.0, *J''*= 14.4 Hz); 3.39-3.44 (m, 1H, C$H_{2b}$); 4.03-4.07 (m, 1H, C*H*); 4.63 (q, 1H, C*H*, *J* = 7.9 Hz); 4.71 (d, 1H, N*H*, *J* = 6.9 Hz); 5.62 (bs, 1H, N*H*); 7.09 (s, 1H, aryl); 7.17 (t, 1H, aryl, *J* = 7.6 Hz); 7.23 (d, 1H, aryl, *J* = 7.4 Hz); 7.39 (d, 1H, aryl, *J* = 8.0 Hz); 7.73 (d, 1H, aryl, *J* = 7.6 Hz); 8.22 (bs, 1H, N*H*). HR-MS m/z calcd for $C_{26}H_{41}N_4O_4$ $[(M + H)]^+$: 473.3122; found 473.3109.

***tert-butyl ((S)-1-(((S)-1-(tert-butylamino)-3-(1H-indol-3-yl)-1-oxopropan-2-yl)amino)-1-oxopent-4-yn-2-yl)carbamate (10)***

Compound **10** was obtained using general procedure **A**, starting from intermediate **4** which was reacted with N-Boc-*L*-propargylglycine. FC in n-hexane/ethyl acetate 2/1, Rf = 0.36. Yellowish oil (80% yield). $^1$H NMR (400 MHz, $CDCl_3$): δ: 1.18 (s, 9H, C$H_3$); 1.36 (s, 9H, C$H_3$); 2.08 (s, 1H, C*H*); 2.56-2.62 (m, 1H, C$H_{2a}$); 2.81-2.85 (m, 1H, C$H_{2b}$); 3.08 (dd, 1H, C$H_{2a}$ *J'*= 7.8, *J''*= 14.4 Hz); 3.46-3.51 (m, 1H, C$H_{2b}$); 4.22-4.24 (m, 1H, C*H*); 4.63-4.69 (m, 1H, C*H*); 5.24 (d, 1H, N*H*, *J* = 4.8 Hz); 5.62 (bs, 1H, N*H*); 7.09 (s, 1H, aryl); 7.16 (t, 1H, aryl, *J* = 7.9 Hz); 7.23 (t, 1H, aryl, *J* = 7.8 Hz); 7.39 (d, 1H, aryl, *J* = 8.0 Hz); 7.75 (d, 1H, aryl, *J* = 7.7 Hz); 8.43 (bs, 1H, N*H*). HR-MS m/z calcd for $C_{25}H_{35}N_4O_4$ $[(M + H)]^+$: 455.2653; found 455.2660.

***tert-butyl ((S)-1-(((S)-1-(([1,1'-biphenyl]-4-ylmethyl)amino)-3-(1H-indol-3-yl)-1-oxopropan-2-yl)amino)-1-oxopent-4-en-2-yl)carbamate (11)***

Obtained from **5** and Boc-*L*-allyl-Gly-OH following the general procedure **A**. FC in hexane/ethyl acetate 3/1, Rf = 0.45. White powder (75% yield). $^1$H NMR (400 MHz, $CD_3OD$): δ: 1.36 (s, 9H, C$H_3$); 2.21-2.26 (m, 1H, C$H_{2a}$); 2.28-2.36 (m, 1H, C$H_{2b}$); 3.02 (dd, 1H, C$H_{2a}$, *J'*= 7.4, *J''*= 14.4 Hz ); 3.14 (dd, 1H, C$H_{2b}$, *J'*= 6.5, *J''*= 14.4 Hz); 3.96-4.02 (m, 1H, C*H*); 4.21-4.32 (m, 2H, C$H_2$); 4.62 (q, 1H, C*H*, *J* = 7.2 Hz); 4.96-5.04 (m, 2H, C$H_2$); 5.61-5.73 (m, 1H, C*H*); 6.87 (d, 1H, aryl, *J* = 8.1 Hz); 6.99 (t, 1H, aryl, *J* = 7.5 Hz); 7.07 (t, 1H, aryl, *J* = 7.8 Hz); 7.13-7.15 (m, 1H aryl); 7.34-7.38 (m, 2H, aryl); 7.46 (t, 2H, aryl, *J* = 7.5 Hz); 7.52 (d, 2H, aryl, *J* = 8.2 Hz); 7.59-7.64 (m, 2H, aryl); 7.93 (d, 1H, aryl, *J* = 8.0 Hz); 8.43 (t, 1H, aryl, *J* = 5.6 Hz); 10.9 (s, 1H, N*H*). HR-MS m/z calcd for $C_{34}H_{39}N_4O_4$ $[(M + H)]^+$: 567.2966; found 567.2958.

***tert-butyl ((S)-1-(((S)-1-(([1,1'-biphenyl]-4-ylmethyl)amino)-3-(1H-indol-3-yl)-1-oxopropan-2-yl)amino)-1-oxopent-4-yn-2-yl)carbamate (12)***

Compound **12** was synthesized in 82% yield starting from intermediate **5** and Boc-*L*-Pra-OH following the general procedure **A**. FC in n-hexane/ ethyl acetate 3/1, Rf = 0.45. White powder. $^1$H NMR (400 MHz, $CD_3OD$): δ: 1.32 (s, 9H, C$H_3$); 2.35 (s, 1H, C*H*); 2.54-2.65 (m, 2H, C$H_2$); 3.27-3.37 (m, 2H, C$H_2$); 4.15 (t, 1H, C*H*, *J* = 6.2 Hz); 4.25-4.37 (m, 2H, C$H_2$); 4.73 (t, 1H, C*H*, *J* = 6.0 Hz); 7.04-7.15 (m, 4H, aryl); 7.33 (t, 1H, aryl, *J* = 7.4 Hz); 7.37-7.47 (m, 6H, aryl); 7.58 (d, 2H, aryl, *J* = 9.2 Hz); 7.65 (d, 1H, aryl, *J* = 7.6 Hz). HR-MS m/z calcd for $C_{34}H_{37}N_4O_4$ $[(M + H)]^+$: 565.2809; found 565.2815.

***tert-butyl ((S)-1-(((S)-1-(benzylamino)-3-(1H-indol-3-yl)-1-oxopropan-2-yl)amino)-1-oxopent-4-en-2-yl)carbamate (13)***

Obtained using general procedure **A** from **6** and Boc-*L*-allyl-Gly-OH. FC in hexane/ethyl acetate 2/1, Rf = 0.40. White powder (78% yield). $^1$H NMR (400 MHz, $CD_3OD$): δ: 1.27 (s, 9H, C$H_3$); 2.25-2.34 (m, 1H, C$H_{2a}$); 2.44-2.48 (m, 1H, C$H_{2b}$); 3.28 (d, 2H, C*H*, *J* = 4.6 Hz); 4.02 (t, 1H, C*H*, *J* = 5.2 Hz ); 4.21-4.26 (m, 1H, C$H_{2a}$); 4.32 (dd, 1H, C$H_{2b}$, *J'* = 3.4, *J''*= 11.9 Hz); 4.70 (t, 1H, C*H*, *J* = 4.5 Hz); 5.04-5.11 (m, 2H, C$H_2$); 5.67-5.75 (m, 1H, C*H*); 7.03-7.10 (m, 5H, aryl); 7.14 (t, 1H, aryl, *J* = 5.6 Hz); 7.20-7.25 (m, 2H, aryl); 7.38 (d, 1H, aryl, *J* = 6.5 Hz); 7.63 (d, 1H, aryl, *J* = 6.2 Hz). HR-MS m/z calcd for $C_{28}H_{35}N_4O_4$ $[(M + H)]^+$: 491.2653; found 491.2661.

***tert-butyl ((S)-1-(((S)-1-(benzylamino)-3-(1H-indol-3-yl)-1-oxopropan-2-yl)amino)-4-methyl-1-oxopentan-2-yl)carbamate (14)***

The intermediate **14** was obtained using *L*-Boc-Leu-OH and **6** as starting material, following general procedure **A**. FC in hexane/ethyl acetate 2/1, Rf = 0.45. White powder (77% yield). $^1$H NMR (400 MHz, DMSO): δ: 0.79 (d, 3H, C$H_3$, *J* = 6.4 Hz); 0.83 (d, 3H, C$H_3$, *J* = 6.5 Hz); 1.24-1.35 (m, 12H, C*H*, C$H_2$, C$H_3$); 3.01-3.15 (m, 2H, C$H_2$); 3.90-3.96 (m, 1H, C*H*); 4.22 (d, 2H, C$H_2$, *J* = 5.6 Hz); 4.59 (q, 1H, CH, *J* = 6.9 Hz ); 6.97 (t, 1H, aryl, *J* = 6.9 Hz); 7.04-7.11 (m, 3H, aryl); 7.18-7.25 (m, 3H, aryl); 7.33 (d, 1H, aryl, *J* = 8.0 Hz); 7.57 (d, 1H, aryl, *J* = 7.7 Hz); 7.81 (d, 1H, aryl, *J* = 8.0 Hz); 8.40 (t, 1H, N*H*, *J* = 5.1 Hz); 10.82 (s, 1H, N*H*). HR-MS m/z calcd for $C_{29}H_{38}N_4O_4$ $[(M + H)]^+$: 506.2888; found 506.2899.

***2-amino-N-(1-(tert-butylamino)-3-(1H-indol-3-yl)-1-oxopropan-2-yl)-3-phenylpropanamide (15)***

Intermediate **15** was synthesized according to the general procedure **B**, starting from **8**. White powder (95% yield). FC in hexane/ethyl acetate 7/3, Rf: 0.47. Yellow oil (55% yield). $^1$H NMR (400 MHz, $CDCl_3$): δ: 1.17 (s, 9H, C$H_3$); 2.71 (dd, 1H, C$H_{2a}$

*J'*= 8.3, *J''*= 13.6 Hz); 3.06 (dd, 1*H*, C$H_{2b}$ *J'*= 8.0, *J''*= 14.5 Hz); 3.13 (dd, 1H, C$H_{2a}$ *J'*= 4.9, *J''*= 13.8 Hz); 3.23 (dd, 1H, C$H_{2b}$, *J'*= 6.5, *J''*= 14.6 Hz); 3.73 (t, 1H, C*H*, *J* = 5.3 Hz ); 4.62 (q, 1H, C*H*, *J* = 7.6 Hz); 5.63 (bs, 1H, N*H*); 7.05 (s, 1H, aryl); 7.11-7.30 (m, 6H, aryl); 7.35 (d, 1H, aryl, *J* = 8.0 Hz); 7.68 (d, 1H, aryl, *J* = 8.0 Hz); 7.88 (d, 1H, aryl, *J* = 7.1 Hz); 8.29 (bs, 1H, N*H*). HR-MS m/z calcd for $C_{24}H_{31}N_4O_2$ $[(M + H)]^+$: 407.2442; found 407.2451.

***2-amino-N-(1-(tert-butylamino)-3-(1H-indol-3-yl)-1-oxopropan-2-yl)-4-methylpentanamide (16)***

Intermediate **16** was synthesized according to the general procedure **B**, starting from **9**. White powder (94% yield). $^1$H NMR (400 MHz, $CD_3OD$): δ: 0.91 (d, 3H, C$H_3$, *J* = 6.5 Hz); 0.94 (d, 3H, C$H_3$, *J* = 6.5 Hz); 1.39-1.48 (m, 1H, C$H_{2a}$); 1.54-1.61 (m, 1H, C$H_{2b}$); 1.65-1.71 (m, 1H, C*H*); 3.24 (dd, 1H, C$H_{2a}$ *J'*= 7.8, *J''*= 14.7 Hz); 3.34 (dd, 1H, C$H_{2b,}$ *J'*= 5.5, *J''*= 14.7 Hz); 3.56 (dd, 1H, C*H*, *J'*= 6.0, *J''*= 8.4 Hz); 7.03 (t, 1H, aryl, *J* = 7.9 Hz); 7.11 (t, 1H, aryl, *J* = 8.1 Hz); 7.13 (s, 1H, aryl); 7.37 (d, 1H, aryl, *J* = 8.1 Hz); 7.55 (d, 1H, aryl, *J* = 7.9 Hz). HR-MS m/z calcd for $C_{21}H_{33}N_4O_2$ $[(M + H)]^+$: 373.2598; found 373.2604.

***tert-butyl ((S)-1-(((S)-1-(tert-butylamino)-3-(1H-indol-3-yl)-1-oxopropan-2-yl)amino)-1-oxopent-4-yn-2-yl)carbamate (17)***

Intermediate **17** was synthesized according to the general procedure **B**, starting from **10**. White powder (92% yield). $^1$H NMR (400 MHz, $CDCl_3$): δ: 1.15 (s, 9H, C$H_3$); 1.96 (t, 1H, C*H*, *J* = 2.6 Hz); 2.47-2.54 (m, 1H, C$H_{2a}$); 2.62-2.68 (m, 1H, C$H_{2b}$); 3.12 (dd, 1H, C$H_{2a}$, *J'*= 8.3, *J''*= 14.4 Hz); 3.30 (dd, 1H, C$H_{2b}$ *J'*= 6.7, *J''*= 15.0 Hz); 3.49 (dd, 1H, C*H*, *J'*= 4.6, *J''*= 7.1 Hz); 4.63 (q, 1H, C*H*, *J* = 8.1 Hz ); 5.57 (bs, 1H, N*H*); 7.07 (s, 1H, aryl); 7.14 (t, 1H, aryl, *J* = 7.2 Hz); 7.21 (t, 1H, aryl, *J* = 7.0 Hz);

7.37 (d, 1H, aryl, *J* = 8.0 Hz); 7.74 (d, 1H, aryl, *J* = 7.8 Hz); 8.49 (bs, 1H, N*H*). HR-MS m/z calcd for $C_{20}H_{27}N_4O_2$ $[(M + H)]^+$: 355.2129; found 355.2136.

***(S)-N-((S)-1-(([1,1'-biphenyl]-4-ylmethyl)amino)-3-(1H-indol-3-yl)-1-oxopropan-2-yl)-2-aminopent-4-enamide (18)***

Intermediate **18** was synthesized according to the general procedure **B**, starting from **11**. White powder (89% yield). $^1$H NMR (400 MHz, $CD_3OD$): δ: 1.95-2.03 (m, 1H, C$H_{2a}$); 2.33-2.38 (m, 1H, C$H_{2b}$); 3.18-3.21 (m, 1H, C*H*); 3.26-3.35 (m, 2H, C$H_2$); 4.28-4.40 (m, 2H, C$H_2$); 4.93-5.04 (m, 3H, C$H_2$ and C*H*); 5.45-5.55 (m, 1H, C*H*); 6.94 (s, 1H, aryl); 7.06-7.11 (m, 3H, aryl); 7.19 (t, 1H, aryl, *J* = 7.7 Hz); 7.34-7.39 (m, 3H, aryl); 7.43-7.47 (m, 4H aryl); 7.56 (d, 1H, aryl, *J* = 7.2 Hz); 7.68 (d, 1H, aryl, *J* = 8.0 Hz); 8.14 (d, 1H, N*H*, *J* = 8.2 Hz); 8.95 (s, 1H, N*H*). HR-MS m/z calcd for $C_{29}H_{31}N_4O_2$ $[(M + H)]^+$: 467.2442; found 467.2436.

***(S)-N-((S)-1-(([1,1'-biphenyl]-4-ylmethyl)amino)-3-(1H-indol-3-yl)-1-oxopropan-2-yl)-2-aminopent-4-ynamide (19)***

Intermediate **19** was synthesized according to the general procedure **B**, starting from **12**. White powder (95% yield). $^1$H NMR (400 MHz, $CD_3OD$): δ: 2.49 (s, 1H, C*H*); 2.66 (dd, 1H, C$H_{2a}$, *J'*= 7.2, *J''*= 14.8 Hz); 2.75 (dd, 1H, C$H_{2b}$, *J'*= 5.1, *J''*= 19.7 Hz); 3.21 (dd, 1H, C$H_{2a}$, *J'*= 6.9, *J''*= 14.4 Hz); 3.29-3.36 (m, 1H, C$H_{2b}$); 3.83 (t, 1H, C*H*, *J* = 5.4 Hz); 4.25 (d, 1H, C$H_{2a}$, *J* = 15.0 Hz); 4.37 (d, 1H, C$H_{2b}$, *J* = 15.0 Hz); 4.78 (t, 1H, C*H*, *J* = 7.3 Hz); 7.03-7.15 (m, 4H aryl); 7.35 (t, 1H, aryl, *J* = 7.6 Hz); 7.37-7.49 (m, 6H, aryl); 7.58 (d, 2H, aryl, *J* = 9.2 Hz); 7.66 (d, 1H, aryl, *J* = 7.6 Hz). HR-MS m/z calcd for $C_{29}H_{29}N_4O_2$ $[(M + H)]^+$: 465.2285; found 465.2292.

***(S)-2-amino-N-((S)-1-(benzylamino)-3-(1H-indol-3-yl)-1-oxopropan-2-yl)pent-4-enamide (20)***

Intermediate **20** was synthesized according to the general procedure **B**, starting from **13**. White powder (93% yield). $^1$H NMR (400 MHz, $CD_3OD$): δ: 2.55-2.61 (m, 1H, C$H_{2a}$); 2.65-2.69 (m, 1H, C$H_{2b}$); 3.19 (dd, 1H, C$H_{2a}$, *J'*= 5.5, *J''*= 11.3 Hz); 3.31 (dd, 1H, C$H_{2b}$, *J'*= 6.3, *J''*= 10.9 Hz); 3.95 (t, 1H, C*H*, *J* = 5.5 Hz ); 4.25 (dd, 1H, C$H_{2a}$, *J'* = 3.7, *J''*= 11.8 Hz); 4.31 (dd, 1H, C$H_{2b}$, *J'* = 4.4, *J''*= 12.0 Hz); 4.77 (t, 1H, C*H*, *J* = 6.0 Hz); 5.21-5.27 (m, 2H, C$H_2$); 5.72-5.80 (m, 1H, C*H*); 7.02-7.07 (m, 3H, aryl); 7.14 (t, 1H, aryl, *J* = 5.7 Hz); 7.21-7.26 (m, 4H, aryl); 7.39 (d, 1H, aryl, *J* = 6.4 Hz); 7.66 (d, 1H, aryl, *J* = 6.3 Hz). HR-MS m/z calcd for $C_{23}H_{27}N_4O_2$ $[(M + H)]^+$: 391.2129; found 391.2135.

***(S)-2-amino-N-((S)-1-(benzylamino)-3-(1H-indol-3-yl)-1-oxopropan-2-yl)-4-methylpentanamide (21)***

Intermediate **21** was synthesized according to the general procedure **B**, starting from **14**. White powder (95% yield). $^1$H NMR (400 MHz, $CD_3OD$): δ: 0.87 (d, 3H, C$H_3$, *J* = 6.6 Hz); 0.90 (d, 3H, C$H_3$, *J* = 6.5 Hz); 1.20-1.28 (m, 1H, C$H_{2a}$); 1.38-1.46 (m, 1H, C$H_{2b}$); 1.56-1.67 (m, 1H, C*H*); 3.27-3.37 (m, 3H, C*H* and C$H_2$); 4.25 (d, 1H, C$H_{2a}$, *J* = 15.0 Hz); 4.32 (d, 1H, C$H_{2b}$, *J* = 15.0 Hz); 4.72 (t, 1H, C*H*, *J* = 7.2 Hz); 7.01-7.13 (m, 6H, aryl); 7.20-7.26 (m, 2H, aryl); 7.36 (d, 1H, aryl, *J* = 8.1 Hz); 7.64 (d, 1H, aryl, *J* = 7.8 Hz). HR-MS m/z calcd for $C_{24}H_{31}N_4O_2$ $[(M + H)]^+$: 407.2442; found 407.2435.

***(S)-2-(([1,1'-biphenyl]-4-ylmethyl)amino)-N-((S)-1-(tert-butylamino)-3-(1H-indol-3-yl)-1-oxopropan-2-yl)-3-phenylpropanamide (22)***

Final product **22** was synthesized in 64% yield starting from **15** and 4-phenylbenzaldehyde, following the general procedure **C**. FC in hexane/ethyl acetate 1/1, Rf = 0.35. Yellowish powder. $^{1}$H NMR (400 MHz, $CDCl_3$): δ: 1.18 (s, 9H, C*H*$_3$); 2.61 (dd, 1H, C*H*$_{2a}$, *J'* = 9.3, *J''* = 13.8 Hz); 3.11-3.17 (m, 2H, C*H*$_{2b}$ and C*H*$_{2a}$); 3.34-3.44 (m, 3H, C*H*, C*H*$_{2b}$ and C*H*$_{2a}$); 3.53, (d, 1H, C*H*$_{2a}$, *J* = 13.4 Hz); 3.70 (d, 1H, C*H*$_{2b}$, *J* = 13.6 Hz); 4.69 (dd, 1H, C*H*, *J'* = 8.1, *J''* = 14.3 Hz); 5.59 (bs, 1H, N*H*); 7.06 (d, 3H, aryl, *J* = 8.1 Hz); 7.12-7.30 (m, 6H, aryl); 7.39 (t, 2H, aryl, *J* = 8.1 Hz); 7.44-7.48 (m, 4H, aryl); 7.58 (d, 2H, aryl, *J* = 8.4 Hz); 7.76 (d, 1H, aryl, *J* = 7.8 Hz); 8.07 (d, 1H, aryl, *J* = 5.8 Hz); 8.39 (bs, 1H, N*H*). $^{13}$C NMR (100 MHz, $CDCl_3$) δ 28.2,28.5, 39.0, 51.1, 52.1, 54.0, 63.0, 111.21, 111.28, 119.2, 119.8, 122.3, 123.2, 127.0, 127.3, 127.5, 128.5, 128.8, 1292, 136.3, 137.2, 138.1, 140.1, 140.9. HR-MS m/z calcd for $C_{37}H_{40}N_4O_2$ $[(M + H)]^+$: 573.3230; found 573.3238.

***2-(([1,1'-biphenyl]-4-ylmethyl)amino)-N-(1-(tert-butylamino)-3-(1H-indol-3-yl)-1-oxopropan-2-yl)-4-methylpentanamide (23)***

Obtained from **16** and 4-phenylbenzaldehyde following the general procedure **C**. FC in hexane/ethyl acetate 1/1, Rf = 0.35. Yellowish powder (56% yield). $^{1}$H NMR (400 MHz, $CDCl_3$): δ: 0.74 (d, 3H, C*H*$_3$, *J* = 6.4 Hz); 0.81 (d, 3H, C*H*$_3$, *J* = 6.4 Hz); 1.16-1.24 (m, 1H, C*H*); 1.40-1.45 (m, 1H, C*H*$_{2a}$); 1.47-1.56 (m, 1H, C*H*$_{2b}$); 3.07 (dd, 1H, C*H*$_{2a}$, J' = 8.0, J"= 14.4 Hz); 3.17-3.20 (m, 1H, C*H*); 3.24 (dd, 1H, C*H*$_{2b}$, *J'*= 6.5, *J''*= 14.5 Hz); 3.54 (d, 1H, C*H*$_{2a}$, J = 12.9 Hz); 4.59 (q, 1H, C*H*); 5.54 (bs, 1H, N*H*); 7.03 (s, 1H, aryl); 7.06 (t, 1H, aryl, *J* = 7.7 Hz); 7.13 (t, 1H, aryl, *J* = 7.2 Hz); 7.18-7.21 (m, 2H, aryl); 7.27 (d, 1H, aryl, J = 8.3 Hz); 7.35 (t, 2H, aryl, J = 7.5 Hz); 7.43-

7.49 (m, 4H, aryl); 7.69 (d, 1H, aryl, *J* = 7.7 Hz); 7.85 (d, 1H, aryl, *J* = 7.9 Hz); 8.06 (s, 1H, N*H*). $^{13}$C NMR (100 MHz, $CDCl_3$) δ 25.0, 28.2, 28.5, 29.7, 42.4, 51.2, 52.1, 54.0, 60.8, 111.2, 111.4, 119.2, 119.8, 122.3, 123.1, 127.1, 127.3, 128.8, 129.0, 136.3, 140.4, 140.8, 170.2. HR-MS m/z calcd for $C_{34}H_{43}N_4O_2$ $[(M + H)]^+$: 539.3381; found 539.3390.

***(S)-2-(([1,1'-biphenyl]-4-ylmethyl)amino)-N-((S)-1-(tert-butylamino)-3-(1H-indol-3-yl)-1-oxopropan-2-yl)pent-4-ynamide (24)***

Synthesized according to the general procedure **C**, starting from intermediate **17** and 4-phenylbenzaldehyde. FC in hexane/ethyl acetate 1/1, Rf = 0.30. White powder (57% yield). $^1$H NMR (400 MHz, $CDCl_3$): δ: 1.24 (s, 9H, C$H_3$); 2.32 (s, 1H, C*H*); 2.43-2.58 (m, 2H, C$H_2$); 3.17-3.26 (m, 2H, C$H_2$); 3.32-3.34 (m, 1H, C*H*); 3.55 (dd, 2H, C$H_2$, J'= 13.2, J"= 15.2 Hz); 4.69 (t, 1H, CH, *J* = 7.3 Hz); 7.03 (t, 1H, aryl, *J* = 7.9 Hz); 7.11 (t, 1H, aryl, *J* = 7.9 Hz); 7.14 (s, 1H, aryl); 7.23 (d, 2H, aryl, *J* = 8.2 Hz); 7.33 (d, 2H, aryl, *J* = 8.9 Hz); 7.42 (t, 2H, aryl, *J* = 7.4 Hz); 7.49 (d, 2H, aryl, *J* = 8.2 Hz); 7.58 (d, 2H, aryl, *J* = 7.2 Hz); 7.68 (d, 1H, aryl, *J* = 7.6 Hz). $^{13}$C NMR (100 MHz, $CDCl_3$) δ 21.7, 27.4, 28.0, 50.8, 54.2, 58.1, 59.6, 71.1, 79.2, 109.5, 110.9, 118.3, 121.1, 123.3, 126.5, 126.8, 127.5, 128.6, 136.7, 138.2, 139.9, 140.8, 171.3, 173.2. HR-MS m/z calcd for $C_{33}H_{37}N_4O_2$ $[(M + H)]^+$: 521.2911; found 521.2918.

***(S)-2-(([1,1'-biphenyl]-4-ylmethyl)amino)-N-((S)-1-(benzylamino)-3-(1H-indol-3-yl)-1-oxopropan-2-yl)-4-methylpentanamide (25)***

Synthesized according to the general procedure **C**, starting from intermediate **21** and 4-phenylbenzaldehyde. FC in hexane/ethyl acetate 1/1, Rf = 0.48. White powder (60% yield). $^1$H NMR (400 MHz, $CD_3OD$): δ: 0.78 (d, 3H, C$H_3$, *J* = 6.6 Hz); 0.88 (d, 3H, C$H_3$, *J* = 6.6 Hz); 1.28-1.40 (m, 2H, C$H_2$); 1.56-1.63 (m, 1H, C*H*); 3.13 (t, 1H,

C*H*, *J* = 6.8 Hz); 3.21 (dd, 1H, C$H_{2a}$, *J'* = 7.9, *J''*= 14.5 Hz); 3.28 (dd, 1H, C$H_{2b}$, *J'* = 6.6, *J''*= 14.6 Hz); 3.48 (dd, 2H, C$H_2$, *J'*= 13.1, *J''*= 25.1 Hz); 4.26 (d, 1H, C$H_{2a}$, *J* = 15.0 Hz); 4.36 (d, 1H, C$H_{2b}$, *J* = 15.0 Hz); 4.82 (t, 1H, C*H*, *J* = 7.8 Hz); 7.03-7.14 (m, 6H, aryl); 7.17-7.27 (m, 5H, aryl); 7.31-7.36 (m, 1H, aryl); 7.41-7.47 (m, 4H, aryl); 7.57 (d, 2H, aryl, *J* = 8.5 Hz); 7.67 (d, 1H, aryl, *J* = 7.8 Hz). $^{13}$C NMR (100 MHz, $CD_3OD$) δ 21.3, 21.9, 24.5, 27.9, 42.5, 42.7, 51.2, 53.7, 60.0, 109.4, 111.0, 118.2, 118.5, 121.1, 123.3, 126.5, 126.7, 126.84, 127.04, 128.1, 128.4, 128.7, 136.7, 138.1, 138.4, 139.8, 140.8, 172.4, 175.9. HR-MS m/z calcd for $C_{37}H_{40}N_4O_2$ $[(M + H)]^+$: 573.3224; found 573.3230.

***(S)-N-((S)-1-(([1,1'-biphenyl]-4-ylmethyl)amino)-3-(1H-indol-3-yl)-1-oxopropan-2-yl)-2-(benzylamino)pent-4-enamide (26)***

Final product **26** was synthesized as a yellow powder in 66% yield starting from **18** and benzaldehyde and following the general procedure **C**. FC in hexane/ethyl acetate 1/1, Rf = 0.45. $^1$H NMR (400 MHz, $CD_3OD$): δ: 2.19-2.31 (m, 2H, C$H_2$); 3.07 (dd, 1H, C$H_{2a}$, *J'*= 8.3, *J''*= 14.4 Hz); 3.18-3.23 (m, 4H, C$H_{2b}$, C$H_2$ and C*H*); 4.25 (q, 2H, C$H_2$, *J* = 15.0 Hz); 4.73-4.76 (m, 1H, C*H*); 4.88-4.94 (m, 2H, C$H_2$); 5.47-5.57 (m, 1H, C*H*); 6.93-7.02 (m, 7H aryl); 7.07 (d, 2H, aryl, *J* = 8.2 Hz); 7.14 (d, 2H, aryl, *J* = 2.8 Hz); 7.21 (t, 1H, aryl, *J* = 6.8 Hz); 7.30 (t, 2H, aryl, *J* = 7.4 Hz); 7.38 (d, 2H, aryl, *J* = 8.2 Hz); 7.45 (d, 2H, aryl, *J* = 7.2 Hz); 7.57(d, 1H, aryl, *J* = 7.6 Hz). $^{13}$C NMR (100 MHz, $CD_3OD$) δ 28.1, 36.4, 42.4, 50.9, 54.0, 60.2, 109.4, 111.1, 118.09, 118.20, 118.6, 121.2, 123.4, 126.49, 126.66, 126.91, 127.6, 128.23, 128.43, 128.7, 132.5, 136.7, 137.2, 140.0, 140.7, 172.1. HR-MS m/z calcd for $C_{36}H_{37}N_4O_2$ $[(M + H)]^+$: 557.2911; found 557.2918.

***(S)-N-((S)-1-(([1,1'-biphenyl]-4-ylmethyl)amino)-3-(1H-indol-3-yl)-1-oxopropan-2-yl)-2-(benzylamino)pent-4-ynamide (27)***

Final product **27** was synthesized in 68% yield starting from **19** and benzaldehyde, following the general procedure **C**. FC in hexane/ethyl acetate 1/1, Rf = 0.40. White powder (55% yield). $^{1}$H NMR (400 MHz, $CD_3OD$): δ: 2.54 (s, 1H, C*H*); 2.79 (dd, 2H, C$H_2$, *J'*= 2.7, *J''*= 6.5 Hz); 3.17 (dd, 1H, C$H_{2a}$, *J'*= 9.4, *J''*= 14.5 Hz); 3.38 (dd, 1H, C$H_{2b}$, *J'*= 6.2, *J''*= 14.8 Hz); 3.43 (d, 1H, C$H_{2a}$, *J* = 13.0 Hz); 3.63 (d, 1H, C$H_{2b}$, *J* = 13.0 Hz); 3.83 (t, 1H, C*H*, *J* = 6.5 Hz); 4.42 (q, 2H, C$H_2$, *J* = 15.0 Hz); 5.01 (dd, 1H, C*H, J'*= 6.0, *J''*= 9.4 Hz); 7.06-7.09 (m, 2H aryl); 7.13 (d, 2H, aryl, *J* = 7.0 Hz); 7.19 (s, 1H, aryl); 7.23-7.26 (m, 3H, aryl); 7.38-7.46 (m, 6H, aryl); 7.55 (d, 2H, aryl, *J* = 8.2 Hz); 7.60 (d, 2H, aryl, *J* = 7.2 Hz); 7.73-7.76 (m, 1H, aryl). $^{13}$C NMR (100 MHz, $CD_3OD$) δ 20.3, 28.3, 42.4, 49.8, 54.4, 57.7, 73.8, 109.5, 111.2, 118.2, 118.6, 121.2, 123.5, 126.5, 126.7, 127.0, 127.4, 127.7, 128.4, 128.8, 129.4, 129.8, 130.3, 136.7, 137.2, 140.1, 140.7, 165.7, 171.6. HR-MS m/z calcd for $C_{36}H_{34}N_4O_2$ $[(M + H)]^+$: 555.2755; found 555.2763.

***(S)-N-((S)-1-(([1,1'-biphenyl]-4-ylmethyl)amino)-3-(1H-indol-3-yl)-1-oxopropan-2-yl)-2-(propylamino)pent-4-ynamide (28)***

Final product **28** was synthesized in 64% starting from **19** and propionaldehyde following the general procedure **C**. FC in hexane/ethyl acetate 1/2, Rf = 0.35. White powder. $^{1}$H NMR (400 MHz, $CD_3OD$): δ: 0.95 (t, 3H, C$H_3$, *J* = 7.4 Hz); 1.36-1.42 (m, 2H, C$H_2$); 1.54-1.58 (m, 2H, C$H_2$); 2.60 (s, 1H, C*H*); 2.80 (dd, 1H, C$H_{2a}$, *J'*= 7.4, *J''*= 17.5 Hz); 2.88 (dd, 1H, C$H_{2b}$, *J'*= 8.1, *J''*= 17.5 Hz); 3.20 (dd, 1H, C$H_{2a}$, *J'*= 7.0, *J''*= 14.3 Hz); 3.31-3.37 (m, 1H, C$H_{2b}$); 4.05 (dd, 1H, C*H*, *J'*= 5.4, *J''*= 7.4 Hz); 4.25 (d, 1H, C$H_{2a}$, *J* = 15.1 Hz); 4.36-4.40 (m, 1H, C$H_{2b}$); 4.78-4.80 (m, 1H, C*H*); 7.03-7.15

(m, 4H aryl); 7.34 (t, 1H, aryl, *J* = 7.4 Hz); 7.38-7.48 (m, 6H, aryl); 7.58 (d, 2H, aryl, *J* = 8.5 Hz); 7.67 (d, 1H, aryl, *J* = 7.9 Hz). $^{13}$C NMR (100 MHz, $CD_3OD$) δ 12.8, 21.1, 27.9, 34.4, 42.4, 51.4, 54.8, 73.7, 104.5, 109.1, 111.0, 118.0, 118.5, 121.2, 123.4, 126.5, 126.9, 127.3, 127.5, 128.4, 136.7, 139.9, 140.7, 167.0, 171.8. HR-MS m/z calcd for $C_{32}H_{35}N_4O_2$ $[(M + H)]^+$: 507.2755; found 507.2747.

***(S)-N-((S)-1-(benzylamino)-3-(1H-indol-3-yl)-1-oxopropan-2-yl)-2-(2-chloroacetamido)pent-4-enamide (29)***

Intermediate **20** (1 mmol) was dissolved in THF and added with TEA (1.2 eq), and chloroacetyl chloride (1.2 eq). The mixture was allowed to react for 20 minutes. Afterward, the reaction mixture was diluted with dichloromethane (20 mL), and the resulting solution was washed successively with water (2 x 25 mL), dried over $Na_2SO_4$ and evaporated to dryness. The crude products were purified by flash chromatography using n-hexane/ethyl acetate 1/1, Rf = 0.38. White powder (62% yield). $^1$H NMR (400 MHz, DMSO): δ: 2.24-2.31 (m, 1H, C$H_{2a}$); 2.37-2.44 (m, 1H, C$H_{2b}$); 2.99 (dd, 1H, C$H_{2a}$, *J'*= 8.1, *J''*= 14.5 Hz); 3.15 (dd, 1H, C$H_{2b}$, *J'*= 4.6, *J''*= 14.5 Hz); 4.09 (dd, 2H, C$H_2$, *J'*= 13.1, *J''*= 15.8 Hz); 4.24-4.26 (m, 2H, C$H_2$); 4.38-4.45 (m, 1H, C*H*); 4.56-4.61 (m, 1H, C*H*); 5.00 (dd, 2H, C$H_2$, *J'*= 17.2, *J''*= 25.5 Hz); 5.61-5.71 (m, 1H, C*H*); 6.98 (t, 1H, aryl, *J* = 7.8 Hz); 7.06 (t, 1H, aryl, *J* = 7.0 Hz); 7.10-7.13 (m, 2H, aryl); 7.19-7.28 (m, 3H, aryl); 7.34 (d, 1H, aryl, *J* = 8.1 Hz); 8.25 (d, 1H, aryl, *J* = 8.0 Hz); 8.40 (t, 1H, aryl, *J* = 5.9 Hz); 10.83 (s, 1H, N*H*). $^{13}$C NMR (100 MHz, DMSO) δ 28.3, 36.9, 40.5, 42.5, 43.0, 52.7, 54.1, 110.3, 111.7, 118.1, 118.9, 121.3, 124.1, 127.1, 127.4, 127.8, 128.6, 134.3, 136.5, 139.6, 166.1, 170.7, 171.6. HR-MS m/z calcd for $C_{25}H_{27}ClN_4O_3$ $[(M + H)]^+$: 467.1844; found 467.1852.

***methyl 1-isobutyl-1H-indole-5-carboxylate (30)***

Intermediate **30** was obtained according to the general procedure **D**, starting from methyl indole-5-carboxylate and 1-iodo-2-methylpropane, as previously described (Kitamura *et. al*, 2022). FC in n-hexane/ethyl acetate 3/1, Rf = 0.4. Yellowish oil (80% yield). $^{1}$H NMR (400 MHz, $CDCl_3$): δ: 0.94 (d, 6H, C*H*$_3$, *J* = 6.7 Hz); 2.17-2.24 (m, 1H, C*H*); 3.93 (d, 2H, C*H*$_2$, *J* = 7.3 Hz); 3.96 (s, 3H, C*H*$_3$); 6.61 (d, 1H, aryl, *J* = 3.2 Hz); 7.14 (d, 1H, aryl, *J* = 3.1 Hz); 7.35 (d, 1H, aryl, *J* = 8.7 Hz); 7.94 (d, 1H, aryl, *J* = 10.1 Hz); 8.44 (s, 1H, aryl). HR-MS m/z calcd for $C_{14}H_{18}NO_2$ $[(M + H)]^+$: 232.1332; found 232.1340.

***methyl 1-methyl-1H-indole-5-carboxylate (31)***

Intermediate **31** was obtained according to the general procedure **D**, starting from methyl indole-5-carboxylate and iodomethane, as previously described (Zhang *et al*., 2021).FC in n-hexane/ethyl acetate 3/1, Rf = 0.4. Yellowish oil (82% yield). $^{1}$H NMR (400 MHz, $CDCl_3$): δ: 3.85 (s, 3H, C*H*$_3$); 3.92 (s, 3H, C*H*$_3$); 6.57 (d, 1H, aryl, *J* = 3.4 Hz); 7.26 (d, 1H, aryl, *J* = 3.4 Hz); 7.43 (d, 1H, aryl, *J* = 9.2 Hz); 7.87 (d, 1H, aryl, *J* = 9.6 Hz); 8.32 (s, 1H, aryl). HR-MS m/z calcd for $C_{11}H_{12}NO_2$ $[(M + H)]^+$: 190.0863; found 190.0871.

***methyl 3-((([1,1'-biphenyl]-4-ylmethyl)amino)methyl)-1-isobutyl-1H-indole-5-carboxylate*** (**32**)

The compound **32** was obtained using general procedure **E**, starting from intermediate **30** which was reacted with 2-([1,1'-biphenyl]-4-yl)ethan-1-amine. FC in dichloromethane/methanol 4.8/0.2. Rf = 0.42. Yellowish oil (70% yield). $^{1}$H NMR (400 MHz, $CDCl_3$): δ: 3.83 (s, 3H, C*H*$_3$); 3.86 (s, 2H, C*H*$_2$); 3.93 (s, 3H, C*H*$_3$); 3.99

(s, 2H, C$H_2$); 7.28 (s, 1H, aryl); 7.32-7.38 (m, 5H, aryl); 7.43 (d, 1H, aryl, *J* = 8.8 Hz); 7.88 (d, 1H, aryl, *J* = 9.2 Hz); 8.35 (s, 1H, aryl). HR-MS m/z calcd for $C_{28}H_{31}N_2O_2$ $[(M + H)]^+$: 427.2380; found 427.2389.

***methyl 3-(((2-([1,1'-biphenyl]-4-yl)ethyl)amino)methyl)-1-isobutyl-1H-indole-5-carboxylate (33)***

The compound **33** was obtained using general procedure **E**, starting from intermediate **31** which was reacted with benzylamine. FC in dichloromethane/methanol 4.8/0.2. Rf = 0.45. Yellowish oil (75% yield). $^1$H NMR (400 MHz, $CDCl_3$): δ: 0.94 (d, 6H, C$H_3$, *J* = 6.6 Hz); 2.14-2.25 (m, 1H, C*H*); 2.94 (t, 2H, C$H_2$, *J* = 7.3 Hz); 3.06 (t, 2H, C$H_2$, *J* = 6.9 Hz); 3.89 (d, 2H, C$H_2$, *J* = 7.3 Hz); 3.94 (s, 3H, C$H_3$); 4.09 (s, 2H, C$H_2$); 7.10 (s, 1H, aryl); 7.31-7.33 (m, 4H, aryl); 7.36 (d, 1H, aryl, *J* = 7.4 Hz); 7.45 (t, 2H, aryl, *J* = 7.8 Hz); 7.55 (d, 2H, aryl, *J* = 8.2 Hz); 7.60 (d, 2H, aryl, *J* = 8.9 Hz); 7.94 (d, 1H, aryl, *J* = 10.1 Hz); 8.43 (s, 1H, N*H*). HR-MS m/z calcd for $C_{29}H_{33}N_2O_2$ $[(M + H)]^+$: 441.2537; found 441.2549.

***methyl 3-((([1,1'-biphenyl]-4-ylmethyl)(benzyl)amino)methyl)-1-isobutyl-1H-indole-5-carboxylate (34)***

Final compound **34** was obtained following general procedure **C**, using as starting materials intermediate **32** and benzaldehyde. FC in dichloromethane/methanol 4.8/0.2. Rf = 0.27. Yellowish oil (78% yield). $^1$H NMR (400 MHz, $CDCl_3$): δ: 0.94 (d, 6H, C$H_3$, *J* = 6.7 Hz); 2.15-2.25 (m, 1H, C*H*); 2.86-2.89 (m, 2H, C$H_2$); 2.94-2.98 (m, 2H, C$H_2$); 3.80 (s, 2H, C$H_2$); 3.89 (d, 2H, C$H_2$, *J* = 7.4 Hz); 3.94 (s, 2H, C$H_2$); 3.99 (s, 3H, C$H_3$); 7.02 (s, 1H, aryl); 7.23 (d, 2H, aryl, *J* = 8.1 Hz); 7.28-7.41 (m, 5H, aryl); 7.45-7.53 (m, 6H, aryl); 7.64 (d, 2H, aryl, *J* = 7.1 Hz); 7.98 (d, 1H, aryl, *J* = 8.7 Hz); 8.54 (s, 1H, aryl). $^{13}$C NMR (100 MHz, $CDCl_3$) δ 203, 29.7, 33.2, 49.2, 51.8, 54.1, 55.2,

58.6, 65.9, 109.2, 114.0, 120.8, 123.0, 126.9, 127.8, 128.3, 128.4, 128.9, 129.4, 138.7, 139.3, 140.0, 141.1, 168.3. HR-MS m/z calcd for $C_{35}H_{38}N_2O_2$ $[(M + H)]^+$: 531.3001; found 531.2994.

***(S)-methyl 3-((N-benzyl-2-((tert-butoxycarbonyl)amino)pent-4-ynamido)methyl)-1-methyl-1H-indole-5-carboxylate (35)***

Final compound **35** was obtained following general procedure **A**, using as starting materials intermediate **33** and Boc-*L*-Pra-OH. FC in dichloromethane/methanol 4.8/0.2. Rf = 0.3. White powder (80% yield). $^1$H NMR (400 MHz, $CD_3OD$): δ: 1.34 (s, 9H, C*H*$_3$); 2.59-2.68 (m, 3H, C*H*$_2$ and C*H*); 3.79 (s, 3H, C*H*$_3$); 3.92 (s, 3H, C*H*$_3$); 4.51-4.63 (m, 4H C*H*$_2$); 5.06 (t, 1H, C*H*, *J* = 6.5 Hz); 7.19-7.44 (m, 5H, aryl); 7.88 (t, 2H, aryl, *J* = 7.1 Hz); 8.21 (s, 1H, aryl); 8.29 (s, 1H, aryl). $^{13}$C NMR (100 MHz, $CD_3OD$) δ 22.0, 27.2, 31.61, 31.74, 39.2, 42.1, 49.2, 49.9, 51.0, 79.3, 111.1, 120.8, 121.1, 122.1, 122.6, 126.8, 127.2, 128.1, 128.4, 130.0, 130.8, 136.4, 136.9, 139.8, 155.8, 168.5, 171.4. HR-MS m/z calcd for $C_{29}H_{33}N_3O_5$ $[(M + H)]^+$: 504.2493; found 504.2501.

***(S)-tert-butyl (1-(benzylamino)-3-(1H-indol-3-yl)-1-oxopropan-2-yl)carbamate (36)***

Synthesized according to the general procedure **A**, starting from Boc-L-Trp-OH and benzylamine.FC in hexane/ethyl acetate 7/3, Rf = 0.45. Yellowish oil (80% yield). 1H NMR (400 MHz, $CD_3OD$): δ: 1.40 (s, 9H, CH 3); 3.10 (dd, 1H, CH 2a, J' = 6.6, J" = 13.8 Hz); 3.25 (dd, 1H, CH 2b, J' = 6.9, J" = 14.4 Hz); 4.19–4.23 (m, 1H, CH); 4.34–4.41 (m, 2H, CH 2); 7.02–7.06 (m,5H, aryl); 7.12 (t, 1H, aryl, J = 7.1 Hz); 7.20–7.25 (m, 2H, aryl); 7.37 (d, 1H, aryl, J = 8.1 Hz); 7.62 (d, 1H, aryl, J = 7.8 Hz). HR-MS m/z calcd for $C_{23}H_{28}N_3O_3$ $[(M + H)]^+$: 394.2125; found 394.2118.

***(S)-2-Amino-N-benzyl-3-(1H-indol-3-yl)propanamide (37)***

Intermediate **37** was synthesized according to the general procedure **B**, starting from **36**. White powder (95% yield). 1H NMR (400 MHz, $CD_3OD$): δ: 3.05 (dd, 1H, CH 2a, J' = 5.8, J" = 10.4 Hz); 3.20 (dd, 1H, CH 2b, J' = 6.0, J" = 10.4 Hz); 3.69 (t, 1H, CH, J = 5.2 Hz); 4.25 (d, 1H, CH 2a, J = 12.6 Hz); 4.35 (d, 1H, CH 2b, J = 12.6 Hz); 7.02–7.07 (m, 5H, aryl); 7.12 (t, 1H, aryl, J = 7.2 Hz); 7.20–7.26 (m, 2H, aryl); 7.39 (d, 1H, aryl, J = 8.2 Hz); 7.64 (d, 1H, aryl, J = 8.0 Hz). HR-MS m/z calcd for $C_{18}H_{20}N_3O$ $[(M + H)]^+$: 294.1601; found 294.1608.

***tert-butyl ((S)-1-(((S)-1-(benzylamino)-3-(1H-indol-3-yl)-1-oxopropan-2-yl)amino)-4-methyl-1-oxopentan-2-yl)carbamate (38)***

Intermediate **38** was synthetized starting from **37** and Boc-*L*-Leu-OH following the general procedure **A**. FC in hexane/ethyl acetate 1/1, R*f*: 0.47. White powder (75% yield). $^1$H NMR (400 MHz, $CD_3OD$): δ 0.89 (d, 3H, C$H_3$, *J* = 6.5 Hz); 0.93 (d, 3H, C$H_3$, *J* = 6.6 Hz); 1.43-1.49 (m, 2H, C$H_2$); 1.56-1.66 (m, 1H, C*H*); 3.28 (d, 2H, C$H_2$, *J* = 6.4 Hz); 3.99 (t, 1H, C*H*, *J* = 7.4 Hz); 4.22 (d, 1H, C$H_{2a}$, *J* = 15.0 Hz); 4.32 (d, 1H, C$H_{2b}$, *J* = 15.0 Hz); 4.68 (t, 1H, C*H*, *J* = 6.3 Hz); 7.02-7.07 (m, 5H, aryl); 7.12 (t, 1H, aryl, *J* = 7.6 Hz); 7.19-7.24 (m, 2H, aryl); 7.37 (d, 1H, aryl, *J* = 8.1 Hz); 7.62 (d, 1H, aryl, *J* = 8.0 Hz). HR-MS m/z calcd for $C_{29}H_{38}N_4O_4$ $[(M + H)]^+$: 507.2966; found 507.2960.

***tert-butyl ((S)-1-(((S)-1-(benzylamino)-3-(1H-indol-3-yl)-1-oxopropan-2-yl)amino)-4-methyl-1-oxopentan-2-yl)carbamate (39)***

Intermediate **39** was synthetized starting from **37** and Boc-D-Leu-OH following the general procedure **A**. FC in hexane/ethyl acetate 1/1, R*f*: 0.47. White powder (72%

yield). $^1$H NMR (400 MHz, DMSO): δ 0.73 (d, 3H, C*H*$_3$, *J* = 6.0 Hz); 0.79 (d, 3H, C*H*$_3$, *J* = 6.1 Hz); 1.13-1.22 (m, 1H, C*H*); 1.23-1.32 (m, 2H, C*H*$_2$); 1.39 (s, 9H, C*H*$_3$); 2.93 (dd, 1H, C*H*$_{2a}$, *J'* = 10.0, *J''* = 14.5 Hz); 3.00-3.04 (m, 2H, C*H*$_2$); 3.23 (dd, 1H, C*H*$_{2b}$, *J'* = 4.5, *J''* = 14.5 Hz); 3.97-4.02 (m, 2H, C*H*); 4.51-4.57 (m, 1H, C*H*); 6.96 (t, 1H, aryl, *J* = 7.2 Hz); 7.05 (t, 1H, aryl, *J* = 7.4 Hz); 7.10 (s, 1H, aryl); 7.13-7.20 (m, 5H, aryl); 7.53 (d, 1H, aryl, *J* = 7.4 Hz); 7.59 (d, 1H, aryl, *J* = 7.8 Hz). HR-MS m/z calcd for $C_{29}H_{38}N_4O_4$ $[(M + H)]^+$: 507.2966; found 507.2968.

***tert-butyl (1-(((S)-1-(benzylamino)-3-(1H-indol-3-yl)-1-oxopropan-2-yl)amino)-1-oxo-3-phenylpropan-2-yl)carbamate (40)***

Intermediate **40** was synthetized starting from **37** and Boc-Phe-OH following the general procedure **A**. FC in hexane/ethyl acetate 7/3, R*f*: 0.49. White powder (82% yield). $^1$H NMR (400 MHz, DMSO): δ 1.29 (s, 9H, 3 C*H*$_3$); 1.72-1.75 (m, 2H, C*H*$_2$); 2.68-2.74 (m, 1H, C*H*$_{2a}$); 2.90 (dd, 1H, C*H*$_{2b}$, *J'* = 10.1, *J''* = 14.0 Hz); 3.00-3.16 (m, 2H, C*H*$_2$); 4.13-4.19 (m, 1H, C*H*,); 4.24 (d, 2H, C*H*$_2$, *J* = 5.6 Hz); 4.59-4.64 (m, 1H, C*H*); 6.94 (d, 1H, aryl, *J* = 8.4 Hz); 6.99 (d, 1H, aryl, *J* = 7.4 Hz); 7.08 (d, 2H, aryl, J= 7.08 Hz); 7.16-7.24 (m, 8H, aryl); 7.34 (d, 1H, aryl, *J* = 8.0 Hz); 7.60 (d, 1H, aryl, *J* = 7.8 Hz); 8.01 (d, 1H, aryl, *J* = 7.9 Hz); 8.42 (t, 1H, NH, *J* = 5.6 Hz); 10.85 (s, 1H, N*H*). HR-MS m/z calcd for $C_{32}H_{36}N_4O_4$ $[(M + H)]^+$: 541.2809; found 541.2811

***tert-butyl (S)-(2-((1-(benzylamino)-3-(1H-indol-3-yl)-1-oxopropan-2-yl)amino)-2-oxoethyl)carbamate (41)***

Intermediate **41** was synthetized starting from **37** and Boc-Gly-OH following the general procedure **A**. FC in hexane/ethyl acetate 1/1, R*f*: 0.47. White powder (80% yield). $^1$H NMR (400 MHz, $CD_3OD$): δ 1.37 (s, 3H, C*H*$_3$); 3.26 (t, 1H, C*H*$_{2a}$, *J* = 6.1 Hz); 3.33 (d, 1H, C*H*$_{2b}$, *J* = 1.6 Hz); 3.65 (d, 1H, C*H*$_{2a}$, *J* = 16.9 Hz); 3.71 (d, 1H, C*H*$_{2b}$,

*J* = 16.9 Hz); 4.25 (d, 1H, C$H_{2a}$, *J* = 15.1 Hz); 4.32 (d, 1H, C$H_{2b,}$ *J* = 15.1 Hz); 4.72 (t, 1H, C*H,* *J* = 6.4 Hz); 7.03-7.06 (m, 4H, aryl); 7.12 (t, 1H, aryl, *J* = 7.1 Hz); 7.19-7.26 (m, 3H, aryl); 7.37 (d, 1H, aryl, *J* = 8.0 Hz); 7.62 (d, 1H, aryl, *J* = 7.8 Hz). HR-MS m/z calcd for $C_{25}H_{30}N_4O_4$ $[(M + H)]^+$: 451.2340; found 451.2338.

***tert-butyl ((S)-1-(((S)-1-(benzylamino)-3-(1H-indol-3-yl)-1-oxopropan-2-yl)amino)-3-(4-hydroxyphenyl)-1-oxopropan-2-yl)carbamate (42)***

Intermediate **42** was synthetized starting from **37** and Boc-*L*-Tyr-OH following the general procedure **A**. FC in hexane/ethyl acetate 4/6, R*f*: 0.47. White powder (65% yield). $^1$H NMR (400 MHz, $CD_3OD$): δ 1.31 (s, 9H, C$H_3$); 2.80 (dd, 1H, C$H_{2a,}$ *J'* = 8.7, *J''* = 13.8 Hz); 2.99 (dd, 1H, C$H_{2b,}$ *J'* = 5.2, *J''* = 13.9 Hz); 3.16-3.30 (m, 2H, C$H_2$); 4.19-4.23 (m, 2H, C$H_{2a}$ and C*H*); 4.30 (d, 1H, C$H_{2b}$, *J* = 15.1 Hz); 4.68 (t, 1H, C*H,* *J* = 6.2 Hz); 6.88 (d, 2H, aryl, *J* = 8.4 Hz); 7.00-7.05 (m, 4H, aryl); 7.09 (d, 2H, aryl, *J* = 8.3 Hz); 7.14-7.23 (m, 5H, aryl); 7.37 (d, 1H, aryl, *J* = 7.9 Hz). HR-MS m/z calcd for $C_{32}H_{36}N_4O_5$ $[(M + H)]^+$: 557.2758; found 557.2761.

***(S)-2-amino-N-((S)-1-(benzylamino)-3-(1H-indol-3-yl)-1-oxopropan-2-yl)-4-methylpentanamide (43)***

Intermediate **43** was synthetized starting from **38** following the general procedure **B**. White powder (93% yield). $^1$H NMR (400 MHz, $CD_3OD$): δ 0.87 (d, 3H, C$H_3$, *J* = 6.6 Hz); 0.90 (d, 3H, C$H_3$, *J* = 6.6 Hz); 1.22-1.31 (m, 1H, C$H_{2a}$); 1.40-1.47 (m, 1H, C$H_{2b}$); 1.56-1.65 (m, 1H, C*H*); 3.18 (dd, 1H, C$H_{2a,}$ *J'* = 7.2, *J''* = 14.4 Hz); 3.29-3.38 (m, 2H, C$H_{2b}$ and C*H*, *J* = 7.4 Hz); 4.25 (d, 1H, C$H_{2a,}$ *J* = 15.0 Hz); 4.33 (d, 1H, C$H_{2b,}$ *J* = 15.0 Hz); 4.73 (t, 1H, C*H*, *J* = 7.3 Hz); 7.01-7.08 (m, 5H, aryl); 7.12 (t, 1H, aryl, *J* = 8.0 Hz); 7.20-7.25 (m, 2H, aryl); 7.37 (d, 1H, aryl, *J* = 8.1 Hz); 7.64 (d, 1H, aryl, *J* = 7.8 Hz). HR-MS m/z calcd for $C_{24}H_{30}N_4O_2$ $[(M + H)]^+$: 407.2442; found 407.2446.

***(R)-2-amino-N-((S)-1-(benzylamino)-3-(1H-indol-3-yl)-1-oxopropan-2-yl)-4-methylpentanamide (44)***

Intermediate **44** was synthetized starting from **39** following the general procedure **B**. White powder (94% yield). $^1$H NMR (400 MHz, $CD_3OD$): δ 0.77 (t, 6H, C*H*$_3$, *J* = 5.7 Hz); 1.17-1.24 (m, 1H, C*H*); 1.28-1.35 (m, 2H, C*H*$_2$); 3.13 (dd, 1H, C*H*$_{2a,}$ *J'* = 8.5, *J''* = 14.5 Hz); 3.27 (t, 1H, C*H*, *J* = 6.8 Hz); 3.33-3.38 (m, 1H, C*H*$_{2b}$); 4.32 (d, 1H, C*H*$_{2a,}$ *J* = 15.0 Hz); 4.37 (d, 1H, C*H*$_{2a,}$ *J* = 15.0 Hz); 4.77 (dd, 1H, C*H, J'* = 6.2, *J''* = 8.5 Hz); 7.03 (t, 1H, aryl, *J* = 7.0 Hz); 7.08 (s, 1H, aryl); 7.13 (t, 1H, aryl, *J* = 6.8 Hz); 7.21-7.29 (m, 2H, aryl); 7.31-7.40 (m, 2H, aryl); 7.64 (d, 1H, aryl, *J* = 7.9 Hz); 7.74 (d, 1H, aryl, *J* = 7.5 Hz); 7.79 (d, 1H, aryl, *J* = 7.6 Hz). HR-MS m/z calcd for $C_{24}H_{30}N_4O_2$ $[(M + H)]^+$: 407.2442; found 407.2438.

***(S)-2-amino-N-((S)-1-(benzylamino)-3-(1H-indol-3-yl)-1-oxopropan-2-yl)-3-phenylpropanamide (45)***

Intermediate **45** was synthetized starting from **40** following the general procedure **B**. White powder (95% yield). $^1$H NMR (400 MHz, $CD_3OD$): δ 3.04 (dd, 1H, C*H*$_{2a,}$ *J'* = 8.1, *J''* = 14.2 Hz); 3.15-3.26 (m, 3H, C*H*$_{2b}$ and C*H*$_2$); 4.13 (t, 1H, C*H*, *J* = 6.2 Hz); 4.21 (d, 1H, C*H*$_{2a}$, *J* = 18.7 Hz); 4.32 (d, 1H, C*H*$_{2b}$, *J* = 18.8 Hz); 4.74 (t, 1H, C*H*, *J* = 7.5 Hz); 7.00 (d, 1H, aryl, *J* = 7.7 Hz); 7.04 (t, 1H, aryl, *J* = 7.8 Hz); 7.13 (t, 1H, aryl, *J* = 7.8 Hz); 7.19-7.24 (m, 5H, aryl); 7.26-7.33 (m, 5H, aryl); 7.38 (d, 1H, aryl, *J* = 7.4 Hz); 7.66 (d, 1H, aryl, *J* = 7.5 Hz). HR-MS m/z calcd for $C_{27}H_{28}N_4O_2$ $[(M + H)]^+$: 441.2285; found 441.2291.

***(S)-2-(2-aminoacetamido)-N-benzyl-3-(1H-indol-3-yl)propanamide (46)***

Intermediate **46** was synthetized starting from **41** following the general procedure **B**. White powder (92% yield). $^{1}$H NMR (400 MHz, $CD_3OD$): δ 3.16 (dd, 1H, C$H_{2a,}$ *J'* = 7.4, *J''* = 14.4 Hz); 3.30 (dd, 1H, C$H_{2b,}$ *J'* = 7.2, *J''* = 15.1 Hz); 3.63 (d, 1H, C$H_{2a}$, *J* = 16.0 Hz); 3.72 (d, 1H, C$H_{2b,}$ *J* = 16.0 Hz); 4.25 (d, 1H, C$H_{2a}$, *J* = 15.0 Hz); 4.33 (d, 1H, C$H_{2b,}$ *J* = 15.0 Hz); 4.77 (t, 1H, C$H$, *J* = 7.3 Hz); 7.02-7.08 (m, 4H, aryl); 7.12 (t, 1H, aryl, *J* = 7.7 Hz); 7.18-7.25 (m, 3H, aryl); 7.37 (d, 1H, aryl, *J* = 8.1 Hz); 7.64 (d, 1H, aryl, *J* = 7.7 Hz). HR-MS m/z calcd for $C_{20}H_{22}N_4O_2$ $[(M + H)]^+$: 351.1816; found 351.1824.

***(S)-2-amino-N-((S)-1-(benzylamino)-3-(1H-indol-3-yl)-1-oxopropan-2-yl)-3-(4-hydroxyphenyl)propanamide (47)***

Intermediate **47** was synthetized starting from **42** following the general procedure **B**. White powder (94% yield). $^{1}$H NMR (400 MHz, $CD_3OD$): δ 2.74 (dd, 1H, C$H_{2a,}$ *J'* = 7.6, *J''* = 13.9 Hz); 2.94 (dd, 1H, C$H_{2b,}$ *J'* = 6.2, *J''* = 14.3 Hz); 3.14-3.27 (m, 2H, C$H_2$); 3.70 (t, 1H, C$H$, *J* = 5.8 Hz); 4.21 (d, 1H, C$H_{2a}$, *J* = 15.0 Hz); 4.33 (d, 1H, C$H_{2b,}$ *J* = 15.0 Hz); 4.71 (t, 1H, C$H$, *J* = 7.2 Hz); 6.74 (d, 2H, aryl, *J* = 8.5 Hz); 7.01-7.05 (m, 6H, aryl); 7.12 (t, 1H, aryl, *J* = 7.1 Hz); 7.19-7.25 (m, 3H, aryl); 7.37 (d, 1H, aryl, *J* = 7.9 Hz); 7.59 (d, 1H, aryl, *J* = 8.0 Hz). HR-MS m/z calcd for $C_{27}H_{28}N_4O_3$ $[(M + H)]^+$: 457.2234; found 457.2229.

***(S)-N-((S)-1-(benzylamino)-3-(1H-indol-3-yl)-1-oxopropan-2-yl)-2-(2-chloroacetamido)-4-methylpentanamide (48)***

Derivative **48** was synthetized starting from **43** and chloroacetyl chloride following the general procedure **F**. FC in ethyl acetate/methanol 9.8/0.2, R*f*: 0.47. Yellowish

powder (55% yield). $^{1}$H NMR (400 MHz, $CD_3OD$): δ: 0.89 (d, 3H, C*H*$_3$, *J* = 6.4 Hz); 0.93 (d, 3H, C*H*$_3$, *J* = 6.4 Hz); 1.53 (t, 2H, C*H*$_2$, *J* = 6.8 Hz); 1.56-1.65 (m, 1H, C*H*); 3.18 (dd, 1H, C*H*$_{2a}$, *J'* = 7.0; *J''* = 14.4 Hz); 3.28-3.33 (m, 1H, C*H*$_{2b}$); 3.98 (q, 2H, C*H*$_2$, *J* = 13.4 Hz); 4.28 (q, 2H, C*H*$_2$, *J* = 13.6 Hz); 4.40 (t, 1H, C*H*, *J* = 7.4 Hz); 4.69 (t, 1H, C*H*, *J* = 7.2 Hz); 7.01-7.06 (m, 5H, aryl); 7.11 (t, 1H, aryl, *J* = 7.2 Hz); 7.18-7.25 (m, 2H, aryl); 7.36 (d, 1H, aryl, *J* = 8.1 Hz); 7.61 (d, 1H, aryl, *J* = 7.8 Hz).$^{13}$C NMR (100 MHz, $CD_3OD$) δ: 20.6, 21.9, 24.4, 27.4, 40.2, 41.6, 42.7, 52.3, 54.4, 109.3, 110.9, 118.0, 118.5, 121.0, 123.3, 126.7, 127.0, 127.4, 128.0, 136.7, 138.0, 168.0, 172.2, 172.6. HR-MS m/z calcd for $C_{26}H_{31}ClN_4O_3$ $[(M + H)]^+$: 483.2157; found 483.2155.

***(S)-2-acrylamido-N-((S)-1-(benzylamino)-3-(1H-indol-3-yl)-1-oxopropan-2-yl)-4-methylpentanamide (49)***

Derivative **49** was synthetized starting from **43** and acryloyl chloride following the general procedure **F**. FC in hexane/ethyl acetate 2/8, R*f*: 0.45. White powder (58% yield). $^{1}$H NMR (400 MHz, DMSO): δ: 0.82 (d, 3H, C*H*$_3$, *J* = 6.5 Hz); 0.86 (d, 3H, C*H*$_3$, *J* = 6.5 Hz); 1.43 (t, 2H, C*H*$_2$, *J* = 6.9 Hz); 1.51-1.57 (m, 1H, C*H*); 3.01 (dd, 1H, C*H*$_{2a}$, *J'* = 7.7, *J''* = 14.6 Hz); 3.15 (dd, 1H, C*H*$_{2b}$, *J'* = 6.2, *J''* = 14.6 Hz); 4.17-4.28 (m, 2H, C*H*$_2$); 4.38-4.44 (m, 1H, C*H*); 4.54-4.60 (m, 1H, C*H*); 5.60 (dd, 1H, C*H*$_{2a}$, *J'* = 2.2, *J''* = 10.1 Hz); 6.09 (dd, 1H, C*H*$_{2b}$, *J'* = 2.2, *J''* = 17.1 Hz); 6.32 (dd, 1H, C*H*$_{2b}$, *J'* = 10.2, *J''* = 17.1 Hz); 6.97 (t, 1H, aryl, *J* = 7.0 Hz); 7.06 (t, 1H, aryl, *J* = 8.0 Hz); 7.08-7.11 (m, 1H, aryl); 7.20-7.26 (m, 2H, aryl); 7.33 (d, 1H, aryl, *J* = 8.4 Hz); 7.57 (d, 1H, aryl, *J* = 7.8 Hz); 8.10 (d, 1H, aryl, *J* = 8.0 Hz); 8.22 (d, 1H, aryl, *J* = 8.1 Hz); 8.36 (t, 1H, aryl, *J* = 6.0 Hz).$^{13}$C NMR (100 MHz, DMSO) δ: 22.0, 23.5, 24.7, 28.1, 41.2, 42.5, 51.6, 54.0, 110.4, 111.7, 118.9, 121.3, 124.0, 126.0, 127.1, 127.4, 127.8,

128.6, 132.0, 136.5, 139.6, 165.0, 171.6, 172.0. HR-MS m/z calcd for $C_{27}H_{32}N_4O_3$ [(M + H)]$^+$: 461.2547; found 461.2549.

***(R)-N-((S)-1-(benzylamino)-3-(1H-indol-3-yl)-1-oxopropan-2-yl)-2-(2-chloroacetamido)-4-methylpentanamide (50)***

Derivative **50** was synthetized starting from **44** and chloroacetyl chloride following the general procedure **F**. FC in ethyl acetate/methanol 9.8/0.2, R*f*: 0.44. White powder (48% yield). $^1$H NMR (400 MHz, $CD_3OD$): δ: 0.73 (d, 3H, C*H*$_3$, *J* = 6.5 Hz); 0.76 (d, 3H, C*H*$_3$, *J* = 6.5 Hz); 1.14-1.21 (m, 1H, C*H*); 1.32 (t, 2H, C*H*$_2$, *J* = 7.4 Hz); 3.08 (dd, 1H, C*H*$_{2a,}$ *J'* = 9.7, *J''* = 14.6 Hz); 3.45 (dd, 1H, C*H*$_{2b,}$ *J'* = 8.3, *J''* = 14.6 Hz); 3.92 (q, 2H, C*H*$_2$, *J* = 13.5 Hz ); 4.21 (t, 1H, C*H*, *J* = 7.6 Hz ); 4.40 (q, 2H, C*H*$_2$, *J* = 15.0 Hz ); 4.78 (dd, 1H, C*H*$_{2a,}$ *J'* = 8.3, *J''* = 14.6 Hz); 7.02 (t, 1H, aryl, *J* = 7.8 Hz); 7.08 (s, 1H, aryl); 7.11 (t, 1H, aryl, *J* = 7.2 Hz); 7.23 (t, 3H, aryl, *J* = 7.6 Hz); 7.27-7.31 (m, 2H, aryl); 7.35 (d, 1H, aryl, *J* = 8.1 Hz); 7.62 (d, 1H, aryl, *J* = 7.9 Hz).$^{13}$C NMR (100 MHz, $CD_3OD$) δ: 21.0, 21.4, 24.1, 27.2, 39.9, 41.4, 42.7, 52.8, 54.3, 109.6, 110.9, 118.0, 118.5, 121.1, 123.2, 126.7, 127.17, 127.22, 128.0, 136.8, 138.3, 168.0, 172.4, 173.1. HR-MS m/z calcd for $C_{26}H_{31}ClN_4O_3$ [(M + H)]$^+$: 483.2157; found 483.2159.

***(S)-N-benzyl-2-((S)-2-(2-chloroacetamido)-3-phenylpropanamido)-3-(1H-indol-3-yl)propenamide (51)***

Derivative **51** was synthetized starting from **45** and chloroacetyl chloride following the general procedure **F**. FC in hexane/ethyl acetate 0.2/9.8, R*f*: 0.42. White powder (68% yield). $^1$H NMR (400 MHz, $CD_3OD$): δ 2.90 (dd, 1H, C*H*$_{2a,}$ *J'* = 8.4, *J''* = 13.9 Hz); 3.07-3.19 (m, 2H, C*H*$_{2b}$ and C*H*$_{2a}$); 3.30 (dd, 1H, C*H*$_{2b,}$ *J'* = 7.3, *J''* = 14.4 Hz); 3.88-3.97 (m, 2H, C*H*$_2$); 4.27 (q, 2H, C*H*$_2$, *J* = 15.0 Hz ); 4.59-4.70 (m, 2H, C*H*); 7.01-7.04 (m, 3H, aryl); 7.12 (t, 1H, aryl, *J* = 7.3 Hz); 7.17-7.26 (m, 9H, aryl); 7.37 (d, 1H,

aryl, *J* = 8.1 Hz); 7.59 (d, 1H, aryl, *J* = 7.9 Hz).$^{13}$C NMR (100 MHz, $CD_3OD$) δ: 27.6, 37.2, 41.5, 42.7, 54.4, 54.9, 109.2, 110.9, 118.0, 118.5, 121.1, 123.4, 126.5, 127.0, 127.4, 128.1, 128.9, 136.5, 138.0, 167.7, 171.2, 172.0 . HR-MS m/z calcd for $C_{29}H_{29}ClN_4O_3$ $[(M + H)]^+$: 517.2001; found 517.2003.

***(S)-N-benzyl-2-(2-(2-chloroacetamido)acetamido)-3-(1H-indol-3-yl)propanamide (52)***

Derivative **52** was synthetized starting from **46** and chloroacetyl chloride following the general procedure **F**. FC in ethyl acetate, R*f*: 0.45. White powder (63% yield). $^1$H NMR (400 MHz, $CD_3OD$): δ 3.06 (dd, 1H, C$H_{2a,}$ *J'* = 7.0, *J''* = 14.4 Hz); 3.16-3.25 (m, 3H, C$H_{2b}$ and C$H_2$); 3.73 (d, 1H, C$H_{2a,}$ *J* = 16.6 Hz); 3.81 (d, 1H, C$H_{2a,}$ *J* = 16.6 Hz); 3.92 (s, 2H, C$H_2$); 4.13 (d, 1H, C$H_{2a,}$ *J* = 15.0 Hz); 4.22 (d, 1H, C$H_{2a,}$ *J* = 15.0 Hz); 4.60 (t, 1H, C*H*, *J* = 7.0 Hz); 6.90-6.95 (m, 4H, aryl); 7.00 (t, 1H, aryl, *J* = 8.0 Hz); 7.08-7.14 (m, 3H, aryl); 7.25 (d, 1H, aryl, *J* = 8.0 Hz); 7.50 (d, 1H, aryl, *J* = 7.9 Hz).$^{13}$C NMR (100 MHz, $CD_3OD$) δ: 27.6, 41.6, 42.4, 42.7, 54.4, 109.2, 110.9, 117.9, 118.5, 121.1, 123.3, 126.6, 127.0, 127.4, 128.0, 136.7, 138.0, 168.5, 169.5, 172.3. HR-MS m/z calcd for $C_{22}H_{23}ClN_4O_3$ $[(M + H)]^+$: 427.1531; found 427.1529.

***(S)-N-benzyl-3-(1H-indol-3-yl)-2-((S)-2-(2-mercaptoacetamido)-3-phenylpropanamido)propanamide (53)***

Derivative **53** was synthetized starting from **45** and 2-mercaptoacetyl chloride following the general procedure **F**. FC in ethyl acetate/methanol 9.5/0.5, R*f*: 0.47. white powder (55% yield). $^1$H NMR (400 MHz, DMSO): δ 2.55 (t, 1H, C$H_{2a,}$ *J* = 8.0 Hz); 2.73-2.80 (m, 1H, C$H_{2b}$); 2.96-3.02 (m, 2H, C$H_{2b}$ and C$H_{2a}$); 3.07 (d, 1H, C$H_{2a,}$ *J* = 8.0 Hz); 3.16 (dd, 1H, C$H_{2b,}$ *J'* = 6.1, *J''* = 14.4 Hz); 4.24-4.27 (m, 2H, C$H_2$); 4.53-4.64 (m, 2H, C*H*); 6.96-7.00 (m, 1H, aryl); 7.04-7.28 (m, 8H, aryl); 7.34 (d, 1H, aryl,

*J* = 8.0 Hz); 7.59-7.62 (m, 1H, aryl); 8.18 (d, 1H, aryl, *J* = 8.2 Hz); 8.24 (t, 1H, aryl, *J* = 7.4 Hz); 8.30 (d, 1H, aryl, *J* = 8.0 Hz); 8.36 (t, 1H, aryl, *J* = 5.8 Hz); 10.84 (s, 1H, N*H*).$^{13}$C NMR (100 MHz, DMSO) δ: 27.4, 28.4, 38.0, 42.1, 42.5, 54.1, 54.6, 110.3, 111.7, 118.7, 118.9, 121.3, 124.1, 126.7, 127.1, 127.4, 127.8, 128.6, 129.7, 136.6, 137.9, 139.6, 168.1, 169.8, 171.1, 171.6. HR-MS m/z calcd for $C_{29}H_{30}N_4O_3S$ [(M + H)]$^+$: 515.2111; found 515.2113.

***(S)-N-benzyl-2-((S)-2-(2-chloroacetamido)-3-(4-hydroxyphenyl)propanamido)-3-(1H-indol-3-yl)propanamide (54)***

Derivative **54** was synthetized starting from **47** and chloroacetyl chloride following the general procedure **F**. FC in ethyl acetate/methanol 9.5/0.5, R*f*: 0.48. White powder (59% yield). $^1$H NMR (400 MHz, $CD_3OD$): δ 2.66 (dd, 1H, C$H_{2a,}$ *J'* = 9.0, *J''* = 13.8 Hz); 2.88 (dd, 1H, C$H_{2a,}$ *J'* = 4.6, *J''* = 13.9 Hz); 3.00 (dd, 1H, C$H_{2a,}$ *J'* = 7.9, *J''* = 14.5 Hz); 3.15 (dd, 1H, C$H_{2a,}$ *J'* = 6.2, *J''* = 14.6 Hz); 4.02 (s, 2H, C$H_2$); 4.21-4.31 (m, 2H, C$H_2$); 4.48-4.53 (m, 1H, C*H*); 4.57-4.62 (m, 1H, C*H*); 6.60 (d, 2H, aryl, *J* = 8.4 Hz); 6.97 (d, 2H, aryl, *J* = 8.2 Hz); 7.05-7.14 (m, 3H, aryl); 7.21-7.28 (m, 2H, aryl); 7.34 (d, 1H, aryl, *J* = 8.1 Hz); 7.61 (d, 1H, aryl, *J* = 7.8 Hz); 8.24 (d, 1H, aryl, *J* = 8.2 Hz); 8.31 (d, 1H, aryl, *J* = 8.0 Hz); 8.36 (t, 1H, aryl, *J* = 6.0 Hz); 9.15 (s, 1H, N*H*); 10.84 (s, 1H, N*H*).$^{13}$C NMR (100 MHz, $CD_3OD$) δ: 28.4, 37.3, 42.5, 42.9, 54.1, 54.7, 110.3, 111.7, 115.3, 118.7, 118.9, 121.3, 124.1, 127.1, 127.4, 127.8, 128.6, 130.6, 136.5, 139.6, 156.2, 165.9, 170.9, 171.6. HR-MS m/z calcd for $C_{29}H_{29}ClN_4O_4$ [(M + H)]$^+$: 533.1950; found 533.1952.

***N-((S)-1-(((S)-1-(benzylamino)-3-(1H-indol-3-yl)-1-oxopropan-2-yl)amino)-1-oxo-3-phenylpropan-2-yl)acrylamide (55)***

Derivative **55** was synthetized starting from **45** and acryloyl chloride following the general procedure **F**. FC in ethyl acetate, R*f*: 0.45. White powder (48% yield). $^{1}$H NMR (400 MHz, $CD_3OD$): δ 2.78 (dd, 1H, C$H_{2a,}$ *J'* = 8.7, *J''* = 14.0 Hz); 2.98 (dd, 1H, C$H_{2b,}$ *J'* = 5.9, *J''* = 13.9 Hz); 3.03-3.17 (m, 2H, C$H_2$); 4.11 (d, 1H, C$H_{2a,}$ *J* = 15.0 Hz); 4.17 (d, 1H, C$H_{2b,}$ *J* = 15.0 Hz); 4.52-4.57 (m, 2H, C*H*); 5.50 (dd, 1H, C$H_{a,}$ *J'* = 2.2, *J''* = 9.8 Hz); 6.00 (dd, 1H, C$H_{2a,}$ *J'* = 2.2, *J''* = 17.0 Hz); 6.08 (dd, 1H, C$H_{2b,}$ *J'* = 9.8, *J''* = 17.1 Hz); 6.88-6.92 (m, 3H, aryl); 6.99 (t, 1H, aryl, *J* = 7.1 Hz); 7.05-7.12 (m, 9H, aryl); 7.23 (d, 1H, aryl, *J* = 8.1 Hz); 7.45 (d, 1H, aryl, *J* = 7.9 Hz).$^{13}$C NMR (100 MHz, $CD_3OD$) δ: 27.5, 37.1, 42.7, 54.4, 54.9, 109.2, 110.9, 118.0, 118.5, 121.0, 123.3, 126.1, 126.4, 126.6, 127.0, 128.0, 128.8, 129.9, 136.7, 136.8, 138.0, 166.7, 171.75, 171.79. HR-MS m/z calcd for $C_{30}H_{30}N_4O_3$ $[(M + H)]^+$: 495.2391; found 495.2392.

***(S)-2-amino-N-((S)-1-(((S)-1-(benzylamino)-3-(1H-indol-3-yl)-1-oxopropan-2-yl)amino)-1-oxo-3-phenylpropan-2-yl)-4-methylpentanamide (56)***

Intermediate **56** was synthetized starting from tert-butyl ((R)-1-(((S)-1-(((S)-1-(benzylamino)-3-(1H-indol-3-yl)-1-oxopropan-2-yl)amino)-1-oxo-3-phenylpropan-2-yl)amino)-4-methyl-1-oxopentan-2-yl)carbamate obtained from **45** and Boc-L-Leu-OH according to the general procedure **A**, following the general procedure **B**. White powder (78% yield). $^{1}$H NMR (400 MHz, $CD_3OD$): δ 0.90 (d, 3H, C$H_3$, *J* = 6.5 Hz); 0.95 (d, 3H, C$H_3$, *J* = 6.5 Hz); 1.63 (t, 2H, C$H_{2,}$ *J* = 6.6 Hz); 1.68-1.74 (m, 1H, C*H*); 2.96 (dd, 1H, C$H_{2a,}$ *J'* = 8.6, *J''* = 14.0 Hz); 3.09-3.14 (m, 1H, C$H_{2b}$); 3.16-3.26 (m, 2H, C$H_2$); 3.80 (t, 1H, C*H*, *J* = 7.5 Hz); 4.18 (d, 1H, C$H_{2a}$, *J* = 15.0 Hz); 4.28 (d, 1H, C$H_{2b}$, *J* = 15.0 Hz); 4.65 (t, 1H, C*H*, *J* = 7.5 Hz); 4.71 (t, 1H, C*H*, *J* = 6.4 Hz); 6.98 (d,

1H, aryl, *J* = 7.7 Hz); 7.03 (t, 1H, aryl, *J* = 7.3 Hz); 7.06 (s, 1H, aryl); 7.12 (t, 1H, aryl, *J* = 7.4 Hz); 7.19-7.24 (m, 9H, aryl); 7.37 (d, 1H, aryl, *J* = 8.1 Hz); 7.61 (d, 1H, aryl, *J* = 7.9 Hz). HR-MS m/z calcd for $C_{33}H_{39}N_5O_3$ $[(M + H)]^+$: 554.3126; found 554.3119.

***(S)-N-((S)-1-(((S)-1-(benzylamino)-3-(1H-indol-3-yl)-1-oxopropan-2-yl)amino)-1-oxo-3-phenylpropan-2-yl)-2-(2-chloroacetamido)-4-methylpentanamide (57)***

Derivative **57** was synthetized starting from **56** and chloroacetyl chloride following the general procedure **F**. FC in ethyl acetate/methanol 9.8/0.2, R*f*: 0.44. White powder (52% yield). $^1$H NMR (400 MHz, DMSO): δ: 0.81 (d, 3H, C*H*$_3$, *J* = 6.5 Hz); 0.84 (d, 3H, C*H*$_3$, *J* = 6.5 Hz); 1.38 (t, 2H, C*H*$_2$, *J* = 7.4 Hz); 1.48-1.54 (m, 1H, C*H*); 2.80 (dd, 1H, C*H*$_{2a,}$ *J'* = 9.3, *J''* = 13.9 Hz); 2.98-3.04 (m, 2H, C*H*$_{2b}$ and C*H*$_{2a}$); 3.14 (dd, 1H, C*H*$_{2b,}$ *J'* = 6.7, *J''* = 14.5 Hz); 4.06 (q, 2H, C*H*$_2$, *J* = 12.9 Hz ); 4.24 (d, 2H, C*H*$_2$, *J* = 5.7 Hz ); 4.28-4.34 (m, 1H, C*H*); 4.52-4.61 (m, 2H, C*H*); 6.98 (t, 1H, aryl, *J* = 7.1 Hz); 7.05-7.09 (m, 2H, aryl); 7.13 (s, 1H, aryl); 7.18-7.26 (m, 5H, aryl); 7.35 (d, 1H, aryl, *J* = 8.0 Hz); 7.59 (d, 1H, aryl, *J* = 7.8 Hz); 8.08-8.14 (m, 2H, aryl); 8.24 (d, 1H, aryl, *J* = 8.3 Hz); 8.34 (t, 1H, aryl, *J* = 6.0 Hz); 10.8 (s, 1H, N*H*).$^{13}$C NMR (100 MHz, DMSO) δ: 22.1, 23.4, 24.6, 28.5, 37.7, 40.3, 40.5, 40.7, 41.3, 42.5, 43.0, 51.8, 54.1, 54.3, 110.2, 111.7, 118.7, 118.9, 121.3, 124.1, 126.7, 127.1, 127.4, 127.8, 128.4, 128.6, 129.7, 136.6, 138.1, 139.5, 166.1, 171.0, 171.5, 171.9. HR-MS m/z calcd for $C_{35}H_{40}ClN_5O_4$ $[(M + H)]^+$: 630.2842; found 630.2844

***(R)-2-amino-N-benzyl-3-(1H-indol-3-yl)propanamide (58)***

Intermediate **58** was synthetized starting from tert-butyl (R)-(1-(benzylamino)-3-(1H-indol-3-yl)-1-oxopropan-2-yl)carbamate, obtained from Boc-D-Trp-OH and benzylamine according to the general procedure **A**, following the general procedure **B**. White powder (88% yield). $^1$H NMR (400 MHz, $CD_3OD$): δ 3.04 (dd, 1H, C*H*$_{2a,}$ *J'*

= 6.8, *J''* = 14.1 Hz); 3.19 (dd, 1H, C$H_{2b,}$ *J'* = 6.7, *J''* = 14.1 Hz); 3.67 (t, 1H, C*H*, *J* = 6.8 Hz); 4.22 (d, 1H, C$H_{2a,}$ *J* = 14.9 Hz); 4.34 (d, 1H, C$H_{2a,}$ *J* = 14.9 Hz); 7.01-7.05 (m, 4H, aryl); 7.12 (t, 1H, aryl, *J* = 7.2 Hz); 7.19-7.24 (m, 3H, aryl); 7.38 (d, 1H, aryl, *J* = 8.0 Hz); 7.63 (d, 1H, aryl, *J* = 7.9 Hz). HR-MS m/z calcd for $C_{18}H_{19}N_3O$ [(M + H)]$^+$: 294.1601; found 294.1597.

***(S)-2-amino-N-((R)-1-(benzylamino)-3-(1H-indol-3-yl)-1-oxopropan-2-yl)-4-methylpentanamide (59)***

Intermediate **59** was synthetized starting from tert-butyl ((R)-1-(((R)-1-(benzylamino)-3-(1H-indol-3-yl)-1-oxopropan-2-yl)amino)-4-methyl-1-oxopentan-2-yl)carbamate, obtained from **58** and Boc-*L*-Leu-OU according to the general procedure **A**, following the general procedure **B**. White powder (78% yield). $^1$H NMR (400 MHz, $CD_3OD$): δ 0.71 (d, 3H, C$H_3$, *J* = 6.4 Hz); 0.75 (d, 3H, C$H_3$, *J* = 6.4 Hz); 1.23-1.30 (m, 3H, C*H* and C$H_2$); 3.11 (t, 1H, C$H_{2a,}$ *J* = 14.1 Hz); 3.48 (dd, 1H, C$H_{2b,}$ *J'* = 4.8, *J''* = 14.6 Hz); 3.90 (t, 1H, C*H*, *J* = 7.4 Hz); 4.34 (d, 1H, C$H_{2a,}$ *J* = 15.0 Hz); 4.45 (d, 1H, C$H_{2a,}$ *J* = 14.8 Hz); 4.81-4.84 (m, 1H, C*H*); 7.02 (t, 1H, aryl, *J* = 7.7 Hz); 7.07 (s, 1H, aryl); 7.10 (t, 1H, aryl, *J* = 7.2 Hz); 7.19-7.28 (m, 5H, aryl); 7.35 (d, 1H, aryl, *J* = 8.1 Hz); 7.63 (d, 1H, aryl, *J* = 7.9 Hz). HR-MS m/z calcd for $C_{24}H_{30}N_4O_2$[(M + H)]$^+$: 407.2442; found 407.2445.

***(S)-N-((R)-1-(benzylamino)-3-(1H-indol-3-yl)-1-oxopropan-2-yl)-2-(2-chloroacetamido)-4-methylpentanamide (60)***

Derivative **60** was synthetized starting from **59** and chloroacetyl chloride following the general procedure **F**. FC in ethyl acetate/methanol 9.8/0.2, R*f*: 0.45. White powder (52% yield). $^1$H NMR (400 MHz, $CD_3OD$): δ: 0.73 (d, 3H, C$H_3$, *J* = 6.5 Hz); 0.76 (d, 3H, C$H_3$, *J* = 6.5 Hz); 1.14-1.21 (m, 1H, C*H*); 1.32 (t, 2H, C$H_2$, *J* = 7.4 Hz); 3.08 (dd,

1H, C$H_{2a,}$ *J'* = 9.7, *J''* = 14.6 Hz); 3.45 (dd, 1H, C$H_{2b,}$ *J'* = 8.3, *J''* = 14.6 Hz); 3.92 (q, 2H, C$H_2$, *J* = 13.5 Hz ); 4.21 (t, 1H, C*H*, *J* = 7.6 Hz ); 4.40 (q, 2H, C$H_2$, *J* = 15.0 Hz ); 4.78 (dd, 1H, C$H_{2a,}$ *J'* = 8.3, *J''* = 14.6 Hz); 7.03 (t, 1H, aryl, *J* = 7.8 Hz); 7.08 (s, 1H, aryl); 7.11 (t, 1H, aryl, *J* = 7.2 Hz); 7.23 (t, 3H, aryl, *J* = 7.6 Hz); 7.27-7.30 (m, 2H, aryl); 7.35 (d, 1H, aryl, *J* = 8.1 Hz); 7.62 (d, 1H, aryl, *J* = 7.9 Hz).$^{13}$C NMR (100 MHz, $CD_3OD$) δ: 21.0, 21.4, 24.1, 27.2, 39.9, 41.4, 42.7, 52.8, 54.3, 109.6, 110.9, 118.0, 118.5, 121.0, 123.2, 126.7, 127.16, 127.22, 128.0, 136.8, 138.3, 168.0, 172.4, 173.1. HR-MS m/z calcd for $C_{26}H_{31}ClN_4O_3$ $[(M + H)]^+$: 483.2157; found 483.2163.

***tert-butyl (S)-(3-(1H-indol-3-yl)-1-((2-morpholinoethyl)amino)-1-oxopropan-2-yl)carbamate (61)***

Intermediate **61** was synthetized starting from Boc-*L*-Trp-OH and 4-(2-aminoethyl)morpholine following the general procedure **A**. FC in ethyl acetate, R*f*: 0.48. Whitish oil (74% yield). $^1$H NMR (400 MHz, $CD_3OD$): δ 1.42 (s, 9H, C$H_3$); 2.24-2.29 (m, 2H, C$H_2$); 2.36 (bs, 4H, C$H_2$); 3.09-3.26 (m, 6H, C$H_2$); 2.87-2.94 (m, 2H, C$H_2$); 3.60 (bs, 4H, C$H_2$); 4.29 (t, 1H, C*H*, *J* = 6.8 Hz); 7.03 (t, 1H, aryl, *J* = 7.0 Hz); 7.09-7.13 (m, 2H, aryl); 7.35 (d, 1H, aryl, *J* = 8.0 Hz); 7.59 (d, 1H, aryl, *J* = 7.9 Hz). HR-MS m/z calcd for $C_{22}H_{32}N_4O_4$ $[(M + H)]^+$: 417.2496; found 417.2499.

***tert-butyl ((S)-1-(((S)-3-(1H-indol-3-yl)-1-((2-morpholinoethyl)amino)-1-oxopropan-2-yl)amino)-1-oxobut-3-en-2-yl)carbamate (62)***

Intermediate **62** was synthetized starting from (S)-2-amino-3-(1H-indol-3-yl)-N-(2-morpholinoethyl)propenamide obtained from **61** according to the general procedure **B**, and Boc-allyl-Gly-OH following the general procedure **A**. FC in ethyl acetate/methanol 9.6/0.4, R*f*: 0.47. Whitish oil (58% yield). $^1$H NMR (400 MHz, $CD_3OD$): δ 1.40 (s, 9H, C$H_3$); 2.12-2.22 (m, 2H, C$H_2$); 2.24-2.36 (m, 4H, C$H_2$); 2.45-

2.51 (m, 1H, C$H_{2a}$); 3.07-3.14 (m, 1H, C$H_{2b}$); 3.18-3.27 (m, 2H, C$H_2$); 3.58 (t, 4H, C$H_2$, *J* = 4.6 Hz); 4.04 (dd, 1H, C*H*, *J'* = 5.1, *J''* = 8.4 Hz); 4.59 (t, 1H, C*H*, *J* = 6.6 Hz); 5.06-5.13 (m, 2H C$H_2$); 5.68-5.76 (m, 1H C*H*); 7.04 (t, 1H, aryl, *J* = 7.6 Hz); 7.12 (d, 1H, aryl, *J* = 8.0 Hz); 7.15 (s, 1H, aryl); 7.35 (d, 1H, aryl, *J* = 8.1 Hz); 7.60 (d, 1H, aryl, *J* = 7.8 Hz). HR-MS m/z calcd for $C_{26}H_{37}N_5O_5$ $[(M + H)]^+$: 500.2867; found 500.2867.

***(S)-N-((S)-3-(1H-indol-3-yl)-1-((2-morpholinoethyl)amino)-1-oxopropan-2-yl)-2-(2-chloroacetamido)pent-4-enamide (63)***

Derivative **63** was synthetized starting from (S)-N-((S)-3-(1H-indol-3-yl)-1-((2-morpholinoethyl)amino)-1-oxopropan-2-yl)-2-aminopent-4-enamide obtained from **62** according to the general procedure **B**, and chloroacetyl chloride following the general procedure **F**. FC in ethyl acetate/methanol 9.5/0.5, R*f*: 0.47. White powder (52% yield). $^1$H NMR (400 MHz, $CD_3OD$): δ: 2.35-2.40 (m, 1H, C$H_{2a}$); 2.45-2.51 (m, 1H, C$H_{2b}$); 3.04-3.14 (m, 4H, C$H_2$); 3.24-3.37 (m, 8H, C$H_2$); 3.39-3.44 (m, 1H, C$H_{2a}$); 3.56-3.62 (m, 1H, C$H_{2b}$); 4.13 (s, 2H, C$H_2$); 4.31 (dd, 1H, C*H, J'* = 5.5; *J''* = 8.3 Hz); 4.52 (t, 1H, C*H*, *J* = 7.4 Hz); 5.04-5.11 (m, 2H, C$H_2$); 5.62-5.72 (m, 1H, C*H*); 7.06 (t, 1H, aryl, *J* = 7.7 Hz); 7.13 (t, 1H, aryl, *J* = 8.0 Hz); 7.19 (s, 1H, aryl); 7.38 (d, 1H, aryl, *J* = 8.1 Hz); 7.61 (d, 1H, aryl, *J* = 7.8 Hz).$^{13}$C NMR (100 MHz, $CD_3OD$) δ: 26.6, 33.6, 35.2, 41.8, 52.1, 54.0, 55.1, 56.5, 63.6, 109.2, 111.1, 117.7, 118.0, 118.6, 121.2, 123.5, 127.4, 132.7, 136.7, 168.5, 172.1, 173.5. HR-MS m/z calcd for $C_{24}H_{32}ClN_5O_4$ $[(M + H)]^+$: 490.2216; found 490.2223.

***methyl (tert-butoxycarbonyl)-L-tryptophyl-L-leucinate (64)***

Intermediate **64** was synthetized starting from Boc-*L*-Trp-OH and *L*-Leu-OMe following the general procedure **A**. FC in hexane/ethyl acetate 7/3, R*f*: 0.47. Whitish

oil (77% yield). $^1$H NMR (400 MHz, $CDCl_3$): δ 0.83-0.89 (m, 6H, C*H*$_3$); 1.42-1.54 (m, 12H, C*H*$_3$ and C*H*$_2$ and C*H*); 3.18-3.24 (m, 2H, C*H*$_2$); 3.62 (s, 3H, C*H*$_3$); 4.47-4.46 (m, 2H, C*H*); 5.30 (bs, 1H, N*H*); 6.46 (bs, 1H, N*H*); 4.29 (t, 1H, C*H*, *J* = 6.8 Hz); 7.04 (s, 1H, aryl); 7.08 (t, 1H, aryl, *J* = 7.8 Hz); 7.16 (t, 1H, aryl, *J* = 7.2 Hz); 7.33 (d, 1H, aryl, *J* = 8.0 Hz); 7.63 (d, 1H, aryl, *J* = 7.8 Hz); 8.83 (s, 1H, N*H*). HR-MS m/z calcd for $C_{23}H_{33}N_3O_5$ $[(M + H)]^+$: 432.2493; found 432.2489.

***tert-butyl ((S)-1-(((S)-1-(benzylamino)-4-methyl-1-oxopentan-2-yl)amino)-3-(1H-indol-3-yl)-1-oxopropan-2-yl)carbamate (65)***

Intermediate **65** was synthetized starting from (tert-butoxycarbonyl)-L-tryptophyl-L-leucine obtained from **64** according to general procedure **G**, and benzylamine following the general procedure **A**. FC in hexane/ethyl acetate 1/1, R*f*: 0.47. White powder (58% yield). $^1$H NMR (400 MHz, $CD_3OD$): δ 0.87-0.92 (m, 6H, C*H*$_3$); 1.19-1.27 (m, 2H, C*H*$_2$); 1.32-1.38 (m, 10H, C*H*$_3$ and C*H*); 3.07-3.12 (m, 1H, C*H*$_{2a}$); 3.23-3.28 (m, 1H, C*H*$_{2b}$); 4.24-4.34 (m, 2H, C*H*$_2$); 4.39-4.42 (m, 2H, C*H*); 4.29 (t, 1H, C*H*, *J* = 6.8 Hz); 7.01-7.12 (m, 4H, aryl); 7.23-7.35 (m, 4H, aryl); 7.61 (d, 1H, aryl, *J* = 7.0 Hz); 7.96 (d, 1H, aryl, *J* = 7.9 Hz). HR-MS m/z calcd for $C_{29}H_{38}N_4O_4$ $[(M + H)]^+$: 507.2966; found 507.2960.

***(S)-N-benzyl-2-((S)-2-(2-chloroacetamido)-3-(1H-indol-3-yl)propanamido)-4-methylpentanamide (66)***

Derivative **66** was synthetized starting from (S)-2-((S)-2-amino-3-(1H-indol-3-yl)propanamido)-N-benzyl-4-methylpentanamide obtained from **65** according to the general procedure B, and chloroacetyl chloride following the general procedure **F**. FC in hexane/ethyl acetate 2/8, R*f*: 0.47. White powder (48% yield). $^1$H NMR (400 MHz, $CD_3OD$): δ: 0.88 (d, 3H, C*H*$_3$, *J* = 6.0 Hz); 0.91 (d, 3H, C*H*$_3$, *J* = 6.0 Hz); 1.56-1.58

(m, 3H, C$H_2$ and C$H$); 3.18 (dd, 1H, C$H_{2a,}$ $J'$ = 7.3, $J''$ = 14.6 Hz); 3.29-3.35 (m, 1H, C$H_{2b}$); 4.02 (dd, 2H, C$H_{2,}$ $J'$ = 13.8; $J''$ = 16.6 Hz); 4.29 (dd, 2H, C$H_{2,}$ $J'$ = 15.0; $J''$ = 20.4 Hz); 4.41 (t, 1H, C$H$, $J$ = 6.1 Hz ); 4.73 (t, 1H, C$H$, $J$ = 6.8 Hz); 7.03 (t, 1H, aryl, $J$ = 7.0 Hz); 7.09-7.12 (m, 2H, aryl); 7.23-7.25 (m, 3H, aryl); 7.29-7.34 (m, 3H, aryl); 7.60 (d, 1H, aryl, $J$ = 6.3 Hz).$^{13}$C NMR (100 MHz, $CD_3OD$) δ: 20.6, 22.0, 24.3, 27.3, 40.4, 41.7, 42.6, 52.0, 54.5, 109.0, 111.0, 118.0, 118.6, 121.2, 123.3, 126.8, 127.0, 127.2, 128.1, 136.6, 138.4, 167.8, 172.1, 172.9. HR-MS m/z calcd for $C_{26}H_{31}ClN_4O_3$ $[(M + H)]^+$: 482.2085; found 482.2078.

***methyl L-tryptophyl-L-leucinate (67)***

Intermediate **67** was synthetized starting from **64** following the general procedure **B**. White powder (88% yield). $^1$H NMR (400 MHz, $CD_3OD$): δ 0.93-0.98 (m, 6H, C$H_3$); 1.22-1.26 (m, 2H, C$H_2$); 1.63-1.68 (m, 1H, C$H$); 3.20-3.27 (m, 1H, C$H_{2a}$); 3.48 (dd, 1H, C$H_{2b,}$ $J'$ = 5.9, $J''$ = 14.9 Hz); 3.70 (s, 3H, C$H_3$); 4.20-4.25 (m, 1H, C$H$); 4.53 (t, 1H, C$H$, $J$ = 7.2 Hz); 7.08 (t, 1H, aryl, $J$ = 7.0 Hz); 7.16 (t, 1H, aryl, $J$ = 7.9 Hz); 7.26 (s, 1H, aryl); 7.40 (d, 1H, aryl, $J$ = 8.1 Hz); 7.70 (d, 1H, aryl, $J$ = 7.8 Hz). HR-MS m/z calcd for $C_{18}H_{25}N_3O_3$ $[(M + H)]^+$: 332.1969; found 332.1965.

***methyl (2-chloroacetyl)-L-tryptophyl-L-leucinate (68)***

Derivative **68** was synthetized starting from **67** and chloroacetyl chloride following the general procedure **F**. FC in hexane/ethyl acetate 2/8, R$f$: 0.47. White powder (66% yield). $^1$H NMR (400 MHz, $CD_3OD$): δ: 0.90 (d, 3H, C$H_3$, $J$ = 6.2 Hz); 0.93 (d, 3H, C$H_3$, $J$ = 6.3 Hz); 1.57-1.68 (m, 3H, C$H_2$ and C$H$); 3.16 (dd, 1H, C$H_{2a,}$ $J'$ = 7.4, $J''$ = 14.7 Hz); 3.30-3.35 (m, 1H, C$H_{2b}$); 3.67 (s, 3H, C$H_3$); 4.02 (dd, 2H, C$H_{2,}$ $J'$ = 13.8; $J''$ = 15.8 Hz); 4.48 (t, 1H, C$H$, $J$ = 7.9 Hz ); 4.75 (t, 1H, C$H$, $J$ = 6.4 Hz); 7.03 (t, 1H, aryl, $J$ = 7.1 Hz); 7.10 (t, 1H, aryl, $J$ = 8.1 Hz); 7.14 (s, 1H, aryl); 7.34 (d, 1H, aryl, $J$

= 8.0 Hz); 7.62 (d, 1H, aryl, *J* = 7.9 Hz).$^{13}$C NMR (100 MHz, $CD_3OD$) δ: 20.5, 21.8, 24.4, 27.5, 40.1, 41.7, 50.8, 51.2, 54.2, 109.0, 110.8, 117.9, 118.4, 121.0, 123.4, 127.5, 136.6, 167.4, 172.1, 172.9. HR-MS m/z calcd for $C_{20}H_{26}ClN_3O_4$ $[(M + H)]^+$: 408.1685; found 408.1678.

***benzyl (S)-(3-(1H-indol-3-yl)-1-(methoxy(methyl)amino)-1-oxopropan-2-yl)carbamate (69)***

Intermediate **69** was synthetized starting from Z-*L*-Trp-OH and N,O-dimethylhydroxylamine hydrochloride following the general procedure **A**. FC in hexane/ethyl acetate 7/3, R*f*: 0.47. Whitish oil (85% yield). $^1$H NMR (400 MHz, $CDCl_3$): δ 3.19-3.25 (m, 4H, C*H*$_3$ and C*H*$_{2a}$); 3.40-3.48 (m, 1H, C*H*$_{2b}$); 3.64 (s, 3H, C*H*$_3$); 5.07-5.18 (m, 2H, C*H*$_2$); 6.03 (d, 1H, C*H*, *J* = 7.6 Hz); 6.97 (s, 1H, aryl); 7.17-7.26 (m, 2H, aryl); 7.34-7.37 (m, 5H, aryl); 7.70 (d, 1H, aryl, *J* = 7.9 Hz); 9.00 (s, 1H, N*H*). HR-MS m/z calcd for $C_{21}H_{23}N_3O_4$ $[(M + H)]^+$: 382.1761; found 382.1758.

**Synthesis of benzyl (S)-(1-(benzylamino)-3-(1H-indol-3-yl)propan-2-yl)carbamate (70)**

Intermediate **69** (0.1 mmol) was dissolved in dry THF under nitrogen atmosphere and the temperature was set at 0°C. The mixture was added with 2.5 eq of 1M $LiAlH_4$ solution in THF and stirred for 6 minutes. Then, the crude was quenched with a solution of citric acid (10% w:w), diluted with DCM, extracted three times, dried over sodium sulfate, and concentrated under vacuum. The obtained aldehyde intermediate was dissolved in dry MeOH under a positive nitrogen flux at room temperature, then benzylamine (1.2 eq) was added. The mixture was stirred at room temperature for 12 hours, then $NaBH_4$ (3 eq) was added. After 30 minutes the organic phase was quenched with a solution of citric acid (10% w:w), concentrated in vacuo, diluted with ethyl

acetate and extracted (3 x 100 mL). The obtained mixture was dried over sodium sulfate, concentrated under vacuum and purified by flash chromatography using mixture of n-hexane/ethyl acetate (4:1 v:v) as mobile phase., R*f*: 0.45. Whitish oil (52% yield). $^1$H NMR (400 MHz, $CDCl_3$): δ 2.38-2.53 (m, 2H, C$H_{2a}$ and C$H_{2a}$ ); 2.67-2.81 (m, 2H, C$H_{2b}$ and C$H_{2b}$); 3.32 (d, 1H, C$H_{2a}$, *J* = 12.9 Hz); 3.43 (d, 1H, C$H_{2b}$, *J* = 12.9 Hz); 3.99 (bs, 1H, C*H*); 4.85 (s, 2H, C$H_2$); 6.80 (s, 1H, aryl); 6.86 (t, 1H, aryl, *J* = 7.1 Hz); 6.92-7.07 (m, 10H, aryl); 7.18 (d, 2H, aryl, *J* = 7.9 Hz); 7.47 (d, 1H, aryl, *J* = 7.7 Hz);. HR-MS m/z calcd for $C_{26}H_{27}N_3O_2$ $[(M + H)]^+$: 414.2176; found 414.2178.

***tert-butyl (S)-(2-amino-3-(1H-indol-3-yl)propyl)(benzyl)carbamate (71)***

Intermediate **71** was synthetized starting from (S)-(1-(benzyl(tert-butoxycarbonyl)amino)-3-(1H-indol-3-yl)propan-2-yl) obtained from **70** using the general procedure **F**, following the general procedure **H**. FC in hexane/ethyl acetate 1/1, R*f*: 0.47. white powder (88% yield). $^1$H NMR (400 MHz, $CD_3OD$): δ 1.45 (s, 9H, C$H_3$); 2.71 (dd, 1H, C$H_{2a,}$ *J'* = 7.4, *J''* = 14.2 Hz); 2.85-2.89 (m, 1H, C$H_{2b}$); 3.30-3.35 (m, 4H, C$H_2$); 3.36-3.42 (m, 1H, C*H*); 7.01 (t, 1H, aryl, *J* = 7.6 Hz); 7.05 (s, 1H, aryl); 7.10-7.14 (m, 3H, aryl); 7.23-7.29 (m, 3H, aryl); 7.36 (d, 1H, aryl, *J* = 7.7 Hz); 7.48 (d, 1H, aryl, *J* = 7.6 Hz). HR-MS m/z calcd for $C_{23}H_{29}N_3O_2$ $[(M + H)]^+$: 380.2333; found 380.2230.

***tert-butyl ((S)-2-((S)-2-aminobut-3-enamido)-3-(1H-indol-3-yl)propyl)(benzyl)carbamate (72)***

Intermediate **72** was synthetized from tert-butyl ((S)-2-((S)-2-((((9H-fluoren-9-yl)methoxy)carbonyl)amino)but-3-enamido)-3-(1H-indol-3-yl)propyl)(benzyl)carbamate, obtained from **71** and Fmoc-*L*-allyl-Gly-OH using the general procedure **A**, following the general procedure **I**. Yellowish powder (78%

yield). $^1$H NMR (400 MHz, $CD_3OD$): δ 1.37 (s, 9H, C*H*$_3$); 2.15-2.23 (m, 1H, C*H*$_{2a}$); 2.26-2.31 (m, 1H, C*H*$_{2b}$); 3.42-3.50 (m, 1H, C*H*); 4.07-4.19 (m, 2H, C*H*$_2$); 4.31-4.42 (m, 2H, C*H*$_2$); 4.50-4.54 (m, 1H, C*H*); 4.95 (d, 1H, C*H*$_{2a}$, *J* = 10.6 Hz); 5.02-5.10 (m, 2H, C*H*$_{2b}$ and C*H*); 7.00-7.03 (m, 2H, aryl); 7.09 (t, 1H, aryl, *J* = 7.9 Hz); 7.27-7.32 (m, 2H, aryl); 7.34-7.39 (m, 2H, aryl); 7.56-7.62 (m, 2H, aryl); 7.77 (t, 1H, aryl, *J* = 7.8 Hz). HR-MS m/z calcd for $C_{27}H_{34}N_4O_3$ $[(M + H)]^+$: 463.2704; found 463.2700.

***tert-butyl ((2S)-2-((2S)-2-(2-aminobut-3-enamido)but-3-enamido)-3-(1H-indol-3-yl)propyl)(benzyl)carbamate (73)***

Intermediate **73** was synthetized from tert-butyl ((8S,11S)-11-((1H-indol-3-yl)methyl)-1-(9H-fluoren-9-yl)-3,6,9-trioxo-5,8-divinyl-2-oxa-4,7,10-triazadodecan-12-yl)(benzyl)carbamate, obtained from **72** and Fmoc-*L*-allyl-Gly-OH using the general procedure **A**, following the general procedure **I**. Yellowish powder (72% yield). $^1$H NMR (400 MHz, $CD_3OD$): δ 1.41 (s, 9H, C*H*$_3$); 2.14-2.24 (m, 1H, C*H*$_{2a}$); 2.29-2.39 (m, 1H, C*H*$_{2b}$); 2.87-2.94 (m, 2H, C*H*$_2$); 3.27 (t, 2H, C*H*$_2$, *J* =7.0 Hz); 3.47-3.58 (m, 1H, C*H*); 4.16-4.27 (m, 1H, C*H*); 4.43-4.51 (m, 1H, C*H*); 5.00-5.10 (m, 2H, C*H*$_{2a}$); 5.53-5.68 (m, 4H, C*H*$_{2b}$ and C*H*); 7.01-7.05 (m, 3H, aryl); 7.11 (t, 1H, aryl, *J* = 8.0 Hz); 7.18-7.23 (m, 4H, aryl); 7.35 (d, 1H, aryl, *J* = 8.2 Hz); 7.60 (t, 1H, aryl, *J* = 8.1 Hz). HR-MS m/z calcd for $C_{31}H_{39}N_5O_4$ $[(M + H)]^+$: 546.3075; found 546.3079.

***(S)-N-((S)-1-(benzylamino)-3-(1H-indol-3-yl)propan-2-yl)-2-((S)-2-(2-chloroacetamido)pent-4-enamido)pent-4-enamide (74)***

Derivative **74** was synthetized starting from tert-butyl benzyl((S)-2-((S)-2-((S)-2-(2-chloroacetamido)pent-4-enamido)pent-4-enamido)-3-(1H-indol-3-yl)propyl)carbamate obtained from **73** and chloroacetyl chloride according to procedure **F**, following the general procedure **B**. White powder (78% yield). $^1$H NMR

(400 MHz, $CD_3OD$): δ: 2.36-2.59 (m, 4H, C*H*$_2$); 2.81-2.86 (m, 2H, C*H*$_2$); 2.95 (dd, 1H, C*H*$_{2a}$, *J'* = 7.3; *J''* = 14.5 Hz); 3.00 (dd, 1H, C*H*$_{2b}$, *J'* = 6.3; *J''* = 14.5 Hz); 3.69 (d, 1H, C*H*$_{2a}$, *J* = 12.8 Hz); 3.82 (d, 1H, C*H*$_{2b}$, *J* = 12.8 Hz); 4.11 (s, 2H, C*H*$_2$); 4.30 (t, 1H, C*H*, *J* = 6.1 Hz); 4.36 (t, 1H, C*H*, *J* = 6.5 Hz); 4.42-4.49 (m, 1H, C*H*); 4.98-5.18 (m, 4H, C*H*$_2$); 5.64-5.83 (m, 2H, C*H*$_2$); 7.04 (t, 1H, aryl, *J* = 7.8 Hz); 7.09-7.13 (m, 2H, aryl); 7.23-7.31 (m, 5H, aryl); 7.35 (d, 1H, aryl, *J* = 7.9 Hz); 7.62 (d, 1H, aryl, *J* = 8.0 Hz).$^{13}$C NMR (100 MHz, $CD_3OD$) δ: 28.2, 35.5, 41.7, 49.1, 51.2, 52.3, 53.8, 110.4, 110.9, 117.4, 117.7, 118.0, 118.4, 121.0, 122.9, 127.2, 127.6, 128.1, 128.5, 129.4, 132.8, 132.2, 136.7, 168.3, 171.9. HR-MS m/z calcd for $C_{30}H_{36}ClN_5O_3$ $[(M + H)]^+$: 550.2579; found 550.2577.

***methyl (S)-2-((S)-2-(((benzyloxy)carbonyl)amino)-3-(1H-indol-3-yl)propanamido)-6-oxo-6-(tritylamino)hexanoate (75)***

Intermediate **75** was synthetized starting from Z-*L*-Trp-OH and *L*-Gln(Trt)-OMe following the general procedure **A**. FC in hexane/ethyl acetate 1/1, R*f*: 0.47. Whitish oil (72% yield). $^1$H NMR (400 MHz, $CD_3OD$): δ 1.75-1.83 (m, 1H, C*H*$_{2a}$); 2.03-2.13 (m, 1H, C*H*$_{2b}$); 2.25-2.32 (m, 1H, C*H*$_{2a}$); 2.34-2.43 (m, 1H, C*H*$_{2b}$); 3.12 (dd, 1H, C*H*$_{2a}$, *J'* = 7.7, *J''* = 14.5 Hz); 3.14 (dd, 1H, C*H*$_{2b}$, *J'* = 6.4, *J''* = 14.5 Hz); 3.64 (s, 3H, C*H*$_3$); 4.43 (t, 1H, C*H*, *J* = 5.9 Hz); 4.89-4.94 (m, 2H, C*H* and C*H*$_{2a}$); 4.96 (d, 1H, C*H*$_{2b}$, *J* = 12.5 Hz); 7.00 (t, 1H, aryl, *J* = 7.2 Hz); 7.09 (t, 1H, aryl, *J* = 7.2 Hz); 7.19-7.29 (m, 21H, aryl); 7.34 (d, 1H, aryl, *J* = 8.4 Hz); 7.59 (d, 1H, aryl, *J* = 8.8 Hz). HR-MS m/z calcd for $C_{45}H_{44}N_4O_6$ $[(M + H)]^+$: 737.3334; found 737.3331.

***methyl (5S,8S,11S)-8-((1H-indol-3-yl)methyl)-1-(9H-fluoren-9-yl)-5-isobutyl-3,6,9-trioxo-11-(4-oxo-4-(tritylamino)butyl)-2-oxa-4,7,10-triazadodecan-12-oate (76)***

Intermediate 76 was synthetized starting from methyl (S)-2-((S)-2-amino-3-(1H-indol-3-yl)propanamido)-6-oxo-6-(tritylamino)hexanoate obtained from 75 using the general procedure H, following the general procedure A. FC in hexane/ethyl acetate 3/7, Rf: 0.47. Whitish oil (68% yield). 1H NMR (400 MHz, CD3OD): δ 0.83 (d, 3H, $CH_3$, J = 6.6 Hz); 0.88 (d, 3H, $CH_3$, J = 6.6 Hz); 1.20-1.29 (m, 1H, $CH_{2a}$); 1.35-1.41 (m, 1H, $CH_{2b}$); 1.48-1.60 (m, 1H, CH); 1.74-1.84 (m, 1H, $CH_{2a}$); 2.03-2.09 (m, 1H, $CH_{2b}$); 2.29-2.35 (m, 2H, $CH_2$); 3.18 (dd, 1H, $CH_{2a}$, J' = 7.8, J" = 14.5 Hz); 3.27-3.33 (m, (s, 3H, $CH_3$); 4.03 (t, 1H, CH, J = 7.5 Hz); 4.15 (t, 1H, CH, J = 9.4 Hz); 4.24 (d, 2H, $CH_2$, J = 7.6 Hz); 4.37-4.41 (m, 1H, CH); 4.64 (t, 1H, CH, J = 6.9 Hz); 6.99 (t, 1H, aryl, J = 7.2 Hz); 7.06 (t, 1H, aryl, J = 7.7 Hz); 7.11 (s, 1H, aryl); 7.15-7.25 (m, 16H, aryl); 7.30 (t, 2H, aryl, J = 7.4 Hz); 7.40 (t, 2H, aryl, J = 7.5 Hz); 7.56 (d, 1H, aryl, J = 7.9 Hz); 7.61 (t, 2H, aryl, J = 7.2 Hz); 7.81 (d, 2H, aryl, J = 7.5 Hz). HR-MS m/z calcd for $C_{58}H_{59}N_5O_7$ $[(M + H)]^+$: 938.4487; found 938.4495.

***methyl (2-chloroacetyl)-L-leucyl-L-tryptophyl-L-glutaminate (77)***

Derivative **77** was synthetized starting from methyl N2-(2-chloroacetyl)-*L*-leucyl-*L*-tryptophyl-N5-trityl-*L*-glutaminate, which was obtained from **76**, previously subjected to Fmoc deprotection according to the general procedure **I** and acylation reaction with chloroacetyl chloride according to the procedure **F**, following the general procedure **B**. White powder (38% yield). $^1$H NMR (400 MHz, $CD_3OD$): δ: 0.88 (d, 3H, C*H*$_3$, *J* = 6.4 Hz); 0.92 (d, 3H, C*H*$_3$, *J* = 6.4 Hz); 1.51 (t, 2H, C*H*$_2$, *J* = 8.2 Hz); 1.58-1.63 (m, 1H, C*H*); 1.86-1.96 (m, 1H, C*H*$_{2a}$); 2.09-2.29 (m, 3H, C*H*$_2$ and C*H*$_{2b}$);

3.19 (dd, 1H, C$H_{2a,}$ *J'* = 7.8, *J''* = 14.7 Hz); 3.29-3.36 (m, 1H, C$H_{2b}$); 3.68 (s, 3H, C$H_3$); 4.01 (q, 2H, C$H_{2,}$ *J* = 13.4 Hz); 4.36-4.43 (m, 1H, C*H*); 4.67 (t, 1H, C*H*, *J* = 6.4 Hz); 7.03 (t, 1H, aryl, *J* = 7.4 Hz); 7.10 (t, 1H, aryl, *J* = 7.8 Hz); 7.14 (s, 1H, aryl); 7.35 (d, 1H, aryl, *J* = 8.0 Hz); 7.60 (d, 1H, aryl, *J* = 7.9 Hz).$^{13}$C NMR (100 MHz, $CD_3OD$) δ: 20.5, 21.9, 24.4, 27.0, 31.0, 40.1, 41.6, 48.0, 51.4, 51.8, 52.3, 54.2, 109.2, 110.9, 117.9, 118.4, 121.0, 123.4, 127.5, 136.6, 168.0, 171.8, 172.5, 172.7, 176.2. HR-MS m/z calcd for $C_{25}H_{34}ClN_5O_6$ $[(M + H)]^+$: 536.2270; found 536.2265.

**Synthesis of methyl benzyl-L-leucinate (78)**

Intermediate **78** was synthetized starting from *L*-Leu-OMe following the general procedure **C**. FC in hexane/ethyl acetate (8:2 v:v) as mobile phase., R*f*: 0.45. Whitish oil (72% yield). $^1$H NMR (400 MHz, $CD_3OD$): δ 0.85 (d, 3H, C$H_3$, *J* = 6.6 Hz); 0.92 (d, 3H, C$H_3$, *J* = 6.6 Hz); 1.50 (t, 2H, C$H_{2,}$ *J* = 8.5 Hz); 1.66-1.74 (m, 1H, C*H*); 3.30 (t, 1H, C*H*, *J* = 7.2 Hz); 3.61 (d, 1H, C$H_{2a,}$ *J* = 13.0); 3.71 (s, 3H, C$H_3$); 3.78 (d, 1H, C$H_{2b,}$ *J* = 13.0); 7.23-7.33 (m, 5H, aryl). HR-MS m/z calcd for $C_{14}H_{21}NO_2$[(M + H)]$^+$: 235.1572; found 235.1566.

***N-benzyl-N-(tert-butoxycarbonyl)-L-leucine (79)***

Intermediate **79** was synthetized starting from methyl N-benzyl-N-(tert-butoxycarbonyl)-*L*-leucinate, obtained from methyl benzyl-*L*-leucinate and di-tert-butyl dicarbonate according to the general procedure **C**, following the general procedure **G**. White powder (38% yield). $^1$H NMR (400 MHz, $CD_3OD$): δ 0.64 (d, 3H, C$H_3$, *J* = 6.2 Hz); 0.77 (d, 3H, C$H_3$, *J* = 6.2 Hz); 1.50-1.60 (m, 11H, C$H_2$ and C$H_3$); 1.63-1.72 (m, 1H, C*H*); 4.20 (t, 1H, C*H*, *J* = 6.1 Hz); 4.28 (d, 1H, C$H_{2a,}$ *J* = 14.2); 4.41 (d, 1H, C$H_{2b,}$ *J* = 14.0); 7.23-7.33 (m, 5H, aryl). HR-MS m/z calcd for $C_{18}H_{27}NO_4$[(M + H)]$^+$: 322.2013; found 322.2017.

***tert-butyl ((S)-1-((((3S,5S,7S)-adamantan-1-yl)methyl)amino)-4-methyl-1-oxopentan-2-yl)(benzyl)carbamate (80)***

Intermediate **80** was synthetized starting from **79** and 1-adamantanemethylamine following the general procedure **A**. FC in hexane/ethyl acetate 7/3, R*f*: 0.47. Whitish oil (68% yield). $^{1}$H NMR (400 MHz, $CD_3OD$): δ 0.89 (d, 6H, C*H*$_3$, *J* = 6.2 Hz); 1.42 (bs, 6H, C*H*$_2$); 1.48 (s, 9H, C*H*$_3$); 1.66 (d, 3H, C*H*$_2$ and C*H*$_{2b}$, *J* = 11.4 Hz); 1.77 (d, 3H, C*H*$_2$ and C*H*$_{2b}$, *J* = 11.4 Hz); 1.96 (bs, 3H, C*H*); 2.78-2.86 (m, 2H, C*H*$_2$); 4.39 (d, 1H, C*H*$_{2a,}$ *J* = 15.1); 4.43 (d, 1H, C*H*$_{2b,}$ *J* = 14.9); 4.60 (bs, 1H, C*H*); 7.23-7.34 (m, 5H, aryl). HR-MS m/z calcd for $C_{29}H_{44}N_2O_3$[(M + H)]$^+$: 469.3425; found 469.3422.

***(S)-N-(((3S,5S,7S)-adamantan-1-yl)methyl)-2-(N-benzyl-2-chloroacetamido)-4-methylpentanamide (81)***

Derivative **81** was synthetized starting from (S)-N-(((3S,5S,7S)-adamantan-1-yl)methyl)-2-(benzylamino)-4-methylpentanamide obtained from **80** according to the general procedure **B**, and chloroacetyl chloride following the general procedure **F**. FC in hexane/ethyl acetate 7/3, R*f*: 0.47. White powder (38% yield). $^{1}$H NMR (400 MHz, $CDCl_3$): δ: 0.87 (d, 3H, C*H*$_3$, *J* = 6.7 Hz); 0.90 (d, 3H, C*H*$_3$, *J* = 6.6 Hz); 1.39-1.58 (bs, 8H, C*H*$_2$); 1.64 (d, 3H, C*H*$_2$ and C*H*$_{2a}$, *J* = 11.8 Hz); 1.73 (d, 3H, C*H*$_2$ and C*H*$_{2b}$, *J* = 12.0 Hz); 1.89-2.00 (m, 4H, C*H*); 2.90 (dd, 1H, C*H*$_{2a,}$ *J'* = 6.0, *J''* = 13.4 Hz); 2.98 (dd, 1H, C*H*$_{2b,}$ *J'* = 6.5, *J''* = 13.4 Hz); 3.98 (s, 2H, C*H*$_2$); 4.66-4.77 (m, 2H, C*H*$_2$); 5.00 (dd, 1H, C*H,* *J'* = 6.2, *J''* = 8.4 Hz); 6.43 (bs, 1H, N*H*); 7.20 (d, 2H, aryl, *J* = 7.4 Hz); 7.32 (d, 1H, aryl, *J* = 7.1 Hz); 7.36-7.40 (m, 2H, aryl).$^{13}$C NMR (100 MHz, $CDCl_3$) δ: 22.3, 22.6, 22.9, 25.2, 28.2, 31.6, 33.7, 37.0, 40.2, 41.8, 48.5, 51.0, 57.2, 128.8, 127.7, 129.1, 136.8, 168.9, 170.2. HR-MS m/z calcd for $C_{26}H_{37}ClN_2O_2$ [(M + H)]$^+$: 444.2544; found 938.4495**.**

**Enzymatic assays**

***Mpro enzymatic assay***

The assay was performed in a volume of 25 µL in black 384-well OptiPlate. A fluorescent FRET substrate (DABCYL-KTSAVLQSGFRKME-EDANS) harboring the cleavage site of SARS-COV-2 Mpro and aqueous buffer solution (40 mM Tris-HCl, pH 8.0, 110 mM NaCl, 2.2 mM KCl, 20% glycerol, 3 mM DTT, 8 mM maltose) were used for the inhibition assay (BPS Bioscience 3CL Protease, MBP-tagged Assay). Mpro recombinant protease, at a final concentration of 150 ng per reaction, was preincubated for 30 min at room temperature with the compounds at different concentrations. Finally, the reaction was initiated by adding 5 µl of the FRET substrate to each well (final concentration, 50 µM). Buffer with the same amount of DMSO (1%) was used as control and Mpro inhibitor GC376 is also included as a positive control. The plate was covered with a TopSeal™-A PLUS sealing film to prevent contamination and evaporation of the samples and incubated for 4 hours at room temperature in subdued light.

The fluorescence signals (excitation/emission, 360 nm/460 nm) of released EDANS were read using a PerkinElmer EnSight multimode plate reader. The experiments were performed in triplicate. The $IC_{50}$ values were calculated using GraphPad Prism 8.0 software by nonlinear regression of dose-response inhibition.

***PLpro enzymatic assay***

The assay was performed in a volume of 50 µL in black 96-well OptiPlate. A fluorometric peptide Z-Arg-Leu-Arg-Gly-Gly-AMC (Z-RLRGG-AMC) was used as substrate in PLpro enzymatic assay (BPS Bioscience Papain-like Protease Assay:

Deubiquitinase Activity). Upon cleavage by PLpro, the fluorescence of the AMC moiety dramatically raises. For steady state measurement, the enzyme was incubated for 30 min at 37 °C (final concentration, 25 ng per reaction) with the compounds at different concentrations in assay buffer (40 mM Tris-HCl, pH 8, 110 mM NaCl, 2.2mM KCl, 0.04% Tween-20, 3 mM DTT, 20% glycerol and 115 mM Imidazole). Then, the reaction was initiated by adding 10 µl of the substrate to each well (final concentration, 250 nM). Buffer with the same amount of DMSO (1%) was used as control and $PL^{pro}$ inhibitor GRL0617 is also included as a positive control. The plate was covered with a TopSeal™-A PLUS sealing film to prevent contamination and evaporation of the samples and incubated in the dark for 50 min at 37 °C. The fluorescence signals (excitation/emission, 360 nm/460 nm) were read using a PerkinElmer EnSight multimode plate reader. The experiments were performed in triplicate. The $IC_{50}$ values were calculated using GraphPad Prism 8.0 software by nonlinear regression of dose-response inhibition.

***SPR binding assay***

SARS-Cov-2 Spike protein (S1) was acquired by Genscript Biotech, NE (cat. no. Z03501-1). Series S Sensor Chip CM5 8 (cat. no. BR100530), His Capture Kit (cat. no. 28995056), Amine Coupling Kit (cat. no. BR100050), HBS-P (cat. no. BR100368) were purchased from Cytiva.

The affinity of synthetic compounds for SARS-CoV-2 Spike protein (S1) was determined by SPR using a Biacore T200 (Cytiva) optical biosensor equipped with research-grade CM5 (Carboxy Methyl Dextran) sensor chip. Prior to the immobilization of the SP protein, a pH scouting was performed as follows. Solutions of 1.25 µM of the ligand in 10 mM sodium acetate with pH values ranging from 4.47

to 6 were prepared and injected onto the surface. The S protein (1.25 μM in 10 mM sodium acetate, pH 4.59) was immobilized by using standard amine-coupling protocol to obtain densities of 11500 RU. HBS-P buffer (0.01 M HEPES pH 7.4, 0.15 M NaCl, 0.005% (v/v) Surfactant P20) diluted 10× with Milli-Q water and supplemented with 5% DMSO was used as a running buffer. Stock solutions of compounds in 100% DMSO were prepared (10 mM). Running buffer was injected at a flow rate of 10 μL/min over the chip to clean and equilibrate the immobilizes sensor surface, then a solvent correction was performed as indicated in Laboratory Guideline 29-0057-18 AA, GE Healthcare Life Sciences. A series of increasing concentrations of compounds (0.75-100 μM) diluted in the ligand buffer were injected at 25 °C with a flow rate of 20 μL/min for 90s (association phase), and then the buffer alone was injected for 600 s (dissociation phase). A regeneration step was not necessary. The first channel was used as a reference surface. The experiments were performed in triplicate. The equilibrium dissociation constants ($K_D$) and kinetic dissociation ($k_d$) and association ($k_a$) constants were calculated from the sensorgrams by global fitting of a 1:1 binding model using evaluation software (v3.1) provided with the Biacore T200 instrument (Cytiva).

**Cellular assay**

SARS-CoV-2 antiviral assay Vero cells (ATCC-CCL81) were grown in Dulbecco's Modified Eagle's Medium (DMEM, ThermoFisher, Belgium) supplemented with 10% fetal calf serum (FCS), 2 mM L-glutamine, 0.1 mM non-essential amino acids, 1 mM sodium pyruvate, and 10 mM HEPES at 37 °C in a 5% $CO_2$ humidified atmosphere.

Variants of concern, kindly provided by Piet Maes (Laboratory of Clinical and Epidemiological Virology, Rega Institute, KU Leuven, Belgium) were used: UC-1074

(Wuhan variant), UC-1075 (Wuhan variant), NVDBB-2220 (Alpha variant) and RG-2674 (Beta variant), 860-J1(Delta variant) and B1.1529BA.1 (Omicron variant). All variants were used after 2–3 passages in cell culture. The infectious virus titer of the different variants was determined in Vero cells and expressed as 50% cell culture infectious dose (CCID50) per mL. For the antiviral assays, Vero cells were seeded in 96-well plates at a density of 1 x $10^4$ cells per well in DMEM 10% FCS medium. After 24 h growth, the medium was removed, and cells were treated with different compound concentrations in DMEM 2% FCS and mocked-infected or SARS-CoV-2-infected with 100 $CCID_{50}$ /well (final volume 200 µl / 450 well). After 5 days of incubation at 37°C, viral CPE was recorded microscopically, and the 50% effective concentration ($EC_{50}$) was calculated for each compound and remdesivir (reference anti-SARS-CoV-2 compound). In parallel, the cytotoxic effects of the compounds were assessed by evaluating the MCC (minimum cytotoxic concentration that causes a microscopically detectable alteration of cell morphology). The effects of the compounds on cell growth were determined by counting the number of cells with a Coulter counter in mock-infected cultures and expressed as the cytostatic concentration required to reduce cell growth by 50% ($CC_{50}$). All SARS-CoV-2-related work was conducted in the high-containment BSL3 facilities of the KU Leuven Rega Institute (3CAPS) under licenses AMV 30112018 SBB 219 2018 0892 and AMV 23102017 SBB 219 2017 0589 according to institutional guidelines.

**Computational details**

3D structures of SARS-CoV-2 Mpro in complex with **A1** antagonist (FJC) (PDB code: 6M0K) (Dai *et al*., 2020) and of SARS-CoV-2 PLpro in complex with non-covalent inhibitor VBY (PDB code: 7JIW) (Osipiuk *et al*., 2020) and with covalent

peptidic inhibitor VIR251 (PDB code: 6WX4) (Rut *et al*., 2020), and of SARS-CoV-2 spike protein (PDB code: 6LZG) (Wang *et al*., 2020), were prepared using the Schrödinger Protein Preparation Wizard workflow. Specifically, water molecules and the co-complexed compounds (ACE2 in the case of spike protein) were deleted, cap termini were included, all hydrogen atoms were added, and bond orders were assigned. Eventually, the prepared .pdb files were converted to the final .mae files. The grids accounted for the subsequent molecular docking calculations were generated analyzing the positions of the related co-crystallized compounds. The focused library of investigated compounds was prepared using LigPrep software (Schrodinger Suite) (Schrodinger Release, 2021). Specifically, all the possible tautomers and protonation states (pH = 7.4 ± 1.0) were generated for each compound, and the obtained structures were minimized using the OPLS 2005 force field. Molecular docking experiments were performed using Glide software (Schrödinger Suite), using the Extra Precision [XP] mode (Schrodinger Release, 2021). In details, 20,000 poses were kept in the starting phase of docking 1200 poses for energy minimization were selected. The scoring window for keeping the initial poses was set to 400.0 and a scaling factor of 0.8 related to van der Waals radii with a partial charge cutoff of 0.15, basing on a 0.5 kcal/mol rejection cutoff for the obtained minimized poses, was considered. In the output file, 10 poses for each compound were saved. Covalent docking experiments were performed using Glide software (Schrödinger Suite). Cys145 was set as the reactive protein residue for SARS-CoV-2 Mpro and Cys111 for SARS-CoV-2 PLpro, whereas the specific reaction type was selected in the related panel according to the specific ligand chemical features. When needed, the specific. cdock "custom chemistry" file was generated. In the output file, 10 poses for each compound were saved.

# CHAPTER 2

# Synthesis and biological evaluation of bicyclic compounds as potential anti-inflammatory agents

## 1.1 Inflammation: an overview

Inflammation is a physiological response of our immune system that can be triggered by a variety of factors such as pathogens, damaged cells, and toxic compounds that can cause damage to our tissues (Chen *et al*., 2018). The inflammatory process includes several stages, each of which is characterized by different mechanisms and chemical mediators.

At first, an acute inflammatory response is triggered, during which there is recruitment of neutrophils from the blood, activation of tissue macrophages, and production of a series of mediators that are intended to remove the damaging stimuli to initiate the healing process and restore homeostasis of damaged tissues (Ward *et al*., 1999). The acute phase of the inflammatory process is characterized by phenomena mainly involving the blood vessels: the main vascular changes are represented by increased secondary blood flow, vasodilation, and increased vascular permeability; these changes lead to the typical symptoms of acute inflammation such as redness, swelling, heat, pain, and loss of tissue function (Chen *et al*., 2018).

Generally, a controlled inflammatory response is beneficial to our body (*e.g.*, in providing protection against infection); however, if the immune system is unable to eliminate the cause of the damage, evolution into chronic inflammation may occur due to excessive production of pro-inflammatory mediators (Medzhitov, 2008).

When inflammation becomes chronic (**Figure 28**), there is an increase in the typical features of the acute phase, including vascular dilatation, increased blood flow, capillary permeability, and migration of neutrophils into the infected tissue (diapedesis); however, the composition of white blood cells changes, and soon short-lived neutrophils are replaced by macrophages and lymphocytes. Thus, the hallmarks of chronic inflammation are the infiltration, at the damaged tissue site, of primary inflammatory cells such as macrophages (both M1 and M2 types), T and B lymphocytes, and plasma cells, which produce inflammatory cytokines, growth factors, and enzymes that contribute to the progression of tissue damage and the formation of granulomas, typical histologic structures of the chronic inflammatory process (Pahwa *et al.*, 2022).

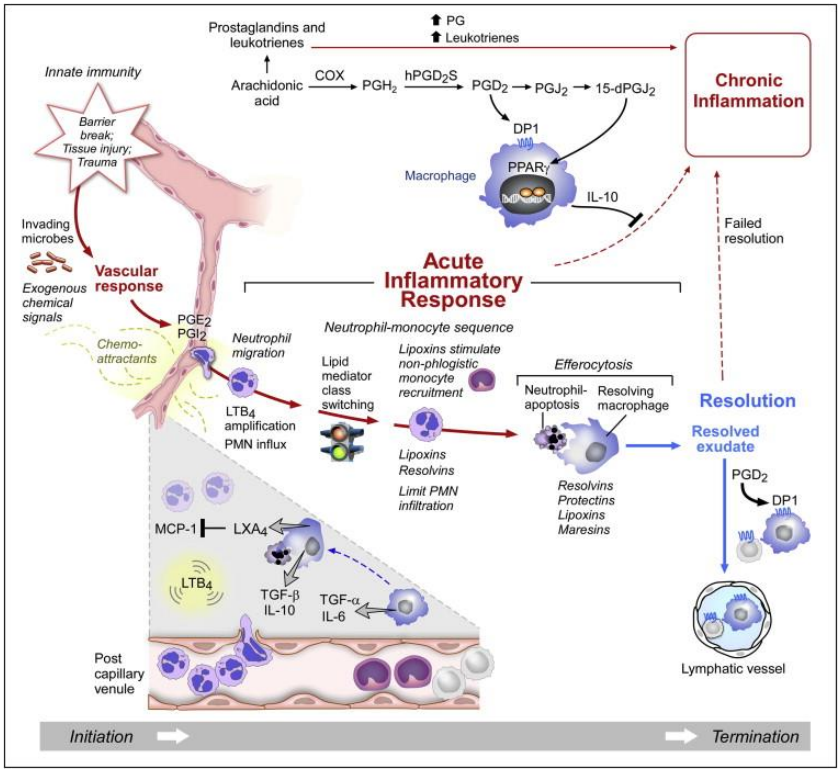


**Figure 28.** *Inflammatory process. (Adapted from Buckley et al., 2014).*

### *1.1.1 The arachidonic acid cascade*

Inflammatory stimuli activate several intracellular signaling pathways that have a major impact on the pathogenesis of numerous chronic inflammatory diseases (Chen *et al*., 2018).

Among these, of considerable interest is the arachidonic acid cascade, which represents a key biochemical pathway for pharmacologically targeting some inflammatory diseases. Arachidonic acid (AA) is a 20-carbon-atom polyunsaturated fatty acid with 4 double bonds, which is released upon hydrolysis of membrane phospholipids by phospholipase A2. The presence of double bonds within the structure makes AA susceptible to metabolization by several mechanisms that lead to the

production of a network of pro-inflammatory and pro-resolving mediators that are critical for the proper functioning of the immune system (Violette *et al*., 2018).

Metabolization of AA (**Figure 29**) can occur through three main pathways:

- The cyclo-oxygenase pathway, which leads to the production of pro-inflammatory vasodilator prostaglandins (such as PGE2 and prostacyclin) and thromboxane, a potent platelet aggregating agent (Pahwa *et al*., 2022).
- The 5-lipoxygenase (5-LOX) pathway, which mediates the production of leukotrienes; this enzyme requires two accessory proteins to exert its activity: the 5-lipoxygenase-activating protein (FLAP) and the coactosin-like protein (CLP). Leukotrienes are a family of lipid mediators of fundamental importance in inflammatory processes, particularly in allergic conditions such as asthma (Duroudier *et al*., 2009).
- The cytochrome P450 (CYP450) monooxygenase pathway, which transforms AA into 20-hydroxyheicosatetraenoic acid (20-HETE) and epoxyeicosatrienoic acids (EETs): the latter undergo a process of hydrolysis by the enzyme soluble epoxide hydrolase (sEH), rapidly transforming into dihydroxyeicosatrienoic acids (DHETs) with mainly pro-inflammatory effects (Kroetz *et al*., 2022).

In contrast, *in vitro* and animal model studies indicate that EETs possess anti-inflammatory activity directed at reducing, resolving, and limiting damage caused by inflammation. Thus, the metabolic pathways mediated by these two enzymes (cytochrome P450 monooxygenase and epoxide hydrolase), represent an important object of study for the treatment of cardiovascular inflammatory diseases. Indeed, studies have shown that enhancing the CYP450 pathway and decreasing EET

hydrolysis by sEH attenuate NF-kB-dependent vascular inflammatory responses *in vivo*, representing valuable therapeutic strategies to combat inflammation (Deng *et al.*, 2011).

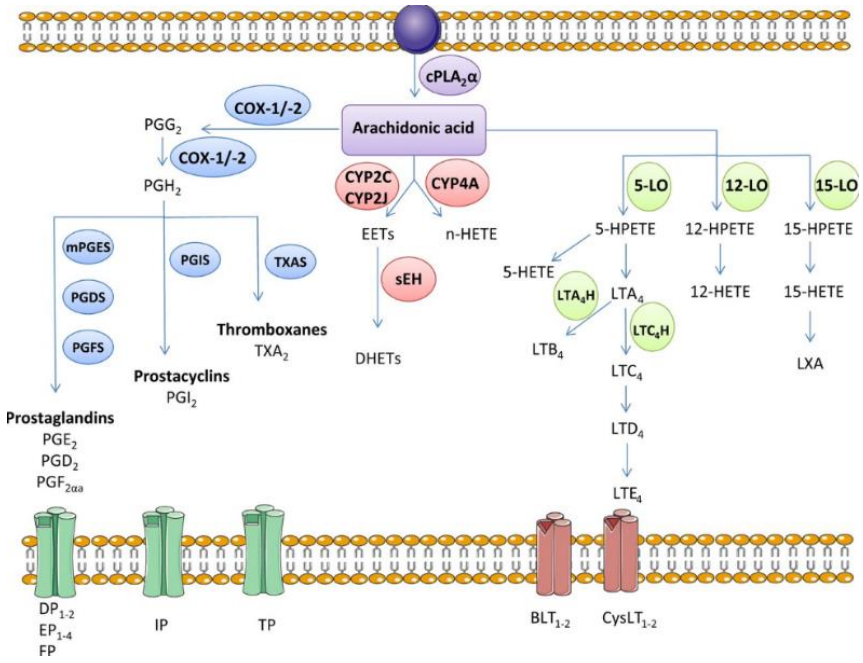


**Figure 29.** *Overview of the arachidonic acid (AA) metabolism pathways. (Adapted from Meirer et al., 2014).*

## 1.2 Lipoxygenases family

Lipoxygenases (LOXs) are non-heme iron-containing dioxygenases (Ivanov *et al.*, 2010) that catalyze dioxygenation of polyunsaturated fatty acids containing at least two isolated cis-double bonds. Specifically in mammals, the most abundant polyenoic fatty acids are linoleic acid and arachidonic acid, which serve as substrates for the different LOX isoforms.

Mammalian LOXs prefer free fatty acids as substrates, so an active LOX pathway requires the release of fatty acids from cell membranes where they are in the form of esters. Once released from membrane phospholipids by the action of cytosolic phospholipase A2, the free fatty acids, mainly arachidonic acid (AA), eicosapentaenoic acid (EPA), and docosahexaenoic acid (DHA), are oxygenated either by cyclooxygenases (COX) to G-prostaglandins or by LOX isoforms to various hydroperoxy derivatives (Haeggstrom *et al*., 2011).

Leukotrienes, lipoxins, epoxylins, resolvins, protectins, and other bioactive lipid mediators derived from AA, EPA, and DHA are just some of the mediators into which the primary substrates of LOXs are subsequently transformed. However, it is possible that LOXs can demonstrate their bioactivity in ways other than the traditional model of the arachidonic acid cascade. There are at least two different possibilities, such as structural modification of complex lipid-protein assemblies and modification of the cellular redox homeostasis, which alter the gene expression pattern (Schewe *et al*., 1975; Belkner *et al*., 1991).

Numerous studies using various gain-of-function (cellular transfection studies, transgenic animals) and loss-of-function (siRNA-mediated expression knockdown, knockout mice) strategies have given a deeper understanding of the biological significance of LOXs in health and disease. These studies have focused on the molecular specifics of how the various LOX-isoforms exhibit their bioactivity.

Six functional LOX genes (ALOX15, ALOX15B, ALOX12, ALOX12B, ALOXE3, and ALOX5) that code for six distinct LOX-isoforms are found in the human genome (Funk *et al*., 2002). All LOX genes are located in a shared gene cluster

on chromosome 17, with the exception of the ALOX5 gene, which was mapped to chromosome 10.

The 12/15-LOX, which is highly expressed in eosinophils (Sigal *et al*., 1988), broncho-alveolar epithelial cells (Sigal *et al*., 1992), and interleukin-4-treated monocytes (Conrad *et al*., 1992), is encoded by the ALOX15 gene. Epithelial cells express 15-LOX2, which is encoded by the ALOX15B gene (Brash *et al*., 1997; Jisaka *et al*., 1997). The platelet-type 12-LOX (pl12-LOX), which the ALOX12 gene encodes, is expressed at high levels in blood platelets (Funk *et al.*, 1990) as well as in the skin. The ALOXE3 gene (Kinzig *et al*., 1999) encodes for two different epidermis-type LOX isoforms that are co-expressed in the skin, while the ALOX12B gene (Boeglin *et al*., 1998) encodes for a 12R-LOX enzyme.

These enzymes appear to be crucial for the establishment of the epidermal water barrier and have been linked to epidermal differentiation (Krieg *et al*., 2014).

Leukotriene production depends heavily on the 5-LOX enzyme that the ALOX5 gene encodes (Samuelsson *et al*., 1987).

### *1.2.1 5-lipoxygenase*

The biosynthesis of leukotrienes (LT), a class of lipid mediators of inflammation produced from arachidonic acid, is catalyzed by 5-lipoxygenase (5-LOX), which operates in two steps (AA). Leukotrienes (LT) are mediators of inflammation that can lead to, among other things, increased vascular permeability and phagocyte chemotaxis. Arachidonic acid (AA) is oxygenated by 5-LOX to produce 5(S)-hydroperoxide-6-trans-8,11,14-cis-eicosatetraenoic acid (5-HPETE), which is further

dehydrated to produce the allyl epoxide leukotriene A4 (Samuelsson *et al*., 1987). Polymorphonuclear leukocytes (neutrophils and eosinophils), monocytes/macrophages, mast cells, B lymphocytes, dendritic cells, and foam cells of human atherosclerotic tissue are the types of leukocytes that most express 5-LOX. The 5-LOX gene has 14 exons and is situated on chromosome 10 (Funk *et al*., 1989). The promoter region resembles the promoters of common house-keeping genes since it has eight GC-boxes but no TATA or CAT boxes.

Leukocytes are the only cells that express 5-LOX in large amounts. The 5-LOX gene core promoter is fully methylated in the cell lines U-937 and HL-60TB, which do not express the 5-LOX protein, but is unmethylated in HL-60 cells, which express the 5-LOX protein during differentiation, according to methylation-specific DNA sequencing (Uhl *et al*., 2002). When reporter gene was methylated in vitro, its activity severely decreased, but 5-aza-2'deoxycytidine treatment of U-937 and HL-60TB cells allowed 5-LOX expression to be restored. Thus, the ability of a cell type to express 5-LOX is determined by DNA methylation.

Through crystallization of 15-LOX present in rabbit reticulocyte, it has been shown that, as in plants, LOXs enzymes in mammals consist of two domains and contain 672 or 673 amino acids (**Figure 30**). Model structure has an N-terminal sandwich (residues 1-114) and a C-terminal catalytic domain (residues 121-673) that bind the prosthetic iron, that is anchorated by a 2-His-1-carboxylate facial triad (Hegg *et al*., 1997). Thus, mutagenesis investigations show that the triad for 5-LOX consists of two conserved His (H372, H550) and the C-terminal Ile-673. H367 and N554 may also serve as alternative ligands for iron (Hammarberg *et al*., 2001).

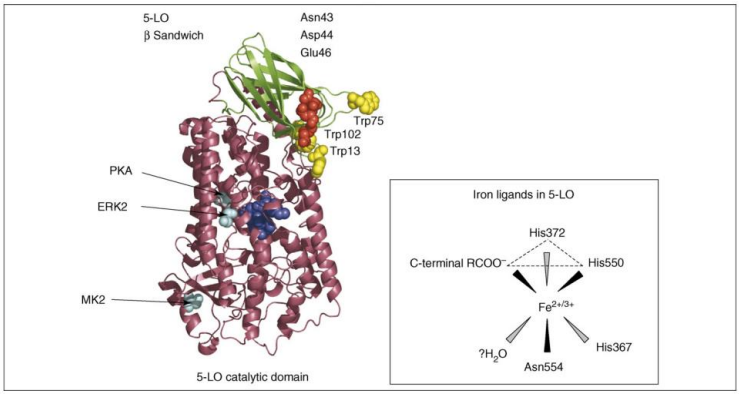


**Figure 30.** *Model of 5-LO based on the crystal structure of the $Fe^{2+}$ form of rabbit reticulocyte 15-LO (PDB 1LOX). (Adapted from Radmark et al., 2007).*

The C2-like β sandwich of the smaller N-terminal domain (residues 1-114) contains the typical ligand-binding loops (Hammarberg *et al*., 2000). It has been demonstrated that 5-LOX residues in these loops bind both $Ca^{2+}$ and cellular membranes, and that $Ca^{2+}$ can activate 5-LOX inducing membrane attachment.

### *1.2.2 5-lipoxygenase pathway*

The 5-lipoxygenase pathway is the main source of pro-inflammatory leukotrienes produced by arachidonic acid metabolism. In the resting cell, 5-LOX is located in the cytosol or in a soluble compartment within the nucleus. Upon activation, 5-LOX migrates to the nuclear envelope, where cytosolic phospholipase A2 (cPLA2) and the 5-LOX activating protein (FLAP) aid the enzyme in the biosynthesis of leukotrienes: cPLA2 releases AA from membrane phospholipids, while membrane-bound FLAP is believed to facilitate AA transfer to the enzyme (Dixon *et al*., 1990). When activated by $Ca^{2+}$, coactosin-like protein (CLP), which is in a complex with cellular 5-LOX, helps to assemble the enzyme on the nuclear membrane (Basavarajappa *et al*., 2014).

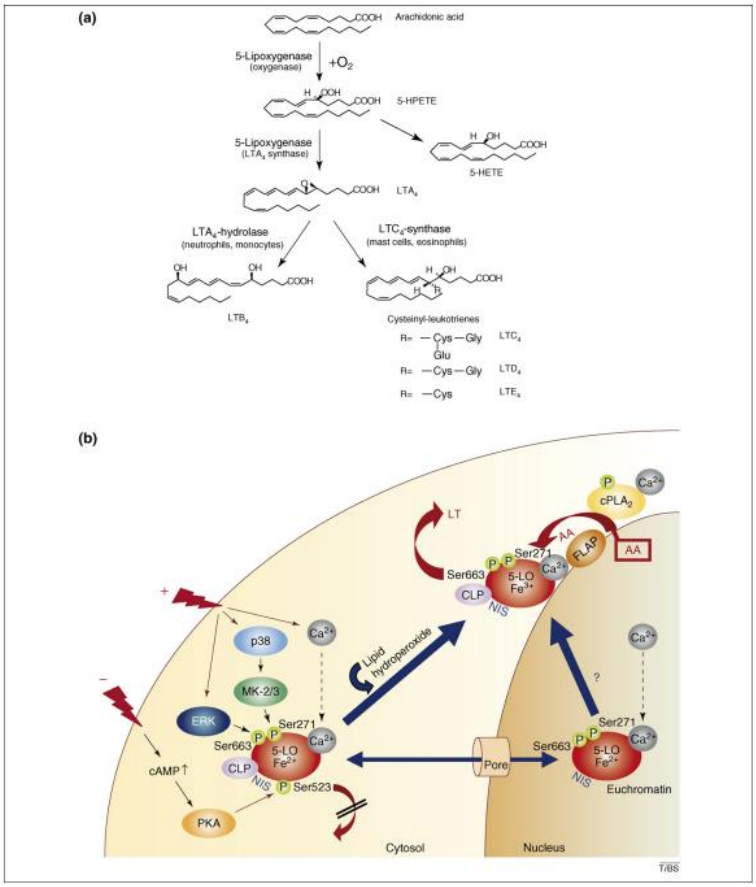


**Figure 31.** *a) Conversion of arachidonic acid to leukotrienes (LTs); b) localization and activation of 5-LOX. (Adapted from Radmark et al., 2007).*

When LT production is stimulated, 5-LOX is activated along with increased $Ca^{2+}$ and/or mitogen-activated protein kinase (MAPK) activity. Iron is oxidized by lipid hydroperoxide to $Fe^{3+}$ while Ser271 is phosphorylated by MAPKAPK-2/3 (MK-2/3), and 5-LOX is also phosphorylated at Ser663 by ERK. On the other hand, a rise in cAMP levels activates protein kinase A (PKA), which phosphorylates Ser523 to stop 5-LOX action (**Figure 31-b**). Once activated, the 5-LOX enzyme converts arachidonic acid to the unstable intermediate known as 5-hydroperoxyeicosatetraenoic acid (5-HPETE), which is subsequently hydrolyzed to 5-hydroxyeicosatetraenoic acid (5-HETE) or converted to the unstable epoxide leukotriene A4 (LTA4) by the formation

of a triene conjugate. (Golden 1998) LTA4 can be further metabolized to cysteinyl leukotrienes (CysLTs): specifically, LTC4 synthetase conjugates LTA4 to glutathione to form LTC4, which can be rapidly converted to LTD4 by a gammaglutamyl transpeptidase and to LTE4 by a dipeptidase. The cysteinyl leukotrienes (LTD4 and LTE4) appear to be involved in most of the main features of asthma, including increased mucus secretion, bronchoconstriction, vasodilation, and increased vascular permeability; indeed, some scientific evidence shows that CysLT production is particularly pronounced in asthmatic subjects. In addition, LTA4 can also be hydrolyzed by a specific zinc metallohydrolase, LTA4 hydrolase, to form LTB4 (**Figure 4**); the latter is able to promote the recruitment of neutrophils to the damaged area, as well as induces the production of cytokines of a proinflammatory nature by immune cells (**Figure 31-a**) (Radmark *et al*., 2007). The cysteinyl leukotrienes and LTB4 act on different G-protein-coupled receptors; specifically, each of them binds at least two different receptors: the CysLTs bind to CYSLTR1 and CYSLTR2 and the LTB4s bind to LTB4R1 and LTB4R2 (Lynch *et al*., 1999; Heise *et al*., 2000).

The function of 5-LOX is closely related to FLAP (5-LOX activating protein), a nuclear membrane-associated protein that is responsible for presenting arachidonic acid to the enzyme, increasing the efficiency with which 5-HPETE is converted to LTA4. According to a recent study, FLAP controls 5-LOX activity in two different ways: first, it causes a flexible and loose association with 5-LOX for effective 5-LOX product synthesis, and then it forms a tight 5-LOX/FLAP complex that stops 5-LOX activity (Plante *et al*., 2006).

### *1.2.3 The role of 5-lipoxygenases in pathophysiological conditions*

5-LOX is involved in the development of several diseases and plays an important role in the control of asthma, mainly due to the production of cysteinyl leukotrienes which, as mentioned earlier, are the main mediators involved in the asthmatic inflammatory process. They, in fact, exert a potent effect on bronchial constriction as a result of binding to the CYSLTR1 receptor, which is found to be expressed exclusively on bronchial smooth muscle cells, but not on epithelial cells; in contrast, the CYSLTR2 receptor is expressed strongly in pulmonary interstitial macrophages and weakly in smooth muscle cells (Lynch *et al*., 1999; Heise *et al*., 2000). In addition to the cysteinyl leukotrienes, LTB4 also appears to be involved in the asthmatic process: it is overproduced in the airways of patients with asthma and COPD (chronic obstructive pulmonary disease) where it causes the migration of inflammatory cells (mast cells, lymphocytes, and eosinophils) as a result of interaction with its receptor (Irvin *et al*., 1997).

Cysteinyl leukotrienes are also key mediators of allergic rhinitis; they modulate nasal allergic inflammation and clinical symptoms (especially sneezing and rhinorrhea) through activation of CYSLTR1 in the nasal mucosa (Lynch *et al*., 1999). There is also evidence for increased production of cysteinyl leukotrienes in the pathogenesis of atopic dermatitis; in fact, increased production of them has been reported in the skin of atopic patients compared with healthy patients (Sadik *et al*., 2013). Several studies have shown that 5-LOX plays a key role in the onset and progression of atherosclerosis, although the mechanisms underlying this involvement are not fully elucidated yet. Alteration of the enzyme's expression in mouse models characterized by LDL receptor deficiency revealed a suppression of atherogenesis,

suggesting how 5-LOX may potentially be involved in the development of this disease (Mehrabian *et al*., 2002). Recent studies suggest that this enzyme may contribute to atherosclerosis at several levels, such as lesion initiation, cell proliferation within the lesion, and destabilization of plaques that may lead to their rupture (Mehrabian *et al*., 2003).

A recent study reported that mouse models characterized by a deficiency in the ALOX5 gene showed protective effects against anxious behaviours, raising the possibility that this gene may modulate neuronal function.

Subsequently, zileuton, a known inhibitor of 5-LOX, was shown to be effective in a transgenic mouse model of Alzheimer's disease, leading to speculation that ALOX5 may be involved in the onset or progression of Alzheimer's disease (Joshi *et al*., 2014).

Immunohistochemistry studies demonstrated increased expression of ALOX5 in Apc468 mouse models, which specifically carry a truncated Apx gene that develops severe polyposis within four months, which suggested that 5-LOX might somehow contribute to the onset of colorectal cancer (Gounari *et al*., 2005).

### 1.3 Soluble epoxide hydrolase

Epoxide hydrolase (EH) is an enzyme found in all living organisms that converts, lipids containing epoxides to 1,2-diols by the addition of a molecule of water (Morisseau, 2013).

Overall, this enzyme has three main roles, detoxification, catabolism and regulation of signaling molecules, which, however, differ from organism to organism. In microorganisms, EH appears to play an important role in the catabolism of naturally

occurring carbon sources, such as tartaric acid or limonene, as well as environmental contaminants, such as epichlorohydrin. In plants, on the other hand, it appears to be important in cuticle formation, stress responses, and defence against pathogens. Several isoforms of the EH enzyme exist in mammals, but the most studied over the years have been soluble epoxide hydrolase (sEH) and microsomal epoxide hydrolase (mEH). Although these two isoforms are mostly localized to the liver, they can be found in almost any tissue and appear to be involved in the detoxification of a wide range of mutagenic, toxic, and carcinogenic xenobiotic epoxides; however, recent studies have clearly identified the roles of these two enzymes (Harris *et al*., 2013).

The sEH is a 120 kDa homodimeric enzyme that belongs to the α/β hydrolase superfamily; it contains a C-terminal hydrolase domain and an N-terminal phosphatase domain (Beetham *et al*., 1993), which are separated by a proline-rich linker (**Figure 32**).

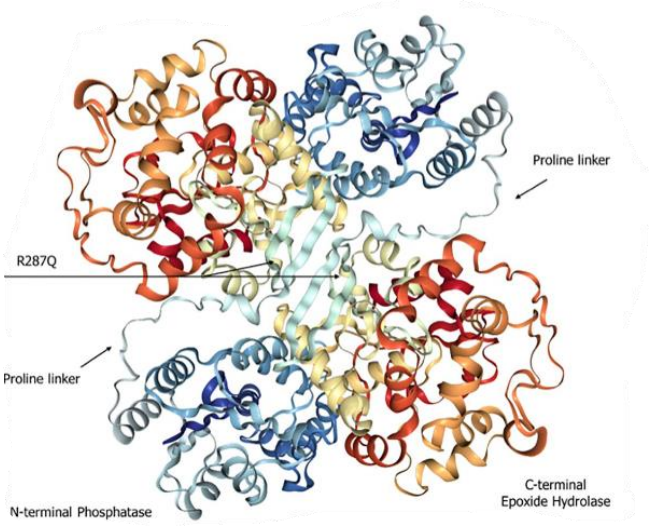


**Figure 32.** *Overall structure of the dimeric form of the human sEH. (Adapted from Domingues et al., 2020).*

As for the phosphatase domain, it appears involved in phosphorylated lipids hydrolysis, such as isoprenoid phosphates and lysophosphatidic acid, which stimulate cell growth, although to date little is known about its activity (Oguro *et al*., 2012).

The C-terminal domain, on the other hand, is responsible for the hydrolysis of epoxides by the addition of water to the three-membered oxirane ring (Spector, 2009). sEH is widely distributed throughout the body, although it is found to be most concentrated in the liver, kidney, intestine and blood vessels of mammals (Enayetallah *et al*., 2004). However, studies have shown that sEH is also found in the brain (Marowsky *et al*., 2009): in fact, it has been found to be expressed at the neuronal level along with CYP450 enzymes that produce EpFA (Iliff *et al*., 2009) and in astrocytes, including astrocyte endings (Marowsky *et al*., 2009).

### *1.3.1 Role of sEH in inflammation process*

The role of the soluble epoxide hydrolase enzyme is to convert epoxy fatty acids (EpFAs) into the corresponding 1,2-diols by adding of a molecule of water. Several scientific evidence has shown that sEH plays a crucial role in the metabolism of polyunsaturated fatty acids (PUFAs) during the inflammatory process. PUFAs are essential for the proper maintenance of body homeostasis (Jump, 2022). The structure and function of neurons, glial cells, and endothelial cells in the brain are known to be regulated by PUFAs (Bazinet *et al*., 2014).

Importantly, because animals cannot synthesize PUFAs, they must be obtained through diet. As discussed previously, the major enzymes that convert PUFAs into bioactive derivatives are cyclooxygenases (COXs), lipoxygenases (LOXs), and

cytochrome P450s (CYPs); in particular, the CYP pathway produces 20-HETE via CYP hydroxylases and epoxy fatty acids (EpFAs) via CYP epoxygenases, such as epoxy-eicosatrienoic acids (EETs) and epoxydocosapentaenoic acids (EDPs). Metabolites produced via the CYP exhibit both pro-inflammatory, such as the 20-hydroxyeicosatetraenoic acid (20-HETE) and anti-inflammatory properties, such as epoxyeicosatrienoic acids (EETs) and epoxydocosapentaenoic acids (EDPs), produced by cytochrome P450 (CYP) hydroxylases and CYP epoxygenases, respectively (**Figure 33**) (Spector, 2009).

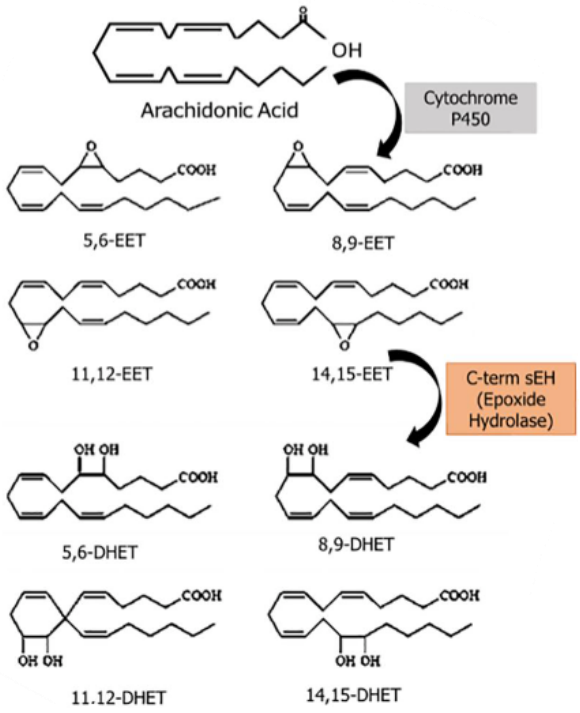


**Figure 33.** *sEH pathway in arachidonic acid metabolism. (Adapted from Domingues et al., 2020).*

Specifically, sEH is responsible for convert EET in DHET, abolishing the anti-inflammatory effects exerted by this metabolite. Initially, the generally accepted mechanism of EHs involved a direct attack of water on the epoxide ring. Later,

Lacourciere *et al*. showed that these enzymes hydrolyze epoxides through the formation of a hydroxy-alkyl covalent intermediate (Morisseau *et al*., 2004), as described in **Figure 34**.

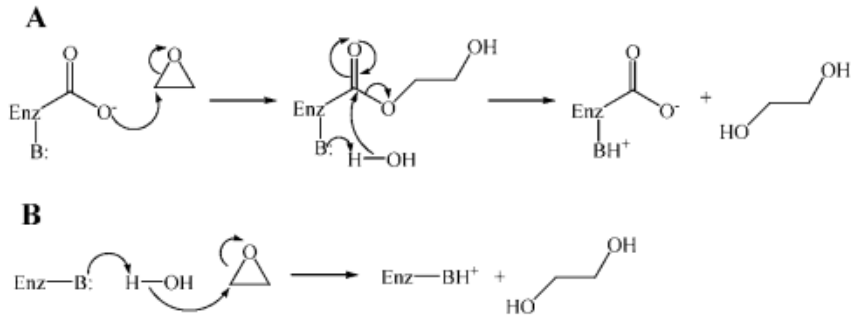


**Figure 34.** *Proposed mechanism for epoxide hydrolase. (Adapted from Morisseau et al., 2004).*

There are multiple mechanisms by which EETs and other EpFAs appear to reduce the inflammatory process. One of these involves the expression inhibition of VCAM-1, E-selectin, and ICAM-1 (Node *et al*., 1999). EETs also decrease TNFα secretion by monocytes by also inhibiting their cell adhesion (Bystrom *et al*., 2011). In addition, EETs can block nuclear translocation of NFkB factor, which in turn reduces the expression of certain enzymes such as calcium insensitive nitric oxide synthase (iNOS), lipoxygenase-5 (LOX-5) and cyclooxygenase-2 (COX-2), which are found to be upregulated during inflammation (Schmelzer *et al*. 2006).

Additional mechanisms reported involve activation of signal transducer and activator of transcription 3 (STAT3) (Williams *et al*., 2004) and activation of other nuclear receptors, such as peroxisome proliferator-activated receptor (PPAR) alpha and gamma.

### *1.3.2 Role of sEH in pathophysiological diseases*

The use of small molecule sEH inhibitors has helped to clarify the role that EpFAs play in several disorders (**Figure 35**).

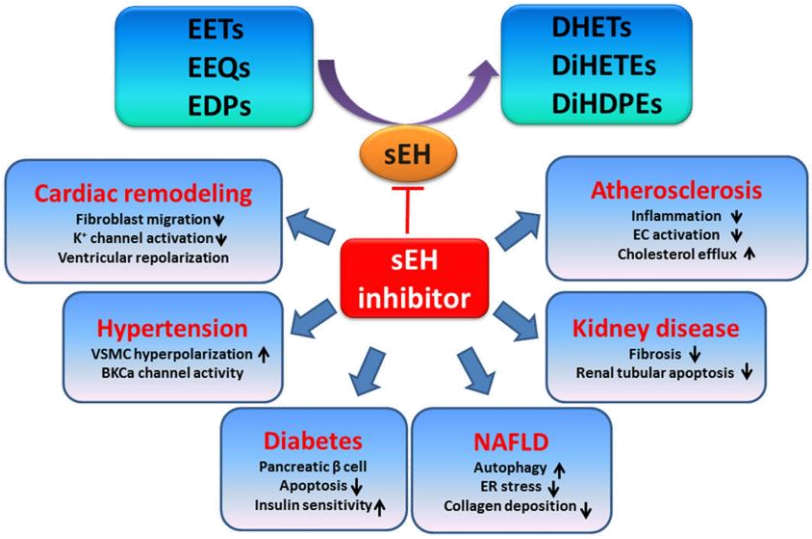


**Figure 35.** *Soluble epoxide hydrolase (sEH) and metabolic diseases (Adapted from He et al., 2016).*

First of all, EpFAs have been shown to be active against inflammatory disorders of the gastrointestinal tract (Zhang *et al*., 2012). Many sEH inhibitors, in fact, have been studied for their ability to chronic inflammatory bowel disease. The use of sEH inhibitors has also been evaluated as an anti-inflammatory therapeutic strategy in chronic arthritis, as an alternative to NSAIDs and corticosteroids, which are characterized by innumerable side effects. In fact, the use of sEH inhibitors and the consequent increase in EET, has been shown to regulate the transcription of several enzymes including COX-2 inducible (Schmelzer *et al*., 2005). Since sEH inhibitors have been shown to reduce hypertension and gastrointestinal complaints often associated with long-term NSAID use, synergistic use of the two drug classes is possible (Liu *et al*., 2010). In addition, high levels of EET appear to be associated with

reduced bone consumption, going to act on osteoclast differentiation *in vivo* through downregulation of ROS.

Certainly, the anti-inflammatory properties of EpFas in the context of cardiovascular diseases are widely reported and demonstrated in the literature. The main mechanisms underlying cardiovascular anti-inflammatory action involve endothelial cells, monocytes, and several receptors including PPAR, GPCR, and TRP channels (Liu *et al*., 2005).

Recently, to evaluate the applicability of the anti-inflammatory properties of EpFAs, effects associated with the use of sEH inhibitors were demonstrated in mouse models of depression. The use of sEHi reduced TNFalpha levels in LPS-treated mice, to induce depression, but not in control mice (Ren *et al*., 2016).

Finally, it appears that the use of sEH inhibitors is responsible for analgesic effects in both acute inflammatory pain (Schmelzer *et al*., 2006) and chronic painful conditions refractory to other therapeutic approaches, paving the way for new therapeutic strategies for pain treatment.

### 1.4 Leukotriene mediated response: pharmacological approach

Suppression of the 5-lipoxygenase pathway is an excellent therapeutic strategy to reduce the leukotriene-mediated inflammatory response and its impact in the development of various diseases. Two different approaches have been developed to reduce the LT-mediated response: leukotriene receptor antagonism and inhibition of leukotriene biosynthesis.

### *1.4.1 Leukotriene receptor antagonists*

Leukotriene receptor antagonists include zafirlukast and montelukast (**Figure 36**).

Specifically, these are antagonists of the CysLT1 receptor of cysteinyl leukotrienes, mediators involved in the mechanisms of bronchoconstriction, vascular permeability, and bronchial eosinophil recruitment.

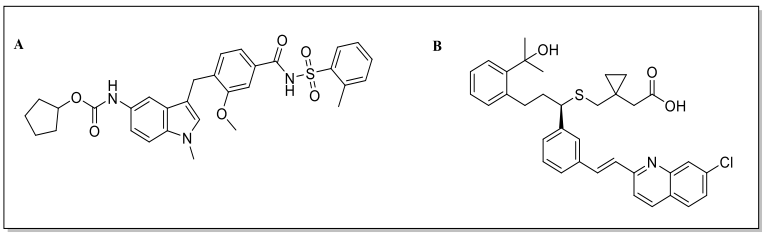


**Figure 36.** *Zafirlukast (A) and montelukast (B).*

Previous studies have also shown that cysteinyl leukotrienes play an important role in airway remodelling in chronic asthma; that is why these two drugs have been approved for the treatment of bronchial asthma, allergic rhinitis, and other allergic diseases (Choi *et al*., 2022). A phase 4 study conducted by Ghent University Hospital and the University of Rostock showed that, following treatment with 10 mg of Montelukast, 86.5% of patients reported a marked reduction in daytime asthma symptoms and 88.5% reported an improvement in night-time symptoms. In addition, an equally high percentage of patients reported a strong or marked improvement in all symptoms of allergic rhinitis, including sneezing, itching, rhinorrhoea, nasal congestion, and lacrimation (Virchow *et al*., 2006).

Although montelukast is considered a fairly safe drug, there are concerns regarding adverse reactions, including the onset of Churg-Strauss syndrome (CSS). A case-crossover study of 78 patients with CSS reported that the use of montelukast was

associated with a 4-fold increase in the risk of onset of CSS within 3 months. In addition, in 2008 the Food and Drug Administration issued a warning regarding the possible association between montelukast use and suicide, and many studies have suggested that use of this drug is associated with neuropsychiatric events such as anxiety, sleep disturbances, depression, and suicidal tendencies (Young *et al*., 2020).

### *1.4.2 Leukotriene biosynthesis inhibitors*

5-LOX inhibitors can be classified into three main groups:

- Active redox compounds. Early screening programs identified many redox-active compounds, such as coumarins or flavonoids, which act as nonselective antioxidants; however, many of them show serious side effects, such as methaemoglobin formation, or poor pharmacokinetic parameters so there has been no further development (Werz *et al*., 2005).

- Iron-ligand inhibitors. These are able to chelate and reduce the ferric iron present in the active site preventing the enzyme from entering the catalytic cycle (**Figure 37**).

These include hydroxamic acid and N-hydroxyurea derivatives (Werz *et al*., 2005).

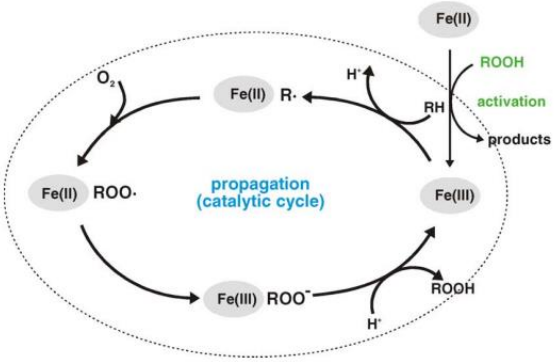


**Figure 37.** *Catalytic cycle of 5-LOX. (Adapted from Werz et al., 2005).*

- Non-redox inhibitors. The disadvantages associated with the use of redox-active inhibitors and iron ligands, such as participation in redox reactions and lack of selectivity, led to the development of non-redox inhibitors. However, although the latter showed high potency in vitro, are unable to strongly inhibit leukotriene synthesis at sites of chronic inflammation (Werz *et al*., 2005).

Currently, zileuton (**Figure 38**), a benzothiophene N-hydroxyurea, is the only 5-lipoxygenase inhibitor approved for the treatment of bronchial asthma (Werz *et al*., 2005): it acts by inhibiting leukotrienes biosynthesis in allergic and inflammatory diseases.

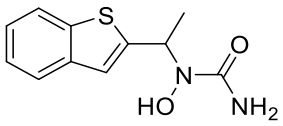


**Figure 38.** *Structure of zileuton.*

Given the crucial role that LTs play in the airway inflammatory process, zileuton represents a useful tool in the management of chronic and persistent asthmatic disease (Kelly *et al*., 2006).

However, zileuton exhibits hepatic toxicity, limiting its clinical use due to the requirement to check liver enzyme levels. It's interesting to note that zileuton's liver damage seems to be a direct toxic consequence unrelated to 5-LOX inhibition (You *et al*., 2020). In fact, zileuton administration is associated with an increase in serum ALT (alanine aminotransferase) levels, and most of these increases (61%) occurred during the first two months of therapy. Therefore, ALT concentration should be monitored once a month for the first three months and every three months in a year, and patients with a history of liver disease or excessive alcohol consumption should use zileuton

with caution. It has been shown that liver toxicity probably involves a sequence of biotransformations leading to 2-acetyl benzothiophene (2-ABT), which is subsequently metabolised to give one or more reactive intermediates. *In vitro* experiments using the human lymphoblastic cell line MCL5 showed that 2-ABT is cytotoxic in a P450-dependent manner (Joshi *et al*., 2003).

### 1.5 Multitarget approach in the treatment of inflammatory diseases

As discussed previously, both 5-lipoxygenase and epoxide hydrolase inhibitors represent an excellent therapeutic strategy for the treatment of inflammatory diseases such as asthma, as inhibition of the 5-lipoxygenase pathway prevents the formation of pro-inflammatory leukotrienes, but also cardiovascular diseases, as inhibition of epoxide hydrolase results in the accumulation of EETs that act at the vascular, renal, and cardiac levels with vasodilatory properties.

Despite this, the clinical use of molecules that act at the level of a single metabolic pathway is not entirely advantageous as it can cause shunting phenomena and amplification of alternative pathways, resulting in decreased efficacy and increased side effects (Morphy *et al*., 2009).

Therefore, polypharmacological approaches appear particularly useful in the design of anti-inflammatory drugs; multitarget drugs, in fact, allow balanced modulation of eicosanoid levels and largely suppress the phenomena of shunting and redirection (Celotti *et al*., 2001).

### *1.5.1 sEH and COX dual inhibitors*

COX inhibitors, known as NSAIDs (non-steroidal anti-inflammatory drugs), have long been considered highly effective drugs in reducing both pain and inflammation.

However, high doses of these compounds cause gastrointestinal erosion due to the reduction of prostaglandins critical for the integrity of the gastric mucosa (Hiesinger *et al*., 2020).

Therefore, selective COX-2 inhibitors, such as rofecoxib and celecoxib, were subsequently developed with the goal of limiting gastrointestinal side effects; however, these drugs exhibit worse cardiovascular side effects than nonselective inhibitors. This evidence has demonstrated how the adverse effects of COX inhibitors cannot be avoided simply by adjusting the selective inhibition of COX-1 and COX-2 (Funk *et al*., 2020).

Contextually, it was discovered that EETs derived from the CYP450 pathway, particularly 8,9-EETs, are metabolized by COX-1 to 11-hydroxy-8,9-EETs with angiogenic effects (Ritter *et al*., 2009).

Based on this finding, the compound PTUPB (**Figure 39**) was developed; it acted as sEH and COX-2 inhibitor but didn't show any activity on COX-1 enzyme, showing analgesic effects in animal models and in pathological conditions such as kidney disease and cancer. In fact, PTUPB significantly suppressed tumor growth and metastasis in a murine lung cancer, breast cancer and glioblastoma model. As an adjuvant, it potentiated cisplatin- and gemcitabine-based chemotherapy regimens in bladder cancer models; moreover, it did not alter the ratio of PGI2 to TXA2, an effect associated with selective COX-2 inhibitors, suggesting how multitarget inhibition is

effective in both enhancing the beneficial effects of therapy and reducing the adverse ones (Jankiewicz *et al*., 2021).

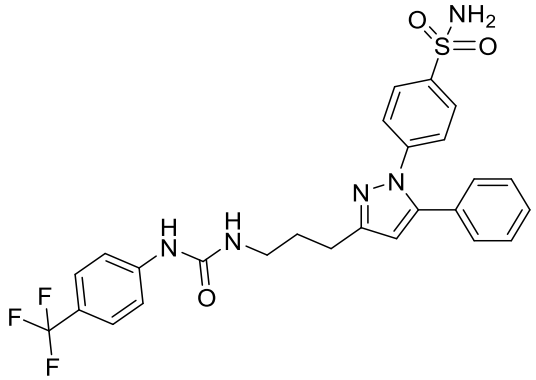

**Figure 39.** *Structure of PTUPB.*

### *1.5.2 sEH and FLAP dual inhibitors*

As discussed above, the FLAP protein is critical in regulating the activity of the 5-LOX enzyme as it is responsible for making AA available to the enzyme itself thus making possible the massive production of pro-inflammatory leukotrienes.

Therefore, another possible useful approach to interfere in the 5-LOX-mediated metabolic pathway is the modulation of FLAP protein activity. Indeed, several studies have observed a greater anti-inflammatory effect using a polypharmacological approach resulting from combining a sEH inhibitor with a FLAP inhibitor on a mouse model (Liu *et al*., 2010). This suggested how the use of dual inhibitors may have similar or even greater efficacy than co-administration; therefore, a virtual screening was performed in which pharmacophoric models based on ligands of FLAP were developed, using known models for sEH instead.

From this screening, 20 hit compounds were identified: among them, diflapolin (**Figure 40**) showed dual inhibition against FLAP and sEH, blocking leukotriene formation and reducing neutrophil infiltration in a mouse model of zymosan-induced peritonitis; it also showed high selectivity and no interaction with other enzymes that metabolize arachidonic acid, such as COX-1/2, 12/15-LOX, LTA4H (Temml *et al*., 2017).

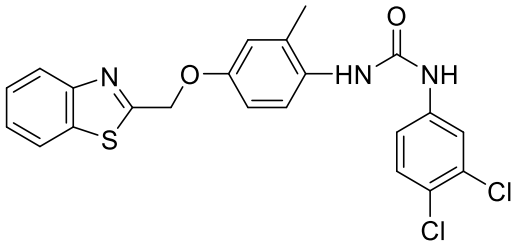


**Figure 40.** *Structure of diflapolin.*

### *1.5.3 sEH and 5-LOX dual inhibitors*

The first dual inhibitors of sEH and 5-LOX were discovered through a virtual screening of 37429 compounds by applying pharmacophoric models for both targets. Specifically, it was observed that benzimidazole scaffold compounds exhibited potent anti-inflammatory activity, inhibiting the action of 5-LOX, while aminoheterocyclic compounds were identified as sEH inhibitors. Based on these observations, new fluorobenzimidazoles were designed and synthesized as potential dual inhibitors of these enzymes. Specifically, the initial scaffold was modified (**Figure 41**) by introducing an aryl ether, responsible for inhibition of 5-LOX, and a benzoic acid, responsible instead for inhibition of sEH (Nandha *et al*., 2018).

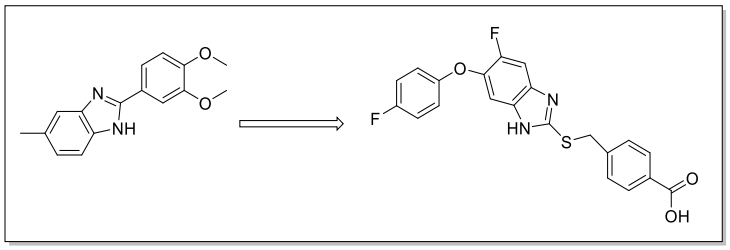


**Figure 41.** *In silico optimization of a dual inhibitor of 5-LOX/sEH.*

The anti-inflammatory effects of these compounds were studied on a rat paw edema model, and some of them showed a significant reduction in edema, comparable to that of the reference compound, ibuprofen. Later, a new series of dual inhibitors of 5-LOX and sEH was developed by linking two pharmacophores (Meirer *et al*., 2013): an imidazopyridine scaffold, derived from a selective inhibitor of 5-LOX (EP6) (Wisniewska *et al*., 2012), and an ureidic scaffold derived instead from a selective inhibitors of sEH (AUDA) (**Figure 42**) (Shen, 2010). From SAR studies, it was observed that in order to maintain the inhibition of sEH without adversely affecting that of 5-LOX, an n-propyl linker between the two drugs is required (Hiesinger *et al*., 2020).

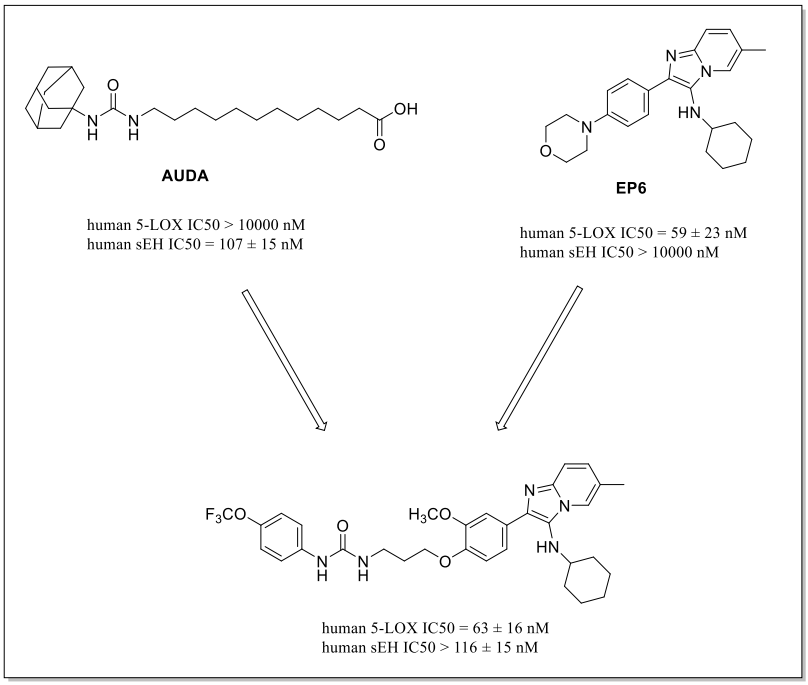


**Figura 42**. *5-LOX/sEH dual inhibitor obtained through the bond between two pharmacophores for 5-LOX and sEH.*

Another dual inhibitor of 5-LOX and sEH is KM55 (**Figure 43**), which was developed by linking, through an n-propyl linker, two pharmacophores: an N-hydroxy-ureide moiety derived from zileuton, and a ureide group derived from an sEH inhibitor, TPAU (Shen, 2010). To evaluate the effect of KM55, the capability of the compound to decrease leukocyte adhesion to endothelial cells was analysed, and the same assay was performed for zileuton and the sEH inhibitor. This study showed that KM55 was able to inhibit leukocyte adhesion to endothelial cells significantly more strongly than the single inhibitors (Meirer *et al*., 2017).

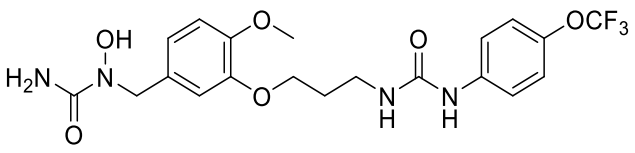

**Figure 43**. *Structure of KM55.*

## 2.1 5-LOX/sEH dual inhibitors: *in silico* evaluation of an in-house molecular library of bicyclic compounds

There is much evidence that multitarget drugs achieve balanced modulation of eicosanoid levels and largely suppress shunting and/or redirection phenomena (Morphy *et al*., 2009; Celotti *et al*., 2009; Hiesinger *et al*., 2020; Funk *et al*., 2007).

So, part of my PhD project focused on the design and synthesis of new indoline-based compounds as dual 5-LOX/sEH inhibitors; the starting point for the development of these molecules involved an integrated approach of *in silico* and *in vitro* assays on an in-house molecular library. Since the benzothiophene moiety of the zileuton is considered the pharmacophore of the molecule, 50 bicyclic compounds were selected from our library and evaluated *in silico*. Given the unavailability of an experimentally solved co-crystal structure of zileuton/5-LOX in the protein database, the binding mode of zileuton (**Figure 44**) was predicted by the use of molecular docking simulations.

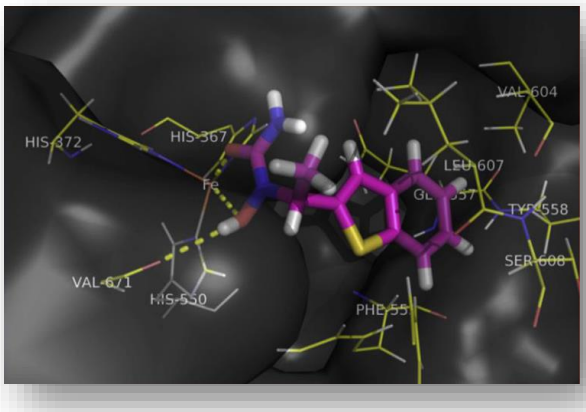


**Figure 44.** *Docking-predicted zileuton/5-LOX interaction. Yellow dashed lines highlight H-bonds.*

By the *in silico* evaluation, nine compounds (series I, **Figure 45**) were selected and tested *in vitro* for their 5-LOX inhibitory properties.

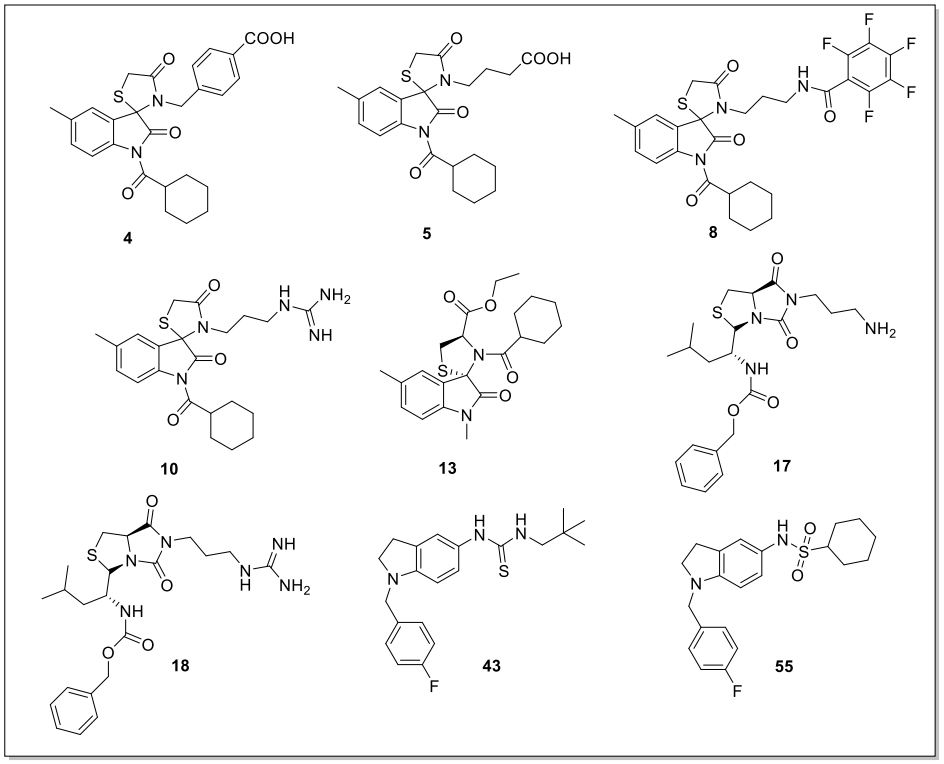


**Figure 45**. *Series I: synthesized derivatives.*

The bicyclic-based molecules, selected for the *in silico* preliminary screening towards 5-LOX, were structurally featured with (*R*)-dihydro-3H,5H-imidazo[1,5-c]thiazole-5,7(6H)-dione, 5-methylindolin-2-one and indoline rings.

For the spiro compounds, both enantiomers were considered in the calculations. The docking outcomes suggested that the indoline-based (**43** and **55** and (*R*)-dihydro-3H,5H-imidazo[1,5-c]thiazole-5,7(6H)-dione **17** and **18**) scaffolds are suitable molecular seeds for 5-LOX inhibitor design thanks to their ability to properly fit into 5-LOX binding pocket, while the spiro compounds (**4**, **5** and **13**) were the less promising scaffolds *in silico*.

### *2.1.1 Biological evaluation of series I: in vitro assays*

The nine derivatives selected from the preliminary *in silico* screening (**Figure 45**) were tested for their 5-LOX-inhibitory activity. At first, we evaluated their effectiveness in activated human polymorphonuclear leukocytes (PMNL), using cell-based assays which allow the analysis of the interference of the test compounds with 5-LOX in a biological environment. Results obtained were corroborated testing compounds against isolated human recombinant 5-LOX, thus allowing the identification of direct interference of the test compound with the target enzyme. The results are summarized in **Table 7**. Only derivative **43** reduced 5-LOX product levels in activated human PMNL ($IC_{50}$ 1.38 ± 0.23 μM). In addition, **43** showed a remarkable inhibitory activity against isolated 5-LOX ($IC_{50}$ 0.45 ± 0.11 μM).

**Table 7.** *Inhibition of 5-LOX product formation in activated PMNL of human isolated 5-LOX. The values are given as mean ± SEM of single determinations obtained in 3-4 independent experiments.* [a]

| *Compound* | *$IC_{50}$ (μM) in PMNL* | *$IC_{50}$ (μM) for isolated 5-LOX* |
|---|---|---|
| ***4*** | >10 | - |
| ***5*** | >10 | - |
| ***8*** | >10 | - |
| ***10*** | >10 | - |
| ***13*** | - | - |
| ***17*** | >10 | - |
| ***18*** | >10 | >25 |
| ***43*** | **1.38 ± 0.23** | **0.45 ± 0.11** |
| ***55*** | >10 | - |

[a]Zileuton, used as positive control at 3 μM gives residual activity of 3.90 ± 4.14 % and 14.24 ± 5.88 % over PMNL and isolated 5-LOX, respectively.

The biological activity of **43** was in agreement with structural observations from molecular docking.

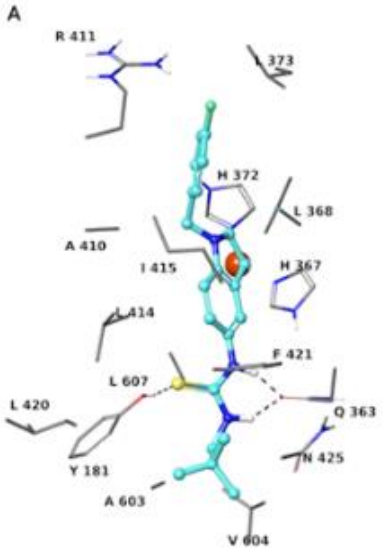


**Figure 46**. *Three-dimensional model of the interactions between **43** and 5-LOX.*

In detail, it was observed that the indoline moiety is placed near the iron atom, hampering the access to the open position of ion coordination sphere, and also contributing to the complex line up by van der Waals interactions with H372, H367, L368, L414, I415, F421, L607. The thiourea group of **43** donates two H-bonds to the side chain of Q363 and accepts a hydrogen bond from Y181 (**Figure 46**). The neopentyl group of **43** establishes van der Waals contacts with Y181, F421, A424, N425, P569, H600, A603. The 4-fluorobenzyl moiety is engaged in an aromatic H-bond with N407 side chain and van der Waals contacts with W147, F151, H372, L368, L373, A410, R411, I415. Furthermore, the fluorine interacts with the side chain of R411.

### *2.1.2 Design of series II*

The remarkable 5-LOX inhibitory activity of **43** together with the observed intermolecular interactions led us to design and synthetize a new series of 19 structurally correlated compounds (**Figure 47**).

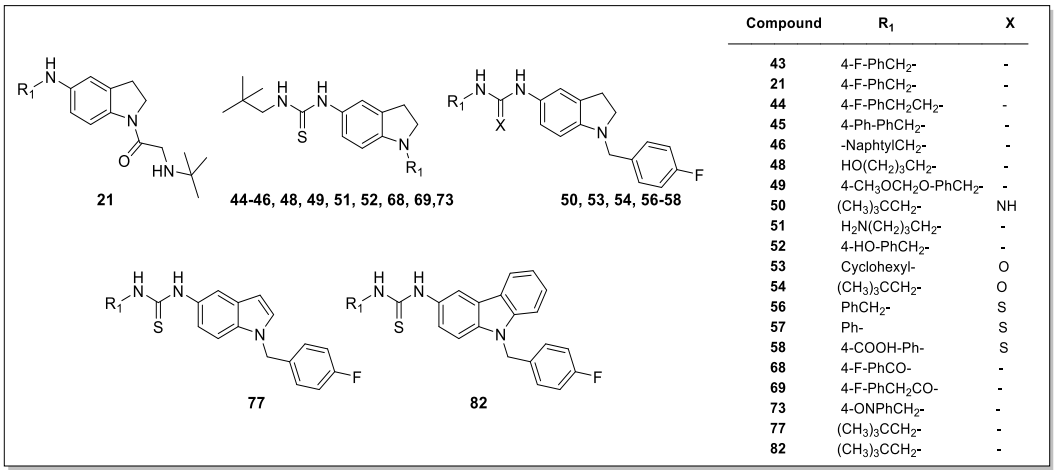


| Compound | $R_1$ | X |
|---|---|---|
| 43 | 4-F-$PhCH_2$- | - |
| 21 | 4-F-$PhCH_2$- | - |
| 44 | 4-F-$PhCH_2CH_2$- | - |
| 45 | 4-Ph-$PhCH_2$- | - |
| 46 | -Naphtyl$CH_2$- | - |
| 48 | $HO(CH_2)_3CH_2$- | - |
| 49 | 4-$CH_3OCH_2O$-$PhCH_2$- | - |
| 50 | $(CH_3)_3CCH_2$- | NH |
| 51 | $H_2N(CH_2)_3CH_2$- | - |
| 52 | 4-HO-$PhCH_2$- | - |
| 53 | Cyclohexyl- | O |
| 54 | $(CH_3)_3CCH_2$- | O |
| 56 | $PhCH_2$- | S |
| 57 | Ph- | S |
| 58 | 4-COOH-Ph- | S |
| 68 | 4-F-PhCO- | - |
| 69 | 4-F-$PhCH_2CO$- | - |
| 73 | 4-ONPh$CH_2$- | - |
| 77 | $(CH_3)_3CCH_2$- | - |
| 82 | $(CH_3)_3CCH_2$- | - |

**Figure 47.** *Series II: synthesized derivatives.*

Specifically, to get clues about structure-activity relationships, we decide to introduce modifications at different positions, including:

1. the tert-butyl moiety (**56**-**58**);
2. the thiourea group (**21**, **50**, **53**, **54**);
3. the 5-fluorobenzyl group (**44**-**49**, **51**, **52**, **68**, **69**, **73**);
4. moreover, we modify the indoline scaffold at C-2 and C-3 (**77**, **82**).

### *2.1.3 Biological evaluation of series II*

All the synthetized compounds were tested to evaluate their anti-inflammatory activity by different *in vitro* assays. Initially, they were challenged for their inhibitory capabilities toward isolated LOX-5 as well as in activated PMNL. Then, considering

the importance of the sEH enzyme in the AA cascade, we questioned whether the parent molecule (compound **43**) and its analogues could affect the activity of this enzyme. Results obtained are summarized in **Table 8**.

**Table 8.** *Inhibition of 5-LOX Product Formation in Activated PMNL, of Human Isolated 5-LOX and Human Isolated sEH. All values are given as mean ± SEM of single determinations obtained in 3−4 independent experiments.*[a]

| *Compounds* | *$IC_{50}$ in PMNL (μM)* | *$IC_{50}$ for isolated 5-LOX (μM)* | *$IC_{50}$ for isolated sEH (μM)* | *Compounds* | *$IC_{50}$ in PMNL (μM)* | *$IC_{50}$ for isolated 5-LOX (μM)* | *$IC_{50}$ for isolated sEH (μM)* |
|---|---|---|---|---|---|---|---|
| ***43*** | 1.38 ± 0.23 | 0.45 ± 0.11 | 1.39 ± 0.45 | **53** | >10 | 0.28 ± 0.02 | 0.061 ± 0.003 |
| ***21*** | >10 | >10 | >10 | **54** | nd | 0.18 ± 0.05 | 0.10±0.01 |
| ***44*** | 4.87 ± 0.41 | 0.38 ± 0.05 | 1.14 ± 0.29 | **56** | 0.95 ± 0.15 | 0.57 ± 0.12 | 3.86 ± 0.79 |
| ***45*** | >10 | 1.48 ± 0.48 | >10 | **57** | 1.98 ± 0.32 | 0.16 ± 0.05 | 10.39 ± 0.37 |
| ***46*** | >10 | 1.02 ± 0.44 | 0.91±0.24 | **58** | >10 | 2.29 ± 0.46 | >10 |
| ***48*** | nd | 9.02 ± 4.20 | >10 | **68** | >10 | >10 | >10 |
| ***49*** | 2.93 ± 0.70 | >10 | 2.40 ± 0.80 | **69** | >10 | >10 | >10 |
| ***50*** | >10 | 1.42 ± 0.23 | >10 | **73** | **0.59 ± 0.09** | **0.41 ± 0.01** | **0.43 ± 0.10** |
| ***51*** | >10 | >10 | >10 | **77** | >10 | >10 | 2.12 ±1.06 |
| ***52*** | 2.90 ± 0.75 | 5.10 ± 2.92 | 0.79 ± 0.52 | **82** | >10 | >10 | >10 |

nd= not determined. [a] Zileuton, used as positive control at 3 μM gives residual activity of 3.90 ± 4.14% and 14.24 ± 5.88% over PMNL and isolated 5-LOX, respectively. AUDA used as positive control at 1 μM gives residual activity of 3.90 ± 4.14% over isolated sEH.

### *2.1.4 Synthesis of series I and II*

Spiro[indoline-3,2'-thiazolidine] derivatives were synthesized according to scheme reported in **Figure 48**.

5-Methylindoline-2,3-dione was reacted with mercaptoacetic acid in presence of stoichiometric amount of 4-(aminomethyl)benzoic acid, or 4-aminobutanoic acid, or tert-butyl (3-aminopropyl)carbamate, to obtain in one step the intermediates **1-3** in 55, 59 and 85% yields, respectively. These intermediates were acylated at N-1 position

with cyclohexane carbonyl chloride, giving final compounds **4** and **5** in 55 and 57% yield respectively, and the Boc-protected intermediate **6** in 72% yield. Intermediate 6 was then subjected to Boc deprotection in DCM/TFA affording the amino derivative **7**, that was coupled with 2,3,4,5,6-pentafluorobenzoyl chloride leading to **8** (65% yield). Besides, the amino group of the intermediate **7** was subjected to guanidination using tert-butyl(((tert-butoxycarbonyl)amino)(1H-pyrazol-1-yl)methylene)carbamate to obtain Boc-protected derivative **9** in 45% yield. Boc removal of the resulting intermediate gave **10** in 92% yield.

5-Methylindoline-2,3-dione also underwent N-1 alkylation with methyl iodide affording derivative **11**, that was treated with *L*-Cys-OEt in ethanol and $NaHCO_3$ to give the corresponding spiro thiazolidine intermediate **12** as diastereoisomeric mixture (3/1 2'R,4'R/2'S,4'R as ratio) in 85% yield. Acylation of this diastereoisomeric mixture using cyclohexane carbonyl chloride yielded final compound **13** (45% yield) as pure isomer (2'S,4'R), in accordance with literature (Bertamino *et al*., 2013).

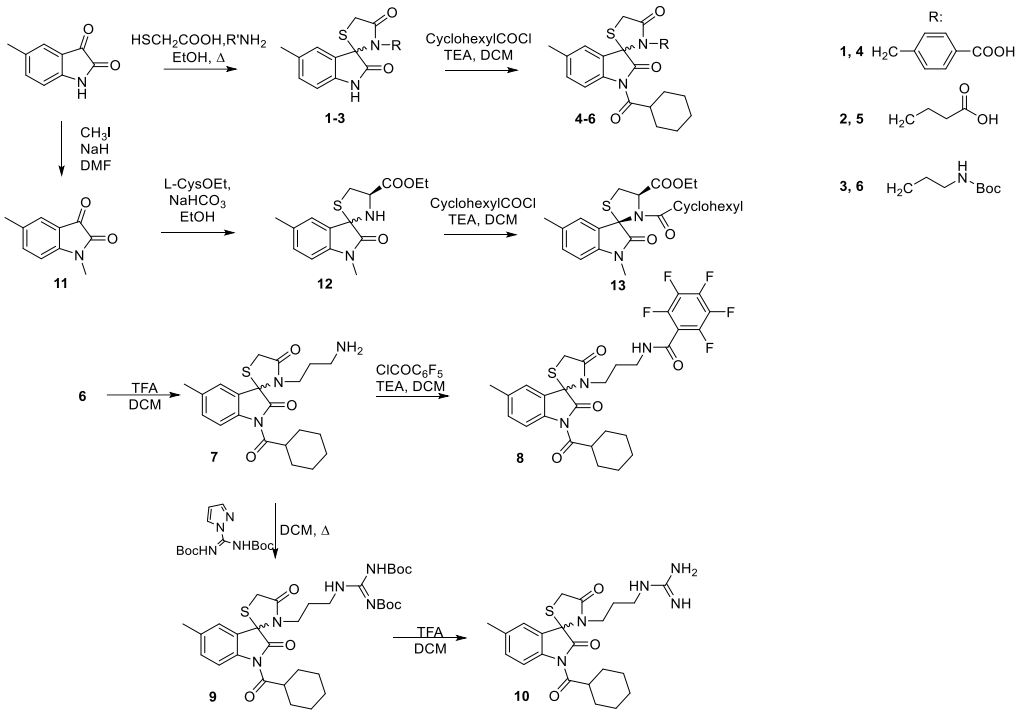


**Figure 48.** *Synthesis of spiro[indoline-3,2'-thiazolidine] derivatives **4**, **5**, **8**, **10** and **13**.*

Derivatives **17** and **18** were obtained as depicted in scheme reported in **Figure 49**. Starting from N-Cbz-L-Leu-OH, reduction of the carboxylic acid function to aldehyde was performed. The aldehyde intermediate was reacted with *L*-Cys-OEt, using the same conditions described above, giving the thiazolidine **15** as diastereoisomeric mixture in 62% yield (3/2 2R,4R,2'S/2S,4R,2'S as ratio). Reaction of **15** with triphosgene and tert-butyl N-(3-aminopropyl)carbamate, followed by a spontaneous intramolecular cyclization gave the hydantoin **16** that, upon removal of the Boc protecting group, afforded the final derivative **17** as pure diastereoisomer (3S,7aR,1'S) in 55% yield.

Stereochemistry was assigned by ROESY NMR spectra (**Figure 50**), assuming retention of configuration for the aminoacid moiety (C-7a and C-1'). A correlation

between H-1' (3.94 ppm) and H-3 (5.22 ppm) was observed, highlighting a cis configuration. On the other hand, the lack of peak correlation between H-7a (3.36 ppm) and H-3 indicates a trans configuration for the two protons. Finally, guanidination of **17**, followed by Boc removal, gave final compound **18** in 55% yield.

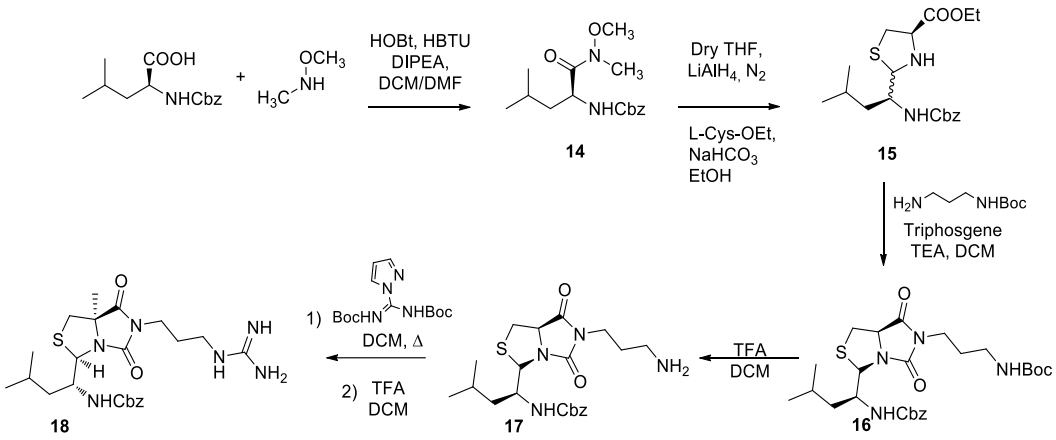


**Figure 49**. *Synthesis of hexahydroimidazo[1,5-c]thiazolidine derivatives **17** and **18**.*

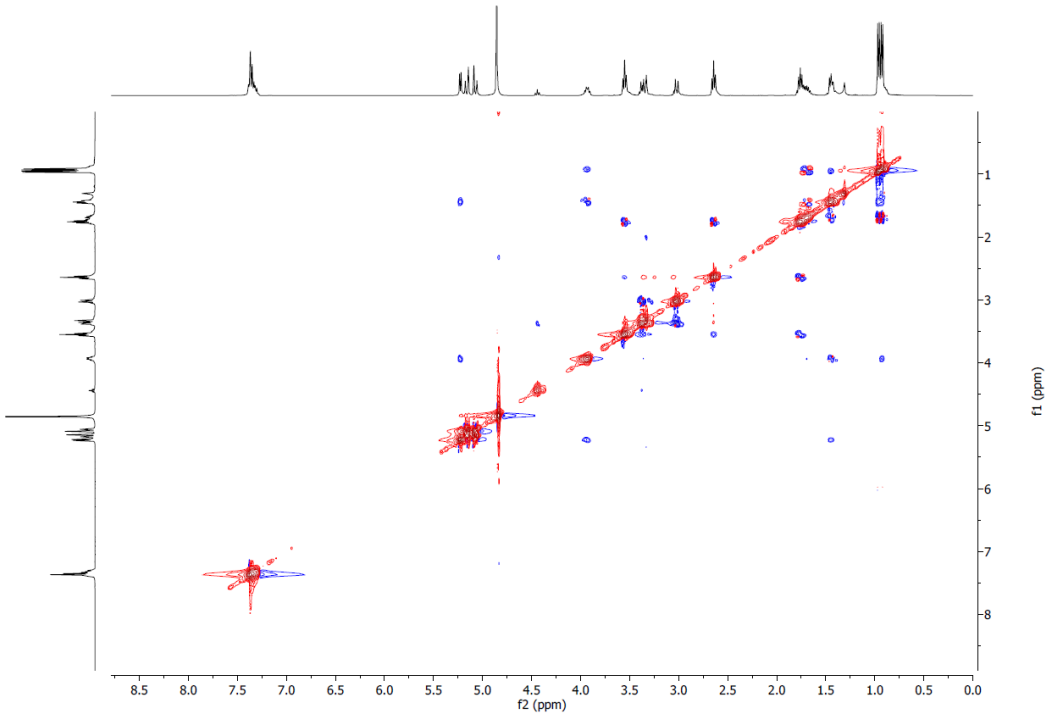


**Figure 50.** *ROESY spectrum of compound **17**.*

Derivatives **21**, **43**-**46**, **48**-**52** were obtained as shown in scheme reported in **Figure 51**.

Starting from 5-nitroindoline, different synthetic approaches were used to decorate both the N-1 and the C-5 positions. Using triphosgene and 2,2-dimethylpropan-1-amine, the urea derivative **19** was obtained in 66% yield. Then, a continuous flow hydrogenation reaction provided the corresponding amine intermediate **20** (61% yield), that was converted to the final compound **21** (58% yield) through a reductive amination reaction with 4-fluorobenzaldehyde. Under the same conditions, N-1 alkylation of 5-nitroindoline was attained, using commercially available aldehydes, leading to the intermediates **22**-**25** in 62-92% yields. Intermediates **26**-**28** were synthesized using the same protocol and the modified aldehydes **26a**, **27a** and **28a** obtained as described in **Figure 51**. Continuous flow hydrogenation of these compounds afforded the corresponding amines **29**-**35** in 58-95% yields. Intermediates **29**-**35** were converted to isothiocyanates **36**-**42** by reaction with $CS_2$ in toluene followed by treatment with ethyl chloroformate (48-77% yields). Reaction of these intermediates with 2,2-dimethylpropan-1-amine yielded thiourea analogues **43**-**49** in 52-67% yields. Compound **43** was further modified to guanidine **50** by reaction with HgO, in presence of $Na_2SO_4$ and $CaCl_2$, followed by addition of $NH_4OH$, as previously described (Ostacolo *et al*., 2020). Compound **47** underwent Boc removal as described before, giving final compound **51**.

Final compound **52** was obtained from **49**, after removal of the MOM protecting group in acid conditions.

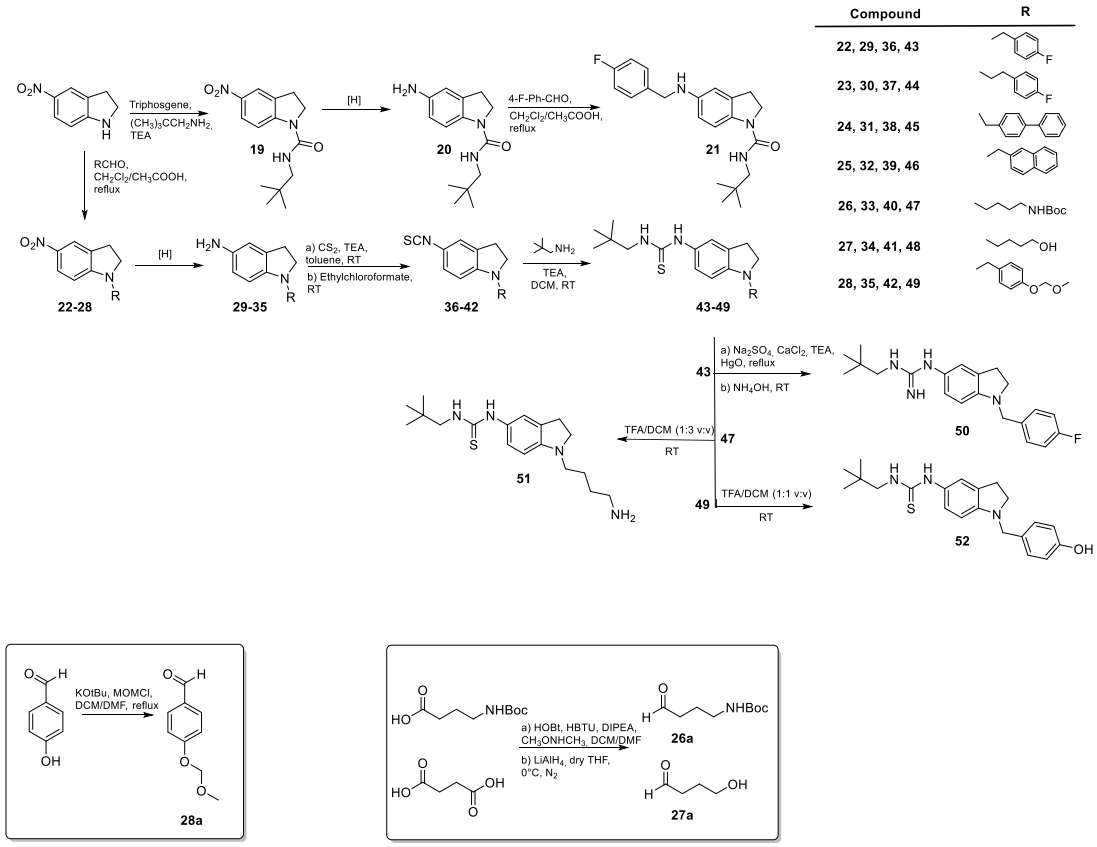








**Figure 51.** *Synthesis of indoline derivatives **21**, **43-46**, **48-52**.*

Indoline derivatives **53-58** were synthesized in according to scheme reported in **Figure 52**.

The intermediate **29** was converted to its carbamic chloride by reaction with triphosgene that, upon reaction with cyclohexylamine and 2,2-dimethyl-1-propanamine, gave urea final compounds **53** and **54** in **72** and 78% yields, respectively. Coupling of **29** with cyclohexane sulfonyl chloride afforded, instead, final compound **55** as previously described (Ostacolo *et al*., 2020).

Previously obtained intermediate **30** was converted into aromatic thiourea analogues by the same method described above in 58-67% yields.

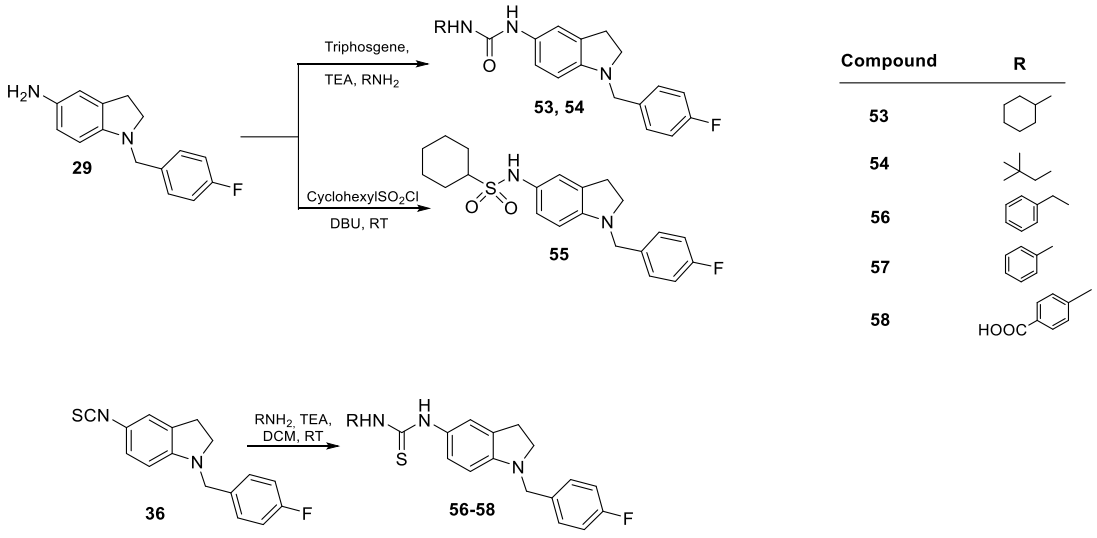


**Figure 52.** *Synthesis of indoline derivatives **53-58**.*

5-Nitroindoline was also decorated at the N-1 by acylation with 4-fluorobenzoyl chloride and 4-fluorophenylacetyl chloride, to give intermediates **59** and **60** in 91 and 88% yields respectively and using di-tert-butyl dicarbonate to give the N-Boc intermediate **61** in 88% yield (**Figure 53**). The use of continuous flow hydrogenation protocol followed by conversion to the isothiocyanates **65-67** (58-62% yield) and reaction with 2,2-dimethylpropan-1-amine gave the final compounds **68** and **69** which were isolated in 65% and 58% yields respectively. On the other hand, intermediate **70** was further reacted using TFA for the removal of the Boc protecting group. The resulting intermediate **71**, was sequentially subjected to reductive amination to form intermediate **72** in 68% yield, and to reduction using Zn in ammonium chloride to give final nitroso compound **73** (64% yield).

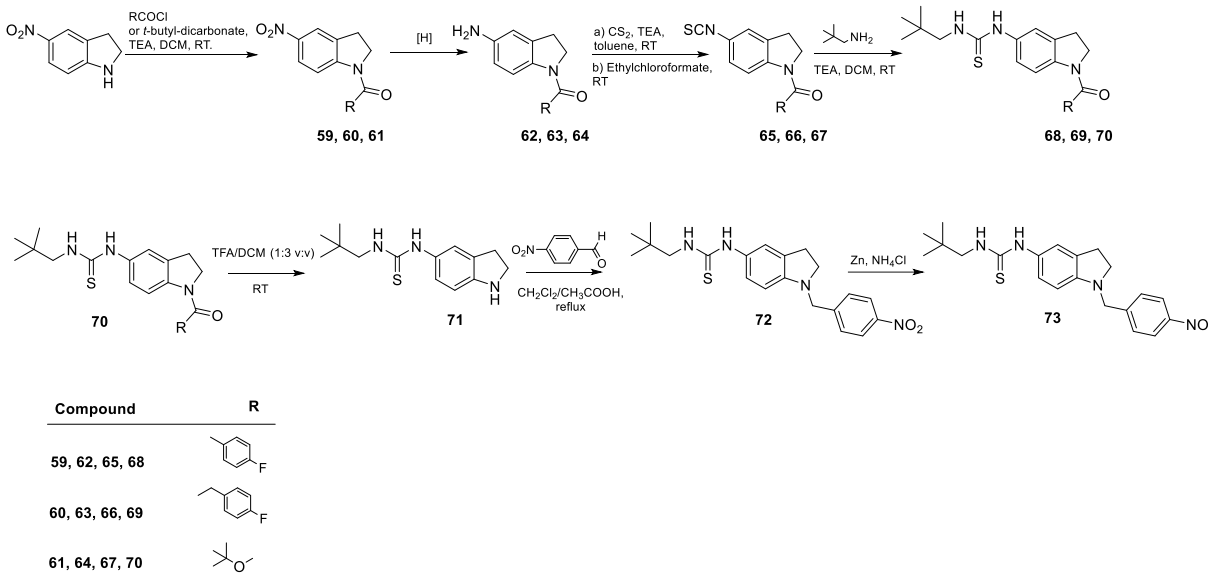


**Figure 53.** *Synthesis of indoline derivatives **68, 69** and **73**.*

Finally, the procedures used for the synthesis of final compounds **77** and **82** are described in scheme reported in **Figure 54**. These molecules were synthesized to expand the SAR clues about dual 5-LOX/sEH inhibitors by increasing planarity and aromaticity of the scaffold with the indole ring and allowing further exploration of the binding site by sterically hindered carbazole moiety.

5-Nitroindole was modified at N-1 using 4-fluorobenzyl bromide by the synthetic strategy previously described (Bertamino *et al*., 2018). The corresponding intermediate **74** was subjected to the same sequential reaction steps described above to give the final thiourea compound **77** (34% overall yield). The same reaction procedures were used, starting from 9-(4-fluorobenzyl)-9H-carbazole (**78**), that upon nitration in nitric acid and acetic anhydride, was transformed to the corresponding thiourea compound **82** (21% overall yield).

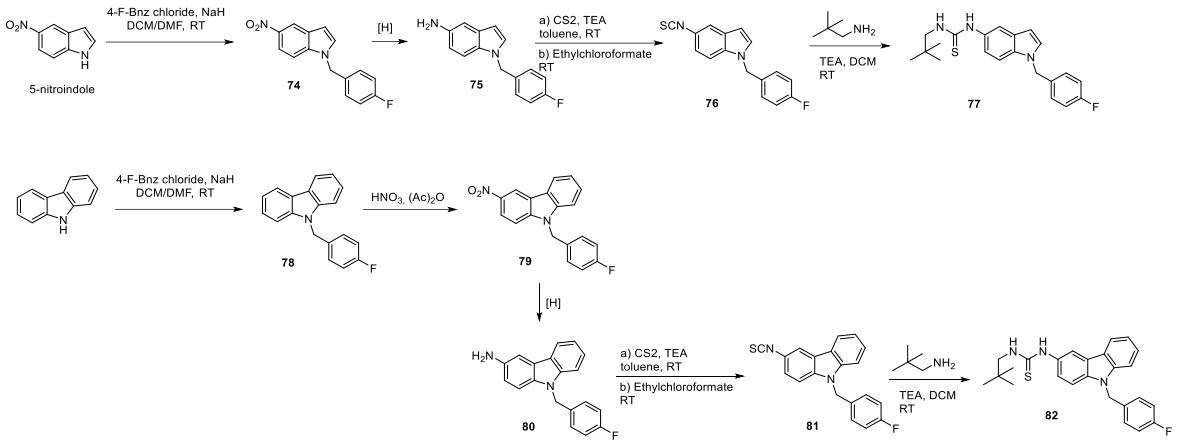


**Figure 54.** *Synthesis of indole derivative **77** and carbazole derivative **82**.*

### *2.1.5 Results discussion: in silico and in vitro integrated approach*

Given the interesting in vitro results obtained from series II, we performed an *in silico* evaluation against 5-LOX and sEH enzymes. The compounds **53**, **54** and **73** exhibited the best experimental outcomes, filling equivalent spaces at the 5-LOX binding site when compared to **43**, and displayed the same pattern of intermolecular contacts by the common structural moieties (**Figure 55B, -C and -D**). In contrast to the parent compound **43**, in **53** and **54** the thiourea is substituted with urea that preserves the same network of H-bonds in the 5-LOX binding pocket. Like the neopentyl group of **43**, the cyclohexyl substituent of **53** gives van der Waals contacts with Y181, F421, A424, N425, P569, H600, A603.

Compounds **53** and **54** inhibited isolated 5-LOX enzyme potently, with $IC_{50}$ of 0.28 ± 0.02 μM and 0.18 ± 0.05 μM, respectively (**Table 8**). With respect to **43**, both compounds showed no 5-LOX inhibitory activity in the cell-based assay. This might be explained by poor membrane permeation, but different reasons cannot be excluded.

Moreover, **53** and **54** also showed a potent inhibitory effect against sEH, with $IC_{50}$ of 61 ± 3 nM and 100 ± 10 nM, respectively (**Table 8**). These data are in accordance

with the literature suggesting that the presence of a urea group is a pivotal requisite for potent sEH inhibition (Sun *et al*., 2021).

Indeed, the two compounds fitted very well in the binding cavity of the enzyme, presenting superimposable conformations with the co-crystallized ligand 34N (**Figure 2B, C**) (Eldrup *et al*., 2009). For both binders, the indoline and 4-fluorobenzyl moieties give π-π interaction with H524 and W525, respectively. Their urea group is involved in a network of four hydrogen bonds with the side chains of D335, Y383 and Y466, unlike **43** that donates a hydrogen bond with its thiourea group (**Figure 56A**). The neopentyl (**54**) and cyclohexyl (**53**) groups are involved in van der Waals contacts with Y336, M339, Q384, Y466, Leu499. It is noteworthy that the contacts found for the indoline, urea and neopentyl/cyclohexyl are also observed with 34N. In **50**, the thiourea was replaced by a guanidine losing the hydrogen bond with Y181 side chain.

The loss of interaction with Y181 seems responsible for a partial loss of activity for compound **50** showing three times higher $IC_{50}$ on isolated 5-LOX compared to **43** (1.42 ± 0.23 *vs* 0.45 ± 0.11 μM).

The most interesting compound of the series is represented by compound **73**. It is noteworthy that **73** structurally differs from all other compounds for the NO group instead of fluorine. The NO group is engaged in hydrogen bonds with side chains of R411, tightening the affinity towards 5-LOX. The phenyl ring in two aromatic H-bonds with backbone CO of L368 and N407 (**Figure 56D**), showing the highest potency against both isolated 5-LOX and PMNL (0.41 ± 0.01 μM and 0.59 ± 0.09 μM, respectively, **Table 8**). Moreover, **73** also exhibited an important efficacy against sEH with an $IC_{50}$ of 0.43 μM ± 0.10 (**Table 8**). We observed that the NO group also favors the binding to sEH by establishing two H-bonds with the backbone NH groups of F497 and H524 (**Figure 56D**). With respect to **73**, the phenol moiety of **52** is only H-bonded

to the backbone CO of N407, justifying a reduced activity on isolated 5-LOX and PMNL ($IC_{50}$ = 5.10 ± 2.92 μM and 2.90 ± 0.75 μM respectively), otherwise sEH inhibition is maintained with an $IC_{50}$ of 0.79 ± 0.52 μM (**Table 8**). In fact, even though the NO and OH groups of **73** and **52** are also hydrogen bonded to backbone NH and CO of H524 and V416 in the sEH binding cavity, their presence displaces the thiourea moiety, compared to urea of **53** and **54**, giving rise to only one H-bond (**Figure 55**), justifying the mild reduction of sEH activity by **53** and **54**.

If compared with **43**, compounds **44**-**49** and **51** present a substantial modification of the substituent at indoline nitrogen that could affect the correct binding into the 5-LOX catalytic site. Specifically, the switch from methylene (**43**) to ethyl linker between 4-fluorophenyl and indoline moieties (**44**) is well tolerated, while further increase of the substituent size (**45**, **46** and **49**) impairs the interaction from the remaining structural portions of the small molecules, especially for **49**. Compound **48** showed a superimposable accommodation of common molecular portions with the parent compound in the 5-LOX binding site, but the hydroxy butyl chain is quite folded although H-bonded to the backbone CO of Q363. All these compounds exhibit a micromolar activity against isolated 5-LOX, except **44** which showed an $IC_{50}$ comparable to **43** (0.38 ± 0.05 μM *vs* 0.45 ± 0.11 μM). However, for derivatives **45** and **48** a decrease of effectiveness against sEH was observed, while their analogues **44**, **46** and **49** act on the same target with an $IC_{50}$ in the low micromolar range. Unfortunately, none of them is effective against 5-LOX in PMNL. Compound **49** binding to sEH could be rationalized using the same considerations made for **53** and **54**. The compound accepts a H-bond from the backbone NH of H524, leading to an unfavorable entropic loss. Like **52** and **73**, increasing the size of the substituent at indoline nitrogen (**44** and **46**) also allows hydrogen bonding with only the side chain

of D335 (**Figure 56F**). Derivative **45**, endowed with a larger substituent at indoline nitrogen than **44** and **46**, is unable to give hydrogen bonds by thiourea moiety.

The conversion of the indoline core to indole (**77**) induces a binding conformation into 5-LOX characterized by less contacts with W147, F151, H372, L368, L373, A410, R411 and I415 reflecting an almost complete loss of 5-LOX and sEH inhibition.

In **82**, the indoline was converted into the more hindered carbazole, resulting in docked poses with distorted structural moieties, especially for thiourea and tricyclic aromatic portion, inducing a total inactivity against both targets. For **56-58** a π-π interaction is observed among the phenyl ring and side chain of F421, unlike the parent compound. Moreover, **56** gives π-π interaction with F359, while **57** and **58** with Y181.

The compounds maintained a good activity in the cell-free assay, but only **56** and **57** are able to affect the 5-LOX activity in PMNL, likely due to their higher lipophilicity than the acid analogue **58**.

In consideration of the data described, taking particularly into account the activity of the synthesized derivatives on 5-LOX in PMNL, more properly resembling the biological environment, we have decided to select compound **73** for further pharmacological characterization of this class of compounds.

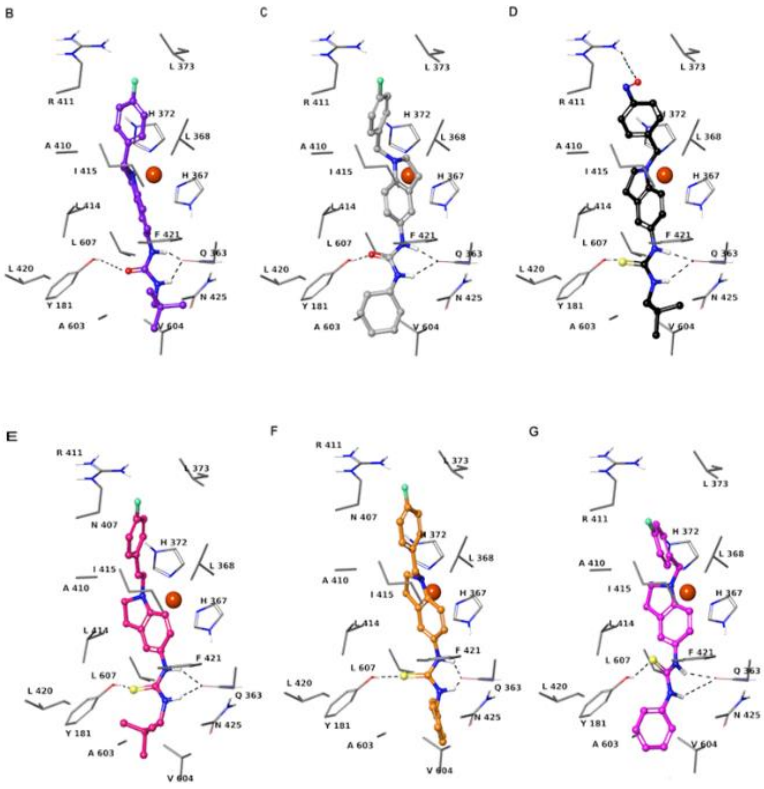


**Figure 55.** *Three-dimensional model of the interactions given by **53** (B), **54** (C), **73** (D), **44** (E), **56** (F) and **57** (G) with 5-LOX.*

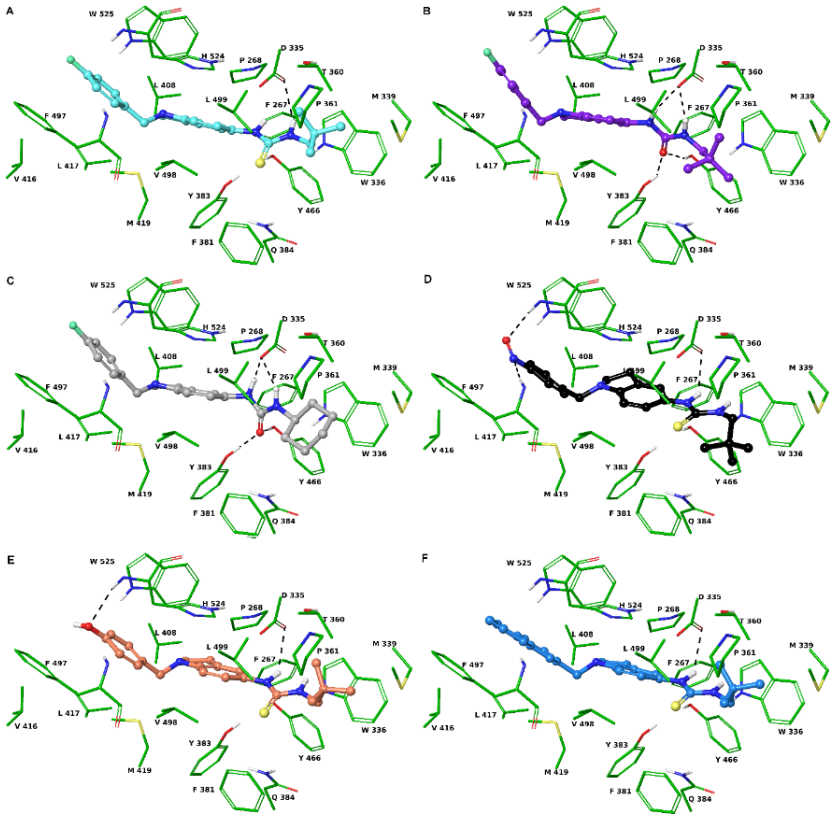


**Figure 56.** *Three-dimensional model of the interactions given by **43** (A), **53** (B), **54** (C), **73** (D), **58** (E) and **46** (F) with sEH.*

### *2.1.6 Evaluation of COX-1 and COX-2 inhibition in intact cells*

Furthermore, we investigated the impact of **73** on COX-1 and COX-2, enzymes within the AA cascade given their role in the biosynthesis of prostanoids in addition to 5-LOX and sEH. A well-established in vitro cell culture assay (J774 murine macrophages) was performed to evaluate the effects of **73** against both COX isoforms (Anzini *et al*., 2013; Biava *et al.*, 2011).

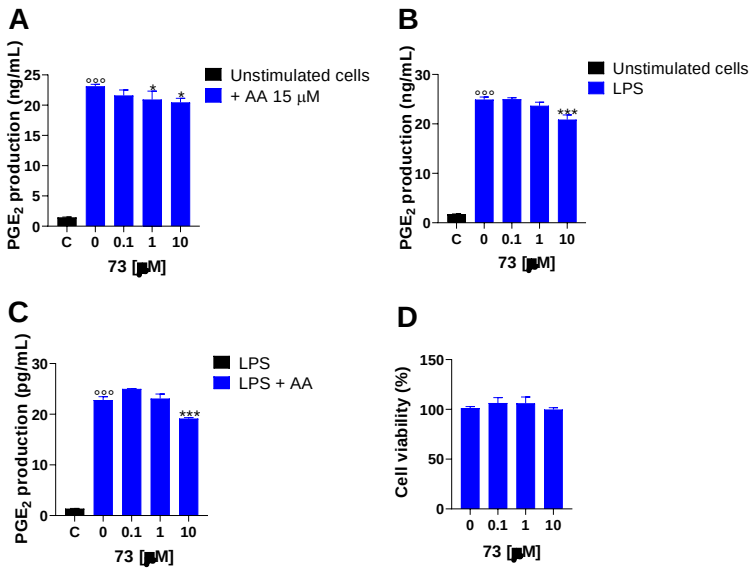


**Figure 57.** *Effect of **73** on COX-1 and COX-2 in intact cells. (A) J774 cells were pre-treated for 2 h with **73** compound (0-10 µM) and then incubated with arachidonic acid (15 µM) for 30 min to stimulate COX-1 activity. (B) J774 cells were pre-treated for 2h with test compound (0-10 µM) and then stimulated for 24 h with LPS (10 µg/mL) to induce COX-2. (C) Cells were stimulated, for 24 h, with LPS (10 µg/mL), to induce COX-2, then pre-treated for 2 h with **73**, and further incubated for 30 min with AA (15 µM). The supernatants were collected for the measurement of $PGE_2$ levels by ELISA assay. (D) Cell viability was evaluated by the mitochondrial-dependent reduction of MTT to formazan.*

Stimulation of J774 macrophages with AA (15 µM) for 30 min induced a significant increase of PGE2 levels in comparison to unstimulated control cells. **73** weakly inhibited production of PGE2 primarily generated via COX-1 at micromolar concentrations (**Figure 57-A**). The same trend was observed for PGE2 production in LPS-stimulated cells in absence (**Figure 57-B**) or presence (**Figure 57-C**) of AA which is mainly mediated by inducible COX-2. These results indicate a higher target selectivity of compound **73** for 5-LOX and sEH enzymes. Finally, cytotoxic effects were excluded since **73** did not impair cell viability at all tested concentrations **(Figure**

**57-D**). Overall, molecular docking and in vitro biological investigations suggest **73** as a promising drug candidate for further in vivo pharmacological studies.

### *2.1.7 Evaluation of in vivo anti-inflammatory effects*

The anti-inflammatory efficacy of compound **73** was evaluated *in vivo* in a zymosan-induced murine peritonitis model at the University of Naples "Federico II" by Prof. Antonietta Rossi's group. This is an experimental model of acute inflammation related to the presence of leukotrienes and other lipid mediators. Zileuton was used as a control (i.p. 35 mg/kg, 30 min before zymosan, **Figure 58A**).

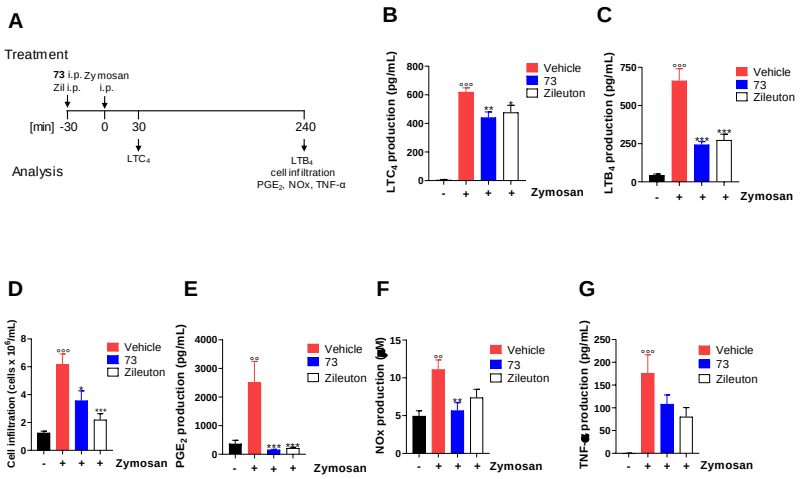


**Figure 58.** *Compound **73** inhibits 5-LOX product formation and limits inflammation in murine peritonitis. (A) Time-scale for zymosan-induced murine peritonitis. Mice received **73** (10 mg/kg, i.p.) or zileuton (10 mg/kg, i.p.) 30 min before zymosan and were killed 30 min (B) or 4 h (C-G) post peritonitis induction injection. (B) $LTC_4$, (C) $LTB_4$, (E) $PGE_2$ and TNF-α (G) levels in the exudate analyzed by ELISA. (D) Immune cell infiltration into the peritoneal cavity. (F) NOx levels in the exudates by Griess assay.*

The zymosan activates murine peritoneal macrophages which in turn are responsible for the production of LTC4. In contrast, the progressive phase of

inflammation is dominated by infiltrating neutrophils, which generate the potent chemoattractant LTB4 and other pro-inflammatory mediators such as PGE2, nitric oxide, and TNF-α. Accordingly, 30 min and 4 h after zymosan injection a significative increase of LTC4 and LTB4 was observed as compared to the unstimulated control group (**Figure 58B and 58C**). The i.p. pre-treatment of mice with **73** (10 mg/kg, 30 min before zymosan, **Figure 58A**) significantly reduced LTC4 and LTB4 levels in the peritoneal exudate, comparable to zileuton (**Figure 58B and 58C**). Since LTB4 is a major chemoattractant for leukocytes, **73** caused a concomitant reduction of leukocyte recruitment in the peritoneal cavity (**Figure 58D**). The in vivo anti-inflammatory effects of **73** were also displayed by a significant inhibition of zymosan-induced PGE2 (**Figure 58E**) and NOx (**Figure 58F**) production as well as by a reduction (not significant) of TNF-α levels (**Figure 58G**) in the peritoneal exudates of zymosan-treated mice.

In addition, to evaluate in vivo sEH inhibition, we measured the levels of several epoxy- and dihydroxy-unsaturated fatty acids in peritoneal exudate upon compound **73** administration, using AUDA as a positive control. In detail, we were unable to measure the levels of (±)5,6-epoxy-8*Z*,11*Z*,14*Z*-eicosatrienoic acid (5,6-EET), (±)8,9-epoxy-5*Z*,11*Z*,14*Z*-eicosatrienoic acid (8,9-EET), and the corresponding dihydroxy derivatives (±)5,6-dihydroxy-8*Z*,11*Z*,14*Z*-eicosatrienoic acid (5,6-DHET) and (±)8,9-dihydroxy-5*Z*,11*Z*,14*Z*-eicosatrienoic acid (8,9-DHET) since their amount was below the LOQ. Thus, quantification was performed only for (±)11,(12)-epoxy-5*Z*,8*Z*,14*Z*-eicosatrienoic acid (11,12-EET), (±)14(15)-epoxy-5*Z*,8*Z*,11*Z*-eicosatrienoic acid (14,15-EET), (±)11,12-dihydroxy-5*Z*,8*Z*,14*Z*-eicosatrienoic acid (11,12-DHET), and (±)14,15-dihydroxy-5*Z*,8*Z*,11*Z*-eicosatrienoic acid (14,15-DHET). We found that the epoxy-unsaturated fatty acid levels were about 8 times higher than the corresponding

dihydroxy-unsaturated fatty acids in both 73- and AUDA-treated mice, in accordance with the sEH inhibition mechanism (**Figure 59**).

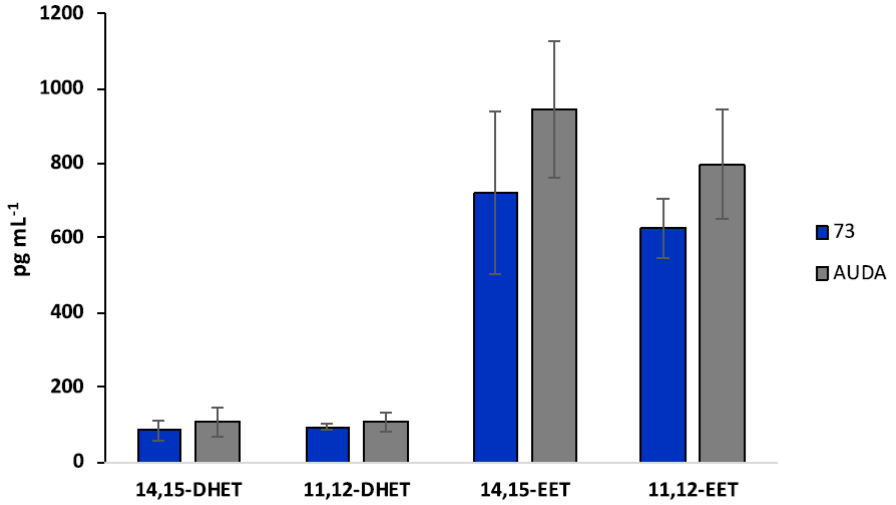


**Figure 59.** *Effect of compound **73** (10 mg/kg, i.p.) and AUDA (10 mg/kg, i.p.) administration on eicosatrienoic acid levels in mouse peritoneal exudate during acute inflammation initiated by zymosan. Values represent means ± S.D.; n = 6 mice for each group.*

Since leukotrienes play a key role in the pathogenesis of asthma by inducing both immune cell infiltration and lung inflammation and bronchoconstriction, the effects of compound **73** were studied in an experimental model of asthma. The experiments were conducted at the University of Naples "Federico II" by Prof. Fiorentina Roviezzo's group. Mice were pretreated with **73** i.p. 30 min before ovalbumin (OVA) injection on days 0 and 7. Animals were sacrificed after 21 days to assess bronchial hyperresponsiveness, lung inflammation, lung LTC4 levels, plasma IgE and Th2 cytokine production (**Figure 60-A**).

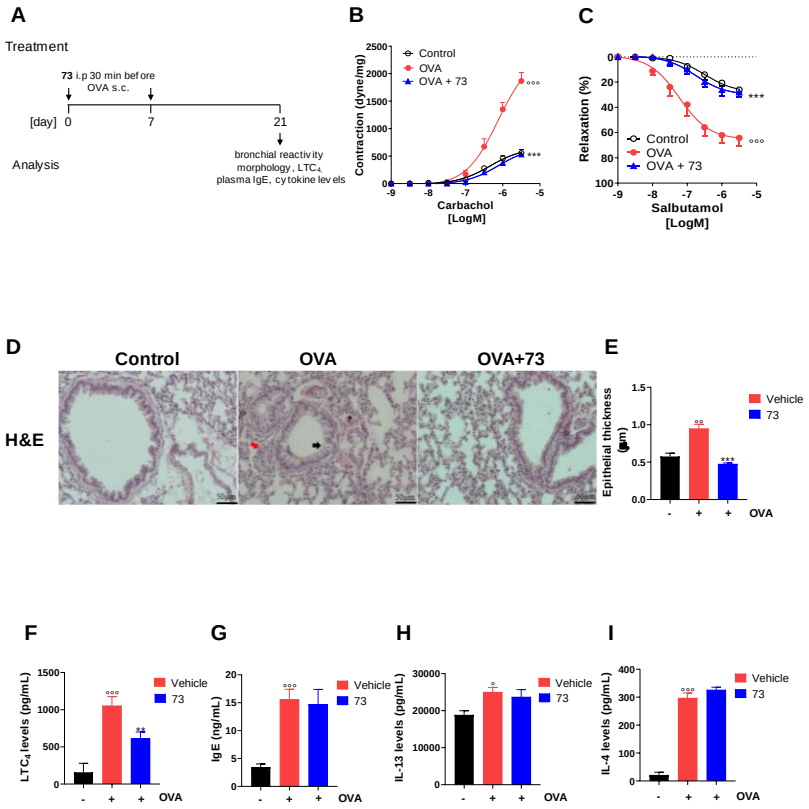


**Figure 60.** *Compound **73** suppresses hallmarks of asthma and pulmonary LT formation in mice sensitized to ovalbumin. (A) Time-scale for the experimental asthma model. Compound **73** (10 mg/kg) was i.p. administered to mice 30 min prior to injection of ovalbumin (OVA) at days 0 and 7. (B) Bronchial reactivity to carbachol or (C) salbutamol. (D) Lung slices were stained for H&E. (E) Epithelial thickness was evaluated using ImageJ Fiji. Pulmonary levels of (F) $LTC_4$, (H) IL-13, (I) IL-4 and (G) plasma IgE levels analyzed by ELISA. Values represent means ± S.E.M.; n = 6 mice for each group. Data were analyzed by two-way ANOVA plus Bonferroni (B and C) and one-way ANOVA plus Bonferroni (E-I). Statistical significance is reported as follows: ° P<0.05; °° P<0.01 and °°° P < 0.001 vs control; ** P < 0.01 and *** P < 0.001 vs OVA + vehicle. Black arrow = bronchial epithelium thickness, red arrow = pulmonary cell infiltration in peribronchial areas, asterisk = pulmonary cell infiltration in perivascular areas (D).*

Sensitization to OVA induced airway hyperresponsiveness to carbacol (**Figure 60B**) and increased bronchial relaxation was observed in response to salbutamol (**Figure 60C**).

Intraperitoneal treatment of mice with 19 reversed OVA-induced bronchial hyperresponsiveness to carbacol (**Figure 60B**) and completely restored bronchial adrenergic relaxation induced by salbutamol (**Figure 60C**). Sensitization to OVA caused airway inflammation by inducing morphological alteration (**Figure 60D**) and increasing the thickness of bronchial epithelium (black arrow) (**Figure 60D and 60E**). In addition, sensitization to OVA promoted lung cell infiltration in the peribronchial (red arrow) and perivascular (asterisk) areas compared with the control group (**Figure 60D**). Pre-treatment with **73** significantly reduced epithelial thickness (**Figure 60E**) in OVA-sensitized mice. The beneficial effect of **73** on lung function was initially associated with reduced lung LTC4 levels in sensitized mice treated with the test compound (**Figure 60F**). However, **73** did not affect the mechanisms of sensitization. In fact, it did not modulate plasma levels of IgE (**Figure 60G**) and pulmonary type 2 T-helper cytokines such as interleukin-13 and interleukin-4 (**Figure 60H and 60I**) in OVA-sensitized mice.

## 2.2 sEH: background

As previously discussed, inhibition of soluble epoxide hydrolase has been shown to be useful for the treatment of inflammatory and pain-related diseases (Wagner *et al*., 2017), and numerous potent sEH inhibitors (sEHIs) present adamantyl or phenyl moieties, such as the clinical candidates AR9281 or EC5026 (**Figure 61**) (Shen *et al*., 2012).

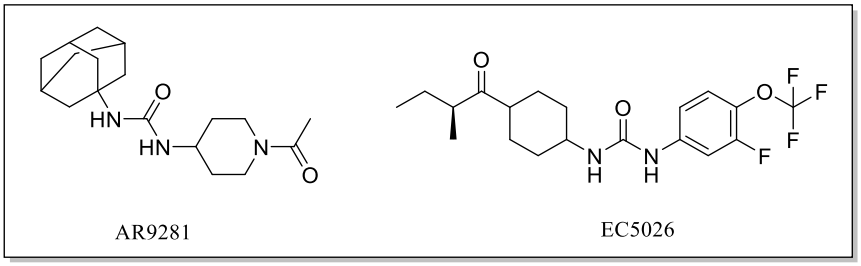


**Figure 61.** *Structure of clinical candidates AR9281 and EC5026.*

sEH has also been shown to play a crucial role in several other metabolic disorders, such as cardiovascular remodelling, hypertension, kidney disease, diabetes and atherosclerosis (He *et al*., 2016). The role of sEH in acute pancreatitis (AP) has previously remained unexplored but a lot of evidence implicates sEH in pancreatic endocrine function. sEH deficiency and pharmacological inhibition promote insulin secretion and reduce islet apoptosis in a type 1 diabetes model and increase islet mass in a mouse model of high fat diet-induced insulin resistance (Bettaieb *et al*., 2015).

### *2.2.1 Design of series I*

Based on previous results where derivative **53** showed a certain selectivity for the enzyme sEH ($IC_{50}$ for isolated sEH = 61.00 ± 3.00 nM, $IC_{50}$ for isolated 5-LOX = 280 ± 20 nM) and considering the involvement of this enzyme in several metabolic disorders, including pancreatitis, we decided to investigate the structure-activity relationships responsible for this selectivity. Thus, starting from derivative **53**, a new series of analogues was designed (**Figure 62**) preserving the indoline scaffold, except for derivative **109** which is characterised by an indole core.

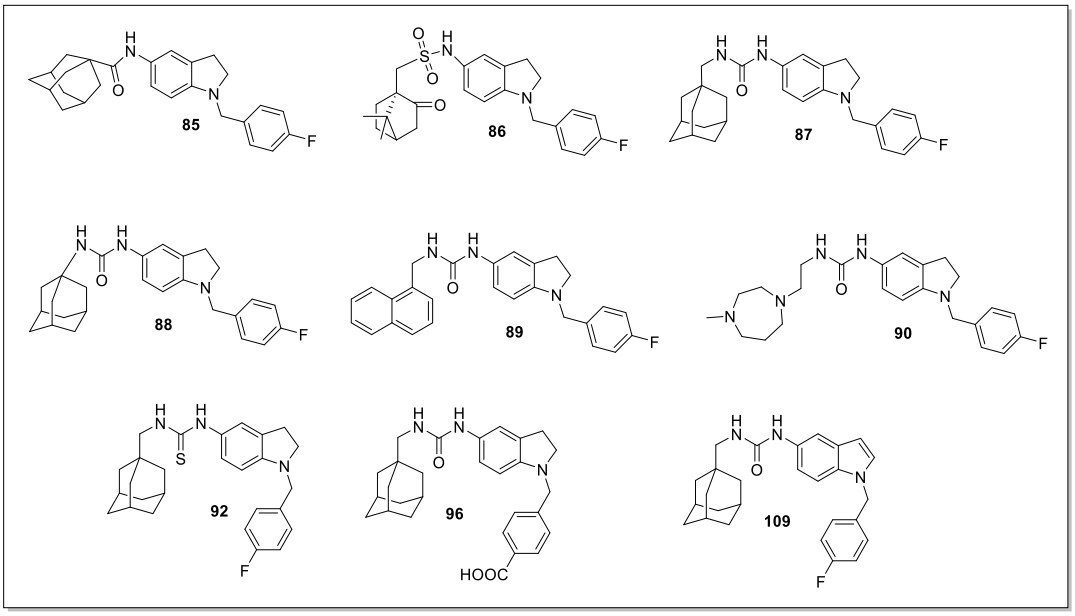


**Figure 62.** *Series I: synthesized derivatives.*

Until now, urea derivatives are the most abundant and effective sEH inhibitors due to the central urea group which binds strongly the catalytic pocket of sEH (Gomez *et al*., 2006). Experimental data showed that the oxygen atom on the urea group forms two hydrogen bonds with the amino acid residues Tyr381 and Tyr465 in the catalytic pocket of sEH (Gomez et al., 2006). In addition, the N-H of the urea group acts as hydrogen bond donor with Asp333 (Gomez *et al*., 2006). Due to their high potency, urea derivatives have been widely developed, in particular to increase solubility and bioavailability for application in the treatment of EpFA-related diseases. For this reason, the ureidic group has been preserved for some analogues (**87**, **88**, **89**, **90**, **96** and **109**), while for other compounds it has been replaced with isosteric groups as sulfonamide (**86**), thioureido (**92**) or amine substituents (**85**) to investigate variations in terms of potency and selectivity. X-ray crystallographic studies have revealed that sEH has an active site characterised by a catalytic triad, at the corner of an L-shaped hydrophobic pocket, that comprises a nucleophilic aspartic acid, which attacks the

carbon of the epoxide, highly polarised by hydrogen bonds with two tyrosine residues, and a histidine-aspartic acid pair, which activates the hydrolysis of the acyl-enzyme intermediate (Sun *et al*., 2020). Therefore, lipophilic groups such as cyclohexyl or adamantyl are commonly present in potent sEH inhibitors to establish hydrophobic interactions with the pocket. Based on this experimental evidence, it was decided to introduce an adamantyl group on the ureidic nitrogen (**87**, **88**, **92**, **96**, **109**) or groups with greater or lesser lipophilicity (**86**, **89**, **90**) in order to explore possible interactions within the binding pocket.

### *2.2.2 Biological evaluation: in vitro assays*

The *in vitro* characterization of this first series of sEH inhibitors involved specific assays on the isolated enzymes, as well as in-cell assays on PMNLs, as previously discussed. Results are summarized in **Table 9**.

Indole derivative **109** showed the highest potency and selectivity towards soluble epoxide hydrolase with an $IC_{50}$ of 1.75 nM, leading the design of a new series of indole and carbazole core analogues.

**Table 9**. *Inhibition of 5-LOX Product Formation in Activated PMNL of Human Isolated 5-LOX and Human isolated sEH. All values are given as mean ± SEM of single determinations obtained in 3−4 independent experiments*[a]

| ***Compounds*** | ***5-LOX residual activity in PMNL (%)*** | ***$IC_{50}$ for isolated 5-LOX (nM)*** | ***$IC_{50}$ for isolated sEH (nM)*** |
|---|---|---|---|
| ***85*** | 53.2 ± 9.9 | 74 ± 18 | 285.1 ± 31.2 |
| ***86*** | 2.5 ± 2.5 | 171 ± 66 | 1800.1 ± 460.2 |
| ***87*** | 73.7 ± 2.8 | 78 ± 53.0 | 11.1 ± 6.0 |
| ***88*** | 35.4 ± 3.1 | 71 ± 16 | 7.22 ± 1.11 |
| ***89*** | 56.3 ± 5.1 | 148 ± 28 | 36.1 ± 7.5 |
| ***90*** | 71.1 ± 6.6 | 1913 ± 942 | >10 |
| ***92*** | >10 | >1000 | 287.8 ± 219.5 |
| ***96*** | 57.7 ± 9.6 | >1000 | 24.1 ± 4.1 |
| ***109*** | 59.4 ± 6.7 | >1000 | **1.752 ± 0.593** |

[a]Zileuton, used as positive control at 3 μM gives residual activity of 3.90 ± 4.14% and 14.24 ± 5.88% over PMNL and isolated 5-LOX, respectively. AUDA used as positive control at 1 μM gives residual activity of 3.90 ± 4.14% over isolated sEH.

### *2.2.3 sEH inhibitors: design of series II*

For the new series of compounds (**Figure 63**), it was decided to keep the indole core unchanged, while for derivative **130**, the latter was replaced by carbazole scaffold, in order to investigate the effects of more hindered structure on inhibitory activity towards the enzyme.

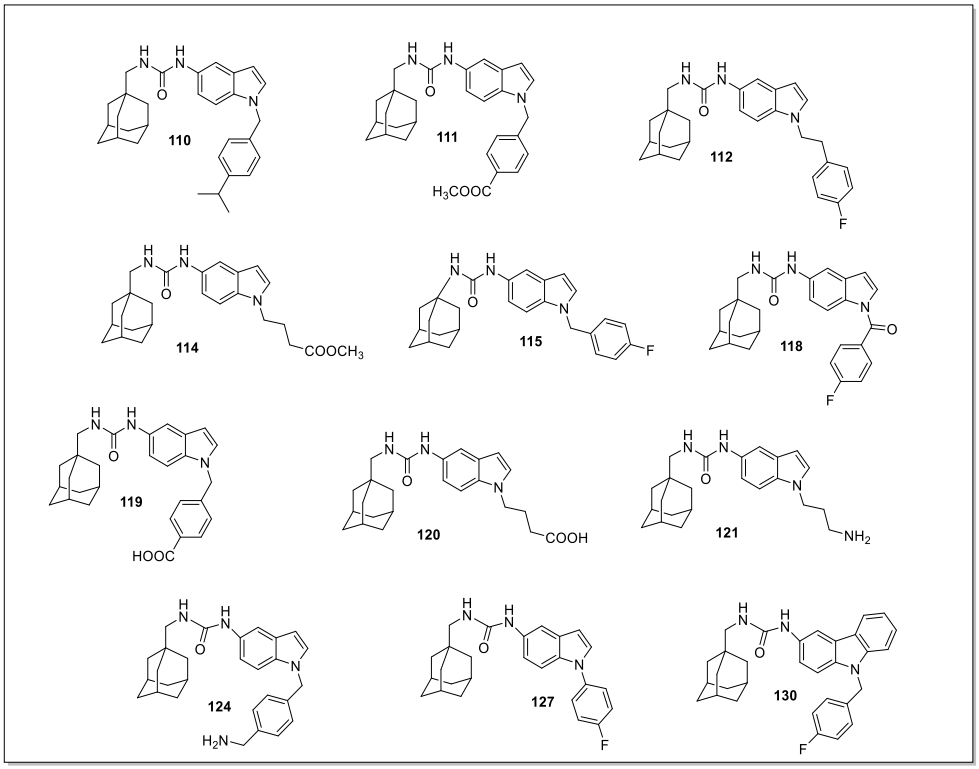


**Figure 63.** *Series II: synthesized derivatives.*

The N-(Adamantyl)urea group remained mainly unchanged, except for derivative **115**, where the methylene bridge between the adamantyl group and the indole scaffold was removed. Most of the changes affected the N-1 substituent of the indole core; in particular, the importance of the p-fluorobenzyl substituent was investigated introducing different group in position 4 of the benzyl moiety (**110**, **111**, **119**, **124**) or substituents with a certain polarity (**120**, **121**), and changing the spacer length between the indole nitrogen and the aromatic group (**112**, **127**) or replacing it with a carbonyl group (**118**).

### *2.2.4 Biological evaluation: in vitro assays*

The *in vitro* characterisation for this second series of molecules was carried out using the same assays discussed above. In particular, the effects of the interest compounds on 5-LOX, both in the cellular environment, and on soluble epoxide hydrolase, were assessed.

**Table 10.** *Inhibition of 5-LOX Product Formation in Activated PMNL, of Human Isolated 5-LOX and Human Isolated sEH. All values are given as mean ± SEM of single determinations obtained in 3−4 independent experiments.*[a]

| *Compounds* | *5-LOX residual activity in PMNL (%)* | *$IC_{50}$ for isolated 5-LOX (nM)* | *$IC_{50}$ for isolated sEH (nM)* |
|---|---|---|---|
| ***110*** | 93.6 ± 4.8 | >1000 | **2.0 ± 1.1** |
| ***111*** | 65.1 ± 9.4 | >1000 | 11.4 ± 3.6 |
| ***112*** | 65.1 ± 6.2 | >1000 | 1.1 ± 0.4 |
| ***114*** | 30.1 ± 4.8 | >1000 | 21.3 ± 11.9 |
| ***115*** | 97.8 ± 0.3 | >1000 | 13.4 ± 3.1 |
| ***118*** | 58.1 ± 5.5 | >1000 | 2.6 ± 0.4 |
| ***119*** | 2.1 ± 1.1 | >1000 | 15.1 ± 7.7 |
| ***120*** | 41.2 ± 7.8 | >1000 | 53.3 ± 15.9 |
| ***121*** | 51.8 ± 13.0 | >1000 | 27.2 ± 11.8 |
| ***124*** | 6.6 ± 4.0 | >1000 | 14.9 ± 4.6 |
| ***127*** | 80.9 ± 1.7 | >1000 | 4.4 ± 0.5 |
| ***130*** | 92.6 ± 4.0 | >1000 | 20.0 ± 3.8 |

[a]Zileuton, used as positive control at 3 μM gives residual activity of 3.90 ± 4.14% over PMNL. AUDA used as positive control at 1 μM gives residual activity of 3.90 ± 4.14% over isolated sEH.

As reported in **Table 10**, the most interesting derivative in the series is certainly compound **110**, which not only showed high potency over sEH ($IC_{50}$ 2.0 ± 1.1 nM) but also a remarkable selectivity (residual activity in PMNL 93.6 ± 4.8 %) compared to the hit compound **109** (residual activity in PMNL 59.4 ± 6.7 %, **Table 9**).

### *2.2.5 Results discussion: molecular docking and evaluation of 5-LOX and sEH inhibition*

Interestingly, the *in vitro* assays showed that only compounds endowed with indoline ring effectively inhibit 5-LOX activity, spanning from nanomolar to low micromolar range. On the contrary, the remaining congeners proved a very weak/absent 5-LOX inhibition. The experimental outcomes were corroborated by in silico analysis, which highlighted that the conversion from indoline to indole/or carbazole ring widen the planar geometry of bicyclic moiety and consequently of nitrogen-substituent bond producing a stiffness that does not allow an appropriate adaptation and consequent accommodation into the binding site. Indeed, no docked poses or distorted ones are found from calculations. The derivative **88** showed the highest inhibitory activity against isolated 5-LOX ($IC_{50}$ = 71.0 ± 16.0 nM), followed by **85** ($IC_{50}$ = 74 ± 18 nM) and **87** ($IC_{50}$ = 78 ± 53.0 nM). The biological activities of **88**, **85** and **87** were in agreement with structural observations from molecular docking (**Figure 64A, 64B and 64C**). The common 4-fluorobenzyl moiety of these compounds is engaged in a π-π stacking with H367 and H372 and a π-cation with $Fe^{2+}$. Both 4-fluorobenzyl and indoline get close to the catalytic iron, obstructing the approach to the open position of ion coordination sphere. The indoline moiety also establishes van der Waals interactions with V175, F177, Y181, I406, L607, I673. These compounds structurally differ for the nature of the linker between indoline and adamantane: an amide group in **85**, a methylene urea in **87**, and an urea group in **88**. For the docked pose of **87** and **88** a π- π stacking between indoline and F177 side chain was observed. In **85**, this π-stacking was not found because the adamantyl group hampers a closer approach to the side chain of F177 due to the shorter linker length between indoline and adamantane. The urea group in both **87** and **88** donates two hydrogen bonds to

amide carbonyl of A606, while accepting an H-bond from side chain of N180. The amide group of **85** accepts two hydrogen bonds from N180 and Q611 and donate an H-bond to the backbone CO of A606. The adamantane group gives van der Waals interactions with surrounding residues, but in **87** it is less enveloped by macromolecular counterparts due to the presence of the methylene. Compounds **86** and **89** showed a comparable inhibition of 5-LOX activity, even though lower than **88** (see **Table 9**). Compared to **88**, the substitution of adamantly group with a naphthalene induced a different conformational arrangement of **89** (**Figure 64D**). Indeed, the indoline ring is 180° rotated respect to **88**, and the urea group shifts toward backbone CO of I673 donating two H-bonds. Compared to **88**, this shift causes the loss of a hydrogen bond and of some van der Waals contacts by indoline ring, while preserving a π-stacking with F177. Moreover, the 4-F-benzyl moved away from H367 losing a π-π interaction. As for **89**, the indoline of **86** is 180° and similar consideration could be inferred (**Figure 64E**). It is noteworthy that **86** differs from **88** for the substitution of urea with a sulphonamide donating an H-bond to side chain of N180. The (1R)-7,7-dimethylbicyclo[2.2.1]heptan-2-one group of **86** is superimposable to the adamantyl of **88**.

The docked pose of **90** showed the 1-ethylene-4-methyl-1,4-diazepane moiety quite folded to establish a hydrogen bond with backbone CO of Q609 with an unfavourable entropic deficiency. Moreover, this induces a 90° rotation of urea group with respect to **88**, with deficiency of a hydrogen bond with N180. Indeed, **90** presented an inhibitory profile in the low micromolar range. Compounds **96** and **92** did not show a proper fit into binding cavity, justifying the very weak inhibition of enzymatic activity, with an $IC_{50}$ higher than 1000 nM as for compound **90**.

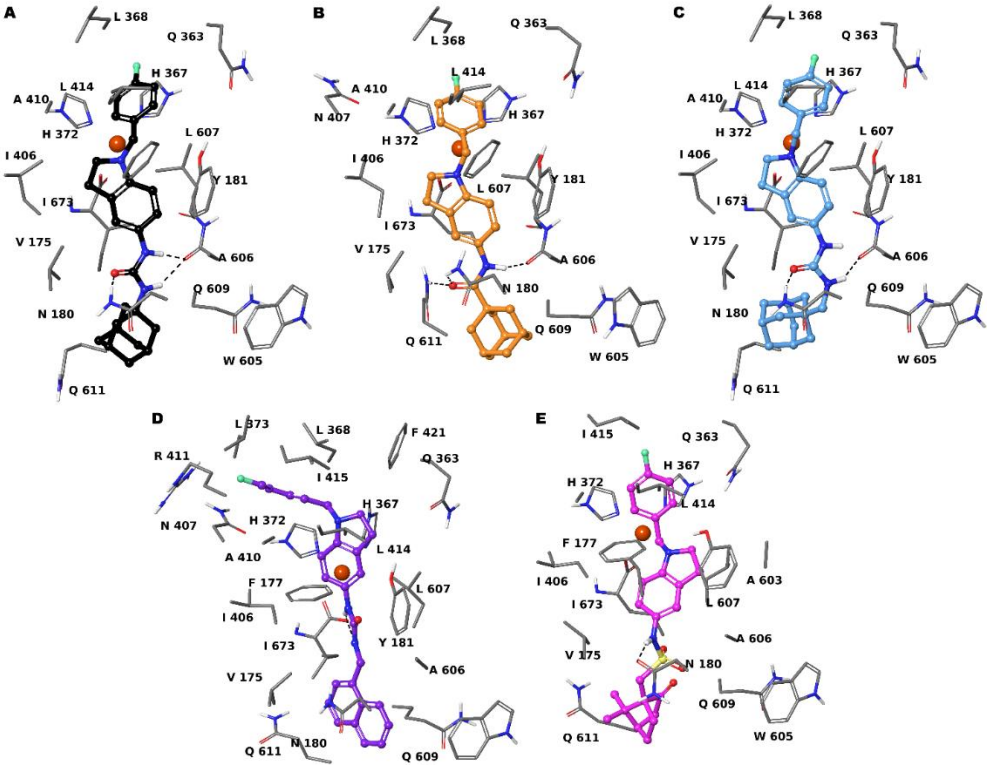


**Figure 64.** *Three-dimensional model of the interactions given by **88** (A), **85** (B), **87** (C), **89** (D) and **86** (E) with 5-LOX.*

The *in vitro* tests against sEH highlighted that most of compounds are active in the nanomolar range with different effectiveness. In particular, five out of twentyone small molecules showed a very potent inhibitory effect (<8 nM): **88**, **109** (**Table 9**), **110**, **112**, and **118** (**Table 10**). They looked well accommodated into binding cavity filling equal room and establishing the same pattern of intermolecular interactions by their identical structural portions (**Figure 65**). In details, the urea group donates two hydrogen bonds to the side chains of D335 and accepts two H-bonds from Y383 and Y466. The adamantyl gives van der Waals contacts with Y336, M339, T360, F381, Q384, Leu499, M503. The indole (**109**, **110**, **112** and **118**) establishes π-π interaction with H524 and W525. In **88**, the indoline is superimposable to the indole moiety of

**109**, **110**, **112** and **118** but does not present the π-stacking with W525, justifying the highest $IC_{50}$ in this set of inhibitors (from 2.8 to 7 times higher than **109**, **110**, **112** and **118**). Interestingly, all these observed intermolecular contacts are also in the 34N/sEH co-crystal structure. All synthesized compounds are endowed with a phenyl ring directly bound to bicyclic nitrogen (**45**) or through a linker: ethylene (**112**), methylene (**109**, **110**) and carbonyl group (**89**). Compared to **118** and **127**, we observed for **109**, **110** and **112** a better π-stacking with W525 thank to higher flexibility of the linker, as demonstrated by their $IC_{50}$ values against sEH. Compounds **87**, **111**, **119** and **124**, showed an inhibitory activity ranging from 10 to 20 nM, slightly inferior respect to the analogues described so far. Compound **87** lacks a π-stacking interaction with W525 since it is endowed with an indoline ring. Compounds **111**, **119** and **124** presented at N1 a benzyl group para-substituted with: a methyl ester, carboxylic acid, and methenamine group, respectively. The presence of this substituent in para position of the benzyl group displaces the urea moiety and indole ring losing a hydrogen bond with N335 and the π-stacking with H524 and W525. However, the methenamine of **124** is hydrogen-bonded with the backbone CO of R410 and V416, whereas the carboxylate group of **119** accepts two H-bonds from the amide backbone of F497 and H524. Compound **111** is only H-bonded to amide backbone of H524 but gives two π-stacking with W525. Interestingly, **115** differs from **88** for the indole ring which confers rigidity.

Thus, **115** rotates 90° its bicyclic portion to fit the binding cavity moving away from W525 but maintaining a π- π with this residue. Similar considerations could be made for 96, which showed an $IC_{50}$ = 24.4 ± 4.1 nM., comparable to compounds **114**, **120** and **121**, all structurally featured with linear alkyl chain at N1, ending with an ester, carboxylic and amine group, respectively.

The amine group of **121** gives ionic interaction with D496, whereas the ester and carboxylic groups of **114** and **120** accept two hydrogen bonds from the backbone NH of F497 and H524.

However, the linear alkyl chain showed few Van der Waals contacts balancing its entropic lost upon binding. For derivative **89** the presence of the naphthalene moiety increases the distance from H524 even though the π-stacking is kept. Moreover, the indoline does not make any π-π interaction with side chain of W525. The compound **130** differs from its congeners for the presence of a carbazole instead of a bicyclic ring (indoline/or indole). This bulkier tricyclic moiety accommodates near Y383 establishing π- π interactions but losing the same contacts with H524 and W525. Moreover, its urea group gives three hydrogen bonds, despite a network of four H-bonds is found for the more active analogues. The conversion of urea in thiourea provides only one hydrogen bond with D335.

This observation agrees with our precious studies and with reported in literature, suggesting that the urea group is a crucial structural requirement to potently inhibit sEH. Moreover, it is herein demonstrated that the amide group is not able to give the network of H-bonds observed for the urea group. Indeed, we noted just three hydrogen bonds in **85**. Moreover, the amide group is shorter than urea group and the adamantyl moiety is too close to some residues such as L499, W336 to give favourable contacts, thus further contributing to explain its high $IC_{50}$ (285.1±31.2 nM). Compounds **86** and **90** are not well accommodated into the binding cavity giving non optimal interactions with the macromolecular counterparts, in accordance with their poor/absent inhibition activities.

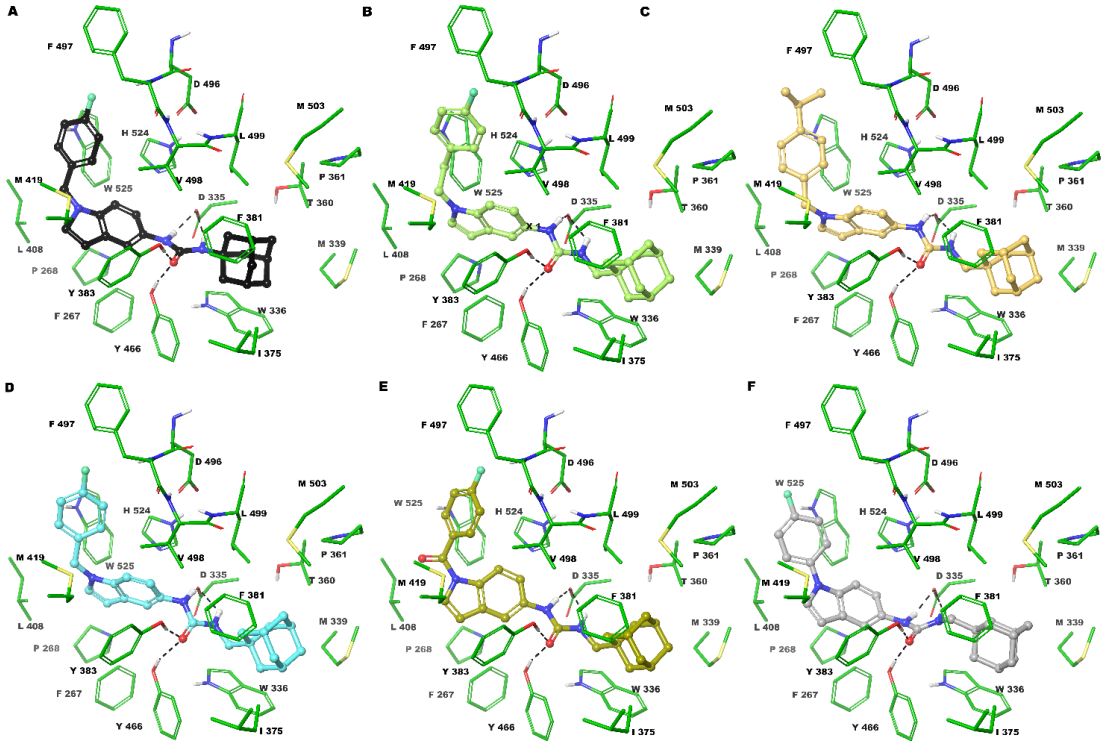


**Figure 65.** *Three-dimensional model of the interactions given by **88** (A), **112** (B), **110** (C), **109** (D), **118** (E) and **127** (F) with sEH.*

### *2.2.6 Synthesis of series I and II*

Final derivatives **85-90**, **92** and **96** were synthesized in accordance with scheme reported in **Figure 66.** Starting from 5-nitroindoline, reductive amination with 4-fluorobenzaldehyde afforded intermediate **83** (92% yield), which was reduced by continuous flow hydrogenation giving aminoindoline **84** in 95% yield. Intermediate **84** was then used as starting material for four different synthetic pathways. Coupling reaction with 1-adamantanecarboxylic acid, using HOBt, HBTU and DIPEA led to final compound **85** in 61% yield, while the treatment with ((1S)-7,7-dimethyl-2-oxobicyclo[2.2.1]heptan-1-yl)methanesulfonyl chloride provided sulfonamidic final derivative **86** (35% yield). When **84** was reacted with triphosgene, TEA and a proper aliphatic amine, ureido compounds **87-90** were obtained in 38-48% of yields,

otherwise, the amino group conversion into isothiocyanide function, by carbon disulfide in toluene, generated intermediate **91**, that was treated with adamantan-1-yl)methanamine to give final compound **92** (38% yield).

The carboxylic derivative **96** was synthesized starting from 5-nitroindoline that was converted in its N-1 Boc-protected analogue, then reduced to its corresponding amino derivative **93**, which was treated with triphosgene, TEA and 1-adamantanemethylamine leading to the ureido compound **94** in 45% yield. Intermediate **95** was obtained, in 55% of yield, after N-1 Boc deprotection and reductive amination with methyl 4-formylbenzoate. The subsequent ester group hydrolysis in NaOH solution gave the final compound **96** in 67% yield.

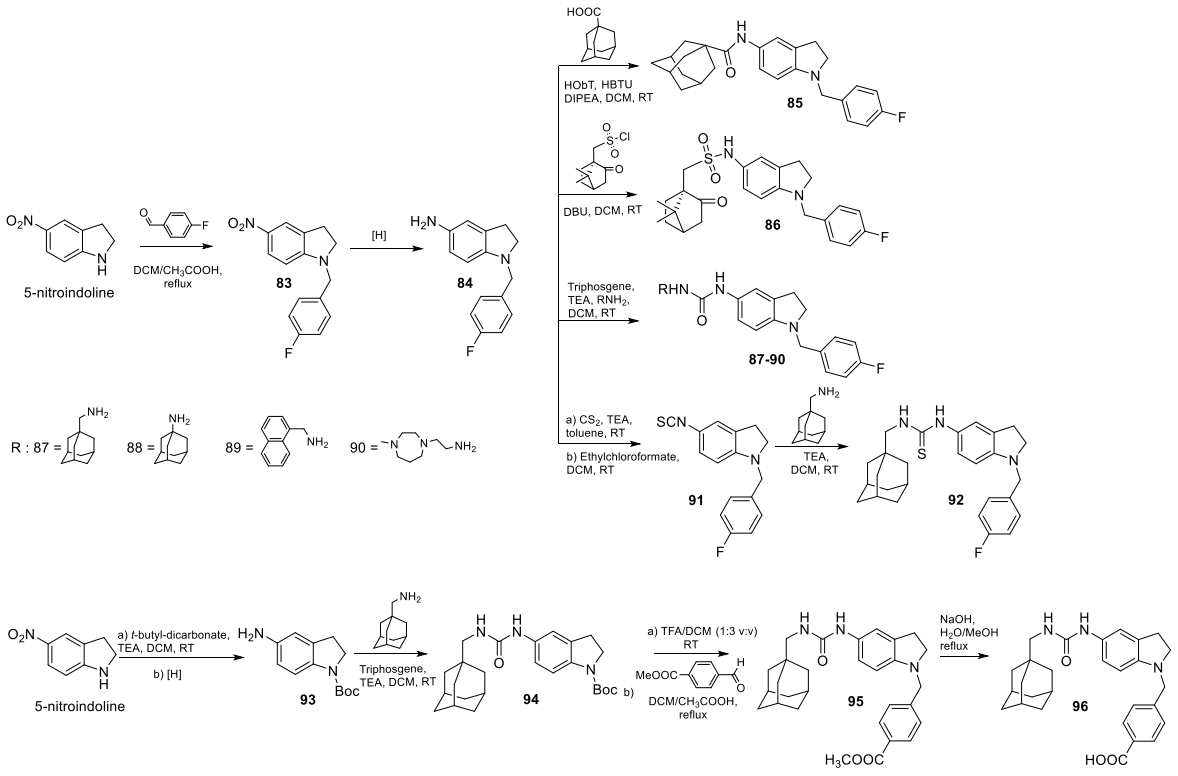


**Figure 66.** *Synthesis of indoline derivatives **85-90**, **92**, **96**.*

Indole final analogues were synthesized as depicted in **Figure 67.**

Starting from 5-nitroindole, an alkylation procedure with different alkyl bromide and sodium hydride provided N-1 alkyl intermediates **97**-**102** in 62-85% yields. Continuous flow hydrogenation led to amino indoles **103**-**108** (55-80%) which were treated with 1-adamantanemethylamine, triphosgene and TEA to give final compounds **109**-**112**, **114** (39-68% yields) and intermediate **113**, while the reaction with 1-adamantylamine furnished derivative **115** in 45% yield. Final derivative **118** was obtained starting from 5-nitroindole, that was coupled with 4-fluorobenzoyl chloride in basic medium to give intermediate **116** (65% yield), whose reduction in the same conditions described above led to compound **117** in 69% yield.

Subsequent treatment with 1-adamantanemethylamine, triphosgene and TEA yielded **118** in 42% yield. Ester group hydrolysis in NaOH solution of **111** and **114** gave final compounds **119** and **120** (62-58%), while reduction of **113**, using $CoCl_2$ and $NaBH_4$ yielded final derivative **121** in 46% yield.

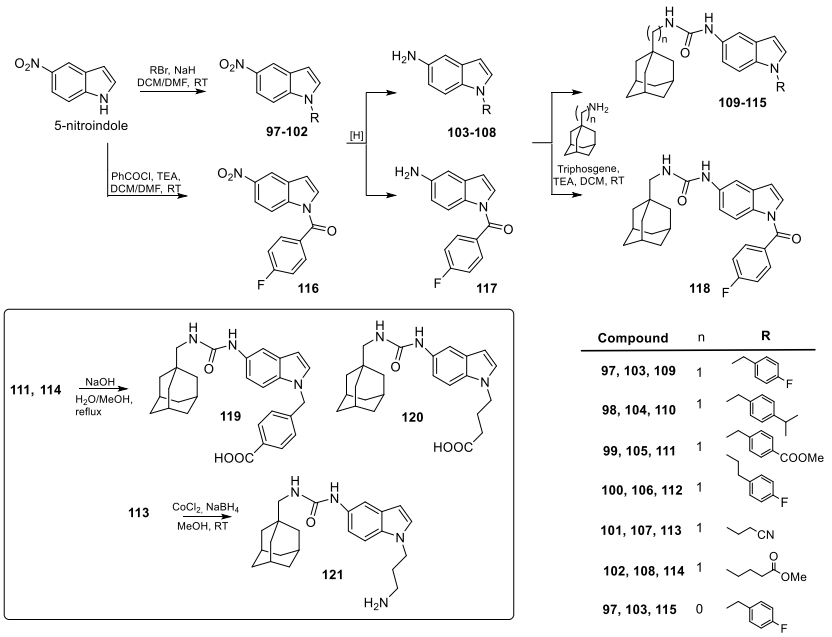


**Figure 67.** *Synthesis of indole derivatives **109-115**, **118-121**.*

The synthetic pathways used to obtain final compounds **124**, **127** and **130** are described in **Figure 68**.

Treating 5-aminoindole with triphosgene, TEA and 1-adamantanemethylamine, ureido intermediate **122** was synthesized (72% yield); alkylation with 4-(bromomethyl)benzonitrile afforded compound **123** in 55% yield, then reduction with $CoCl_2$ and $NaBH_4$ led to final derivative **124** in 48% yield. Compound **127** was obtained starting from 5-nitroindole using an alternative synthetic pathway. N-1 substitution using 4-fluoroiodobenzene, $Cs_2CO_3$ as base and CuI as catalyst led to N1-aryl indole **125** in 35% yield. The subsequent Pd/C catalysed reduction, in presence of hydrazine afforded amino indole intermediate **126** in 65% yield, which was reacted with triphosgene, TEA and 1-adamantanemethylamine yielded final derivative **127** (32% yield). The synthesis of carbazole intermediate **128** was performed by the N-1 carbazole alkylation using NaH and 4-fluorobenzyl chloride (97% yield). The nitration procedure using $HNO_3$ in acetic anhydride and the subsequent nitro group reduction, afforded the amino carbazole compound **129** in 90% yield. Finally, the treatment with triphosgene, TEA and 1-adamantanemethylamine furnished compound **130** (65% yield).

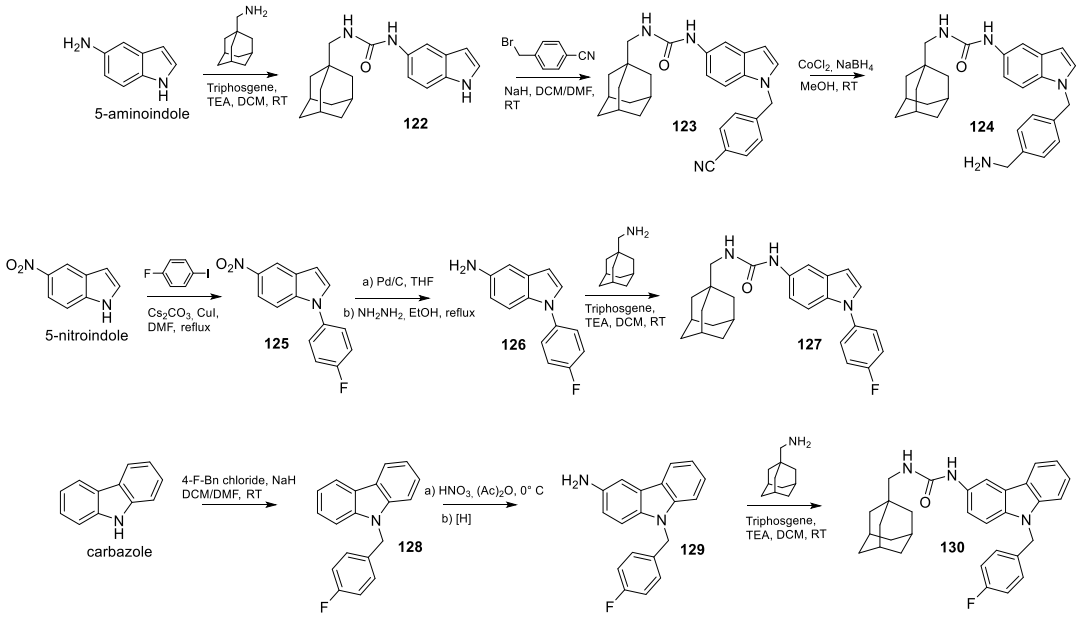


**Figure 68.** *Synthesis of indole derivatives **124**, **127** and carbazole compound **130**.*

## 3.1. Conclusions

Metabolic pathways involving arachidonic acid (AA) play key roles in cardiovascular biology, carcinogenesis, and in many inflammatory diseases such as asthma or arthritis; for this reason, part of my PhD project involved the study of two enzymatic targets involved in the metabolism of arachidonic acid through two different pathways: the 5-LOX enzyme, that results in the formation of proinflammatory leukotrienes, and the sEH enzyme that instead leads to the formation of proinflammatory dihydroxyeicosatrienoic acids (DHET). This chapter described the design, synthesis, and pharmacological characterization of a series of indoline-based small molecules designed as dual inhibitors of 5-LOX/sEH enzymes through a combined approach of in silico and in vitro techniques. In vitro characterization of the first series led to the identification of the indoline derivative **73** as a good candidate for further pharmacological studies ($IC_{50}$ = 0.59 ± 0.09 μM in PMNL, 0.41 ± 0.01 μM

on isolated 5-LOX and 0.43 ± 0.10 μM on isolated sEH). Then, it was evaluated, for its in vivo anti-inflammatory efficacy, in two different murine models: zymosan-induced peritonitis and ovalbumin-induced asthma. The collected data showed that compound **73** displayed in vivo anti-inflammatory effects, decreasing the LT levels as well as cell infiltration and the levels of proinflammatory mediators in the peritonitis model; moreover, **73** reversed the OVA-induced airway inflammatory response by decreasing LTC4 levels. These results pave the way for the rational design of 5-LOX/sEH dual inhibitors and for further investigation of their potential use as anti-inflammatory agents. Then, attention was focused on sEH as involved in numerous metabolic disorders, and starting with derivative **53**, which showed some selectivity toward this enzyme, additional series of analogues were designed and synthesized. The *in vitro* analysis of this novel series led to the identification of indole derivative **110**, characterized by high potency and selectivity toward soluble epoxide hydrolase ($IC_{50}$ >1000 nM on isolated 5-LOX and 2.0 ± 1.1 nM on isolated sEH) and paving the way for the optimization of new potential inhibitors.

### 4.1. Experimental section

**General:** all reagents and solvents used were purchased from Sigma-Aldrich (Milan, Italy) unless otherwise stated. Reactions were performed under magnetic stirring in round-bottomed flasks unless otherwise noted. Moisture-sensitive reactions were conducted in oven-dried glassware under nitrogen stream, using freshly distilled solvents. TLC analysis of reaction mixtures was performed on precoated glass silica gel plates (F254, 0.25 mm, VWR International), while crude products were purified by the Isolera Spektra One automated flash chromatography system (Biotage, Uppsala,

Sweden), using commercial silica gel cartridges (SNAP KP-Sil, Biotage). NMR spectra were recorded on a Bruker Avance 400 MHz apparatus, at room temperature. Chemical shifts were reported in δ values (ppm) relative to internal $Me_4Si$ for $^1H$ and $^{13}C$ NMR. J values were reported in hertz (Hz). $^1H$ NMR peaks were described using the following abbreviations: s (singlet), d (doublet), t (triplet), and m (multiplet). HR-MS spectra were recorded by LTQ-Orbitrap-XL-ETD mass spectrometer (Thermo Scientific, Bremen, Germany), equipped with an ESI source. All the final compounds showed a purity ≥95% as assessed by RP-UHPLC-PDA analysis, performed using a Nexera UHPLC system (Shimadzu, Kyoto, Japan) consisting of a CBM-40 lite controller, two LC-40B X3 pumps, an SPD-M 40 photo diode array detector, a CTO-30A column oven and, a SIL-40C X3 autosampler. The chromatographic analysis was accomplished on a Kinetex® Evo C18 column, 150 × 2.1 mm × 2.6 µm (Phenomenex®, Bologna, Italy) maintained at 40 °C. The optimal mobile phase consisted of 0.1% HCOOH/H2O v/v (A) and 0.1% HCOOH/ACN v/v (B) delivered at constant flow rate of 0.3 mL /min -1. Analysis was performed in gradient elution as follows: 0–20.00 min, 5–95% B; 20.00–25.00 min, isocratic to 95% B; then five minutes for column re-equilibration. Data acquisition was set in the range 190–800 nm and chromatograms were monitored at 254 nm.

**General procedure A: thiazolidinone synthesis.**

5-Methylisatin (1.0 mmol) was dissolved in ethanol (50 mL) and the solution was warmed at 100 °C. Mercaptoacetic acid (1.5 mmol) and 4-(aminomethyl)benzoic acid, or 4-aminobutanoic acid, or N-Boc-1,3-propanediamine (0.5 mmol) were added and the mixture was stirred for 120 min. Then, 5.0 mL of a solution of $NaHCO_3$ (10% v:v) was added and the organic phase was evaporated in *vacuo*. The crude was dissolved

in dichloromethane and a basic aqueous solution ($Na_2CO_3$ 2N) was employed to wash the organic phase (3 x 100 mL). The dichloromethane layer was then dried on $Na_2SO_4$, filtered and evaporated under *vacuo*. Flash chromatography on silica gel, using different eluent systems yielded intermediates **1-3**.

**General procedure B: N-acylation.**

0,5 mmol of proper intermediate, were dissolved in dichloromethane and the proper commercially available acyl chloride or di-*tert*-butyl dicarbonate (0.6 mmol) and triethylamine or DBU (0.6 mmol) were added. The mixture was stirred at room temperature for 30 minutes. Subsequently, water was added and the organic phase was washed for three times, dried on $Na_2SO_4$, filtered and evaporated. Flash chromatography on silica gel was performed to purified N-acyl compounds, using the proper eluent system.

**General procedure C: N-alkylation.**

The proper compound (0.15 mmol) was dissolved in DMF under magnetic stirring, and the temperature was set to 0 °C. To this solution, 0.23 mmol of NaH were added portion wise and the mixture was allowed to react for 30 min. Then, 0.23 mmol of methyl iodide or 4-fluorobenzyl chloride in DMF were added dropwise and the reaction was warmed to room temperature and maintained under stirring for further 12 h. Then, reaction was quenched by 10% aqueous solution of citric acid and washed with brine. Organic layer was separated, dried over anhydrous $Na_2SO_4$, filtered, and evaporated in vacuo. Crude product was purified by flash chromatography using n-hexane/ethyl acetate (4:1 v:v) as mobile phase, to obtain desired intermediates

**General Procedure D: Boc removal.**

The N-Boc protected intermediates (0.2 mmol) were dissolved in a mixture of TFA/DCM (1/3, v/v), and triisopropylsilane (TIS, 0.05 mmol) was added. The reaction was stirred at room temperature for 2 h. Then, a solution of NaOH (2 N) was added until pH 7. The mixture was diluted with water and dichloromethane, and the organic phase was extracted, dried over $Na_2SO_4$, filtered, and concentrated under vacuum. The intermediates obtained were not further purified.

**General Procedure E: guanidine group introduction.**

Proper intermediate (0.5 mmol) was dissolved in DCM and N,N′-Di-Boc-1H-pyrazole-1-carboxamidine (0.6 mmol), triethylamine (0.5 mmol) and N,N-dimethyl aminopyridine (0.35 mmol) were added and the reaction was warmed at 65°C for 4 hours. Then the mixture was cooled and washed with a $NaHCO_3$ aqueous solution (10% v:v) for three times. Chromatographic purification on silica gel using different eluents, gave guanidine compound.

**General Procedure F: urea formation.**

Aminic compounds **(**0.1 mmol) were dissolved in dichloromethane and triphosgene (0.025 mmol) and triethylamine (0.12 mmol) were added. The mixture was reacted for 30 minutes and the second amine (2,2-dimethylpropan-1-amine, or cyclohexylamine) was introduced and the reaction was stirred for 1 hour at room temperature. Then, the organic solvent was treated with water (3 x 100 mL) and the organic phase was dried over $Na_2SO_4$, filtered and evaporated. Ureidic compounds were isolated after flash chromatography using different ratio of n-hexane/ethyl acetate as mobile phase.

**General Procedure G: reductive amination.**

The proper nitro derivative (0.1 mmol) was dissolved in a solution of DCM/$CH_3COOH$ (5:1 v/v) at room temperature. To this solution an amount of 0.2 mmol of the proper aldehyde was added and the mixture was warmed to reflux for 1.5 hours. Then, an amount of 0.18 mmol of sodium triacetoxyborohydride was added portion wise and the mixture was allowed to reflux for further 3−5 hours. After cooling to room temperature, NaOH 1 N was added. The organic phase was separated and extracted one more time with the alkaline solution. Then it was dried over $Na_2SO_4$, filtered, and concentrated in vacuo. The crude products were purified by column chromatography using different mixtures of n-hexane/ethyl acetate as eluent.

**General Procedure H: continuous Flow Hydrogenation**.

Reduction of 5-nitroindoline, 5-nitroindole and 5-nitrocarbazole derivatives was performed by continuous flow hydrogenation employing the H-Cube hydrogenator and commercially available Pd/C 10% cartridges as catalyst. Initial nitro compounds were dissolved in a mixture of tetrahydrofuran (THF)/$CH_3OH$ (1:1, v/v) at a final concentration of 0.1 M and was pumped at a flow rate of 1.0 mL/min. Temperature was set at 30°C, while the hydrogen inlet pressure was set at 10 bar. Finally, the reaction solution was evaporated in vacuo and the obtained products used in the following step without further purification.

**General procedure I: synthesis of isothiocyanide.**

The proper amine (0.1 mmol) was dissolved in toluene and 0.1 mmol of triethylamine, 0.2 mmol of carbon disulfide were added and reacted overnight. Subsequently, the organic phase was concentrated *in vacuo* and the crude was

dissolved in dichloromethane and 0.1 mmol of TEA and 0.1 mmol of ethyl chloroformate were added and the mixture was stirred for 12 hours at room temperature. Then, an aqueous solution (10% w/w) of $NaHCO_3$ was added (3 x 100 mL) and the extracted organic solvent was dried on $Na_2SO_4$, filtered and evaporated. Isothiocyanide derivatives were obtained after flash chromatography using n-hexane/ethyl acetate as eluent.

**General procedure J: synthesis of thioureas**.

Isothiocyanide derivatives (0.1 mmol) were solubilised in dichloromethane at room temperature and 0.15 mmol of triethylamine and 0.15 mmol of proper amine were added and the mixture was reacted for 30 minutes. Then, organic phase was treated with an aqueous solution (10% w/w) of $NaHCO_3$ (3 x 100 mL) and subsequently with HCl 2M (3 x 100 mL). Dichloromethane phase was dried on $Na_2SO_4$, filtered and concentrated. Flash chromatography using n-hexane/ethyl acetate as eluent afforded thioureidic compounds.

**General Procedure K: hydrolysis.**

To a solution of the proper ester intermediate (1 mmol) dissolved in methanol, 5 mL of NaOH 1M aqueous solution were added. The reaction mixture was stirred at 100 °C until the complete disappearance of the starting material, evidenced by TLC. The aqueous phase was quenched with 20 mL of HCl 2M, diluted with ethyl acetate and extracted. Then the organic layer was filtered, dried over anhydrous $Na_2SO_4$ and evaporated in vacuo affording the final derivatives without further purification.

**General procedure L: nitrile reduction.**

To a solution of proper intermediate (0.5 mmol) in methanol $CoCl_2$ (0.5 mmol) and $NaBH_4$ (2 mmol) were added. The temperature was set a 0 °C and reaction mixture was stirred for 2 hours. Then the organic phase was concentrated, added with water and extracted with ethyl acetate (3 x 50 mL). The organic layer was separated, dried over anhydrous $Na_2SO_4$, filtered, and evaporated. Crude products were purified by flash chromatography using ethyl acetate/methanol as mobile phase, furnishing final derivatives.

***4-((5-methyl-2,4'-dioxospiro[indoline-3,2'-thiazolidin]-3'-yl)methyl)benzoic acid (1)***

Intermediate **1** was synthesized according to the general procedure **A**, starting from 5-methylisatin and 4-(aminomethyl)benzoic acid. FC in hexane/ethyl acetate 3/7, R*f*: 0.48. Yellowish oil (55% yield). $^1$H NMR (400 MHz, $CD_3OD$): δ: 2.13 (s, 3H, C$H_3$); 3.88 (d, 1H, C$H_{2a}$, *J* = 15.4 Hz); 4.17 (d, 1H, C$H_{2a}$, *J* = 14.7 Hz); 4.22 (d, 1H, C$H_{2b}$, *J* = 15.3 Hz); 4.53 (d, 1H, C$H_{2b}$, *J* = 14.7 Hz); 6.76 (d, 2H, aryl, *J* = 8.0 Hz); 6.81 (s, 1H, aryl); 6.98 (d, 2H, aryl, *J* = 8.1 Hz); 7.11 (d, 1H, aryl, *J* = 8.0 Hz); 7.79 (d, 2H, aryl, *J* = 7.9 Hz). HR-MS m/z calcd for $C_{19}H_{16}N_2O_4S$ $[(M + H)]^+$: 369.0904; found 369.0907.

***4-(5-methyl-2,4'-dioxospiro[indoline-3,2'-thiazolidin]-3'-yl)butanoic acid (2)***

Intermediate **2** was synthesized according to the general procedure **A**, starting from 5-methylisatin and 4-aminobutanoic acid. FC in hexane/ethyl acetate 3/7, R*f*: 0.38. Yellow powder (59% yield). $^1$H NMR (400 MHz, $CD_3OD$): δ: 1.51-1.64 (m, 2H, C$H_2$); 2.18-2.33 (m, 5H, C$H_2$ and C$H_3$); 2.93-3.00 (m, 1H, C$H_{2a}$); 3.32-3.40 (m, 1H, C$H_{2b}$); 3.64 (d, 1H, C$H_{2a}$, *J* = 15.2 Hz); 4.08 (d, 1H, C$H_{2b}$, *J* = 15.2 Hz); 6.78 (d, 1H, aryl, *J*

= 7.9 Hz); 7.06-7.09 (m, 2H, aryl). HR-MS m/z calcd for $C_{15}H_{16}N_2O_4S$ $[(M + H)]^+$: 321.0904; found 321.0911.

***tert-butyl (3-(5-methyl-2,4'-dioxospiro[indoline-3,2'-thiazolidin]-3'-yl)propyl)carbamate (3)***

Intermediate **3** was synthesized according to the general procedure **A**, starting from 5-methylisatin and N-Boc-1,3-propanediamine. FC in hexane/ethyl acetate 7/3, R*f*: 0.48. Yellow powder (85% yield). $^1$H NMR (400 MHz, $CDCl_3$): δ: 1.34 (s, 9H, C*H*$_3$); 1.45-1.51 (m, 2H, C*H*$_2$); 2.28 (s, 3H, C*H*$_3$); 2.85-3.01 (m, 3H, C*H*$_{2a,}$ and C*H*$_2$); 3.25-3.32 (m, 1H, C*H*$_{2b}$); 3.63 (d, 1H, C*H*$_{2a}$, *J* = 15.9 Hz); 4.09 (d, 1H, C*H*$_{2b}$, *J* = 15.8 Hz); 5.22 (bs, 1H, N*H*); 6.74 (d, 1H, aryl, *J* = 7.0 Hz); 7.08 (d, 1H, aryl, *J* = 8.4 Hz); 7.19 (s, 1H, aryl); 8.09 (s, 1H, N*H*). HR-MS m/z calcd for $C_{19}H_{25}N_3O_4S$ $[(M + H)]^+$: 392.1639; found 392.1634.

***4-((1-(cyclohexanecarbonyl)-5-methyl-2,4'-dioxospiro[indoline-3,2'-thiazolidin]-3'-yl)methyl)benzoic acid (4)***

Derivative **4** was synthesized starting from **1** and cyclohexane carbonyl chloride following the procedure **B**. FC in hexane/ethyl acetate 3/7, R*f*: 0.48. Yellow oil (55% yield). $^1$H NMR (400 MHz, $CDCl_3$): δ: 1.07-1.37 (m, 7H, C*H*$_2$); 1.56-1.68 (m, 2H, C*H*$_2$); 1.73 (d, 1H, C*H*$_{2b,}$ *J* = 12.4 Hz); 2.25 (s, 3H, C*H*$_3$); 2.83-2.90 (m, 1H, C*H*$_2$); 3.74 (d, 1H, C*H*$_{2a}$, *J* = 15.3 Hz); 3.98 (d, 1H, C*H*$_{2a}$, *J* = 14.7 Hz); 4.17 (d, 1H, C*H*$_{2b}$, *J* = 15.3 Hz); 4.74 (d, 1H, C*H*$_{2b}$, *J* = 14.7 Hz); 6.90 (d, 2H, aryl, *J* = 8.3 Hz); 7.02 (s, 1H, aryl); 7.18-7.21 (m, 1H, aryl); 7.81 (d, 2H, aryl, *J* = 8.3 Hz); 8.00 (d, 1H, aryl, *J* = 8.4 Hz). $^{13}$C NMR (100 MHz, $CDCl_3$): δ: 21.0, 25.3, 25.7, 28.6, 29.1, 33.0, 44.5, 46.3, 69.1, 117.4, 122.3, 126.4, 129.1, 129.5, 130.2, 132.7, 135.9, 138.3, 140.5, 170.8, 172.3,

174.9, 176.5. HR-MS m/z calcd for $C_{26}H_{26}N_2O_5S$ $[(M + H)]^+$: 479.1635; found 479.1641.

***4-(1-(cyclohexanecarbonyl)-5-methyl-2,4'-dioxospiro[indoline-3,2'-thiazolidin]-3'-yl)butanoic acid (5)***

Derivative **5** was synthesized starting from **2** and cyclohexane carbonyl chloride following the procedure **B**. FC in hexane/ethyl acetate 1/1, R*f*: 0.47. Yellow oil (57% yield). $^1$H NMR (400 MHz, $CD_3OD$): δ: 1.12-1.58 (m, 7H, C*H*$_2$); 1.66 (d, 1H, C*H*$_{2b,}$ *J* = 12.5 Hz); 1.75 (d, 1H, C*H*$_{2b,}$ *J* = 12.8 Hz); 1.88 (d, 1H, C*H*$_{2b,}$ *J* = 9.5 Hz); 2.18 (dd, 2H, C*H*$_{2,}$ *J'* = 7.1, *J''* = 13.0 Hz); 2.32 (s, 3H, C*H*$_3$); 2.98-3.05 (m, 1H, C*H*$_2$*a*); 3.12-3.20 (m, 1H, C*H*$_{2b}$); 3.38-3.52 (m, 3H, C*H*$_2$ and C*H*); 3.64 (d, 1H, C*H*$_{2a}$, *J* = 15.1 Hz); 4.06 (d, 1H, C*H*$_{2b}$, *J* = 15.1 Hz); 7.16-7.20 (m, 2H, aryl); 8.08 (d, 1H, aryl, *J* = 8.4 Hz). $^{13}$C NMR (100 MHz, $CD_3OD$): δ: 21.1, 23.1, 25.5, 25.8, 29.0, 31.0, 32.8, 42.7, 44.7, 65.9, 117.4, 123.2, 126.0, 132.5, 136.1, 138.2, 172.6, 172.8, 175.8, 176.8. HR-MS m/z calcd for $C_{22}H_{26}N_2O_5S$ $[(M + H)]^+$: 431.1635; found 431.1630.

***tert-butyl (3-(1-(cyclohexanecarbonyl)-5-methyl-2,4'-dioxospiro[indoline-3,2'-thiazolidin]-3'-yl)propyl)carbamate (6)***

Intermediate **6** was synthesized starting from **3** and cyclohexane carbonyl chloride following the procedure **B**. FC in hexane/ethyl acetate 8/2, R*f*: 0.45. Yellow oil (72% yield). $^1$H NMR (400 MHz, $CDCl_3$): δ: 1.25 (t, 2H, C*H*$_2$, *J* = 7.1 Hz); 1.40 (s, 9H, C*H*$_3$); 1.43-1.53 (m, 5H, C*H*$_2$); 1.72 (d, 1H, C*H*$_2$, *J* = 12.4 Hz); 1.82 (d, 2H, C*H*$_2$, *J* = 12.3 Hz); 1.92 (d, 2H, C*H*$_2$, *J* = 12.3 Hz); 2.38 (s, 3H, C*H*$_3$); 3.00-3.07 (m, 2H, C*H*$_2$); 3.10-3.17 (m, 1H, C*H*$_{2a}$); 3.21-3.28 (m, 1H, C*H*$_{2b}$); 3.50 (t, 1H, C*H*$_{,}$ *J* = 11.1 Hz); 3.72 (d, 1H, C*H*$_{2a}$, *J* = 15.2 Hz); 4.13 (d, 1H, C*H*$_{2b}$, *J* = 15.1 Hz); 5.12 (bs, 1H, N*H*); 7.23

(s, 1H, aryl); 7.26 (d, 1H, aryl, *J* = 8.5 Hz); 8.13 (d, 1H, aryl, *J* = 8.4 Hz). HR-MS m/z calcd for $C_{26}H_{35}N_3O_5S$ $[(M + H)]^+$: 502.2370; found 502.2374.

***3'-(3-aminopropyl)-1-(cyclohexanecarbonyl)-5-methylspiro[indoline-3,2'-thiazolidine]-2,4'-dione (7)***

Obtained from intermediate **6** following the general procedure **D**. FC in dichloromethane/methanol 9.5/0.5, R*f*: 0.45. Yellowish powder (93% yield). $^1$H NMR (400 MHz, $CDCl_3$): δ: 1.22-1.32 (m, 1H, C*H*$_2$); 1.36-1.46 (m, 2H, C*H*$_2$); 1.49-1.57 (m, 3H, C*H*$_2$); 1.76 (d, 1H, C*H*$_2$, *J* = 12.8 Hz); 1.85 (d, 2H, C*H*$_2$, *J* = 12.4 Hz); 1.91-1.98 (m, 3H, C*H*$_2$); 2.41 (s, 3H, C*H*$_3$); 3.04 (bs, 1H, N*H*); 3.26-3.40 (m, 3H, C*H*$_2$ and C*H*); 3.49 (t, 2H, C*H*$_2$, *J* = 9.4 Hz); 3.82 (d, 1H, C*H*$_{2a}$, *J* = 15.6 Hz); 4.22 (d, 1H, C*H*$_{2b}$, *J* = 15.1 Hz); 7.23 (s, 1H, aryl); 7.31 (d, 1H, aryl, *J* = 8.3 Hz); 8.16 (d, 1H, aryl, *J* = 8.2 Hz). HR-MS m/z calcd for $C_{21}H_{27}N_3O_3S$ $[(M + H)]^+$: 402.1846; found 402.1844.

***N-(3-(1-(cyclohexanecarbonyl)-5-methyl-2,4'-dioxospiro[indoline-3,2'-thiazolidin]-3'-yl)propyl)-2,3,4,5,6-pentafluorobenzamide (8)***

Derivative **8** was synthesized starting from **7** and 2,3,4,5,6-pentafluorobenzoyl chloride following the procedure **B**. FC in dichloromethane/ethyl acetate 9.8/0.2, R*f*: 0.45. Yellow oil (65% yield). $^1$H NMR (400 MHz, $CD_3OD$): δ: 1.19-1.44 (m, 7H, C*H*$_2$); 1.49-1.57 (m, 2H, C*H*$_2$); 1.63 (d, 1H, C*H*$_{2b}$, *J* = 12.3 Hz); 1.84-1.85 (m, 2H, C*H*$_2$); 2.28 (s, 3H, C*H*$_3$); 3.10 (dd, 1H, C*H*$_{2a}$, *J'* = 6.4, *J''* = 9.0 Hz); 3.16-3.18 (m, 1H, C*H*$_{2b}$); 3.19-3.22 (m, 2H, C*H*$_2$); 3.41-3.48 (m, 1H, C*H*); 3.74, (d, 1H, C*H*$_{2a}$, *J* = 15.9 Hz); 3.99 (d, 1H, C*H*$_{2b}$ , *J* = 15.8 Hz); 7.20 (d, 1H, aryl, *J* = 7.1 Hz); 7.29 (s, 1H, aryl); 8.00 (d, 1H, aryl, *J* = 8.4 Hz). $^{13}$C NMR (100 MHz, $CD_3OD$): δ: 19.6, 25.2, 25.4, 25.6, 27.4, 28.6, 28.9, 32.1, 37.1, 41.1, 44.6, 69.8, 116.8, 123.1, 126.0, 132.1, 136.3, 138.2,

173.6, 176.0, 176.4. HR-MS m/z calcd for $C_{28}H_{26}F_5N_3O_4S$ $[(M + H)]^+$: 596.1637; found 596.1642.

***1-(3-(1-(cyclohexanecarbonyl)-5-methyl-2,4'-dioxospiro[indoline-3,2'-thiazolidin]-3'-yl) 1,3-diboc-2-(propyl))guanidine (9)***

Intermediate **9** was synthesized starting from **7** and N-Boc-1H-pyrazole-1-carboxamidine following the procedure **E**. FC in dichloromethane/methanol 9/1, R*f*: 0.49. Yellowish oil (45% yield). $^1$H NMR (400 MHz, $CDCl_3$): δ: 1.43 (s, 18H, C$H_3$); 1.46-1.56 (m, 7H, C$H_2$); 1.64 (d, 1H, C$H_{2a,}$ $J$ = 12.4 Hz); 1.72-1.78 (m, 2H C$H_{2,}$); 1.86 (d, 2H, C$H_{2,}$ $J$ = 12.6 Hz); 2.31 (s, 3H, C$H_3$); 3.10 (t, 2H, C$H_{2,}$ $J$ = 6.2 Hz); 3.31 (t, 2H, C$H_{2,}$ $J$ = 7.4 Hz); 3.39-3.46 (m, 1H, C$H$); 3.68 (d, 1H, C$H_{2a}$, $J$ = 15.0 Hz); 4.06 (d, 1H, C$H_{2b}$, $J$ = 15.2 Hz); 7.14 (s, 1H, aryl); 7.17 (d, 1H, aryl, $J$ = 8.4 Hz); 8.06 (d, 1H, aryl, $J$ = 8.4 Hz). HR-MS m/z calcd for $C_{32}H_{45}N_5O_7S$ $[(M + H)]^+$: 644.3112; found 644.3113.

***1-(3-(1-(cyclohexanecarbonyl)-5-methyl-2,4'-dioxospiro[indoline-3,2'-thiazolidin]-3'-yl)propyl)guanidine (10)***

Derivative **10** was obtained following general procedure **D**, starting from **9**. FC in dichloromethane/methanol 9/1, R*f*: 0.49. Yellow oil (92% yield). $^1$H NMR (400 MHz, $CD_3OD$): δ: 1.29-1.60 (m, 7H, C$H_2$); 1.73 (d, 1H, C$H_{2a,}$ $J$ = 12.2 Hz); 1.80-1.85 (m, 2H C$H_{2,}$); 1.94 (d, 2H, C$H_{2,}$ $J$ = 12.2 Hz); 2.40 (s, 3H, C$H_3$); 3.13 (t, 2H, C$H_{2,}$ $J$ = 6.8 Hz); 3.21 (t, 2H, C$H_{2,}$ $J$ = 7.2 Hz); 3.52-3.57 (m, 1H, C$H$); 3.86 (d, 1H, C$H_{2a}$, $J$ = 15.5 Hz); 4.10 (d, 1H, C$H_{2b}$, $J$ = 15.5 Hz); 7.33 (d, 1H, aryl, $J$ = 8.4 Hz); 7.38 (s, 1H, aryl); 8.10 (d, 1H, aryl, $J$ = 8.4 Hz). $^{13}$C NMR (100 MHz, $CD_3OD$): δ: 19.7, 25.5, 25.6, 28.6, 28.9, 32.2, 38.2, 40.4, 44.6, 69.8, 116.9, 123.0, 125.9, 132.3, 136.3, 138.2, 157.2,

173.9, 176.0, 176.4. HR-MS m/z calcd for $C_{22}H_{29}N_5O_2S$ $[(M + H)]^+$: 444.2064; found 444.2070.

***1,5-dimethylindoline-2,3-dione (11)***

Intermediate **11** was obtained following general procedure **C**, starting from 5-methylisatin which was reacted with methyl iodide. FC in hexane/ethyl acetate 8/2, R*f*: 0.45. Yellow powder (74% yield). $^1$H and DEPT NMR spectra are in accordance with the literature (Bertamino *et al*., 2013).

**Synthesis of (2'S,4'R) and (2'R,4'R)-ethyl 1,5-dimethyl-2-oxospiro[indoline-3,2'-thiazolidine]-4'-carboxylate (12)**

To an ethanolic solution of 1,5-dimethylindoline-2,3-dione (**11**, 0.1 mmol) 0.15 mmol of *L*-Cys-OEt and 0.2 mmol of $NaHCO_3$ were added and the solution was stirred at room temperature for 3 hours. Then ethanol was evaporated in vacuo and the crude was dissolved in dichloromethane and washed with water (3 x 150 mL). Organic phase was dried over $Na_2SO_4$, filtered and evaporated. Diastereoisomeric mixture of thiazolidines **12** was almost quantitatively isolated, without other treatments. FC in hexane/ethyl acetate 7/3, R*f*: 0.48. Yellow oil (85% yield). $^1$H and $^{13}$C NMR spectra are in accordance with the literature (Bertamino *et al*., 2013).

***(2'S,4'R)-ethyl 3'-(cyclohexanecarbonyl)-1,5-dimethyl-2-oxospiro[indoline-3,2'-thiazolidine]-4'-carboxylate (13)***

Derivative **13** was synthesized according to the general procedure **B**, starting **12** and cyclohexane carbonyl chloride. FC in hexane/ethyl acetate 7/3, R*f*: 0.45. Yellow oil (45% yield). $^1$H and DEPT NMR spectra are in accordance with the literature (Bertamino *et al*., 2013).

**Synthesis of (S)-benzyl (1-(methoxy(methyl)amino)-4-methyl-1-oxopentan-2-yl)carbamate (14)**

To a solution of Z-*L*-Leu-OH (0.1 mmol), or 4-((tert-butoxycarbonyl)amino)butanoic acid, or succinic acid in DCM/DMF (1/1) 0.12 mmol of HOBt, 0.12 mmol of HBTU and 0.24 mmol of diisopropylethylamine, at room temperature, were added. After 30 min 0.12 mmol of N,O-dimethyl hydroxylamine were added and the reaction was mixed at room temperature overnight. Then, the crude was washed with water (3 x 50 mL), 10% aqueous solution of citric acid (3 x 50 mL) and saturated aqueous solution of sodium bicarbonate (3 x 50 mL). The combined organic layer was dried over anhydrous sodium sulfate, filtered, concentrated and purified by flash chromatography in 70:30 n-hexane/ethyl acetate to give the Weinreb amide **14**. FC in hexane/ethyl acetate 7/3, R*f*: 0.52. Yellowish oil (90% yield). $^{1}$H NMR (400 MHz, $CDCl_3$): δ: 0.95 (d, 3H, C*H*$_3$, *J* = 6.2 Hz); 0.98 (d, 3H, C*H*$_3$, *J* = 6.4 Hz); 1.49 (t, 2H, C*H*$_2$, *J* = 6.8 Hz); 1.70-1.78 (m, 1H, *CH*); 3.22 (s, 3H, *CH*$_3$); 3.82 (s, 3H, O*CH*$_3$); 4.80-4.84 (m, 1H, *CH*); 5.11 (q, 2H, *CH*$_2$); 5.36 (d, 1H, N*H*, *J* = 8.7 Hz); 7.33-7.37 (m, 5H, aryl). ESI-MS *m/z* calcd for $C_{16}H_{24}N_2O_4$ $[(M + H)]^+$: 307.1652; found 307.1649.

**Synthesis of (2R,4R,2'S) and (2S,4R,2'S)-ethyl 2-(1-(((benzyloxy)carbonyl)amino)-3-methylbutyl)thiazolidine-4-carboxylate (15)**

The obtained N-methoxy-N-methylcarbamoyl derivative (0.09 mmol) was dissolved in dry THF and mixed at 0°C under nitrogen atmosphere. Then 0.25 mmol of $LiAlH_4$ (1 M in THF) were added and the reaction was mixed at 0°C for 6 minutes. The crude was washed with 10% aqueous solution of citric acid (3 x 50 mL) and the

organic layer was dried over anhydrous sodium sulfate, filtered and concentrated. No further purification was performed for the aldehyde intermediate.

Z-*L*-Leu-H (0.1 mmol) intermediate was dissolved in ethanol, then 0.12 mmol of *L*-Cys-OEt and 0.12 mmol of $NaHCO_3$ were added and the reaction was mixed at room temperature overnight. The solvent was removed in vacuo and the crude was diluted with DCM and washed with water (3 x 50 mL). The collected organic layer was dried over anhydrous sodium sulfate, filtered, concentrated and purified by flash chromatography in 40:10 n-hexane/ethyl acetate to obtain intermediate **15**. FC in hexane/ethyl acetate 7/3, R*f*: 0.57. Yellowish oil (62% yield). $^1$H NMR (400 MHz, $CDCl_3$): δ: 0.93-0.99 (m, 3H, C*H*$_3$); 1.26-1.33 (m, 6H, 2C*H*$_3$); 1.36-1.43 (m, 2H, C*H*$_2$); 1.68-1.76 (m, 1H, C*H*); 2.69 (t, 1H, *CH*$_{2a,}$ *J* = 10.0 Hz); 3.22-3.28 (m, 1H, *CH*$_{2b}$); 3.77-3.84 (m, 1H, *CH*); 4.15 (q, 2H, *CH*$_2$); 4.20-4.28 (m, 2H, C*H*$_2$); 7.33-7.40 (m, 5H, aryl). ESI-MS *m/z* calcd for $C_{19}H_{28}N_2O_4S[(M + H)]^+$: 381.1843; found 381.1840.

**Synthesis of (3*S*,7a*R*,1'*S*) benzyl (1-(6-(3-((tert-butoxycarbonyl)amino)propyl)-5,7-dioxotetrahydro-1H,3H-imidazo[1,5-c]thiazol-3-yl)-3-methylbutyl)carbamate (16)**

To 0.1 mmol of intermediate **15** dissolved in dichloromethane, 0.025 mmol of triphosgene, 0.12 mmol of TEA and 0.12 mmol of N-Boc-1,3-propanediamine were added. The reaction was mixed at room temperature for 20 minutes and then mildly heated to allow the intramolecular cyclization generating hydantoin derivative **16**. Then the solution was washed with water (3 x 20 mL). The combined organic layer was dried over anhydrous sodium sulfate, filtered, concentrated and purified by flash chromatography in 50/50 of n-hexane/ethyl acetate. FC in hexane/ethyl acetate 1/1, R*f*: 0.55. Yellow oil (55% yield). $^1$H NMR (400 MHz, $CDCl_3$): δ: 0.95 (d, 3H, C*H*$_{3,}$ *J*

= 6.2 Hz); 1.51 (s, 9H, C*H*$_3$); 1.67-1.73 (m, 1H, C*H*); 1.84-1.90 (m, 2H, C*H*$_2$); 2.96 (t, 1H, *CH*$_{2a,}$ *J* = 9.9 Hz); 3.31 (t, 1H, *CH*$_{2b,}$ *J* = 8.6 Hz); 3.41-3.48 (m, 2H, *CH*$_2$); 3.48-3.56 (m, 2H, *CH*$_2$); 4.14-4.18 (m, 1H, *CH*); 4.31 (t, 1H, *CH*, *J* = 7.1 Hz); 5.12 (s, 2H, C*H*$_2$); 5.30 (s, 2H, C*H*$_2$); 7.28-7.36 (m, 5H, aryl). ESI-MS *m/z* calcd for $C_{26}H_{38}N_4O_6S$ $[(M + H)]^+$: 535.2585; found 535.2585.

***(3S,7aR,1'S) benzyl (1-(6-(3-aminopropyl)-5,7-dioxohexahydroimidazo[1,5-c]thiazol-3-yl)-3-methylbutyl)carbamate (17)***

Derivative **17** was synthesized starting from intermediate **16** following the procedure **D**. FC in dichloromethane/methanol 8/2, R*f*: 0.51. Yellow oil (87% yield). $^1$H NMR (400 MHz, $CD_3OD$): δ: 0.93 (d, 3H, C*H*$_{3,}$ *J* = 6.2 Hz); 0.96 (d, 3H, C*H*$_{3,}$ *J* = 6.4 Hz); 1.42-1.46 (m, 2H, C*H*$_2$); 1.66-1.79 (m, 3H, C*H*$_2$ and *CH*); 2.64 (t, 2H, *CH*$_{2,}$ *J* = 6.9 Hz); 3.02 (d, 1H, *CH*$_{2a}$, *J* = 11.0 Hz); 3.33-3.37 (m, 2H, C*H*$_{2b}$ and *CH*); 3.55 (t, 2H, C*H*$_2$, *J* = 6.7 Hz); 3.91-3.96 (m, 1H, C*H*); 5.07 (d, 1H, *CH*$_2$*a*, *J* = 12.5 Hz); 5.16 (d, 1H, *CH*$_{2b}$, *J* = 12.5 Hz); 5.22 (d, 1H, *CH*, *J* = 6.1 Hz); 7.30-7.39 (m, 5H, aryl). $^{13}$C NMR (100 MHz, $CD_3OD$): δ: 20.5, 22.5, 24.7, 30.1, 31.8, 36.0, 37.9, 40.3, 53.7, 65.0, 66.1, 67.5, 127.3, 127.6, 128.1, 137.1, 157.4, 158.8, 171.9. ESI-MS *m/z* calcd for $C_{21}H_{30}N_4O_4S$ $[(M + H)]^+$: 435.2061; found 435.2051.

***(3S,7aR,1'S)-benzyl (1-(6-(3-guanidinopropyl)-5,7-dioxohexahydroimidazo[1,5-c]thiazol-3-yl)-3-methylbutyl)carbamate (18)***

Derivative **18** was synthesized starting from **17** and N-Boc-1H-1-carboxamidine following the procedure **E**. FC in ethyl acetate/methanol 8/2, R*f*: 0.52. Yellow oil (55% yield). $^1$H NMR (400 MHz, $CD_3OD$): δ: 0.93 (d, 3H, C*H*$_{3,}$ *J* = 6.2 Hz); 0.96 (d, 3H, C*H*$_{3,}$ *J* = 6.4 Hz); 1.43 (t, 2H, C*H*$_{2,}$ *J* = 7.0 Hz); 1.66-1.73 (m, 1H, *CH*); 1.83-1.90 (m, 2H, *CH*$_2$); 3.04 (t, 1H, *CH*$_{2a,}$ *J* = 10.8 Hz); 3.18 (t, 2H, *CH*$_{2,}$ *J* = 6.8 Hz); 3.33-3.39 (m,

1H, C$H_{2b}$); 3.56 (t, 2H, C$H_2$, $J$ = 6.7 Hz); 3.95-4.00 (m, 1H, C$H$); 4.44 (t, 1H, C$H$, $J$ = 8.0 Hz); 5.07 (d, 1H, $CH_{2a}$, $J$ = 12.5 Hz); 5.16 (d, 1H, $CH_{2b}$, $J$ = 12.5 Hz); 5.23 (d, 1H, $CH$, $J$ = 5.6 Hz); 7.29-7.38 (m, 5H, aryl). $^{13}$C NMR (100 MHz, $CD_3OD$): δ: 20.5, 22.5, 24.6, 27.0, 31.6, 35.8, 38.3, 40.4, 48.5, 53.7, 65.1, 66.1, 67.3, 127.3, 127.6, 128.1, 137.1, 157.4, 158.4, 171.8. ESI-MS *m/z* calcd for $C_{22}H_{32}N_6O_4S$ $[(M + H)]^+$: 477.2279; found 477.2271.

***N-neopentyl-5-nitroindoline-1-carboxamide (19)***

Obtained from intermediate 5-nitroindoline and 2,2-dimethylpropan-1-amine following the general procedure **F**. FC in hexane/ethyl acetate 8/2, R*f*: 0.47. Yellow oil (66% yield). $^1$H NMR (400 MHz, $CDCl_3$): δ: 0.99 (s, 9H, C$H_3$); 3.20 (d, 2H, C$H_2$, $J$ = 4.9 Hz); 3.32 (t, 2H, C$H_2$, $J$ = 7.0 Hz); 4.09 (t, 2H, C$H_2$, $J$ = 6.9 Hz); 4.78 (bs, 1H, N$H$); 8.02 (s, 1H, aryl); 8.07 (d, 1H, aryl, $J$ = 7.2 Hz); 8.13 (d, 1H, aryl, $J$ = 7.0 Hz). ESI-MS *m/z* calcd for $C_{14}H_{19}N_3O_3$ $[(M + H)]^+$: 278.1499; found 278.1502.

***5-amino-N-neopentylindoline-1-carboxamide (20)***

Intermediate **20** was synthesized according to the general procedure **H**, starting from **19**. FC in hexane/ethyl acetate 7/3, R*f*: 0.47. White solid (61% yield). $^1$H NMR (400 MHz, $CD_3OD$): δ: 0.96 (s, 9H, C$H_3$); 3.09-3.12 (m, 4H, C$H_2$); 3.93 (t, 2H, C$H_2$, $J$ = 7.0 Hz); 6.57 (d, 1H, aryl, $J$ = 6.8 Hz); 6.65 (s, 1H, aryl); 7.58 (d, 1H, aryl, $J$ = 6.8 Hz). ESI-MS *m/z* calcd for $C_{14}H_{21}N_3O$ $[(M + H)]^+$: 248.1757; found, 248.1755.

***5-((4-fluorobenzyl)amino)-N-neopentylindoline-1-carboxamide (21)***

Derivative **21** was synthesized according to the general procedure **G**, starting from **20** and 4-fluorobenzaldehyde. FC in hexane/ethyl acetate 7/3, R*f*: 0.47. Yellow oil (58% yield). $^1$H NMR (400 MHz, $CD_3OD$): δ: 0.94 (s, 9H, C$H_3$); 3.06-3.10 (m, 4H,

C$H_2$); 3.91 (t, 2H, C$H_2$, $J$ = 8.6 Hz); 4.26 (s, 2H, C$H_2$); 6.46 (d, 1H, aryl, $J$ = 8.6 Hz); 6.55 (s, 1H, aryl); 7.03 (t, 2H, aryl, $J$ = 8.8 Hz); 7.36-7.40 (m, 2H, aryl); 7.54 (d, 1H, aryl, $J$ = 8.6 Hz). $^{13}$C NMR (100 MHz, $CD_3OD$): δ: 26.3, 27.7, 31.9, 50.7, 110.0, 111.7, 114.4, 114.9, 128.8, 131.7, 134.9, 136.1, 144.1, 156.4, 160.7, 163.1. ESI-MS *m/z* calcd for $C_{21}H_{26}FN_3O$ $[(M + H)]^+$: 356.2133; found 356.2139.

***1-(4-fluorobenzyl)-5-nitroindoline (22)***

Intermediate **22** was synthesized starting from 5-nitroindoline e and 4-fluorobenzaldehyde following the procedure **G**. FC in hexane/ethyl acetate 8/2, R*f*: 0.48. Yellow oil (90% yield). $^1$H NMR (400 MHz, $CDCl_3$): δ: 3.11 (t, 2H, C$H_2$, $J$ = 8.6 Hz); 3.63 (t, 2H, C$H_2$, $J$ = 8.9 Hz); 4.42 (s, 2H, C$H_2$); 6.38 (d, 1H, aryl, $J$ = 8.8 Hz); 7.07 (t, 2H, aryl, $J$ = 8.6 Hz); 7.24-7.28 (m, 2H, aryl); 7.93 (s, 1H, aryl); 8.07 (d, 1H, aryl, $J$ = 8.8 Hz). ESI-MS *m/z* calcd for $C_{15}H_{13}FN_2O_2$ $[(M + H)]^+$: 273.1034; found 273.1039.

***1-(4-fluorophenethyl)-5-nitroindoline (23)***

Intermediate **23** was synthesized starting from 5-nitroindoline e and (4-fluorophenyl)acetaldehyde following the procedure **G**. FC in hexane/ethyl acetate 8/2, R*f*: 0.47. Yellow oil (85% yield). $^1$H NMR (400 MHz, $CDCl_3$): δ: 2.89 (t, 2H, C$H_2$, $J$ = 7.2 Hz); 3.04 (t, 2H, C$H_2$, $J$ = 8.6 Hz); 3.48 (t, 2H, C$H_2$, $J$ = 7.5 Hz); 3.61 (t, 2H, C$H_2$, $J$ = 8.8 Hz); 6.18 (d, 1H, aryl, $J$ = 8.8 Hz); 7.00 (t, 2H, aryl, $J$ = 8.7 Hz); 7.16-7.20 (m, 2H, aryl); 7.84 (s, 1H, aryl); 8.00 (d, 1H, aryl, $J$ = 6.6 Hz). ESI-MS *m/z* calcd for $C_{16}H_{15}FN_2O_2$ $[(M + H)]^+$: 287.1190; found 287.1184.

***1-([1,1'-biphenyl]-4-ylmethyl)-5-nitroindoline (24)***

Obtained from 5-nitroindoline and biphenyl-4-carboxaldehyde following the general procedure **G**. FC in hexane/ethyl acetate 9/1, R*f*: 0.48. Yellow oil (68% yield). $^1$H NMR (400 MHz, $CDCl_3$): δ: 3.05 (t, 2H, C*H*$_2$, *J* = 8.4 Hz); 3.61 (t, 2H, C*H*$_2$, *J* = 8.8 Hz); 4.41 (s, 2H, C*H*$_2$); 6.33 (d, 1H, aryl, *J* = 8.8 Hz); 7.25-7.30 (m, 2H, aryl); 7.37 (t, 1H, aryl, *J* = 7.8 Hz); 7.49-7.62 (m, 6H, aryl); 7.86 (s, 1H, aryl); 8.00 (d, 1H, aryl, *J* = 10.8 Hz). ESI-MS *m/z* calcd for $C_{21}H_{18}N_2O_2$ $[(M + H)]^+$: 331.1441; found 331.1445.

***1-(naphthalen-2-ylmethyl)-5-nitroindoline (25)***

Obtained from 5-nitroindoline and 2-naphthaldehyde following the general procedure **G**. FC in hexane/ethyl acetate 9/1, R*f*: 0.52. Yellow oil (65% yield). $^1$H NMR (400 MHz, $CDCl_3$): δ: 3.14 (t, 2H, C*H*$_2$, *J* = 8.6 Hz); 3.69 (t, 2H, C*H*$_2$, *J* = 8.9 Hz); 4.61 (s, 2H, C*H*$_2$); 6.45 (d, 1H, aryl, *J* = 8.8 Hz); 7.40 (d, 1H, aryl, *J* = 10.1 Hz); 7.50-7.54 (m, 2H, aryl); 7.73 (s, 1H, aryl); 7.82-7.88 (m, 3H, aryl); 7.96 (s, 1H, aryl); 8.09 (d, 1H, aryl, *J* = 9.2 Hz). ESI-MS *m/z* calcd for $C_{19}H_{16}N_2O_2$ $[(M + H)]^+$: 305.1285; found 305.1291.

***tert-butyl (4-(5-nitroindolin-1-yl)butyl)carbamate (26)***

Obtained from 5-nitroindoline and *tert*-butyl (4-oxobutyl)carbamate following the general procedure **G**. FC in hexane/ethyl acetate 8/2, R*f*: 0.48. Yellow oil (62% yield). $^1$H NMR (400 MHz, $CDCl_3$): δ: 1.19 (s, 9H, C*H*$_3$); 1.65-1.72 (m, 4H, C*H*$_2$); 3.14 (t, 2H, C*H*$_2$, *J* = 7.8 Hz); 3.30 (t, 2H, C*H*$_2$, *J* = 8.0 Hz); 3.54 (t, 2H, C*H*$_2$, *J* = 7.6 Hz); 3.71 (t, 2H, C*H*$_2$, *J* = 7.8 Hz); 5.17 (bs, 1H, N*H*); 6.65 (d, 1H, aryl, *J* = 8.2 Hz); 7.81 (s, 1H, aryl); 8.05 (d, 1H, aryl, *J* = 9.6 Hz). ESI-MS *m/z* calcd for $C_{17}H_{25}N_3O_4$ $[(M + H)]^+$: 336.1918; found 336.1922.

***4-(5-nitroindolin-1-yl)butan-1-ol (27)***

Intermediate **27** was synthesized according to the general procedure **G**, starting from 5-nitroindoline and 4-hydroxybutanal. FC in hexane/ethyl acetate 1/1, R*f*: 0.47. Yellow oil (65% yield). $^1$H NMR (400 MHz, $CD_3OD$): δ: 1.46-1.53 (m, 2H, C*H*$_2$); 1.57-1.65 (m, 2H, C*H*$_2$); 2.97 (t, 2H, C*H*$_2$, *J* = 8.5 Hz); 3.20-3.25 (m, 2H, C*H*$_2$); 3.50 (t, 2H, C*H*$_2$, *J* = 6.3 Hz); 3.59 (t, 2H, C*H*$_2$, *J* = 8.8 Hz); 6.30 (d, 1H, aryl, *J* = 8.9 Hz); 7.74 (s, 1H, aryl); 7.90 (d, 1H, aryl, *J* = 8.9 Hz). ESI-MS *m/z* calcd for $C_{12}H_{16}N_2O_3$ $[(M + H)]^+$: 236.1155; found 236.1160.

**Synthesis of 4-(methoxymethoxy)benzaldehyde (28a)**

4-Hydroxybenzaldehyde (0.2 mmol) was dissolved in DMF and 0.3 mmol of potassium *tert*-butoxide and 0.3 mmol of methoxymethyl chloride were introduced and the solution was refluxed for 4 hours. The mixture was diluted with dichloromethane and washed with HCl 2M (3 x 100 mL), organic phase was dried on anhydrous $Na_2SO_4$, filtered and concentrated. Flash chromatography in n-hexane/ethyl acetate 9/1 as ratio afforded the MOM-protected compound **28a** in rather quantitative yield. FC in hexane/ethyl acetate 9/1, R*f*: 0.39. White solid (97% yield). $^1$H NMR (400 MHz, $CDCl_3$): δ: 3.51 (s, 3H, C*H*$_3$); 5.28 (s, 2H, C*H*$_2$); 7.17 (d, 2H, aryl, *J* = 8.2 Hz); 7.86 (d, 2H, aryl, *J* = 8.4 Hz); 9.92 (s, 1H, CO*H*).

***1-(4-(methoxymethoxy)benzyl)-5-nitroindoline (28)***

Intermediate **28** was synthesized according to the general procedure **G**, starting from 5-nitroindoline and 4-(methoxymethoxy)benzaldehyde. FC in hexane/ethyl acetate 9/1, R*f*: 0.48. Yellow oil (92% yield). $^1$H NMR (400 MHz, $CDCl_3$): δ: 3.09 (t, 2H, C*H*$_2$, *J* = 8.8 Hz); 3.50 (s, 3H, C*H*$_3$); 3.63 (t, 2H, C*H*$_2$, *J* = 8.6 Hz); 4.39 (s, 2H, C*H*$_2$); 5.19 (s, 2H, C*H*$_2$); 6.39 (d, 1H, aryl, *J* = 8.8 Hz); 7.04 (d, 2H, aryl, *J* = 8.6 Hz);

7.20 (d, 2H, aryl, $J$ = 8.6 Hz); 7.92 (s, 1H, aryl); 8.07 (d, 1H, aryl, $J$ = 11.0 Hz). ESI-MS *m/z* calcd for $C_{17}H_{18}N_2O_4$ $[(M + H)]^+$: 315.1339; found 315.1336.

***1-(4-fluorobenzyl)indolin-5-amine (29)***

Intermediate **29** was obtained following general procedure **H**, starting **22**. FC in hexane/ethyl acetate 1/1, R*f*: 0.41. White solid (95% yield). $^1$H NMR (400 MHz, $CDCl_3$): δ: 2.79 (t, 2H, C$H_2$, $J$ = 7.4 Hz); 3.08 (t, 2H, C$H_2$, $J$ = 7.6 Hz); 3.26 (bs, 2H, N$H_2$); 4.01 (s, 2H, C$H_2$); 6.26 (d, 1H, aryl, $J$ = 8.1 Hz); 6.37 (d, 1H, aryl, $J$ = 8.0 Hz); 6.50 (s, 1H, aryl); 6.93 (t, 2H, aryl, $J$ = 8.7 Hz); 7.24-7.27 (m, 2H, aryl). ESI-MS *m/z* calcd for $C_{15}H_{15}FN_2$ $[(M + H)]^+$: 243.1292; found 243.1300.

***1-(4-fluorophenethyl)indolin-5-amine (30)***

Intermediate **30** was obtained following general procedure **H**, starting from **23**. FC in hexane/ethyl acetate 7/3, R*f*: 0.48. Yellow oil (82% yield). $^1$H NMR (400 MHz, $CDCl_3$): δ: 2.88 (t, 2H, C$H_2$, $J$ = 7.3 Hz); 3.13-3.32 (m, 6H, C$H_2$); 6.38 (d, 1H, aryl, $J$ = 8.0 Hz); 6.49 (d, 1H, aryl, $J$ = 8.2 Hz); 6.59 (s, 1H, aryl); 7.02 (t, 2H, aryl, $J$ = 8.7 Hz); 7.21-7.26 (m, 2H, aryl). ESI-MS *m/z* calcd for $C_{16}H_{17}FN_2$ $[(M + H)]^+$: 257.1449; found 257.1455.

***1-([1,1'-biphenyl]-4-ylmethyl)indolin-5-amine (31)***

Intermediate **31** was obtained following general procedure **H**, starting from **24**. FC in hexane/ethyl acetate 1/1, R*f*: 0.50. Yellow oil (65% yield). $^1$H NMR (400 MHz, $CDCl_3$): δ: 2.78 (t, 2H, C$H_2$, $J$ = 7.6 Hz); 3.14 (t, 2H, C$H_2$, $J$ = 7.6 Hz); 3.87 (bs, 2H, N$H_2$); 4.10 (s, 2H, C$H_2$); 6.31 (d, 1H, aryl, $J$ = 8.2 Hz); 6.95 (t, 1H, aryl, $J$ = 7.8 Hz); 7.14-7.18 (m, 3H, aryl); 7.26 (s, 1H, aryl); 7.46 (s, 1H, aryl); 7.90-7.98 (m, 5H, aryl). ESI-MS *m/z* calcd for $C_{21}H_{20}N_2$ $[(M + H)]^+$: 301.1699; found 301.1705.

***1-(naphthalen-2-ylmethyl)indolin-5-amine (32)***

Intermediate **32** was obtained following general procedure **H**, starting from **25**. FC in hexane/ethyl acetate 7/3, R*f*: 0.47. Yellow oil (59% yield). $^1$H NMR (400 MHz, $CDCl_3$): δ: 2.92 (t, 2H, C*H*$_2$, *J* = 7.5 Hz); 3.20 (t, 2H, C*H*$_2$, *J* = 7.4 Hz); 3.55 (bs, 2H, N*H*$_2$); 4.14 (s, 2H, C*H*$_2$); 6.29 (d, 1H, aryl, *J* = 7.8 Hz); 7.01-7.08 (m, 2H, aryl); 7.13 (s, 1H, aryl); 7.86-7.95 (m, 6H, aryl). ESI-MS *m/z* calcd for $C_{19}H_{18}N_2$ $[(M + H)]^+$: 275.1543; found 275.1539.

***tert-butyl (4-(5-aminoindolin-1-yl)butyl)carbamate (33)***

Intermediate **33** was synthesized starting from **26** following the procedure **H**. FC in hexane/ethyl acetate 1/1, R*f*: 0.47. Yellow oil (59% yield). $^1$H NMR (400 MHz, $CDCl_3$): δ: 1.12 (s, 9H, C*H*$_3$); 1.58-1.62 (m, 2H, C*H*$_2$); 1.69-1.73 (m, 2H, C*H*$_2$); 2.85 (t, 2H, C*H*$_2$, *J* = 7.4 Hz); 3.04 (t, 2H, C*H*$_2$, *J* = 7.6 Hz); 3.19 (t, 2H, C*H*$_2$, *J* = 7.6 Hz); 3.20 (t, 2H, C*H*$_2$, *J* = 7.4 Hz); 5.21 (bs, 1H, N*H*); 6.23-6.29 (m, 2H, aryl); 7.68 (s, 1H, aryl). ESI-MS *m/z* calcd for $C_{17}H_{27}N_3O_2$ $[(M + H)]^+$: 306.2176; found 306.2182.

***4-(5-aminoindolin-1-yl)butan-1-ol (34)***

Intermediate **34** was synthesized starting from **27** following the procedure **H**. FC in hexane/ethyl acetate 2/8, R*f*: 0.48. Yellow oil (58% yield). $^1$H NMR (400 MHz, $CD_3OD$): δ: 2.43-2.49 (m, 2H, C*H*$_2$); 2.74-2.78 (m, 2H, C*H*$_2$); 2.86 (t, 2H, C*H*$_2$, *J* = 8.5 Hz); 3.02 (t, 2H, C*H*$_2$, *J* = 8.2 Hz); 4.09-4.24 (m, 4H, C*H*$_2$); 6.43 (d, 1H, aryl, *J* = 8.6 Hz); 6.53 (s, 1H, aryl); 7.75 (d, 1H, aryl, *J* = 8.6 Hz). ESI-MS *m/z* calcd for $C_{12}H_{18}N_2O$ $[(M + H)]^+$: 207.1492; found 207.1488.

***1-(4-(methoxymethoxy)benzyl)indolin-5-amine (35)***

Intermediate **35** was synthesized starting from **28** following the procedure **H**. FC in hexane/ethyl acetate 1/1, R*f*: 0.47. White solid (90% yield). $^1$H NMR (400 MHz, $CDCl_3$): δ: 3.00 (t, 2H, C*H*$_2$, *J* = 8.7 Hz); 3.39 (s, 3H, C*H*$_3$); 3.44 (t, 2H, C*H*$_2$, *J* = 8.6 Hz); 4.21 (s, 2H, C*H*$_2$); 5.03 (s, 2H, C*H*$_2$); 6.20 (d, 1H, aryl, *J* = 8.4 Hz); 6.95 (d, 2H, aryl, *J* = 8.2 Hz); 7.07 (d, 2H, aryl, *J* = 8.1 Hz); 7.77 (s, 1H, aryl); 7.93 (d, 1H, aryl, *J* = 10.2 Hz). ESI-MS *m/z* calcd for $C_{17}H_{20}N_2O_2$ $[(M + H)]^+$: 285.1598; found 285.1604.

***1-(4-fluorobenzyl)-5-thiocyanatoindoline (36)***

Obtained from intermediate **29** following the general procedure **I**. FC in hexane/ethyl acetate 9/1, R*f*: 0.48. White solid (58% yield). $^1$H NMR (400 MHz, $CDCl_3$): δ: 2.99 (t, 2H, C*H*$_2$, *J* = 8.4 Hz); 3.40 (t, 2H, C*H*$_2$, *J* = 8.5 Hz); 4.26 (s, 2H, C*H*$_2$); 6.37 (d, 1H, aryl, *J* = 8.3 Hz); 6.94 (s, 1H, aryl); 6.97 (d, 1H, aryl, *J* = 5.5 Hz); 7.05 (t, 2H, aryl, *J* = 8.6 Hz); 7.28-7.32 (m, 2H, aryl). ESI-MS *m/z* calcd for $C_{16}H_{13}FN_2S$ $[(M + H)]^+$: 285.0856; found 285.0849.

***1-(4-fluorophenethyl)-5-isothiocyanatoindoline (37)***

Obtained from intermediate **30** following the general procedure **I**. FC in hexane/ethyl acetate 9/1, R*f*: 0.47. Yellow oil (62% yield). $^1$H NMR (400 MHz, $CDCl_3$): δ: 2.75 (t, 2H, C*H*$_2$, *J* = 7.1 Hz); 2.86 (t, 2H, C*H*$_2$, *J* = 8.4 Hz); 3.22 (t, 2H, C*H*$_2$, *J* = 7.7 Hz); 3.46 (t, 2H, C*H*$_2$, *J* = 8.5 Hz); 6.16 (d, 1H, aryl, *J* = 8.9 Hz); 6.82-6.84 (m, 2H, aryl); 6.90 (t, 2H, aryl, *J* = 8.7 Hz); 7.07-7.11 (m, 2H, aryl). ESI-MS *m/z* calcd for $C_{17}H_{15}FN_2S$ $[(M + H)]^+$: 299.1013; found 299.1018.

***1-([1,1'-biphenyl]-4-ylmethyl)-5-isothiocyanatoindoline (38)***

Intermediate **38** was synthesized starting from **31** following the procedure **I**. FC in hexane/ethyl acetate 9.5/0.5, R*f*: 0.47. Yellow oil (57% yield). $^1$H NMR (400 MHz, $CDCl_3$): δ: 2.76 (t, 2H, C*H*$_2$, *J* = 7.6 Hz); 3.12 (t, 2H, C*H*$_2$, *J* = 8.0 Hz); 4.13 (s, 2H, C*H*$_2$); 6.35 (d, 1H, aryl, *J* = 8.1 Hz); 6.60 (t, 1H, aryl, *J* = 8.4 Hz); 7.07-7.12 (m, 2H, aryl); 7.18 (d, 1H, aryl, *J* = 8.6 Hz); 7.29 (s, 1H, aryl); 7.55 (d, 1H, aryl, *J* = 8.4 Hz); 7.86-7.94 (m, 5H, aryl). ESI-MS *m/z* calcd for $C_{22}H_{18}N_2S$ $[(M + H)]^+$: 343.1263; found 343.1258.

***5-isothiocyanato-1-(naphthalen-2-ylmethyl)indoline (39)***

Intermediate **39** was synthesized starting from **32** following the procedure **I**. FC in hexane/ethyl acetate 9.5/0.5, R*f*: 0.47. Yellow oil (48% yield). $^1$H NMR (400 MHz, $CDCl_3$): δ: 2.90 (t, 2H, C*H*$_2$, *J* = 7.4 Hz); 3.14 (t, 2H, C*H*$_2$, *J* = 8.0 Hz); 4.22 (s, 2H, C*H*$_2$); 6.41 (d, 1H, aryl, *J* = 8.4 Hz); 6.90-6.96 (m, 2H, aryl); 7.08 (d, 1H, aryl, *J* = 8.3 Hz); 7.41 (s, 1H, aryl); 7.65-7.78 (m, 5H, aryl). ESI-MS *m/z* calcd for $C_{20}H_{16}N_2S$ $[(M + H)]^+$: 317.1107; found 317.1104.

***tert-butyl (4-(5-isothiocyanatoindolin-1-yl)butyl)carbamate (40)***

Intermediate **40** was synthesized starting from **33** following the procedure **I**. FC in hexane/ethyl acetate 9.5/0.5, R*f*: 0.52. Yellow oil (57% yield). $^1$H NMR (400 MHz, $CDCl_3$): δ: 1.20 (s, 9H, C*H*$_3$); 1.58-1.63 (m, 2H, C*H*$_2$); 1.70-1.75 (m, 2H, C*H*$_2$); 2.81 (t, 2H, C*H*$_2$, *J* = 7.8 Hz); 3.00 (t, 2H, C*H*$_2$, *J* = 8.0 Hz); 3.14 (t, 2H, C*H*$_2$, *J* = 7.8 Hz); 3.25 (t, 2H, C*H*$_2$, *J* = 7.6 Hz); 5.05 (bs, 1H, N*H*); 6.49 (d, 1H, aryl, *J* = 9.4 Hz); 7.22 (s, 1H, aryl); 8.03 (d, 1H, aryl, *J* = 11.2 Hz). ESI-MS *m/z* calcd for $C_{18}H_{25}N_3O_2S$ $[(M + H)]^+$: 348.1740; found 348.1736.

***4-(5-isothiocyanatoindolin-1-yl)butan-1-ol (41)***

Intermediate **41** was synthesized starting from **34** following the procedure **I**. FC in hexane/ethyl acetate 1/1, R*f*: 0.50. Yellow oil (45% yield). $^{1}$H NMR (400 MHz, $CD_3OD$): δ: 1.68-1.76 (m, 4H, C*H*$_2$); 3.00 (t, 2H, C*H*$_2$, *J* = 8.0 Hz); 3.15 (t, 2H, C*H*$_2$, *J* = 4.0 Hz); 3.48 (t, 2H, C*H*$_2$, *J* = 4.0 Hz); 3.73 (t, 2H, C*H*$_2$, *J* = 4.0 Hz); 6.41 (d, 1H, aryl, *J* = 8.0 Hz); 6.97-6.99 (m, 2H, aryl). ESI-MS *m/z* calcd for $C_{13}H_{16}N_2OS$ [(M + H)]$^+$: 248.0978; found 248.0984.

***5-isothiocyanato-1-(4-(methoxymethoxy)benzyl)indoline (42)***

Obtained from intermediate **35** following the general procedure **I**. FC in hexane/ethyl acetate 9/1, R*f*: 0.47. Yellow oil (77% yield). $^{1}$H NMR (400 MHz, $CDCl_3$): δ: 2.97 (t, 2H, C*H*$_2$, *J* = 8.4 Hz); 3.40 (t, 2H, C*H*$_2$, *J* = 8.5 Hz); 3.51 (s, 3H, C*H*$_3$); 4.23 (s, 2H, C*H*$_2$); 5.19 (s, 2H, C*H*$_2$); 6.39 (d, 1H, aryl, *J* = 8.0 Hz); 6.94-6.96 (m, 2H, aryl); 7.03 (d, 2H, aryl, *J* = 8.6 Hz); 7.25 (d, 2H, aryl, *J* = 8.6 Hz). ESI-MS *m/z* calcd for $C_{18}H_{18}N_2O_2S$ [(M + H)]$^+$: 327.1162; found 327.1155.

***1-(1-(4-fluorobenzyl)indolin-5-yl)-3-neopentylthiourea (43)***

Synthesis of **43** was previously described by Ostacolo and coworkers.

Derivative **43** was synthesized according to the general procedure **J**, starting from **36** and 2,2-dimethylpropan-1-amine. FC in hexane/ethyl acetate 7/3, Rf: 0.45. Yellow oil (52% yield). $^{1}$H and DEPT NMR spectra are in accordance with the literature (Ostacolo *et al*., 2020).

***1-(1-(4-fluorophenethyl)indolin-5-yl)-3-neopentylthiourea (44)***

Derivative **44** was synthesized according to the general procedure **J**, starting from **37** and 2,2-dimethylpropan-1-amine. FC in dichloromethane/ethyl acetate 9.5/0.5, R*f*:

0.47. Yellow oil (65% yield). $^{1}$H NMR (400 MHz, $CD_3OD$): δ: 0.91 (s, 9H, C*H*$_3$); 2.89 (t, 2H, C*H*$_2$, *J* = 7.1 Hz); 2.95 (t, 2H, C*H*$_2$, *J* = 8.4 Hz); 3.33-3.37 (m, 2H, C*H*$_2$); 3.43 (t, 4H, C*H*$_2$, *J* = 8.4 Hz); 6.46 (d, 1H, aryl, *J* = 8.2 Hz); 6.89 (d, 1H, aryl, *J* = 8.2 Hz); 6.94 (s, 1H, aryl); 7.01 (t, 2H, aryl, *J* = 8.8 Hz); 7.27-7.31 (m, 2H, aryl). $^{13}$C NMR (100 MHz, $CD_3OD$): δ: 26.4, 27.8, 32.2, 50.4, 52.8, 55.4, 106.4, 114.5, 114.7, 122.6, 125.4, 130.2, 131.3, 135.8, 151.4, 160.4, 162.8, 181.6. ESI-MS *m/z* calcd for $C_{22}H_{28}FN_3S$ $[(M + H)]^+$: 386.2061; found 386.2055.

***1-(1-([1,1'-biphenyl]-4-ylmethyl)indolin-5-yl)-3-neopentylthiourea (45)***

Derivative **45** was synthesized according to the general procedure **J**, starting from **38** and 2,2-dimethylpropan-1-amine. FC in hexane/ethyl acetate 8/2, R*f*: 0.47. Yellow oil (63% yield). $^{1}$H NMR (400 MHz, $CD_3OD$): δ: 0.80 (s, 9H, C*H*$_3$); 2.87 (t, 2H, C*H*$_2$, *J* = 7.1 Hz); 3.29 (t, 2H, C*H*$_2$, *J* = 8.3 Hz); 3.33 (bs, 2H, C*H*$_2$); 4.23 (s, 2H, C*H*$_2$); 6.49 (d, 1H, aryl, *J* = 8.2 Hz); 6.81 (d, 1H, aryl, *J* = 6.4 Hz); 6.88 (s, 1H, aryl); 7.22 (t, 2H, aryl, *J* = 7.4 Hz); 7.30-7.35 (m, 4H, aryl); 7.50 (t, 4H, aryl, *J* = 8.0 Hz). $^{13}$C NMR (100 MHz, $CD_3OD$): δ: 26.4, 27.8, 29.4, 52.6, 53.2, 55.4, 106.9, 122.7, 125.3, 126.5, 126.7, 128.4, 137.2, 140.1, 140.8, 151.7, 181.7. ESI-MS *m/z* calcd for $C_{27}H_{31}N_3S$ $[(M + H)]^+$: 430.2311; found 430.2306.

***1-(1-(naphthalen-2-ylmethyl)indolin-5-yl)-3-neopentylthiourea (46)***

Derivative **46** was synthesized according to the general procedure **J**, starting from **39** and 2,2-dimethylpropan-1-amine. FC in hexane/ethyl acetate 7/3, R*f*: 0.46. White solid (55% yield). $^{1}$H NMR (400 MHz, $CD_3OD$): δ: 0.92 (s, 9H, C*H*$_3$); 3.00 (t, 2H, C*H*$_2$, *J* = 8.4 Hz); 3.37-3.45 (m, 4H, C*H*$_2$); 4.46 (s, 2H, C*H*$_2$); 6.62 (d, 1H, aryl, *J* = 8.2 Hz); 6.91-6.93 (m, 1H, aryl); 7.00 (s, 1H, aryl); 7.46-7.53 (m, 3H, aryl); 7.81-7.86 (m, 5H, aryl); $^{13}$C NMR (100 MHz, $CDCl_3$): δ: 26.4, 27.8, 53.2, 53.4, 55.4, 106.9, 122.7,

125.4, 125.7, 125.8, 126.2, 127.2, 127.3, 127.8, 132.9, 133.5, 135.7, 151.7, 175.0. ESI-MS *m/z* calcd for $C_{25}H_{29}N_3S$ $[(M + H)]^+$: 404.2155; found 404.2160.

***tert-butyl (4-(5-(3-neopentylthioureido)indolin-1-yl)butyl)carbamate (47)***

Intermediate **47** was synthesized starting from **40** and 2,2-dimethylpropan-1-amine following the procedure **J**. FC in hexane/ethyl acetate 7/3, R*f*: 0.48. Yellow oil (52% yield). $^1$H NMR (400 MHz, $CD_3OD$): δ: 0.89 (s, 9H, C*H*$_3$); 1.16 (s, 9H, C*H*$_3$); 1.65-1.74 (m, 4H, C*H*$_2$); 3.00 (t, 4H, C*H*$_2$, *J* = 7.4 Hz); 3.09 (t, 2H, C*H*$_2$, *J* = 7.0 Hz); 3.43 (t, 4H, C*H*$_2$, *J* = 8.2 Hz); 5.48 (bs, 1H, N*H*); 6.60 (d, 1H, aryl, *J* = 8.5 Hz); 7.01 (d, 1H, aryl, *J* = 9.1 Hz); 7.03 (s, 1H, aryl). ESI-MS *m/z* calcd for $C_{23}H_{38}N_4O_2S$ $[(M + H)]^+$: 435.2788; found 435.2782.

***1-(1-(4-hydroxybutyl)indolin-5-yl)-3-neopentylthiourea (48)***

Derivative **48** was synthesized according to the general procedure **J**, starting from **41** and 2,2-dimethylpropan-1-amine. FC in dichloromethane/ethyl acetate 7/3, R*f*: 0.49. Yellow oil (55% yield). $^1$H NMR (400 MHz, $CD_3OD$): δ: 0.91 (s, 9H, C*H*$_3$); 1.61-1.74 (m, 4H, C*H*$_2$); 2.96 (t, 2H, C*H*$_2$, *J* = 8.4 Hz); 3.12 (t, 2H, C*H*$_2$, *J* = 7.2 Hz); 3.37-3.45 (m, 4H, C*H*$_2$); 3.63 (t, 2H, C*H*$_2$, *J* = 7.2 Hz); 6.52 (d, 1H, aryl, *J* = 8.2 Hz); 6.92 (d, 1H, aryl, *J* = 8.2 Hz); 6.96 (s, 1H, aryl). $^{13}$C NMR (100 MHz, $CD_3OD$): δ: 23.4, 26.4, 27.8, 29.8, 48.7, 52.8, 55.4, 61.3, 106.6, 122.6, 125.4, 131.4, 151.9, 181.6. ESI-MS *m/z* calcd for $C_{18}H_{29}N_3OS$ $[(M + H)]^+$: 336.2104; found 336.2107.

***1-(1-(4-(methoxymethoxy)benzyl)indolin-5-yl)-3-neopentylthiourea (49)***

Derivative **49** was synthesized according to the general procedure **J**, starting from **42** and 2,2-dimethylpropan-1-amine. FC in hexane/ethyl acetate 1/1, R*f*: 0.47. Yellow oil (65% yield). $^1$H NMR (400 MHz, DMSO): δ: 0.89 (s, 9H, C*H*$_3$); 2.87 (t, 2H, C*H*$_2$,

*J* = 8.4 Hz); 3.24 (t, 2H, C*H*$_2$, *J* = 8.2 Hz); 3.31-3.33 (m, 5H, C*H*$_2$ and C*H*$_3$); 4.19 (s, 2H, C*H*$_2$); 5.17 (s, 2H, C*H*$_2$); 6.55 (d, 1H, aryl, *J* = 8.3 Hz); 6.89 (d, 1H, aryl, *J* = 8.3 Hz); 6.98-7.03 (m, 3H, aryl); 7.09 (bs, 1H, N*H*); 7.27 (d, 2H, aryl, *J* = 8.6 Hz); 9.15 (bs, 1H, N*H*). $^{13}$C NMR (100 MHz, DMSO): δ: 27.8, 28.3, 52.5, 53.4, 55.3, 56.0, 94.4, 107.0, 116.6, 122.4, 124.4, 129.7, 130.6, 131.7, 150.4, 156.4, 182.1. ESI-MS *m/z* calcd for $C_{23}H_{31}N_3O_2S$ $[(M + H)]^+$: 414.2210; found 414.2206.

***1-benzyl-3-(1-(4-fluorobenzyl)indolin-5-yl)thiourea (50)***

Derivative **50** was synthesized according to the general procedure **J**, starting from **36** and benzylamine. FC in hexane/ethyl acetate 7/3, R*f*: 0.47. Yellow oil (58% yield). $^1$H NMR (400 MHz, $CDCl_3$): δ: 2.97 (t, 2H, C*H*$_2$, *J* = 8.4 Hz); 3.38 (t, 2H, C*H*$_2$, *J* = 8.4 Hz); 4.22 (s, 2H, *CH*$_2$); 4.89 (d, 2H, C*H*$_2$, *J* = 5.5 Hz); 6.12 (bs, 1H, N*H*); 6.40 (d, 1H, aryl, *J* = 8.2 Hz); 6.89-6.93 (m, 2H, aryl); 7.04 (t, 2H, aryl, *J* = 8.6 Hz); 7.28-7.37 (m, 7H, aryl); 7.63 (bs, 1H, N*H*). $^{13}$C NMR (100 MHz, $CDCl_3$): δ: 28.2, 49.3, 52.4, 53.4, 107.0, 115.4, 115.6, 123.4, 125.0, 126.3, 127.6, 128.7, 129.3, 132.0, 133.3, 137.7, 152.2, 163.4, 181.9. ESI-MS *m/z* calcd for $C_{23}H_{22}FN_3S$ $[(M + H)]^+$: 392.1591; found 392.1599.

***1-(1-(4-fluorobenzyl)indolin-5-yl)-3-phenylthiourea (51)***

Derivative **51** was synthesized according to the general procedure **J**, starting from **36** and aniline. FC in hexane/ethyl acetate 8/2, R*f*: 0.48. Yellow oil (67% yield). $^1$H NMR (400 MHz, $CD_3OD$): δ: 2.96 (t, 2H, C*H*$_2$, *J* = 8.3 Hz); 3.32 (t, 2H, C*H*$_2$, *J* = 8.3 Hz); 4.25 (s, 2H, *CH*$_2$); 6.54 (d, 2H, aryl, *J* = 8.3 Hz); 6.96 (d, 1H, aryl, *J* = 8.2 Hz); 7.06 (t, 3H, aryl, *J* = 11.1 Hz); 7.19 (t, 1H, aryl, *J* = 7.2 Hz); 7.32-7.41 (m, 5H, aryl). $^{13}$C NMR (100 MHz, $CD_3OD$): δ: 27.8, 52.4, 53.3, 106.7, 114.6, 114.8, 122.5, 124.8,

125.3, 128.4, 129.5, 131.0, 134.2, 139.0, 151.3, 160.9, 163.3, 180.6. ESI-MS *m/z* calcd for $C_{22}H_{20}FN_3S$ $[(M + H)]^+$: 378.1435; found 378.1442.

***4-(3-(1-(4-fluorobenzyl)indolin-5-yl)thioureido)benzoic acid (52)***

Derivative **52** was synthesized according to the general procedure **J**, starting from **36** and 4-aminobenzoyc acid. FC in ethyl acetate/methanol 9.8/0.2, R*f*: 0.55. Yellow oil (62% yield). $^1$H NMR (400 MHz, $CD_3OD$): δ: 2.85 (t, 2H, C*H*$_2$, *J* = 8.3 Hz); 3.21 (t, 2H, C*H*$_2$, *J* = 8.3 Hz); 4.15 (s, 2H, *CH*$_2$); 6.43 (d, 2H, aryl, *J* = 8.3 Hz); 6.87 (d, 1H, aryl, *J* = 10.2 Hz); 6.96 (d, 2H, aryl, *J* = 8.8 Hz); 7.26-7.30 (m, 2H, aryl, *J* = 7.2 Hz); 7.47 (d, 2H, aryl, *J* = 8.6 Hz); 7.85 (d, 2H, aryl, *J* = 8.6 Hz). $^{13}$C NMR (100 MHz, $CD_3OD$): δ: 27.8, 52.4, 53.3, 106.7, 114.6, 114.8, 122.3, 122.8, 124.7, 127.3, 129.4, 129.9, 143.5, 151.2, 160.9, 163.1, 180.4. ESI-MS *m/z* calcd for $C_{23}H_{20}FN_3O_2S$ $[(M + H)]^+$: 421.1260; found 421.1253.

**Synthesis of 1-(1-(4-fluorobenzyl)indolin-5-yl)-3-neopentylguanidine (53)**

Derivative **53** was obtained following general procedure **F**, starting from **29** which was reacted with cyclohexylamine. FC in hexane/ethyl acetate 7/3, R*f*: 0.47. Yellow oil (72% yield). $^1$H NMR (400 MHz, DMSO): δ: 1.09-1.20 (m, 3H, C*H*$_2$); 1.24-1.36 (m, 2H, C*H*$_2$); 1.53-1.56 (m, 1H, C*H*$_2$); 1.63-1.67 (m, 2H, C*H*$_2$); 1.77-1.80 (m, 2H, C*H*$_2$); 2.82 (t, 2H, C*H*$_2$, *J* = 8.2 Hz); 3.14 (t, 2H, C*H*$_2$, *J* = 8.1 Hz); 3.40-3.51 (m, 1H, C*H*); 4.05 (s, 1H, N*H*); 4.16 (s, 2H, C*H*$_2$); 5.84 (d, 1H, aryl, *J* = 7.9 Hz); 6.47 (d, 1H, aryl, *J* = 8.4 Hz); 6.90 (d, 1H, aryl, *J* = 8.3 Hz); 7.13-7.19 (m, 2H, aryl); 7.37-7.41 (m, 2H, aryl); 7.85 (s, 1H, N*H*). $^{13}$C NMR (100 MHz, DMSO): δ: 24.9, 25.7, 28.7, 33.6, 40.0, 53.3, 53.8, 107.7, 115.4, 115.6, 116.7, 117.8, 130.40, 130.52, 132.0, 135.1, 147.6, 155.3, 162.9. ESI-MS *m/z* calcd for $C_{22}H_{27}FN_3O$ $[(M + H)]^+$: 368.4671; found 368.4678.

***1-cyclohexyl-3-(1-(4-fluorobenzyl)indolin-5-yl)urea (54)***

Derivative **54** was obtained following general procedure **F**, starting from **29** which was reacted with cyclohexylamine. FC in hexane/ethyl acetate 7/3, R*f*: 0.47. Yellow oil (78% yield). $^{1}$H NMR (400 MHz, DMSO): δ: 1.09-1.20 (m, 3H, C*H*$_2$); 1.24-1.36 (m, 2H, C*H*$_2$); 1.53-1.56 (m, 1H, C*H*$_2$); 1.63-1.67 (m, 2H, C*H*$_2$); 1.77-1.80 (m, 2H, C*H*$_2$); 2.82 (t, 2H, C*H*$_2$, *J* = 8.2 Hz); 3.14 (t, 2H, C*H*$_2$, *J* = 8.1 Hz); 3.40-3.51 (m, 1H, C*H*); 4.05 (s, 1H, N*H*); 4.16 (s, 2H, C*H*$_2$); 5.84 (d, 1H, aryl, *J* = 7.9 Hz); 6.47 (d, 1H, aryl, *J* = 8.4 Hz); 6.90 (d, 1H, aryl, *J* = 8.3 Hz); 7.13-7.19 (m, 2H, aryl); 7.37-7.41 (m, 2H, aryl); 7.85 (s, 1H, N*H*). $^{13}$C NMR (100 MHz, DMSO): δ: 24.9, 25.7, 28.7, 33.6, 40.0, 53.3, 53.8, 107.7, 115.4, 115.6, 116.7, 117.8, 130.40, 130.52, 132.0, 135.1, 147.6, 155.3, 162.9. ESI-MS *m/z* calcd for $C_{22}H_{27}FN_3O$ $[(M + H)]^+$: 368.4671; found 368.4678.

***1-(1-(4-fluorobenzyl)indolin-5-yl)-3-neopentylurea (55)***

Derivative **55** was obtained following general procedure **F**, starting from **29** which was reacted with 2,2-dimethylpropan-1-amine. FC in dichloromethane/ethyl acetate 7/3, R*f*: 0.45. Yellow oil (72% yield). $^{1}$H NMR (400 MHz, $CD_3OD$): δ: 0.82 (s, 9H, C*H*$_3$); 2.79 (t, 2H, C*H*$_2$, *J* = 8.1 Hz); 2.89 (s, 2H, C*H*$_2$); 3.11 (t, 2H, C*H*$_2$, *J* = 8.1 Hz); 4.07 (s, 2H, C*H*$_2$); 6.38 (d, 1H, aryl, *J* = 8.3 Hz); 6.81 (d, 1H, aryl, *J* = 10.3 Hz); 6.92-6.98 (m, 3H, aryl); 7.26-7.29 (m, 2H, aryl). $^{13}$C NMR (100 MHz, $CD_3OD$): δ: 26.1, 28.1, 31.5, 50.7, 53.2, 53.6, 107.2, 114.5, 114.7, 118.4, 120.1, 129.5, 130.2, 130.8, 134.4, 148.8, 158.1, 160.9, 163.3. ESI-MS *m/z* calcd for $C_{21}H_{26}FN_3O$ $[(M + H)]^+$: 356.2133; found 356.2128.

**Synthesis of N-(1-(4-fluorobenzyl)indolin-5-yl)cyclohexanesulfonamide (56)**

0.1 mmol of intermediate **29** were dissolved in dry DCM under a nitrogen positive pressure.

To this solution, 0.12 mmol of 1,8-diazabicyclo[5.4.0]undec-7-ene were added. The solution was stirred at room temperature for 15 minutes, then, 0.15 mmol of cyclohexyl sulfonyl chloride were introduced and further stirred for 2 hours. The reaction was then washed with a saturated solution of $NaHCO_3$ and brine. The organic phase was extracted, dried over anhydrous $Na_2SO_4$, filtered, and concentrated in vacuo. Final product was purified using 50:50 mixture of n-hexane/ethyl acetate as eluent. FC in hexane/ethyl acetate 8/2, R*f*: 0.44. Off white oil (78% yield). $^1$H and DEPT NMR spectra are in accordance with the literature (Ostacolo *et al*., 2020). ESI-MS *m/z* calcd for $C_{21}H_{25}FN_2O_2S$ $[(M + H)]^+$: 389.1694; found 389.1687.

***1-(1-(4-aminobutyl)indolin-5-yl)-3-neopentylthiourea (57)***

Derivative **57** was synthesized starting from **47** following the procedure **D**. FC ethyl acetate/methanol 9/1, R*f*: 0.42. Yellow oil (52% yield). $^1$H NMR (400 MHz, $CD_3OD$): δ: 0.92 (s, 9H, C*H*$_3$); 1.71-1.79 (m, 4H, C*H*$_2$); 2.98 (t, 4H, C*H*$_2$, *J* = 6.6 Hz); 3.14 (t, 2H, C*H*$_2$, *J* = 6.2 Hz); 3.41 (t, 2H, C*H*$_2$, *J* = 8.3 Hz); 3.45 (bs, 2H, C*H*$_2$); 6.54 (d, 1H, aryl, *J* = 8.2 Hz); 6.94 (d, 1H, aryl, *J* = 8.3 Hz); 6.98 (s, 1H, aryl). $^{13}$C NMR (100 MHz, $CD_3OD$): δ: 23.7, 24.3, 25.4, 27.2, 31.2, 47.3, 51.9, 54.4, 105.2, 121.9, 124.7, 126.3, 130.3, 150.7, 180.8. ESI-MS *m/z* calcd for $C_{18}H_{30}N_4S$ $[(M + H)]^+$: 335.2264; found 335.2270.

**Synthesis of 1-(1-(4-hydroxybenzyl)indolin-5-yl)-3-neopentylthiourea (58)**

Methoxymethyl protecting group was removed by dissolving compound **49** in a solution of DCM/TFA (10 mL, 1:1 v:v) at room temperature for 3 hours. After quenching by $Na_2CO_3$, the mixture was washed with water (3 x 100 mL) and the organic layer was dried on $Na_2SO_4$, filtered and evaporated *in vacuo*. Final derivative was obtained after flash chromatography in hexane/ethyl acetate 7/3. FC in hexane/ethyl acetate 7/3, R*f*: 0.51. Yellow oil (62% yield). $^1$H NMR (400 MHz, $CD_3OD$): δ: 0.91 (s, 9H, C*H*$_3$); 2.93 (t, 2H, C*H*$_2$, *J* = 8.3 Hz); 3.30 (t, 2H, C*H*$_2$, *J* = 8.2 Hz); 3.44 (bs, 2H, C*H*$_2$); 4.18 (s, 2H, C*H*$_2$); 6.59 (d, 1H, aryl, *J* = 8.2 Hz); 6.76 (d, 2H, aryl, *J* = 8.5 Hz); 6.91 (d, 1H, aryl, *J* = 8.2 Hz); 6.96 (s, 1H, aryl); 7.18 (d, 2H, aryl, *J* = 8.5 Hz). $^{13}$C NMR (100 MHz, $CD_3OD$): δ: 26.4, 27.7, 32.01, 52.4, 52.9, 55.4, 107.0, 114.8, 122.7, 125.3, 128.6, 129.1, 151.7, 156.4, 181.6. ESI-MS *m/z* calcd for $C_{21}H_{27}N_3OS$ $[(M + H)]^+$: 370.1948; found 370.1956.

***(4-fluorophenyl)(5-nitroindolin-1-yl)methanone (59)***

Intermediate **59** was synthesized starting from 5-nitroindoline and 4-fluorobenzoyl chloride following the procedure **B**. FC in hexane/ethyl acetate 8/2, R*f*: 0.47. Yellow oil (91% yield). $^1$H NMR (400 MHz, $CD_3OD$): δ: 3.16 (t, 2H, C*H*$_2$, *J* = 8.3 Hz); 4.12 (t, 2H, C*H*$_2$, *J* = 8.4 Hz); 7.11 (t, 2H, aryl, *J* = 8.6 Hz); 7.20 (s, 1H, aryl); 7.52-7.56 (m, 2H, aryl); 8.02-8.04 (m, 2H, aryl). ESI-MS *m/z* calcd for $C_{15}H_{11}FN_2O_3$ $[(M + H)]^+$: 287.0826; found 287.0830.

***2-(4-fluorophenyl)-1-(5-nitroindolin-1-yl)ethanone (60)***

Intermediate **60** was synthesized starting from 5-nitroindoline and 4-fluorophenylacethyl chloride following the procedure **B**. FC in hexane/ethyl acetate

8/2, R*f*: 0.47. Yellow oil (88% yield). $^1$H NMR (400 MHz, $CD_3OD$): δ: 3.31 (t, 2H, C*H*$_2$, *J* = 6.8 Hz); 3.84 (s, 2H, C*H*$_2$); 4.25 (t, 2H, C*H*$_2$, *J* = 7.0 Hz); 7.08 (t, 2H, aryl, *J* = 6.9 Hz); 7.29 (t, 2H, aryl, *J* = 5.0 Hz); 8.05 (s, 1H, aryl); 8.14 (d, 1H, aryl, *J* = 8.9 Hz); 8.34 (d, 1H, aryl, *J* = 7.0 Hz). ESI-MS *m/z* calcd for $C_{16}H_{13}FN_2O_3$ $[(M + H)]^+$: 301.0983; found 301.0977.

***tert-butyl 5-nitroindoline-1-carboxylate (61)***

Intermediate **61** was synthesized starting from 5-nitroindoline and di-*tert*-butyl dicarbonate following the procedure **B**. FC in hexane/ethyl acetate 8/2, R*f*: 0.45. Yellow solid (88% yield). $^1$H NMR (400 MHz, $CDCl_3$): δ: 1.60 (s, 9H, C*H*$_3$); 3.19 (t, 2H, C*H*$_2$, *J* = 8.7 Hz); 4.11 (t, 2H, C*H*$_2$, *J* = 9.0 Hz); 7.28 (d, 1H, aryl, *J* = 7.7 Hz); 8.02 (s, 1H, aryl); 8.12 (d, 1H, aryl, *J* = 11.0 Hz). ESI-MS *m/z* calcd for $C_{13}H_{16}N_2O_4$ $[(M + H)]^+$: 265.1183; found 265.1190.

***(5-aminoindolin-1-yl)(4-fluorophenyl)methanone (62)***

Obtained from intermediate **59** following the general procedure **H**. FC in hexane/ethyl acetate 1/1, R*f*: 0.49. Yellow oil (87% yield). $^1$H NMR (400 MHz, $CDCl_3$): δ: 3.05 (t, 2H, C*H*$_2$, *J* = 8.1 Hz); 3.61 (bs, 2H, N*H*$_2$); 4.02 (bs, 2H, C*H*$_2$); 6.59 (bs, 3H, aryl); 7.13 (t, 2H, aryl, *J* = 8.7 Hz); 7.58 (t, 2H, aryl, *J* = 5.5 Hz). ESI-MS *m/z* calcd for $C_{15}H_{13}FN_2O$ $[(M + H)]^+$: 257.1085; found 257.1081.

***1-(5-aminoindolin-1-yl)-2-(4-fluorophenyl)ethanone (63)***

Obtained from intermediate **60** following the general procedure **H**. FC in hexane/ethyl acetate 1/1, R*f*: 0.47. Yellow oil (85% yield). $^1$H NMR (400 MHz, $CD_3OD$): δ: 3.11 (t, 2H, C*H*$_2$, *J* = 6.6 Hz); 3.84 (s, 2H, C*H*$_2$); 4.12 (t, 2H, C*H*$_2$, *J* = 6.7 Hz); 6.57 (d, 1H, aryl, *J* = 6.8 Hz); 6.66 (s, 1H, aryl); 7.09 (t, 2H, aryl, *J* = 7.0 Hz);

7.34 (t, 2H, aryl, $J$ = 4.4 Hz); 7.90 (d, 1H, aryl, $J$ = 6.8 Hz). ESI-MS *m/z* calcd for $C_{16}H_{15}FN_2O$ $[(M + H)]^+$: 271.1241; found 271.1235.

***tert-butyl 5-aminoindoline-1-carboxylate (64)***

Obtained from intermediate **61** following the general procedure **H**. FC in hexane/ethyl acetate 1/1, R*f*: 0.48. White solid (85% yield). $^1$H NMR (400 MHz, $CDCl_3$): δ: 1.53 (s, 9H, C$H_3$); 2.96 (t, 2H, C$H_2$, $J$ = 7.2 Hz); 3.89 (bs, 2H, C$H_2$); 6.46-6.48 (m, 3H, aryl). ESI-MS *m/z* calcd for $C_{13}H_{18}N_2O_2$ $[(M + H)]^+$: 235.1441; found 235.1447.

***(4-fluorophenyl)(5-isothiocyanatoindolin-1-yl)methanone (65)***

Obtained from intermediate **62** following the general procedure **I**. FC in hexane/ethyl acetate 9/1, R*f*: 0.52. Yellow oil (58% yield). $^1$H NMR (400 MHz, $CDCl_3$): δ: 3.05 (t, 2H, C$H_2$, $J$ = 8.3 Hz); 4.03 (t, 2H, C$H_2$, $J$ = 8.3 Hz); 6.96-7.02 (m, 3H, aryl); 7.08 (t, 2H, aryl, $J$ = 8.6 Hz); 7.48-7.52 (m, 2H, aryl). ESI-MS *m/z* calcd for $C_{16}H_{11}FN_2OS$ $[(M + H)]^+$: 299.0649; found 299.0653.

***2-(4-fluorophenyl)-1-(5-isothiocyanatoindolin-1-yl)ethanone (66)***

Obtained from intermediate **63** following the general procedure **I**. FC in hexane/ethyl acetate 9/1, R*f*: 0.44. Yellow oil (62% yield). $^1$H NMR (400 MHz, DMSO): δ: 3.17 (t, 2H, C$H_2$, $J$ = 7.0 Hz); 3.89 (s, 2H, C$H_2$); 4.21 (t, 2H, C$H_2$, $J$ = 6.8 Hz); 7.02 (d, 1H, aryl, $J$ = 6.4 Hz); 7.14-7.18 (m, 2H, aryl); 7.32 (bs, 2H, aryl); 7.39 (s, 1H, aryl); 7.93 (d, 1H, aryl, $J$ = 7.0 Hz). ESI-MS *m/z* calcd for $C_{17}H_{13}FN_2OS$ $[(M + H)]^+$: 312.0727; found 312.0734.

***tert-butyl 5-isothiocyanatoindoline-1-carboxylate (67)***

Obtained from intermediate **64** following the general procedure **I**. FC in hexane/ethyl acetate 8/2, R*f*: 0.47. Yellow oil (58% yield). $^{1}$H NMR (400 MHz, $CDCl_3$): δ: 1.58 (s, 9H, C*H*$_3$); 3.09 (t, 2H, C*H*$_2$, *J* = 8.7 Hz); 4.02 (t, 2H, C*H*$_2$, *J* = 8.7 Hz); 6.92-6.96 (m, 3H, aryl). ESI-MS *m/z* calcd for $C_{14}H_{16}N_2O_2S$ $[(M + H)]^+$: 277.1005; found 277.1001.

***1-(1-(4-fluorobenzoyl)indolin-5-yl)-3-neopentylthiourea (68)***

Derivative **68** was synthesized according to the general procedure **J**, starting from **65** and 2,2-dimethylpropan-1-amine. FC in dichloromethane/ethyl acetate 8/2, R*f*: 0.48. Yellow oil (65% yield). $^{1}$H NMR (400 MHz, $CDCl_3$): δ: 0.91 (s, 9H, C*H*$_3$); 3.15 (t, 2H, C*H*$_2$, *J* = 8.2 Hz); 3.47 (bs, 2H, *CH*$_2$); 4.12 (t, 2H, C*H*$_2$, *J* = 8.1 Hz); 7.04 (bs, 1H, N*H*); 7.13-7.17 (m, 4H, aryl); 7.57-7.61 (m, 3H, aryl). $^{13}$C NMR (100 MHz, $CDCl_3$) δ 27.5, 28.2, 51.1, 56.5, 115.7, 115.9, 122.4, 124.6, 129.6, 132.0, 132.5, 134.6, 141.8, 162.7, 165.2, 168.1, 181.0. ESI-MS *m/z* calcd for $C_{21}H_{24}FN_3OS$ $[(M + H)]^+$: 386.1697; found 386.1703.

***1-(1-(2-(4-fluorophenyl)acetyl)indolin-5-yl)-3-neopentylthiourea (69)***

Derivative **69** was synthesized according to the general procedure **J**, starting from **66** and 2,2-dimethylpropan-1-amine FC in hexane/ethyl acetate 7/3, R*f*: 0.47. Yellow oil (58% yield). $^{1}$H NMR (400 MHz, $CD_3OD$): δ: 0.96 (s, 9H, *CH*$_3$); 3.21 (t, 2H, C*H*$_2$, *J* = 8.5 Hz); 3.47 (bs, 2H, C*H*$_2$); 3.88 (s, 2H, *CH*$_2$); 4.21 (t, 2H, C*H*$_2$, *J* = 8.5 Hz); 7.06-7.10 (m, 3H, aryl); 7.32-7.35 (m, 3H, aryl); 8.11 (d, 1H, aryl, *J* = 8.6 Hz). $^{13}$C NMR (100 MHz, $CD_3OD$) δ 26.4, 27.4, 41.3, 55.3, 114.7, 115.0, 116.8, 130.5, 130.9, 140.6,

160.8, 163.2, 170.1. ESI-MS *m/z* calcd for $C_{22}H_{26}FN_3OS$ $[(M + H)]^+$: 400.1853; found 400.1859.

***tert-butyl 5-(3-neopentylthioureido)indoline-1-carboxylate (70)***

Intermediate **70** was synthesized according to the general procedure **J**, starting from **67** and 2,2-dimethylpropan-1-amine FC in hexane/ethyl acetate 7/3, R*f*: 0.47. Yellow oil (52% yield). $^1$H NMR (400 MHz, $CDCl_3$): δ: 0.82 (s, 9H, C*H*$_3$); 0.87 (s, 9H, C*H*$_3$); 3.03 (t, 2H, C*H*$_2$, *J* = 8.7 Hz); 3.95 (t, 2H, C*H*$_2$, *J* = 8.7 Hz); 7.03-7.06 (m, 3H, aryl); 7.46 (bs, 1H, N*H*). ESI-MS *m/z* calcd for $C_{19}H_{29}N_3O_2S$ $[(M + H)]^+$: 364.2053; found 364.2060.

***1-(indolin-5-yl)-3-neopentylthiourea (71)***

Obtained from intermediate **70** following the general procedure **D**. FC in hexane/ethyl acetate 1/1, R*f*: 0.47. White oil (95% yield). $^1$H NMR (400 MHz, $CDCl_3$): δ: 0.91 (s, 9H, C*H*$_3$); 3.04 (t, 2H, C*H*$_2$, *J* = 8.7 Hz); 3.55 (t, 2H, C*H*$_2$, *J* = 8.3 Hz); 6.72 (d, 1H, aryl, *J* = 8.2 Hz); 6.92 (d, 1H, aryl, *J* = 10.2 Hz); 7.06 (s, 1H, aryl). ESI-MS *m/z* calcd for $C_{14}H_{21}N_3S$ $[(M + H)]^+$: 264.1529; found, 264.1538.

***1-neopentyl-3-(1-(4-nitrobenzyl)indolin-5-yl)thiourea (72)***

Intermediate **72** was synthesized according to the general procedure **G**, starting from **71** and 4-nitrobenzaldehyde. FC in hexane/ethyl acetate 7/3, R*f*: 0.48. Yellowish oil (68% yield). $^1$H NMR (400 MHz, $CDCl_3$): δ: 0.92 (s, 9H, C*H*$_3$); 3.08 (t, 2H, C*H*$_2$, *J* = 6.7 Hz); 3.50 (t, 2H, C*H*$_2$, *J* = 6.7 Hz); 4.41 (s, 2H, C*H*$_2$); 6.45 (d, 1H, aryl, *J* = 6.6 Hz); 6.95 (d, 1H, aryl, *J* = 6.5 Hz); 7.06 (s, 1H, aryl); 7.57 (d, 2H, aryl, *J* = 6.8 Hz); 8.25 (d, 2H, aryl, *J* = 7.0 Hz). ESI-MS *m/z* calcd for $C_{21}H_{26}N_4O_2S$ $[(M + H)]^+$: 399.1849; found 399.1842.

**Synthesis of 1-neopentyl-3-(1-(4-nitrosobenzyl)indolin-5-yl)thiourea (73)**

0.05 mmol of **72** were solubilized in MeOH, then 0.25 mmol of zinc dust and 0.25 mmol of ammonium chloride were introduced and the solution was refluxed for 1 hour.

Afterwards, the mixture was cooled to room temperature and filtered over celite, methanolic phase was evaporated and the residue was washed with 10% w:w aqueous solution of $NaHCO_3$, dried over $Na_2SO_4$, filtered and concentrated in vacuo. Final derivative **73** was isolated after flash chromatography using dichloromethane/ethyl acetate 9/1 as eluent. FC in dichloromethane/ethyl acetate 9/1, R*f*: 0.49. Yellowish solid (64% yield). $^1$H NMR (400 MHz, $CD_3OD$): δ: 0.91 (s, 9H, C*H*$_3$); 2.91 (t, 2H, C*H*$_2$, *J* = 8.3 Hz); 3.28 (t, 2H, C*H*$_2$, *J* = 8.3 Hz); 3.44 (bs, 2H, C*H*$_2$); 4.14 (s, 2H, C*H*$_2$); 6.58 (d, 1H, aryl, *J* = 8.3 Hz); 6.73 (d, 2H, aryl, *J* = 8.4 Hz); 6.90 (d, 1H, aryl, *J* = 8.3 Hz); 6.95 (s, 1H, aryl); 7.11 (d, 2H, aryl, *J* = 8.3 Hz). $^{13}$C NMR (100 MHz, $CD_3OD$): δ: 26.4, 27.7, 32.0, 52.5, 52.9, 55.4, 107.0, 115.5, 115.7, 122.7, 125.3, 127.6, 128.9, 129.9, 131.6, 146.0, 151.7, 181.6. ESI-MS *m/z* calcd for $C_{21}H_{26}N_4OS$ $[(M + H)]^+$: 383.1900; found 383.1905.

***1-(4-fluorobenzyl)-5-nitro-1H-indole (74)***

Intermediate **74** was synthesized starting from 5-nitroindole and 4-fluorobenzyl chloride following the procedure **C**. FC in hexane/ethyl acetate 8/2, R*f*: 0.47. Yellow oil (85% yield). $^1$H NMR (400 MHz, $CDCl_3$): δ: 5.35 (s, 2H, C*H*$_2$); 6.74 (d, 1H, aryl, *J* = 3.1 Hz); 7.02 (t, 2H, aryl, *J* = 8.1 Hz); 7.08-7.12 (m, 2H, aryl); 7.28-7.31 (m, 2H, aryl); 8.03 (s, 1H, aryl); 8.08 (d, 1H, aryl, *J* = 9.1 Hz); 8.60 (s, 1H, N*H*). ESI-MS *m/z* calcd for $C_{15}H_{11}FN_2O_2$ $[(M + H)]^+$: 271.0877; found 271.0884.

***1-(4-fluorobenzyl)-1H-indol-5-amine (75)***

Intermediate **75** was synthesized starting from **74** following the procedure **H**. FC in hexane/ethyl acetate 7/3, R*f*: 0.52. Yellow oil (82% yield). $^{1}$H NMR (400 MHz, $CDCl_3$): δ: 3.46 (bs, 2H, N*H*$_2$); 5.24 (s, 2H, C*H*$_2$); 6.40 (d, 1H, aryl, *J* = 3.0 Hz); 6.67 (dd, 1H, aryl, *J'* = 2.2, Hz *J''* = 6.4 Hz); 6.98-7.02 (m, 3H, aryl); 7.06-7.11 (m, 4H, aryl). ESI-MS *m/z* calcd for $C_{15}H_{13}N_2$ $[(M + H)]^+$: 241.1136; found 241.1129.

***1-(4-fluorobenzyl)-5-isothiocyanato-1H-indole (76)***

Intermediate **76** was obtained following general procedure **I**, starting from **75**. FC in hexane/ethyl acetate 9/1, R*f*: 0.47. Yellow oil (64% yield). $^{1}$H NMR (400 MHz, $CDCl_3$): δ: 5.13 (s, 2H, C*H*$_2$); 6.29 (d, 1H, aryl, *J* = 2.6 Hz); 6.51 (dd, 1H, aryl, *J'* = 2.1, Hz *J''* = 8.7 Hz); 6.81 (d, 1H, aryl, *J* = 1.9 Hz); 6.87-7.01 (m, 5H, aryl); 7.19 (s, 1H, aryl). ESI-MS *m/z* calcd for $C_{16}H_{11}FN_2S$ $[(M + H)]^+$: 283.0700; found 283.0702.

***1-(1-(4-fluorobenzyl)-1H-indol-5-yl)-3-neopentylthiourea (77)***

Derivative **77** was obtained following general procedure **J**, starting from **76** which was reacted with 2,2-dimethylpropan-1-amine. FC in hexane/ethyl acetate 7/3, R*f*: 0.48. Yellow oil (76% yield). $^{1}$H NMR (400 MHz, $CDCl_3$): δ: 0.77 (s, 9H, C*H*$_3$); 3.40 (d, 2H, C*H*$_2$, *J* = 5.5 Hz); 5.23 (s, 2H, C*H*$_2$); 5.93 (bs, 1H, N*H*); 6.50 (d, 1H, aryl, *J* = 3.1 Hz); 6.91-6.96 (m, 2H, aryl); 7.01 (t, 2H, aryl, *J* = 5.3 Hz); 7.14 (d, 1H, aryl, *J* = 3.1 Hz); 7.21 (t, 2H, aryl, *J* = 9.3 Hz); 7.43 (s, 1H, aryl); 7.62 (bs, 1H, N*H*). $^{13}$C NMR (100 MHz, $CDCl_3$): δ: 27.4, 49.8, 56.6, 102.3, 111.1, 115.7, 116.0, 119.1, 120.4, 127.7, 128.4, 129.6, 130.0, 132.6, 135.3, 161.2, 163.6, 181.8. ESI-MS *m/z* calcd for $C_{21}H_{24}FN_3S$ $[(M + H)]^+$: 370.1748; found 370.1752.

***9-(4-fluorobenzyl)-9H-carbazole (78)***

Intermediate **78** was obtained following general procedure **C**, starting from carbazole which was reacted with 4-fluorobenzyl chloride. FC in hexane/ethyl acetate 7/3, R*f*: 0.47. Yellow oil (97% yield). $^1$H NMR (400 MHz, $CDCl_3$): δ: 5.30 (s, 2H, C*H*$_2$); 6.80 (t, 2H, aryl, *J* = 9.0 Hz); 6.94-6.98 (m, 2H, aryl); 7.15 (t, 2H, aryl, *J* = 8.0 Hz); 7.20 (d, 2H, aryl, *J* = 8.4 Hz); 7.32 (t, 2H, aryl, *J* = 8.8 Hz); 8.02 (d, 2H, aryl, *J* = 8.2 Hz). ESI-MS *m/z* calcd for $C_{19}H_{14}FN_2$ $[(M + H)]^+$: 276.1183; found 276.1177.

**Synthesis of 9-(4-fluorobenzyl)-3-nitro-9H-carbazole (79)**

Intermediate **78** (0.1 mmol) was solubilized in acetic anhydride and cooled to 0°C. To this solution 0.05 mmol of nitric acid were added and the solution was stirred for further 2 hours. Then the mixture was quenched with a 2M NaOH solution and extracted with dichloromethane. The organic layer was dried over anhydrous $Na_2SO_4$, filtered and concentrated in vacuo. Purification by flash chromatography using dichloromethane/hexane 8/2 as mobile phase afforded intermediate **79**. FC in dichloromethane/hexane 8/2, R*f*: 0.47. Yellow solid (77% yield). $^1$H NMR (400 MHz, $CDCl_3$): δ: 5.47 (s, 2H, C*H*$_2$); 6.91 (t, 2H, aryl, *J* = 8.6 Hz); 7.01-7.05 (m, 2H, aryl); 7.16-7.20 (m, 2H, aryl); 7.29-7.36 (m, 2H, aryl); 7.47 (t, 1H, aryl, *J* = 8.2 Hz); 8.12 (d, 1H, aryl, *J* = 7.8 Hz); 8.29 (d, 1H, aryl, *J* = 8.8 Hz); 8.99 (s, 1H, aryl). ESI-MS *m/z* calcd for $C_{19}H_{14}FN_2O_2$ $[(M + H)]^+$: 321.1034; found 321.1040.

***9-(4-fluorobenzyl)-9H-carbazol-3-amine (80)***

Intermediate **80** was obtained following general procedure **H**, starting from **79**. FC in hexane/ethyl acetate 2/8, R*f*: 0.40. Yellowish solid (90% yield). $^1$H NMR (400 MHz, $CDCl_3$): δ: 3.48 (bs, 2H, N*H*$_2$); 5.31 (s, 2H, C*H*$_2$); 6.78-6.86 (m, 3H, aryl); 6.97-7.00

(m, 2H, aryl); 7.04 (d, 1H, aryl, *J* = 8.5 Hz); 7.10 (t, 1H, aryl, *J* = 7.8 Hz); 7.19 (d, 1H, aryl, *J* = 8.2 Hz); 7.30 (t, 1H, aryl, *J* = 7.1 Hz); 7.37 (s, 1H, aryl); 7.93 (d, 1H, aryl, *J* = 7.8 Hz). ESI-MS *m/z* calcd for $C_{19}H_{15}FN_2$ $[(M + H)]^+$: 291.1292; found 291.1300.

***9-(4-fluorobenzyl)-3-isothiocyanato-9H-carbazole (81)***

Intermediate **81** was obtained following general procedure **I**, starting from **80**. FC in hexane/ethyl acetate 9/1, R*f*: 0.47. Yellowish oil (55% yield). $^1$H NMR (400 MHz, $CDCl_3$): δ: 5.49 (s, 2H, C*H*$_2$); 6.96 (t, 2H, aryl, *J* = 8.6 Hz); 7.08-7.12 (m, 2H, aryl); 7.27-7.34 (m, 2H, aryl); 7.04 (d, 1H, aryl, *J* = 8.2 Hz); 7.38 (d, 1H, aryl, *J* = 8.2 Hz); 7.51 (t, 1H, aryl, *J* = 8.2 Hz); 8.00 (s, 1H, aryl); 8.09 (d, 1H, aryl, *J* = 7.8 Hz). ESI-MS *m/z* calcd for $C_{20}H_{13}FN_2S$ $[(M + H)]^+$: 333.0856; found 333.0864.

***1-(9-(4-fluorobenzyl)-9H-carbazol-3-yl)-3-neopentylthiourea (82)***

Derivative **82** was synthesized starting from **81** and 2,2-dimethylpropan-1-amine following the procedure **J**. FC in dichloromethane/ethyl acetate 9.5/0.5, R*f*: 0.52. Yellowish oil (58% yield). $^1$H NMR (400 MHz, $CD_3OD$): δ: 0.94 (s, 9H, C*H*$_3$); 3.48 (bs, 2H, C*H*$_2$); 5.59 (s, 2H, C*H*$_2$); 6.97 (t, 2H, aryl, *J* = 8.7 Hz); 7.15-7.18 (m, 2H, aryl); 7.24 (t, 1H, aryl, *J* = 7.8 Hz); 7.34 (d, 1H, aryl, *J* = 8.1 Hz); 7.43-7.52 (m, 3H, aryl); 8.07-8.11 (m, 2H, aryl). $^{13}$C NMR (100 MHz, $CD_3OD$): δ: 26.4, 45.2, 55.4, 109.0, 109.5, 114.8, 115.1, 117.7, 119.2, 120.0, 122.5, 123.4, 124.0, 126.1, 128.2, 133.4, 139.0, 141.2, 160.9, 163.3, 182.0. ESI-MS *m/z* calcd for $C_{25}H_{26}FN_3S$ $[(M + H)]^+$: 420.1904; found 420.1911.

***1-(4-fluorobenzyl)-5-nitroindoline (83)***

Intermediate **83** was obtained from 5-nitroindoline e and 4-fluorobenzaldehyde following the general procedure **G**. FC in hexane/ethyl acetate 8/2, R*f*: 0.48. Yellow

oil (92% yield). $^1$H NMR (400 MHz, $CDCl_3$): δ: 3.11 (t, 2H, C*H*$_2$, *J* = 8.6 Hz); 3.63 (t, 2H, C*H*$_2$, *J* = 8.9 Hz); 4.42 (s, 2H, C*H*$_2$); 6.38 (d, 1H, aryl, *J* = 8.8 Hz); 7.07 (t, 2H, aryl, *J* = 8.6 Hz); 7.24-7.28 (m, 2H, aryl); 7.93 (s, 1H, aryl); 8.07 (d, 1H, aryl, *J* = 8.8 Hz). ESI-MS *m/z* calcd for $C_{15}H_{13}FN_2O_2$ $[(M + H)]^+$: 273.1034; found 273.1039.

***1-(4-fluorobenzyl)indolin-5-amine (84)***

Intermediate **84** was obtained from **83** following general procedure **H**. FC in hexane/ethyl acetate 1/1, R*f*: 0.41. White solid (95% yield). $^1$H NMR (400 MHz, $CDCl_3$): δ: 2.79 (t, 2H, C*H*$_2$, *J* = 7.4 Hz); 3.08 (t, 2H, C*H*$_2$, *J* = 7.6 Hz); 3.26 (bs, 2H, N*H*$_2$); 4.01 (s, 2H, C*H*$_2$); 6.26 (d, 1H, aryl, *J* = 8.1 Hz); 6.37 (d, 1H, aryl, *J* = 8.0 Hz); 6.50 (s, 1H, aryl); 6.93 (t, 2H, aryl, *J* = 8.7 Hz); 7.24-7.27 (m, 2H, aryl). ESI-MS *m/z* calcd for $C_{15}H_{15}FN_2$ $[(M + H)]^+$: 243.1292; found 243.1300.

**Synthesis of (3r,5r,7r)-N-(1-(4-fluorobenzyl)indolin-5-yl)adamantane-1-carboxamide (85)**

To a solution of 1-adamantanecarboxylic acid (0.1 mmol) in DCM 0.12 mmol of HOBt, 0.12 mmol of HBTU and 0.24 mmol of DIPEA were added and the mixture was stirred at room temperature for 30 minutes. Then 0.1 mmol of intermediate **84** were added and the reaction was mixed at room temperature for further 12 hours. Later the crude was washed with water (3 x 50 mL), 10% aqueous solution of citric acid (3 x 50 mL) and saturated aqueous solution of $NaHCO_3$ (3 x 50 mL). The organic phase was dried over anhydrous $Na_2SO_4$, filtered and concentrated in vacuo. Flash chromatography using n-hexane/ethyl acetate (7/3, v/v) furnished the final derivative **85** as a white powder in 61% yield. R*f*: 0.48. $^1$H NMR (400 MHz, DMSO): δ: 1.70 (bs, 6H, C*H*$_2$); 1.88 (bs, 6H, C*H*$_2$); 2.01 (bs, 3H, C*H*); 2.85 (t, 2H, C*H*$_2$, *J* = 8.3 Hz); 3.19 (t, 2H, C*H*$_2$, *J* = 8.1 Hz); 4.21 (s, 2H, C*H*$_2$); 6.53 (d, 1H, aryl, *J* = 8.4 Hz); 7.15-7.19

(m, 3H, aryl); 7.32 (s, 1H, aryl) 7.37-7.40 (m, 2H, aryl); 8.77 (s, 1H, N*H*). $^{13}$C NMR (100 MHz, DMSO) δ 28.2, 28.5, 36.6, 39.0, 52.8, 53.5, 107.1, 115.4, 115.6, 118.9, 120.4, 130.0, 130.5, 149.0, 160.6, 163.0, 175.7. HR-MS m/z calcd for $C_{26}H_{29}FN_2O$ $[(M + H)]^+$: 405.2337; found 405.2343.

***1-((1S)-7,7-dimethyl-2-oxobicyclo[2.2.1]heptan-1-yl)-N-(1-(4-fluorobenzyl)indolin-5-yl)methanesulfonamide (86)***

Derivative **86** was obtained from **84** following general procedure **B**. FC in dichloromethane/hexane 8/2, R*f*: 0.45. Yellowish oil (35% yield). $^1$H NMR (400 MHz, $CDCl_3$): δ: 0.83 (s, 3H, C*H*$_3$); 0.90 (s, 3H, C*H*$_3$); 1.38-1.43 (m, 2H, C*H*$_2$); 1.96-2.04 (m, 2H, C*H*$_2$); 2.06-2.12 (m, 2H, C*H*$_2$); 2.40 (dd, 1H, C*H, J'* = 2.3; *J''* = 18.6 Hz); 2.72 (d, 1H, C*H*$_{2a,}$ *J* = 15.3 Hz); 2.89 (t, 2H, C*H*$_{2,}$ *J* = 8.2 Hz); 3.22-3.27 (m, 2H, C*H*$_2$); 3.35 (d, 1H, C*H*$_{2b,}$ *J* = 15.2 Hz); 4.12 (s, 2H, C*H*$_2$); 6.32 (d, 1H, aryl, *J* = 8.3 Hz); 6.84 (d, 1H, aryl, *J* = 10.2 Hz); 6.95 (t, 2H, aryl, *J* = 8.6 Hz); 7.01 (s, 1H, aryl); 7.23-7.26 (m, 2H, aryl); 7.35 (s, 1H, N*H*). $^{13}$C NMR (100 MHz, $CDCl_3$) δ 19.4, 20.0, 27.1, 27.8, 28.4, 29.7, 42.9, 43.1, 48.3, 49.1, 53.7, 59.9, 115.3, 115.6, 121.6, 123.3, 129.7, 161.0, 163.4, 217.6. HR-MS m/z calcd for $C_{25}H_{29}N_2FO_3S$ $[(M + H)]^+$: 596.1637; found 596.1642.

***1-(((3r,5r,7r)-adamantan-1-yl)methyl)-3-(1-(4-fluorobenzyl)indolin-5-yl)urea (87)***

Derivative **87** was synthetized starting from **84** and 1-adamantanemethylamine following the general procedure **F**. FC in hexane/ethyl acetate 1/1, R*f*: 0.47. white powder (38% yield). $^1$H NMR (400 MHz, DMSO): δ: 1.45 (bs, 6H, C*H*$_2$); 1.59 (d, 3H, C*H*$_2$ and C*H*$_{2a}$, *J* = 12.1 Hz); 1.68 (d, 3H, C*H*$_2$ and C*H*$_{2b}$, *J* = 12.0 Hz); 1.94 (bs, 3H, C*H*); 2.77 (d, 2H, C*H*$_2$, *J* = 5.8 Hz); 2.83 (t, 2H, C*H*$_{2,}$ *J* = 8.0 Hz); 3.14 (t, 2H, C*H*$_{2,}$ *J*

= 8.0 Hz); 4.16 (s, 2H, C*H*$_2$); 5.90 (t, 1H, N*H*, *J* = 6.1 Hz); 6.47 (d, 1H, aryl, *J* = 8.4 Hz); 6.91 (d, 1H, aryl, *J* = 8.3 Hz); 7.14-7.18 (m, 3H, aryl); 7.37-7.41 (m, 2H, aryl); 7.95 (s, 1H, N*H*). $^{13}$C NMR (100 MHz, DMSO) δ 28.2, 28.7, 34.0, 37.1, 51.3, 53.3, 53.8, 107.7, 115.4, 116.5, 117.6, 130.4, 130.6, 132.2, 135.1, 147.6, 156.3, 160.5, 162.9. HR-MS m/z calcd for $C_{27}H_{32}FN_3O$ [(M + H)]$^+$: 434.2602; found 433.2527.

***1-((3s,5s,7s)-adamantan-1-yl)-3-(1-(4-fluorobenzyl)indolin-5-yl)urea (88)***

Obtained from **84** and 1-adamantylamine following the general procedure **F**. FC in hexane/ethyl acetate 9.8/0.2, R*f*: 0.47. Yellowish powder (42% yield). $^1$H NMR (400 MHz, DMSO): δ: 1.63 (bs, 6H, C*H*$_2$); 1.92 (bs, 6H, C*H*$_2$); 2.02 (bs, 3H, C*H*); 2.82 (t, 2H, C*H*$_2$, *J* = 8.2 Hz); 3.13 (t, 2H, C*H*$_2$, *J* = 8.0 Hz); 4.15 (s, 2H, C*H*$_2$); 5.66 (s, 1H, N*H*); 6.46 (d, 1H, aryl, *J* = 8.3 Hz); 6.86 (d, 1H, aryl, *J* = 8.9 Hz); 7.14-7.18 (m, 2H, aryl); 7.37-7.40 (m, 3H, aryl); 7.82 (bs, 1H, N*H*). $^{13}$C NMR (100 MHz, DMSO) δ 28.7, 29.4, 36.6, 42.3, 50.0, 53.3, 53.8, 107.7, 115.4, 115.6, 116.5, 117.5, 130.4, 130.5, 132.2, 135.1, 147.5, 154.9, 160.5, 162.9. HR-MS m/z calcd for $C_{26}H_{30}FN_3O$ [(M + H)]$^+$: 421.2416; found 421.2484.

***1-(1-(4-fluorobenzyl)indolin-5-yl)-3-(naphthalen-1-ylmethyl)urea (89)***

Obtained from **84** and 1-naphthylmethylamine following the general procedure **F**. FC in hexane/ethyl acetate 9.8/0.2, R*f*: 0.45. Yellowish powder (48% yield). $^1$H NMR (400 MHz, DMSO): δ: 2.84 (t, 2H, C*H*$_2$, *J* = 7.8 Hz); 2.85 (t, 2H, C*H*$_2$, *J* = 8.0 Hz); 4.17 (s, 2H, C*H*$_2$); 5.97 (t, 1H, N*H*, *J* = 5.7 Hz); 6.44 (d, 1H, aryl, *J* = 8.4 Hz); 6.90 (d, 1H, aryl, *J* = 7.8 Hz); 7.18 (s, 1H, aryl); 7.48 (d, 2H, aryl, *J* = 8.2 Hz); 7.92 (d, 2H, aryl, *J* = 8.2 Hz); 8.05 (s, 1H, N*H*). $^{13}$C NMR (100 MHz, DMSO) δ 28.7, 41.3, 53.2, 53.8, 107.7, 115.4, 115.6, 116.9, 118.0, 124.0, 125.8, 126.0, 126.3, 126.7, 127.9, 129.0,

130.40, 130.48, 130.56, 131.4, 131.8, 133.8, 135.1, 136.2, 147.8, 155.9, 162.9. HR-MS m/z calcd for $C_{27}H_{24}N_3FO_3$ $[(M + H)]^+$: 426.1976; found 426.1979.

***1-(1-(4-fluorobenzyl)indolin-5-yl)-3-(2-(4-methyl-1,4-diazepan-1-yl)ethyl)urea (90)***

Obtained from **84** and 2-(4-methyl-1,4-diazepan-1-yl)ethanamine following the general procedure **F**. FC in dichloromethane/methanol 7/3, R*f*: 0.41. Yellow oil (45% yield). $^1$H NMR (400 MHz, $CD_3OD$): δ: 1.83-1.89 (m, 2H, C*H*$_2$); 2.41 (s, 3H, C*H*$_3$); 2.65 (t, 2H, C*H*$_2$, *J* = 6.3 Hz); 2.72-2.81 (m, 8H, C*H*$_2$); 2.92 (t, 2H, C*H*$_2$, *J* = 8.2 Hz); 3.23-3.29 (m, 4H, C*H*$_2$); 4.20 (s, 2H, C*H*$_2$); 6.51 (d, 1H, aryl, *J* = 8.3 Hz); 6.93 (d, 1H, aryl, *J* = 8.4 Hz); 7.05-7.09 (m, 3H, aryl); 7.38-7.42 (m, 2H, aryl). $^{13}$C NMR (100 MHz, $CD_3OD$) δ 26.1, 28.1, 37.3, 45.3, 52.6, 53.1, 53.6, 53.8, 56.2, 57.3, 107.2, 114.6, 114.8, 119.2, 120.9, 129.5, 129.7, 130.9, 134.4, 149.2, 158.1, 163.3. HR-MS m/z calcd for $C_{24}H_{32}FN_5O$ $[(M + H)]^+$: 426.2664; found 426.2666.

***1-(4-fluorobenzyl)-5-thiocyanatoindoline (91)***

Obtained from **84** following the general procedure **I**. FC in n-hexane/ethyl acetate 9/1, R*f*: 0.48. Whitish oil (58% yield). $^1$H NMR (400 MHz, $CDCl_3$): δ: 2.99 (t, 2H, C*H*$_2$, *J* = 8.4 Hz); 3.40 (t, 2H, C*H*$_2$, *J* = 8.5 Hz); 4.26 (s, 2H, C*H*$_2$); 6.37 (d, 1H, aryl, *J* = 8.3 Hz); 6.94 (s, 1H, aryl); 6.97 (d, 1H, aryl, *J* = 5.5 Hz); 7.05 (t, 2H, aryl, *J* = 8.6 Hz); 7.28-7.32 (m, 2H, aryl). ESI-MS *m/z* calcd for $C_{16}H_{13}FN_2S$ $[(M + H)]^+$: 285.0856; found 285.0849.

***1-(((3r,5r,7r)-adamantan-1-yl)methyl)-3-(1-(4-fluorobenzyl)indolin-5-yl)thiourea (92)***

Obtained from **91** and 1-adamantanemethylamine following the general procedure **J**. FC in n-hexane/ethyl acetate 9.8/0.2, R*f*: 0.43. Yellow oil (38% yield). $^{1}$H NMR (400 MHz, $CDCl_3$): δ: 1.39 (bs, 6H, C*H*$_2$); 1.52 (d, 3H, C*H*$_2$ and C*H*$_{2a}$, *J* = 11.6 Hz); 1.63 (d, 3H, C*H*$_2$ and C*H*$_{2b}$, *J* = 12.1 Hz); 1.89 (bs, 3H, C*H*); 2.91 (t, 2H, C*H*$_2$, *J* = 8.4 Hz); 3.29-3.34 (m, 4H, C*H*$_2$); 4.18 (s, 2H, C*H*$_2$); 5.89 (bs, 1H, N*H*); 6.40 (d, 1H, aryl, *J* = 6.6 Hz); 6.84 (d, 1H, aryl, *J* = 8.2 Hz); 6.88 (s, 1H, aryl); 6.96 (t, 2H, aryl, *J* = 8.6 Hz); 7.20-7.25 (m, 3H, aryl); 7.43 (s, 1H, N*H*). $^{13}$C NMR (100 MHz, $CDCl_3$) δ 28.18, 28.21, 34.2, 36.9, 40.5, 52.6, 53.4, 56.8, 107.2, 115.4, 115.6, 123.3, 126.1, 129.4, 132.0, 161.0, 163.4, 181.9. HR-MS m/z calcd for $C_{27}H_{32}FN_3S$ $[(M + H)]^+$: 449.2301; found 450.2368.

***tert-butyl 5-nitroindoline-1-carboxylate (93)***

Intermediate **93** was obtained from 5-nitroindoline following the general procedures **B** and **H**. FC in hexane/ethyl acetate 8/2, R*f*: 0.45. Yellow solid (88% yield). $^{1}$H NMR (400 MHz, $CDCl_3$): δ: 1.60 (s, 9H, C*H*$_3$); 3.19 (t, 2H, C*H*$_2$, *J* = 8.7 Hz); 4.11 (t, 2H, C*H*$_2$, *J* = 9.0 Hz); 7.28 (d, 1H, aryl, *J* = 7.7 Hz); 8.02 (s, 1H, aryl); 8.12 (d, 1H, aryl, *J* = 11.0 Hz). ESI-MS *m/z* calcd for $C_{13}H_{16}N_2O_4$ $[(M + H)]^+$: 265.1183; found 265.1190.

***tert-butyl 5-(3-(((3r,5r,7r)-adamantan-1-yl)methyl)ureido)indoline-1-carboxylate (94)***

Intermediate **94** was obtained starting from **93** and 1-adamantanemethylamine following the general procedure **F**. FC in hexane/ethyl acetate 3/7, R*f*: 0.48. Yellow oil (45% yield). $^{1}$H NMR (400 MHz, $CDCl_3$): δ: 1.49 (s, 9H, C*H*$_3$); 1.57 (bs, 6H, C*H*$_2$); 1.63 (d, 3H, C*H*$_2$ and C*H*$_{2a}$, *J* = 13.0 Hz); 1.72 (d, 3H, C*H*$_2$ and C*H*$_{2b}$, *J* = 12.0 Hz); 1.98 (bs, 3H, C*H*); 2.87 (s, 2H, C*H*$_2$); 3.05 (t, 2H, C*H*$_2$, *J* = 8.6 Hz); 3.97 (t, 2H, C*H*$_2$,

*J* = 7.7 Hz); 5.17 (bs, 1H, N*H*); 6.97 ( bs, 2H, aryl); 7.25 (bs, 1H, aryl); 7.74 (bs, 1H, N*H*). HR-MS m/z calcd for $C_{25}H_{35}N_3O_3$ $[(M + H)]^+$: 426.2751; found 426.2745

***methyl 4-((5-(3-(((3r,5r,7r)-adamantan-1-yl)methyl)ureido)indolin-1-yl)methyl)benzoate (95)***

Intermediate **95** was obtained from **94** following the general procedures **D** and **G**. FC in hexane/ethyl acetate 3/7, R*f*: 0.46. Yellowish oil (55% yield). $^1$H NMR (400 MHz, $CD_3OD$): δ: 1.52 (bs, 6H, C$H_2$); 1.68 (d, 3H, C$H_2$ and C$H_{2a}$, *J* = 11.6 Hz); 1.78 (d, 3H, C$H_2$ and C$H_{2b}$, *J* = 12.1 Hz); 1.97 (bs, 3H, C*H*); 2.83 (s, 2H, C$H_2$); 2.95 (t, 2H, C$H_2$, *J* = 7.2 Hz); 3.27 (t, 2H, C$H_2$, *J* = 7.6 Hz); 3.90 (s, 3H, C$H_3$); 4.27 (s, 2H, C$H_2$); 6.44 (d, 1H, aryl, *J* = 8.0 Hz); 6.92 (d, 1H, aryl, *J* = 8.1 Hz); 7.11 (s, 1H, aryl); 7.50 (d, 2H, aryl, *J* = 8.2 Hz); 7.99 (d, 2H, aryl, *J* = 7.8 Hz). HR-MS m/z calcd for $C_{29}H_{35}N_3O_3$ $[(M + H)]^+$: 474.2751; found 474.2760.

***4-((5-(3-(((3r,5r,7r)-adamantan-1-yl)methyl)ureido)indolin-1-yl)methyl)benzoic acid (96)***

Obtained from **95** following the general procedure **K**. Precipitated from MeOH/$Et_2O$. Whitish powder (67% yield). $^1$H NMR (400 MHz, DMSO): δ: 1.44 (bs, 6H, C$H_2$); 1.60 (d, 3H, C$H_2$ and C$H_{2a}$, *J* = 11.4 Hz); 1.67 (d, 3H, C$H_2$ and C$H_{2b}$, *J* = 12.0 Hz); 1.94 (bs, 3H, C*H*); 2.76 (d, 2H, C$H_2$, *J* = 5.9 Hz); 2.85 (t, 2H, C$H_2$, *J* = 8.0 Hz); 3.19 (t, 2H, C$H_2$, *J* = 8.0 Hz); 4.25 (s, 2H, C$H_2$); 5.97 (t, 1H, N*H*, *J* = 5.7 Hz); 6.44 (d, 1H, aryl, *J* = 8.4 Hz); 6.90 (d, 1H, aryl, *J* = 7.8 Hz); 7.18 (s, 1H, aryl); 7.48 (d, 2H, aryl, *J* = 8.2 Hz); 7.92 (d, 2H, aryl, *J* = 8.2 Hz); 8.05 (s, 1H, N*H*). $^{13}$C NMR (100 MHz, DMSO) δ 28.8, 34.0, 37.1, 51.3, 54.1, 107.7, 116.4, 117.5, 128.5, 129.89, 129.95, 130.5, 132.4, 144.4, 147.5, 156.4, 167.7. HR-MS m/z calcd for $C_{28}H_{33}N_3O_3$ $[(M - H)]^-$: 458.2449; found 458.2852.

***1-(4-fluorobenzyl)-5-nitro-1H-indole (97)***

Intermediate **97** was obtained from 5-nitroindole and 4-fluorobenzyl bromide following the general procedure **C**. FC in hexane/ethyl acetate 8/2, R*f*: 0.47. Yellow oil (85% yield). $^1$H NMR (400 MHz, $CDCl_3$): δ: 5.35 (s, 2H, C*H*$_2$); 6.74 (d, 1H, aryl, *J* = 3.1 Hz); 7.02 (t, 2H, aryl, *J* = 8.1 Hz); 7.08-7.12 (m, 2H, aryl); 7.28-7.31 (m, 2H, aryl); 8.03 (s, 1H, aryl); 8.08 (d, 1H, aryl, *J* = 9.1 Hz); 8.60 (s, 1H, N*H*). ESI-MS *m/z* calcd for $C_{15}H_{11}FN_2O_2$ $[(M + H)]^+$: 271.0877; found 271.0884.

***1-(4-isopropylbenzyl)-5-nitro-1H-indole (98)***

Intermediate **98** was synthetized starting from 5-nitroindole and 4-isopropylbenzyl bromide following the general procedure **C**. FC in hexane/ethyl acetate 9/1, R*f*: 0.45. Yellow oil (85% yield). $^1$H NMR (400 MHz, $CDCl_3$): δ: 1.13 (d, 6H, C*H*$_3$, *J* = 6.9 Hz); 2.74-2.84 (m, 1H, C*H*); 5.20 (s, 2H, C*H*$_2$); 6.62 (d, 1H, aryl, *J* = 3.8 Hz); 6.95 (d, 2H, aryl, *J* = 8.2 Hz); 7.10 (d, 2H, aryl, *J* = 8.3 Hz); 7.18-7.24 (m, 2H, aryl); 7.99 (d, 1H, aryl, *J* = 9.2 Hz); 8.50 (s, 1H, aryl). HR-MS m/z calcd for $C_{18}H_{18}N_2O_2$ $[(M + H)]^+$: 295.1441; found 295.1438.

***methyl 4-((5-nitro-1H-indol-1-yl)methyl)benzoate (99)***

Intermediate **99** was synthetized starting from 5-nitroindole and methyl 4-(bromomethyl)benzoate following the general procedure **C**. FC in hexane/ethyl acetate 1/1, R*f*: 0.47. Yellowish oil (72% yield). $^1$H NMR (400 MHz, $CD_3OD$): δ: 3.76 (s, 3H, C*H*$_3$); 5.46 (s, 2H, C*H*$_2$); 6.69 (s, 1H, aryl); 7.14 (d, 2H, aryl, *J* = 8.2 Hz); 7.33 (d, 1H, aryl, *J* = 7.8 Hz); 7.45 (s, 1H, aryl); 7.85 (d, 2H, aryl, *J* = 8.0 Hz); 7.93 (d, 1H, aryl, *J* = 8.6 Hz); 8.48 (s, 1H, aryl). HR-MS m/z calcd for $C_{17}H_{14}N_2O_4$ $[(M + H)]^+$: 311.1026; found 311.1028.

***1-(4-fluorophenethyl)-5-nitro-1H-indole (100)***

Intermediate **100** was synthetized starting from 5-nitroindole and methyl 4-fluorophenethyl bromide following the general procedure **C**. FC in dichloromethane/hexane 9.8/0.2, R*f*: 0.46. Yellowish oil (62% yield). $^{1}$H NMR (400 MHz, $CDCl_3$): δ: 3.04 (t, 2H, C*H*$_2$, *J* = 6.9 Hz); 4.30 (t, 2H, C*H*$_2$, *J* = 6.9 Hz); 6.54 (d, 1H, aryl, *J* = 3.8 Hz); 6.98 (s, 1H, aryl); 6.82-6.86 (m, 3H, aryl); 6.94 (d, 1H, aryl, *J* = 4.2 Hz); 7.15-7.19 (m, 2H, aryl); 8.00 (d, 1H, aryl, *J* = 11.3 Hz); 8.51 (s, 1H, aryl). HR-MS m/z calcd for $C_{16}H_{13}FN_2O_2$ $[(M + H)]^+$: 285.1034; found 285.1026.

***3-(5-nitro-1H-indol-1-yl)propanenitrile (101)***

Intermediate **101** was synthetized starting from 5-nitroindole and methyl 3-bromopropionitrile following the general procedure **C**. FC in hexane/ethyl acetate 3/7, R*f*: 0.45. Yellow oil (85% yield). $^{1}$H NMR (400 MHz, $CDCl_3$): δ: 2.91 (t, 2H, C*H*$_2$, *J* = 6.6 Hz); 4.54 (t, 2H, C*H*$_2$, *J* = 6.6 Hz); 6.78 (d, 1H, aryl, *J* = 3.3 Hz); 7.28 (s, 1H, aryl); 7.35-7.40 (m, 2H, aryl); 8.18 (d, 1H, aryl, *J* = 9.1 Hz); 8.62 (s, 1H, aryl). HR-MS m/z calcd for $C_{11}H_9N_2O_2$ $[(M + H)]^+$: 216.0868; found 216.0765.

***methyl 4-(5-nitro-1H-indol-1-yl)butanoate (102)***

Intermediate **102** was synthetized starting from 5-nitroindole and methyl 4-bromobutanoate following the general procedure **C**. FC in dichloromethane/hexane 9/1, R*f*: 0.45. Orange oil (62% yield). $^{1}$H NMR (400 MHz, $CD_3OD$): δ: 2.12-2.19 (m, 2H, C*H*$_2$); 2.33 (t, 2H, C*H*$_2$, *J* = 6.9 Hz); 3.84 (s, 3H, C*H*$_3$); 4.32 (t, 2H, C*H*$_2$, *J* = 6.9 Hz); 6.73 (d, 1H, aryl, *J* = 3.9 Hz); 7.47 (d, 1H, aryl, *J* = 3.8 Hz); 7.58 (d, 1H, aryl, *J* = 7.8 Hz); 8.57 (s, 1H, aryl). $^{13}$C NMR (100 MHz, $CDCl_3$) δ 25.4, 28.3, 30.8, 34.1,

37.0, 40.2, 45.5, 51.7, 51.9, 101.5, 110.1, 117.4, 119.8, 129.0, 129.2, 129.8, 134.2, 137.2. HR-MS m/z calcd for $C_{13}H_{14}N_2O_4$ $[(M + H)]^+$: 263.1026; found 263.1019.

***1-(4-fluorobenzyl)-1H-indol-5-amine (103)***

Intermediate **103** was obtained from **97** following the general procedure **H**. FC in hexane/ethyl acetate 7/3, R*f*: 0.52. Yellow oil (80% yield). $^1$H NMR (400 MHz, $CDCl_3$): δ: 3.46 (bs, 2H, N*H*$_2$); 5.24 (s, 2H, C*H*$_2$); 6.40 (d, 1H, aryl, *J* = 3.0 Hz); 6.67 (dd, 1H, aryl, *J'* = 2.2, Hz *J''* = 6.4 Hz); 6.98-7.02 (m, 3H, aryl); 7.06-7.11 (m, 4H, aryl). ESI-MS *m/z* calcd for $C_{15}H_{13}N_2$ $[(M + H)]^+$: 241.1136; found 241.1129.

***1-(4-isopropylbenzyl)-1H-indol-5-amine (104)***

Intermediate **104** was obtained from **98** following the general procedure **H**. FC in hexane/ethyl acetate 3/7, R*f*: 0.48. Whitish oil (65% yield). $^1$H NMR (400 MHz, $CDCl_3$): δ: 1.28 (d, 6H, C*H*$_3$, *J* = 6.9 Hz); 2.89-2.97 (m, 1H, C*H*); 3.49 (bs, 2H, N*H*$_2$); 5.26 (s, 2H, C*H*$_2$); 6.41 (s, 1H, aryl); 6.69 (d, 2H, aryl, *J* = 8.7 Hz); 7.00 (s, 1H, aryl); 7.09-7.21 (m, 5, aryl). HR-MS m/z calcd for $C_{18}H_{20}N_2$ $[(M + H)]^+$: 265.1699; found 265.1705.

***methyl 4-((5-amino-1H-indol-1-yl)methyl)benzoate (105)***

Intermediate **105** was obtained from **99** following the general procedure **H**. FC in dichloromethane/ethyl acetate 8/2, R*f*: 0.48. Yellowish powder (65% yield). $^1$H NMR (400 MHz, $CD_3OD$): δ: 3.88 (s, 3H, C*H*$_3$); 5.40 (s, 2H, C*H*$_2$); 6.34 (d, 1H, aryl, *J* = 2.9 Hz); 6.68 (d, 1H, aryl, *J* = 10.5 Hz); 7.00 (s, 1H, aryl); 7.05 (d, 1H, aryl, *J* = 8.6 Hz); 7.17-7.20 (m, 3H, aryl); 7.93 (d, 2H, aryl, *J* = 8.3 Hz). HR-MS m/z calcd for $C_{17}H_{16}N_2O_2$ $[(M + H)]^+$: 281.1285; found 281.1290.

***1-(4-fluorophenethyl)-1H-indol-5-amine (106)***

Intermediate **106** was obtained from **100** following the general procedure **H**. FC in dichloromethane/ethyl acetate 1/1, R*f*: 0.50. Yellowish solid (55% yield). $^1$H NMR (400 MHz, $CDCl_3$): δ: 2.93 (t, 2H, C*H*$_2$, *J* = 7.2 Hz); 3.44 (bs, 2H, N*H*$_2$); 4.13 (t, 2H, C*H*$_2$, *J* = 7.2 Hz); 6.14 (d, 1H, aryl, *J* = 2.9 Hz); 6.58 (dd, 1H, aryl, *J'* = 2.2, *J''* = 8.6 Hz); 6.69 (d, 1H, aryl, *J* = 3.0 Hz); 6.80-6.89 (m, 5H, aryl); 7.01 (d, 1H, aryl, , *J* = 8.2 Hz). HR-MS m/z calcd for $C_{16}H_{15}FN_2$ $[(M + H)]^+$: 255.1292; found 255.1299.

***3-(5-amino-1H-indol-1-yl)propanenitrile (107)***

Intermediate **107** was obtained from **101** following the general procedure **H**. FC in dichloromethane/ethyl acetate 9.8/0.2, R*f*: 0.46. Yellowish powder (62% yield). $^1$H NMR (400 MHz, $CDCl_3$): δ: 2.99 (t, 2H, C*H*$_2$, *J* = 6.8 Hz); 4.57 (t, 2H, C*H*$_2$, *J* = 6.8 Hz); 5.15 (bs, 2H, N*H*$_2$); 6.60 (d, 1H, aryl, *J* = 3.2 Hz); 7.20 (dd, 1H, aryl, *J'* = 2.1, *J''* = 8.7 Hz); 7.47 (d, 1H, aryl, *J* = 3.1 Hz); 7.63-7.68 (m, 2H, aryl). HR-MS m/z calcd for $C_{11}H_{11}N_3$ $[(M + H)]^+$: 186.1026; found 186.1023.

***methyl 4-(5-amino-1H-indol-1-yl)butanoate (108)***

Intermediate **108** was obtained from **102** following the general procedure **H**. FC in hexane/ethyl acetate 1/1, R*f*: 0.48. Withish oil (77% yield). $^1$H NMR (400 MHz, $CD_3OD$): δ: 2.02-2.09 (m, 2H, C*H*$_2$); 2.23 (t, 2H, C*H*$_2$, *J* = 7.0 Hz); 3.79 (s, 3H, C*H*$_3$); 4.11 (t, 2H, C*H*$_2$, *J* = 6.8 Hz); 6.24 (d, 1H, aryl, *J* = 3.2 Hz); 6.73 (d, 1H, aryl, *J* = 8.6 Hz); 6.96 (s, 1H, aryl); 7.04 (d, 1H, aryl, *J* = 2.8 Hz); 7.19 (d, 1H, aryl, *J* = 8.6 Hz). HR-MS m/z calcd for $C_{13}H_{16}N_2O_2$ $[(M + H)]^+$: 233.1285; found 233.1291.

***1-(((3r,5r,7r)-adamantan-1-yl)methyl)-3-(1-(4-fluorobenzyl)-1H-indol-5-yl)urea (109)***

Obtained from **103** and 1-adamantanemethylamine following the general procedure **F**. FC in hexane/ethyl acetate 1/1, R*f*: 0.48. white powder (68% yield). $^{1}$H NMR (400 MHz, $CDCl_3$): δ: 1.45 (bs, 6H, C$H_2$); 1.60-1.63 (m, 3H, C$H_2$ and C$H_{2a}$); 1.70 (d, 3H, C$H_2$ and C$H_{2b}$, *J* = 12.0 Hz); 1.97 (bs, 3H, C*H*); 2.94 (d, 2H, C$H_2$, *J* = 6.3 Hz); 3.51 (d, 1H, N*H*, *J* = 4.5 Hz); 4.77 (t, 1H, N*H*, *J* = 6.0 Hz); 5.31 (s, 2H, C$H_2$); 6.17 (s, 1H, aryl); 6.55 (s, 1H, aryl); 7.01 (t, 1H, aryl, *J* = 8.7 Hz); 7.06-7.12 (m, 2H, aryl); 7.18 (d, 1H, aryl, *J* = 3.1 Hz); 7.25 (d, 1H, aryl, *J* = 8.6 Hz); 7.56 (s, 1H, aryl). $^{13}$C NMR (100 MHz, $CDCl_3$) δ 28.2, 34.0, 37.0, 40.2, 49.7, 51.9, 102.0, 110.5, 115.7, 115.9, 117.7, 120.1, 128.4, 129.4, 130.0, 132.9, 134.0, 157.6, 163.5. HR-MS m/z calcd for $C_{27}H_{30}FN_3O$ $[(M + H)]^+$: 432.2446; found 432.2430.

***1-(((3r,5r,7r)-adamantan-1-yl)methyl)-3-(1-(4-isopropylbenzyl)-1H-indol-5-yl)urea (110)***

Obtained from **104** and 1-adamantanemethylamine following the general procedure **F**. FC in dichloromethane/ethyl acetate 8/2, R*f*: 0.46. Yellowish powder (58% yield). $^{1}$H NMR (400 MHz, $CDCl_3$): δ: 1.24 (d, 6H, C$H_3$, *J* = 6.9 Hz); 1.45 (bs, 6H, C$H_2$); 1.62 (d, 3H, C$H_2$ and C$H_{2a}$, *J* = 11.6 Hz); 1.71 (d, 3H, C$H_2$ and C$H_{2b}$, *J* = 12.1 Hz); 1.97 (bs, 3H, C*H*); 2.86-2.91 (m, 1H, C*H*); 2.94 (s, 2H, C$H_2$); 4.82 (bs, 1H, N*H*); 5.31 (s, 2H, C$H_2$); 6.24 (bs, 1H, N*H*); 6.54 (s, 1H, aryl); 7.07 (d, 3H, aryl, *J* = 12.1 Hz); 7.19 (d, 3H, aryl, *J* = 8.3 Hz); 7.29 (d, 1H, aryl, *J* = 4.7 Hz); 7.55 (s, 1H, aryl). $^{13}$C NMR (100 MHz, $CDCl_3$) δ 23.9, 28.3, 33.8, 34.0, 37.0, 40.2, 50.1, 52.9, 101.7, 110.6, 117.7, 120.0, 126.8, 129.3, 129.57, 129.69, 134.47, 134.67, 148.6, 157.7. HR-MS m/z calcd for $C_{30}H_{37}N_3O$ $[(M + H)]^+$: 456.3009; found 596.1642.

***methyl 4-((5-(3-(((3r,5r,7r)-adamantan-1-yl)methyl)ureido)-1H-indol-1-yl)methyl)benzoate (111)***

Obtained from **105** and 1-adamantanemethylamine following the general procedure **F**. FC in hexane/ethyl acetate 1/1, R*f*: 0.48. Yellow oil (39% yield). $^{1}$H NMR (400 MHz, $CDCl_3$): δ: 1.45 (bs, 6H, C$H_2$); 1.60 (d, 3H, C$H_2$ and C$H_{2a}$, *J* = 11.6 Hz); 1.69-1.73 (m, 3H, C$H_2$ and C$H_{2b}$); 1.95 (bs, 3H, C*H*); 2.94 (d, 2H, C$H_2$, *J* = 6.3 Hz); 3.91 (s, 2H, C$H_3$); 4.92 (t, 1H, N*H*, *J* = 6.2 Hz); 5.38 (s, 2H, C$H_2$); 6.44 (s, 1H, aryl); 6.56 (s, 1H, aryl); 7.08 (d, 1H, aryl, *J* = 10.5 Hz); 7.14-7.19 (m, 3H, aryl); 7.59 (s, 1H, aryl); 7.98 (d, 2H, aryl, *J* = 8.3 Hz). $^{13}$C NMR (100 MHz, $CDCl_3$) δ 28.3, 34.0, 37.0, 40.2, 50.1, 51.9, 52.2, 102.2, 110.3, 116.9, 119.7, 126.6, 129.4, 129.7, 130.1, 130.4, 134.3, 142.4, 157.6, 166.6. HR-MS m/z calcd for $C_{29}H_{33}N_3O_3$ $[(M + H)]^+$: 596.1637; found 596.1642.

***1-(((3r,5r,7r)-adamantan-1-yl)methyl)-3-(1-(4-fluorophenethyl)-1H-indol-5-yl)urea (112)***

Obtained from **106** and 1-adamantanemethylamine following the general procedure **F**. FC in dichloromethane/ethyl acetate 7/3, R*f*: 0.48. Yellowish oil (41% yield). $^{1}$H NMR (400 MHz, $CD_3OD$): δ: 1.57 (bs, 6H, C$H_2$); 1.70 (d, 3H, C$H_2$ and C$H_{2a}$, *J* = 11.5 Hz); 1.79 (d, 3H, C$H_2$ and C$H_{2b}$, *J* = 12.1 Hz); 2.00 (bs, 3H, C*H*); 2.92 (s, 2H, C$H_2$); 3.08 (t, 2H, C$H_2$, *J* = 6.9 Hz); 4.36 (t, 2H, C$H_2$, *J* = 6.9 Hz); 6.91 (t, 2H, aryl, *J* = 8.8 Hz); 6.98 (s, 1H, aryl); 7.01-7.07 (m, 3H, aryl); 7.26 (d, 2H, aryl, *J* = 8.7 Hz); 7.53 (s, 1H, aryl). $^{13}$C NMR (100 MHz, $CD_3OD$) δ 28.4, 33.7, 35.4, 36.7, 39.9, 51.3, 109.2, 112.8, 114.5, 114.7, 116.3, 128.4, 128.9, 130.2, 130.9, 133.1, 134.8, 158.4, 160.5, 162.9. HR-MS m/z calcd for $C_{28}H_{32}FN_3O$ $[(M + H)]^+$: 596.1637; found 596.1642.

***1-(((3r,5r,7r)-adamantan-1-yl)methyl)-3-(1-(2-cyanoethyl)-1H-indol-5-yl)urea (113)***

Intermediate **113** was obtained from **107** and 1-adamantanemethylamine following the general procedure **F**. FC in hexane/ethyl acetate 7/3, R*f*: 0.44. Yellowish oil (65% yield). $^{1}$H NMR (400 MHz, $CDCl_3$): δ: 1.37 (bs, 6H, C$H_2$); 1.53 (d, 3H, C$H_2$ and C$H_{2a}$, $J$ = 11.6 Hz); 1.64 (d, 3H, C$H_2$ and C$H_{2b}$, $J$ = 12.1 Hz); 1.89 (bs, 3H, C$H$); 2.77 (t, 2H, C$H_2$, $J$ = 7.0 Hz); 2.87 (s, 2H, C$H_2$); 4.38 (t, 2H, C$H_2$, $J$ = 6.7 Hz); 6.47 (d, 1H, aryl, $J$ = 2.4 Hz); 7.08 (d, 1H, aryl, $J$ = 8.5 Hz); 7.13 (d, 1H, aryl, $J$ = 2.6 Hz); 7.23 (d, 1H, aryl, $J$ = 8.4 Hz); 7.47 (s, 1H, aryl). HR-MS m/z calcd for $C_{23}H_{28}N_4O$ $[(M + H)]^+$: 377.2336; found 377.2340.

***methyl 4-(5-(3-(((3r,5r,7r)-adamantan-1-yl)methyl)ureido)-1H-indol-1-yl)butanoate (114)***

Obtained from **107** and 1-adamantanemethylamine following the general procedure **F**. FC in hexane/ethyl acetate 3/7, R*f*: 0.49. Whitish oil (42% yield). $^{1}$H NMR (400 MHz, $CDCl_3$): δ: 1.37 (bs, 6H, C$H_2$); 1.53 (d, 3H, C$H_2$ and C$H_{2a}$, $J$ = 11.6 Hz); 1.62 (d, 3H, C$H_2$ and C$H_{2b}$, $J$ = 12.1 Hz); 1.87 (bs, 3H, C$H$); 2.05-2.12 (m, 2H, C$H_2$); 2.23 (t, 2H, C$H_2$, $J$ = 6.7 Hz); 2.85 (s, 2H, C$H_2$); 3.60 (s, 3H, C$H_3$); 4.12 (t, 2H, C$H_2$, $J$ = 6.9 Hz); 6.36-6.40 (m, 2H, aryl and N$H$); 7.02-7.04 (m, 2H, aryl); 7.25 (d, 1H, aryl, $J$ = 8.6 Hz); 7.45 (s, 1H, aryl). $^{13}$C NMR (100 MHz, $CDCl_3$) δ 25.4, 28.3, 30.8, 34.1, 37.0, 40.2, 45.5, 51.7, 51.9, 101.5, 110.1, 117.4, 119.8, 129.0, 129.2, 129.8, 134.2, 137.2. HR-MS m/z calcd for $C_{25}H_{33}N_3O_3$ $[(M + H)]^+$: 596.1637; found 596.1642.

***1-((3s,5s,7s)-adamantan-1-yl)-3-(1-(4-fluorobenzyl)-1H-indol-5-yl)urea (115)***

Obtained from **103** and 1-adamantanamine following the general procedure **F**. FC in hexane/ethyl acetate 1/1, R*f*: 0.51. Yellow oil (45% yield). $^{1}$H NMR (400 MHz, $CD_3OD$): δ: 1.62 (bs, 10H, C$H_2$); 1.93-1.96 (m, 15H, C$H_2$ and C*H*); 5.22 (s, 2H, C$H_2$); 6.31 (d, 1H, aryl, *J* = 4.6 Hz); 6.89 (t, 3H, aryl, *J* = 10.4 Hz); 7.02-7.05 (m, 2H, aryl); 7.09 (d, 1H, aryl, *J* = 8.8 Hz); 7.13 (d, 1H, aryl, *J* = 3.1 Hz); 7.41 (s, 1H, aryl). $^{13}$C NMR (100 MHz, $CD_3OD$) δ 29.3, 29.7, 36.2, 42.0, 100.9, 109.4, 112.3, 114.7, 116.3, 128.3, 128.7, 129.2, 131.4, 133.1, 134.2, 156.8, 160.9, 163.4. HR-MS m/z calcd for $C_{26}H_{28}FN_3O$ $[(M + H)]^+$: 596.1637; found 596.1642.

***(4-fluorophenyl)(5-nitro-1H-indol-1-yl)methanone (116)***

Obtained from 5-nitroindole and 4-fluorobenzoyl chloride following the general procedure **B**. FC in hexane/ethyl acetate 8/2, R*f*: 0.45. Yellowish oil (65% yield). $^{1}$H NMR (400 MHz, $CDCl_3$): δ: 6.71 (d, 1H, aryl, *J* = 3.7 Hz); 7.19 (t, 2H, aryl, *J* = 8.7 Hz); 7.40 (d, 1H, aryl, *J* = 3.8 Hz); 7.73-7.76 (m, 2H, aryl); 8.21 (dd, 1H, aryl, *J'* = 2.2, *J''* = 9.1 Hz); 8.39 (d, 1H, aryl, *J* = 9.1 Hz); 8.47 (d, 1H, aryl, *J* = 2.2 Hz).

***(5-amino-1H-indol-1-yl)(4-fluorophenyl)methanone (117)***

Intermediate **117** was synthetized starting from **116** following the general procedure **H**. FC in hexane/ethyl acetate 3/7, R*f*: 0.42. Yellowish solid (69% yield). $^{1}$H NMR (400 MHz, $CDCl_3$): δ: 3.12 (bs, 2H, N$H_2$); 6.39 (d, 1H, aryl, *J* = 3.7 Hz); 6.70 (dd, 1H, aryl, *J'* = 2.2, *J''* = 8.7 Hz); 6.79 (d, 1H, aryl, *J* = 2.2 Hz); 7.09-7.15 (m, 3H, aryl); 7.65-7.69 (m, 2H, aryl); 8.10 (d, 1H, aryl, *J* = 8.7 Hz). HR-MS m/z calcd for $C_{27}H_{28}FN_3O_2$ $[(M + H)]^+$: 255.0928; found 255.0925.

***1-(((3r,5r,7r)-adamantan-1-yl)methyl)-3-(1-(4-fluorobenzoyl)-1H-indol-5-yl)urea (118)***

Obtained from **117** and 1-adamantanemethylamine following the general procedure **F**. FC in hexane/ethyl acetate 1/1, R*f*: 0.45. Whitish oil (42% yield). $^{1}$H NMR (400 MHz, $CDCl_3$): δ: 1.41 (bs, 6H, C$H_2$); 1.53 (d, 3H, C$H_2$ and C$H_{2a}$, *J* = 11.8 Hz); 1.63 (d, 3H, C$H_2$ and C$H_{2b}$, *J* = 12.1 Hz); 1.89 (bs, 3H, C*H*); 2.89 (s, 2H, C$H_2$); 6.48 (s, 1H, aryl); 7.06-7.19 (m, 4H, aryl); 7.62-7.68 (m, 3H, aryl); 8.19 (d, 1H, aryl, *J* = 8.8 Hz). $^{13}$C NMR (100 MHz, $CDCl_3$) δ 28.2, 33.9, 37.0, 40.2, 52.0, 108.9, 114.1, 115.8, 116.0, 116.9, 119.6, 128.2, 130.5, 131.66, 131.79, 132.9, 134.7, 156.9, 163.6, 166.1, 167.3. HR-MS m/z calcd for $C_{27}H_{28}FN_3O_2$ $[(M + H)]^+$: 596.1637; found 596.1642.

***4-((5-(3-(((3r,5r,7r)-adamantan-1-yl)methyl)ureido)-1H-indol-1-yl)methyl)benzoic acid (119)***

Obtained from **111** following the general procedure **K**. Precipitated from MeOH/$Et_2O$ as a white powder, (62% yield). $^{1}$H NMR (400 MHz, $CD_3OD$): δ: 1.55 (bs, 6H, C$H_2$); 1.70 (d, 3H, C$H_2$ and C$H_{2a}$, *J* = 11.7 Hz); 1.79 (d, 3H, C$H_2$ and C$H_{2b}$, *J* = 11.7 Hz); 1.99 (bs, 3H, C*H*); 2.90 (s, 2H, C$H_2$); 5.45 (s, 2H, C$H_2$); 6.48 (s, 1H, aryl); 7.04 (d, 1H, aryl, *J* = 8.7 Hz); 7.18-7.22 (m, 3H, aryl); 7.29 (d, 1H, aryl, *J* = 3.1 Hz); 7.59 (s, 1H, aryl); 7.94 (d, 2H, aryl, *J* = 8.3 Hz). $^{13}$C NMR (100 MHz, $CD_3OD$) δ 28.4, 33.6, 36.7, 39.9, 49.2, 51.2, 109.5, 112.7, 116.6, 126.3, 129.2, 129.67, 129.78, 131.4, 133.3, 143.6, 158.3, 168.1. HR-MS m/z calcd for $C_{28}H_{31}N_3O_3$ $[(M - H)]^+$: 456.2293; found 456.2292.

***4-(5-(3-(((3r,5r,7r)-adamantan-1-yl)methyl)ureido)-1H-indol-1-yl)butanoic acid (120)***

Obtained from **114** following the general procedure **K**. Precipitated from MeOH/$Et_2O$ as a white powder, (58% yield). $^1$H NMR (400 MHz, $CD_3OD$): δ: 1.43 (bs, 6H, C*H*$_2$); 1.57 (d, 3H, C*H*$_2$ and C*H*$_{2a}$, *J* = 11.6 Hz); 1.65 (d, 3H, C*H*$_2$ and C*H*$_{2b}$, *J* = 12.1 Hz); 1.87 (bs, 3H, C*H*); 1.94-1.99 (m, 2H, C*H*$_2$); 2.13 (t, 2H, C*H*$_2$, *J* = 7.0 Hz); 2.79 (s, 2H, C*H*$_2$); 4.09 (t, 2H, C*H*$_2$, *J* = 6.9 Hz); 6.96 (d, 1H, aryl, *J* = 8.7 Hz); 7.06 (s, 1H, aryl); 7.23 (d, 2H, aryl, *J* = 8.7 Hz); 7.43 (s, 1H, aryl). $^{13}$C NMR (100 MHz, $CD_3OD$) δ 25.3, 28.4, 30.2, 33.6, 36.7, 39.9, 44.8, 51.2, 100.4, 109.2, 112.8, 116.4, 128.3, 128.9, 131.0, 133.2, 158.3, 175.2. HR-MS m/z calcd for $C_{24}H_{31}N_3O_3$ [(M - H)]$^+$: 408.2293; found 408.2298.

***1-(((3r,5r,7r)-adamantan-1-yl)methyl)-3-(1-(3-aminopropyl)-1H-indol-5-yl)urea (121)***

Obtained from **113** following the general procedure **L**. FC in ethyl acetate/methanol 7/3, R*f*: 0.38. Yellowish solid (46% yield). $^1$H NMR (400 MHz, $CD_3OD$): δ: 1.45 (bs, 6H, C*H*$_2$); 1.58 (d, 3H, C*H*$_2$ and C*H*$_{2a}$, *J* = 11.6 Hz); 1.67 (d, 3H, C*H*$_2$ and C*H*$_{2b}$, *J* = 12.1 Hz); 1.88-1.95 (m, 5H, C*H* and C*H*$_2$); 2.57 (t, 2H, C*H*$_2$, *J* = 7.0 Hz); 2.79 (s, 2H, C*H*$_2$); 4.12 (t, 2H, C*H*$_2$, *J* = 6.8 Hz); 6.27 (s, 1H, aryl); 6.99 (d, 1H, aryl, *J* = 8.7 Hz); 7.09 (s, 1H, aryl); 7.23 (d, 1H, aryl, *J* = 8.7 Hz); 7.42 (s, 1H, aryl). $^{13}$C NMR (100 MHz, $CD_3OD$) δ 28.4, 36.8, 38.1, 39.9, 43.3, 51.2, 100.5, 109.1, 112.6, 116.3, 128.3, 129.0, 131.2, 133.1, 158.3. HR-MS m/z calcd for $C_{23}H_{32}N_4O$ [(M + H)]$^+$: 596.1637; found 596.1642.

***1-(((3r,5r,7r)-adamantan-1-yl)methyl)-3-(1-(4-cyanobenzyl)-1H-indol-5-yl)urea (122)***

Intermediate **122** was synthetized starting from 5-aminoindole and 1-adamantanemethylamine following the general procedure **F**. Precipitated from MeOH/$Et_2O$ as a whitish powder, (72% yield). $^1$H NMR (400 MHz, $CDCl_3$): δ: 1.48 (bs, 6H, C*H*$_2$); 1.55 (d, 3H, C*H*$_2$ and C*H*$_{2a}$, *J* = 11.1 Hz); 1.66 (d, 3H, C*H*$_2$ and C*H*$_{2b}$, *J* = 12.0 Hz); 1.94 (bs, 3H, C*H*); 2.89 (d, 2H, C*H*$_2$, *J* = 4.3 Hz); 6.50 (s, 1H, aryl); 7.00 (d, 1H, aryl, *J* = 8.0 Hz); 7.22 (s, 1H, aryl); 7.35 (d, 1H, aryl, *J* = 8.5 Hz); 7.46 (s, 1H, aryl); 8.25 (s, 1H, N*H*). HR-MS m/z calcd for $C_{28}H_{30}N_4O$ $[(M + H)]^+$: 439.2492; found 439.2487.

***1-(((3r,5r,7r)-adamantan-1-yl)methyl)-3-(1-(4-cyanobenzyl)-1H-indol-5-yl)urea (123)***

Intermediate **123** was synthetized starting from **122** and 4-(bromomethyl)benzonitrile following the general procedure **C**. FC in dichloromethane/ethyl acetate 8/2, R*f*: 0.44. Yellow oil (55% yield). $^1$H NMR (400 MHz, $CDCl_3$): δ: 1.45 (bs, 6H, C*H*$_2$); 1.58 (d, 3H, C*H*$_2$ and C*H*$_{2a}$, *J* = 11.4 Hz); 1.70 (d, 3H, C*H*$_2$ and C*H*$_{2b}$, *J* = 12.1 Hz); 1.94 (bs, 3H, C*H*); 2.93 (d, 2H, C*H*$_2$, *J* = 4.5 Hz); 5.36 (s, 2H, C*H*$_2$); 6.55 (s, 1H, aryl); 6.72 (s, 1H, aryl); 7.11-7.15 (m, 4H, aryl); 7.55-7.60 (m, 3H, aryl). HR-MS m/z calcd for $C_{28}H_{30}N_4O$ $[(M + H)]^+$: 439.2492; found 439.2487.

***1-(((3r,5r,7r)-adamantan-1-yl)methyl)-3-(1-(4-(aminomethyl)benzyl)-1H-indol-5-yl)urea (124)***

Obtained from **123** following the general procedure **L**. FC in ethyl acetate/methanol 8/2, R*f*: 0.38. Yellow oil (48% yield). $^{1}$H NMR (400 MHz, $CD_3OD$): δ: 1.56 (bs, 6H, C$H_2$); 1.70 (d, 3H, C$H_2$ and C$H_{2a}$, *J* = 11.7 Hz); 1.78 (d, 3H, C$H_2$ and C$H_{2b}$, *J* = 12.1 Hz); 1.99 (bs, 3H, C*H*); 2.90 (s, 2H, C$H_2$); 3.80 (s, 2H, C$H_2$); 5.35 (s, 2H, C$H_2$); 6.43 (s, 1H, aryl); 7.03 (d, 1H, aryl, *J* = 10.7 Hz); 7.11 (d, 2H, aryl, *J* = 8.0 Hz); 7.21 (d, 1H, aryl, *J* = 8.7 Hz); 7.26-7.29 (m, 3H, aryl); 7.56 (s, 1H, aryl). $^{13}$C NMR (100 MHz, $CD_3OD$) δ 28.4, 29.3, 36.8, 39.9, 44.5, 49.3, 51.2, 100.7, 109.6, 112.6, 116.4, 126.8, 127.6, 128.9, 129.2, 131.2, 133.3, 137.3, 140.0, 158.3. HR-MS m/z calcd for $C_{28}H_{34}N_4O$ $[(M + H)]^+$: 443.2805; found

**Synthesis of 1-(4-fluorophenyl)-5-nitro-1H-indole (125)**

To a solution of 5-nitroindole (0.5 mmol) in dry DMF, under positive nitrogen flow, $Cs_2CO_3$ (1 mmol), CuI (0.07 mmol), and 4-fluoroiodobenzene (0.5 mmol) were added. The mixture was stirred at 120 °C for 12 hours, then water was added, and the mixture was extracted with dichloromethane (2 x 50 mL), dried over $Na_2SO_4$, and concentrated in vacuo. The crude product was purified by flash chromatography using n-hexane/ethyl acetate (8/2, v/v) as eluent. R*f*: 0.44. Yellow powder (35% yield). $^{1}$H NMR (400 MHz, $CD_3OD$): δ: 6.83 (d, 1H, aryl, *J* = 3.3 Hz); 7.23-7.30 (m, 2H, aryl); 7.43-7.59 (m, 3H, aryl); 7.86 (d, 1H, aryl, *J* = 8.6 Hz); 8.01 (dd, 1H, aryl, *J'* = 2.3, *J''* 9.1 Hz); 8.55 (s, 1H, aryl). HR-MS m/z calcd for $C_{14}H_9FN_2O_2$ $[(M + H)]^+$: 257.0721; found 257.0725.

**Synthesis of 1-(4-fluorophenyl)-1H-indol-5-amine (126)**

Intermediate **125** was dissolved in THF and Pd/C (0.01 mmol) was added. The mixture was stirred at 60 °C for 10 minutes. Then $NH_2NH_2$. $H_2O$ (1.5 mmol) was added and the mixture was stirred at 60 °C for further 12 hours. After cooling, ethyl acetate was added and the organic phase was washed with a saturated solution of $NaHCO_3$ (3 × 50 mL), dried over anhydrous $Na_2SO_4$, filtered, concentrated, and purified by column chromatography using n-hexane/ethyl acetate (1/1) as mobile phase. R*f*: 0.45 (65% yield). $^1$H NMR (400 MHz, $CD_3OD$): δ: 6.43 (d, 1H, aryl, *J* = 2.5 Hz); 6.70 (dd, 1H, aryl, *J'* = 2.4, *J''* 8.2 Hz); 6.99 (d, 1H, aryl, *J* = 2.5 Hz); 7.14-7.25 (m, 3H, aryl); 7.29-7.40 (m, 3H, aryl). HR-MS m/z calcd for $C_{14}H_{11}FN_2$ [(M + H)]$^+$: 227.0979; found 227.0984.

***1-(((3r,5r,7r)-adamantan-1-yl)methyl)-3-(1-(4-fluorophenyl)-1H-indol-5-yl)urea (127)***

Obtained from **126** following the general procedure **F**. FC in hexane/ethyl acetate 7/3, R*f*: 0.44. Yellow oil (32% yield). $^1$H NMR (400 MHz, $CD_3OD$): δ: 1.45 (bs, 6H, C$H_2$); 1.59 (d, 3H, C$H_2$ and C$H_{2a}$, *J* = 11.6 Hz); 1.66 (d, 3H, C$H_2$ and C$H_{2b}$, *J* = 12.1 Hz); 1.88 (bs, 3H, C*H*); 2.81-2.82 (m, 2H, C$H_2$); 6.48 (s, 1H, aryl); 7.00 (d, 1H, aryl, *J* = 8.8 Hz); 7.17 (t, 2H, aryl, *J* = 8.7 Hz); 7.26-7.28 (m, 2H, aryl); 7.40-7.43 (m, 2H, aryl); 7.54 (s, 1H, aryl). $^{13}$C NMR (100 MHz, $CD_3OD$) δ 28.4, 33.6, 36.8, 39.9, 51.2, 103.0, 109.8, 112.2, 115.9, 116.7, 125.7, 128.3, 129.7, 132.4, 132.8, 136.1, 158.0, 159.8, 162.2. HR-MS m/z calcd for $C_{26}H_{28}FN_3O$ [(M + H)]$^+$: 596.1637; found 596.1642.

**Synthesis of 9-(4-fluorobenzyl)-9H-carbazole (128)**

Intermediate **128** was synthetized starting from carbazole and 4-fluorobenzyl chloride following **general procedure C**. FC in hexane/ethyl acetate 7/3, R*f*: 0.47. Yellow oil (97% yield). $^1$H NMR (400 MHz, $CDCl_3$): δ: 5.30 (s, 2H, C$H_2$); 6.80 (t, 2H, aryl, *J* = 9.0 Hz); 6.94-6.98 (m, 2H, aryl); 7.15 (t, 2H, aryl, *J* = 8.0 Hz); 7.20 (d, 2H, aryl, *J* = 8.4 Hz); 7.32 (t, 2H, aryl, *J* = 8.8 Hz); 8.02 (d, 2H, aryl, *J* = 8.2 Hz). ESI-MS *m/z* calcd for $C_{19}H_{14}FN_2$ $[(M + H)]^+$: 276.1183; found 276.1177.

***9-(4-fluorobenzyl)-9H-carbazol-3-amine (129)***

Intermediate **129** was obtained following general procedure **H**, starting from **128** that was obtained by carbazole nitration procedure described earlier for the intermediate **79**. FC in hexane/ethyl acetate 2/8, R*f*: 0.40. Yellowish solid (90% yield). $^1$H NMR (400 MHz, $CDCl_3$): δ: 3.48 (bs, 2H, N$H_2$); 5.31 (s, 2H, C$H_2$); 6.78-6.86 (m, 3H, aryl); 6.97-7.00 (m, 2H, aryl); 7.04 (d, 1H, aryl, *J* = 8.5 Hz); 7.10 (t, 1H, aryl, *J* = 7.8 Hz); 7.19 (d, 1H, aryl, *J* = 8.2 Hz); 7.30 (t, 1H, aryl, *J* = 7.1 Hz); 7.37 (s, 1H, aryl); 7.93 (d, 1H, aryl, *J* = 7.8 Hz). ESI-MS *m/z* calcd for $C_{19}H_{15}FN_2$ $[(M + H)]^+$: 291.1292; found 291.1300.

***1-(((3r,5r,7r)-adamantan-1-yl)methyl)-3-(9-(4-fluorobenzyl)-9H-carbazol-3-yl)urea (130)***

Obtained from **129** and 1-adamantanemethylamine following the general procedure **F**. FC in hexane/ethyl acetate 1/1, R*f*: 0.45. Yellowish solid (65% yield). $^1$H NMR (400 MHz, $CD_3OD$): δ: 1.47 (bs, 6H, C$H_2$); 1.60 (d, 3H, C$H_2$ and C$H_{2a}$, *J* = 11.7 Hz); 1.67 (d, 3H, C$H_2$ and C$H_{2b}$, *J* = 12.1 Hz); 1.89 (bs, 3H, C*H*); 2.83 (d, 2H, C$H_2$, *J* = 6.0 Hz); 5.44 (s, 2H, C$H_2$); 5.93 (t, 1H, aryl, *J* = 6.1 Hz); 6.86 (t, 2H, aryl, *J* = 8.8 Hz); 7.01-

7.10 (m, 2H, aryl); 7.18-7.33 (m, 4H, aryl); 7.95 (d, 1H, aryl, $J$ = 7.8 Hz); 8.05 (s, 1H, aryl). $^{13}$C NMR (100 MHz, $CD_3OD$) δ 28.4, 33.7, 36.8, 39.9, 45.1, 48.4, 51.3, 53.4, 108.8, 112.1, 114.8, 115.0, 118.7, 119.8, 122.8, 123.1, 125.6, 128.1, 131.5, 133.7, 141.0, 158.1, 160.9, 163.3. HR-MS m/z calcd for $C_{31}H_{32}FNO$ $[(M + H)]^+$: 596.1637; found 596.1642.

**Computational details**

The ligand geometries were built by through Build Panel of Maestro (version 11) as follows: OPLS3 force field (Harder et al., 2016), the Polak-Ribier conjugate gradient algorithm (PRCG, 9 x $10^7$ steps, maximum derivative less than 0.001 kcal/mol), using a GB/SA (generalized Born/surface area) solvent treatment (Still *et al*., 1990) 52 to mimic the presence of $H_2O$.

The so obtained structures were processed with LigPrep, generating all possible tautomers, stereoisomers, and protonation states at a pH of 7.0 ± 1.0. The structures of 5-LOX (PDB ID: 3O8Y) (Gilbert *et al*., 2011) and SEH (PDB ID: 3I28) (Eldrup *et al*., 2009) for the docking calculations were processed by Protein Preparation Wizard (Madhavi *et al*., 2013) in details: ligand, buffer ions and water molecules were deleted; all hydrogens were added and bond order assigned, missing side chains and loops were checked; residue alternate positions were checked considering the A conformation; the side chain charges were assigned considering their $pK_a$ at physiological pH of 7.4.

For binding investigation towards 5-LOX, the Induced Fit Docking (Farid *et al*., Sherman *et al*., 2006) was applied, using the extended protocol, generating 80 ligand–protein poses at XP precision. The grid was centered on $Fe^{2+}$ with the inner box of 10 Å, and the outer one automatically generated. The conformational search was performed allowing the sample ring conformations of the small molecules, with an

energy window of 2.5 kcal/mol. For Prime refinement, the default values were used. For docking calculations on sEH, Glide software (Friesner *et al*., 2006) employed to dock the ligand against sEH. To validate the docking methodology, the co-crystallized ligand sn34 with SEH was docked and the obtained conformation was compared with the experimental one (RMSD = 0.486 Å) (Di Micco *et al*., 2018; Giordano *et al*., 2018; Giordano *et al*., 2019). An inner and outer receptor grid boxes of 10 Å and 17 Å, respectively, centered on x, y, and z coordinates: 75.42, -9.30, 68.12. In the first step Standard Precision (SP) was applied along with default parameters, producing one pose per ligand. These poses from the SP calculations were utilized as input conformations for two rounds of predictions in the Extra Precision (XP) Glide mode: flexible ligand; only amide bond trans conformation allowed; nitrogen inversion and ring conformations (with an energy cutoff of 2.5 kcal/mol) sampling. The enhanced sampling mode was utilized, saving 10,000 poses/ligand for the initial docking step and 1,000 poses/ligand for energy minimization. 1,000 maximum output structures/ligand were kept applying 0.8 as the scaling factor for van der Waals radii and 0.15 as the partial charge cutoff. Post-docking optimization was executed on docked poses, filtering through 100 maximum number of poses and 0.5 kcal/mol cutoff to reject obtained minimized conformations. The energy contributions of Epik state penalty, aromatic bonds and intramolecular H-bond reward were considered in the predictions. The docking outcome analysis and figure preparation were carried out by Maestro (version 11).

**Cell-free 5-LOX activity assay**

Human recombinant 5-LOX was expressed in *E. coli* Bl21 (DE3) cells that were transformed with pT3–5LO (wt 5-LOX) plasmid and purified on an ATP-agarose

column (Econo-Pac®, Bio-Rad, Hercules, CA) by affinity chromatography (Fischer *et al*., 2003; Pein *et a*l., 2018); Rossi et al., 2002)). In a first step, *E. coli* was lysed in 50 mM triethanolamine/HCl pH 8.0 with EDTA (5 mM), soybean trypsin inhibitor (60 µg/mL), phenylmethylsulphonyl fluoride (1 mM), dithiothreitol (1 mM), and lysozyme (1 mg/mL) and sonified 3 times for 15 s. The homogenate was centrifuged at 40,000 × g for 20 min at 4°C. The supernatant was transferred to an ATP-agarose column (Sigma-Aldrich, Deisenhofen, Germany), which was sequentially washed with PBS pH 7.4, 1 mM EDTA, 50 mM phosphate buffer pH 7.4, 0.5 M NaCl, 1 mM EDTA, and finally 50 mM phosphate buffer pH 7.4 plus 1 mM EDTA. The enzyme was eluted with 50 mM phosphate buffer pH 7.4, 1 mM EDTA, and 20 mM ATP. Purified 5-LOX (0.5 µg in PBS pH 7.4 containing 1 mM EDTA) was pre-incubated with vehicle (DMSO) or test compounds for 15 min on ice. 5-LOX product formation was started by addition of arachidonic acid (Sigma-Aldrich; 20 µM) and $CaCl_2$ (2 mM) and stopped by an equal volume of ice-cold methanol containing $PGB_1$ (200 ng) as internal standard after 10 min at 37°C. Major 5-LOX metabolites (all-*trans* isomers of $LTB_4$ and 5-HETE) were extracted on Sep-Pak C18 35 cc Vac Cartridges (Waters, Milford, MA), separated by RP-HPLC on a Nova-Pak C18 Radial-Pak Column (4 µm, 5×100 mm, Waters) under isocratic conditions (73% methanol/27% water/0.007% trifluoroacetic acid) at a flow rate of 1.2 mL/min and detected at 235 and 280 nm

**5-LOX product formation by human PMNL**

Human PMNL were freshly isolated from leukocyte concentrates that were obtained from the Institute for Transfusion Medicine of the University Hospital Jena (Germany). Thus, venous blood was collected in heparinized tubes (16 U heparin/mL blood), with informed consent of registered male and female healthy adult volunteers

(18-65 years) who were fasted for at least 12 h. These volunteers regularly donated blood (every 8-12 weeks) and were physically inspected by a clinician. They had not taken antibiotics or anti-inflammatory drugs for more than 10 days before blood donation and were free of apparent infections, inflammatory disorders, or acute allergic reactions. Leukocytes were concentrated by centrifugation (4000g/20 min/20 °C) of freshly withdrawn blood and subjected to density gradient centrifugation on a lymphocyte separation medium (LSM 1077, GE Healthcare, Freiburg, Germany). Erythrocytes were removed by dextran sedimentation and hypotonic lysis. PMNL were obtained from the cell pellet. Freshly isolated PMNL ($5 \times 10^6$) suspended in PBS pH 7.4 with 1 mg/mL glucose were preincubated with the test compounds for 15 min on ice. 5-LOX product formation in PMNL was triggered by addition of $Ca^{2+}$-ionophore A23187 (2.5 μM; Sigma-Aldrich) followed by incubation for 10 min at 37 °C. The reaction was stopped with an equal volume of methanol containing $PGB_1$ (200 ng) as internal standard. Major 5-LOX metabolites (all-trans isomers of LTB and 5-HETE) and, for PMNL, additionally $LTB_4$ were extracted and analyzed by RP-HPLC as described for the determination of cell-free 5-LOX activity.

**sEH Activity**

Human recombinant sEH was expressed in Sf9 insect cells and purified by affinity chromatography. Briefly, Sf9 cells were infected with a recombinant baculovirus and lysed after 72 h in 50 mM $NaHPO_4$ pH 8, 300 mM NaCl, 10% glycerol, 1 mM EDTA, 1 mM phenylmethanesulfonylfluoride fluoride, 10 μg/mL leupeptin, and 60 μg/mL STI by sonication (3 × 10 s, 4°C). Sequential centrifugation at 20,000g (10 min, 4 °C) and 100,000g (60 min, 4 °C) yielded a supernatant, which was subjected to benzylthio-sepharose affinity chromatography. Elution with 4-fluorochalcone oxide in PBS pH

7.4 with 1 mM dithiothreitol and 1 mM EDTA yielded sEH, which was dialyzed and concentrated. Purified sEH (60 ng) in 25 mM Tris HCl pH 7 with 0.1 mg/mL bovine serum albumin (BSA) was preincubated with the vehicle (DMSO) or test compounds for 1 min at room temperature. The sEH substrate PHOME (20 µM, Cayman Chemicals) was added to start the enzymatic reaction, which was stopped after 60 min in the darkness by addition of $ZnSO_4$ (200 mM). The formation of the fluorescent product 6-methoxynaphtaldehyde was measured using a NOVOstar fluorescence microplate reader (BMG Labtech, Ortenberg, Germany), with excitation at 330 and emission at 465 nm.

**Cell Culture**

Murine monocyte/macrophage J774 cell line was obtained from the American Type Culture Collection (ATTC TIB 67). The cell line was grown in adhesion in Dulbecco's modified Eagles medium (DMEM) supplemented with glutamine (2 mM, Aurogene Rome, Italy), Hepes (25 mM, Aurogene Rome, Italy), penicillin (100 U/mL, Aurogene Rome, Italy), streptomycin (100 µg/mL, Aurogene Rome, Italy), fetal bovine serum (FBS, 10%, Aurogene Rome, Italy) and sodium pyruvate (1.2%, Aurogene Rome, Italy) (DMEM completed). The cells were plated at a density of $1 \times 10^6$ cells in 75 $cm^2$ culture flasks and maintained at 37°C under 5% $CO_2$ in a humidified incubator until 90% confluence. The culture medium was changed every 2 days. Before a confluent monolayer appeared, sub-culturing cell process was carried out.

**Assessment of COX-1 activity**

Cells ($0.5 \times 10^6$ cells/mL) were pre-treated with **73** (0,1-10 µM) for 2 h and further incubated for 30 min with AA (15 µM). At the end of the incubation the supernatants were collected for the measurement of $PGE_2$ levels with commercially available

ELISA kits according to the manufacturer's instructions (R&D Systems, Aurogene, Rome, Italy).

**Assessment of COX-2 activity**

Cells ($0.5 \times 10^6$ cells/mL) were stimulated, for 24 h, with lipopolysaccharide, LPS from *E. coli*, Serotype 0111:B4, (10 μg/mL; 100 μL in DMEM completed with FBS, Sigma Aldrich, Milan, Italy), to induce COX-2, then pre-treated for 2 h with test compound (0-10 μM), and further incubated for 30 min with AA (15 μM). In another set of experiments, cells were pre-treated for 2 h in the absence or presence of test compound and then stimulated for 24 h with LPS (10 μg/mL). The supernatants were collected for the measurement of $PGE_2$ levels by ELISA assay (R&D Systems, Aurogene, Rome, Italy).

**Cell viability**

Cell respiration, an indicator of cell viability, was assessed by the mitochondrial-dependent reduction of 3-(4,5-dimethylthiazol-2-yl)-2,5-diphenyltetrazolium bromide (MTT; Sigma Aldrich, Milan, Italy) to formazan. Cells were plated to a seeding density of $1.0 \times 10^5$ in 96 multiwell. After stimulation with test compound for 24 h, cells were incubated in 96-well plates with MTT (0.2 mg/mL), for 1 h. Culture medium was removed by aspiration and the cells were lysed in DMSO (0.1 mL). The extent of reduction of MTT to formazan within cells was quantified by the measurement of $OD_{550}$.

**Animals**

Male CD-1 mice (33−39 g, 8 weeks, Charles River Laboratories; Calco, Italy) and female BALB/c mice (20 g, 8 weeks, Charles River Laboratories) were fed with

standard rodent chow and water and acclimated for 4 days at a 12 h light and 12 h dark schedule in a constant air-conditioned environment (21 ± 2°C). Mice were randomly assigned to groups, and experiments were carried out during the light phase. Experimental procedures were conducted in conformity with Italian (D.L. 26/2014) and European (directive 2010/63/EU) regulations on the protection of animals used for scientific purposes and approved by the Italian Ministry.

**Zymosan-Induced Peritonitis**

CD-1 mice were pre-treated i.p. with **73** (10 mg/kg), Zileuton (10 mg/kg) or vehicle (0.5 mL, DMSO 2% in saline) 30 min before zymosan (2 mg/mL in saline, i.p., 0.5 mL, Sigma-Aldrich). Mice were sacrificed by inhalation of $CO_2$ after 30 min or 4 h to analyze peritoneal $LTC_4$ (30 min), $LTB_4$, cell infiltration, $PGE_2$, nitrite/nitrate (NOx) and TNF-α peritoneal exudate levels. Peritoneal exudates were collected and centrifugated, cells were counted in exudates after trypan blue staining. Levels of $LTB_4$, $LTC_4$, $PGE_2$ (Cayman Chemical, BertinPharma, Montigny Le Bretonneux, France) and TNF-α (R&D Systems, Aurogene, Rome, Italy) were quantified in the exudate by ELISA according to the manufacturer's instructions. Measurements of nitrite and nitrate (NOx) was based on the reduction of nitrate to nitrite by cadmium (Fischer *et al*., 2003) and subsequent determination of nitrite by Griess reaction. The reduction of nitrate to nitrite was performed in a microplate: 40 µL of STB (75% $NH_4Cl$ 0,49M and 25% of $Na_2B_4O_7$ 0,06M) and 115 µL of nitrate standard curves or samples were pipetted in each well. Cadmium granules (2-2.5 g) were rinsed three times with deionized distilled water and then they were added to samples. The microplate was then shaken automatically for 90 min. Subsequently, 155 µL of the mixture from each well was centrifugated, then 100 µL of supernatants were

transferred into another microplate. 100 µL of Griess reagent (0.1% naphthylethylenediamide dihydrochloride in $H_2O$ and 1% sulphanilamide in 5% concentrated $H_2PO_4$; vol. 1:1; Sigma Aldrich, Milan, Italy) was added and absorbance was measured within 10 minutes in a spectrophotometer at a wavelength of 540 nm.

**Experimental Model of Murine Asthma**

BALB/c mice were treated with 0.4 mL s.c. of a suspension containing 100 µg of ovalbumin (OVA) absorbed to 3.3 mg of aluminum hydroxide gel on days 0 and 7 (Pein *et al*., 2018; Rossi *et al*., 2002). Compound **73** (10 mg/kg) or vehicle (dimethyl sulfoxide 4%, 0.5 mL) were administered i.p. 30 min (Fig. 5A) before each OVA administration. Animals were killed at days 21 by an overdose of enflurane, and lungs, bronchi and plasma collected. In particular, blood was collected by intracardiac puncture using citrate as an anticoagulant. Then plasma was obtained by centrifugation at 800 × g at 4 °C for 10 minutes and immediately frozen at -80 °C (Tu *et al*., 2010).

Total IgE levels were measured by ELISA kit (BD Biosciences, Pharmingen, San Jose, CA). Bronchi were cut in rings of 1 to 2 mm length, placed in organ baths, and fixed to an isometric force transducer 7006 connected to a Powerlab 800 (AD Instruments, Ugo Basile, Comerio, Italy). After stretching the rings to a resting tension of 0.5g and equilibration for at least 30 min, the rings were challenged with carbachol (1 µM) until a reproducible response was observed. To assess bronchial reactivity, the cumulative response to carbachol (0.001 to 3.16 µM) and salbutamol (0.01 to 30 µM) was measured (Wang *et al*., 2014). Results were expressed as dyne per mg tissue.

The right lung lobes harvested from mice was rapidly fixed in formalin 4%. The tissues were embedded in paraffin and 7 µm cryosections were cut. The slices were processed to remove the paraffin and, following the rehydratation, hematoxylin and

eosin (H&E) staining was performed. Sections were analysed by using Leica Microsystem with a scale bar of 50 µm (H&E). Pulmonary cell-infiltration and epithelial thickness were evaluated by using ImageJ Fiji software (Wang *et al*., 2014).

Left lung were isolated and homogenized in PBS (Sigma Aldrich, Milan, Italy). The homogenate was centrifuged (4 °C, 6000 × g, 10 min) (Wang *et al*., 2014). The levels of $LTC_4$ (Cayman Chemical, BertinPharma, Montigny Le Bretonneux, France), IL13 and IL4 (Invitrogen, Vienna, Austria) were measured by ELISA according to the manufacturer's instructions. The levels of $LTC_4$, IL13 and IL4 were expressed as pg/mL.

**Statistical analysis**

The results are expressed as mean ± S.E.M of the mean of n observations, where n represents the number of animals or number of experiments performed at different days. Statistical evaluation was performed by one–way or two-way ANOVA using GraphPad InStat (Graphpad Software Inc., San Diego, CA) followed by a Bonferroni post-hoc test for multiple comparisons, respectively. Post hoc tests were run only when F achieved $P < 0.05$ and there was no significant variance in the homogeneity. A P value <0.05 was used to define statistically significant differences between mean values.

**References**

Anzini, M.; Di Capua, A.; Valenti, S.; Brogi, S.; Rovini, M.; Giuliani, G.; Cappelli, A.; Vomero, S.; Chiasserini, L.; Sega, A.; Poce, G.; Giorgi, G.; Calderone, V.; Martelli, A.; Testai, L.; Sautebin, L.; Rossi, A.; Pace, S.; Ghelardini, C.; Di Cesare Mannelli, L.; Benetti, V.; Giordani, A.; Anzellotti, P.; Dovizio, M.; Patrignani, P.; Biava, M. Novel Analgesic/Anti-Inflammatory Agents: 1,5-Diarylpyrrole Nitrooxyalkyl Ethers and Related Compounds as Cyclooxygenase-2 Inhibiting Nitric Oxide Donors. *Journal of Medicinal Chemistry*. **2013**, 56: 3191−3206.

Assiri, A.; Al-Tawfiq, J. A.; Al-Rabeeah, A. A.; Al-Rabiah, F. A.; Al-Hajjar, S.; Al- Barrak, A.; Flemban, H.; Al-Nassir, W. N.; Balkhy, H. H.; Al-Hakeem, R. F.; Makhdoom, H. Q.; Zumla, A. I.; Memish, Z. A. Epidemiological, demographic, and clinical characteristics of 47 cases of Middle East respiratory syndrome coronavirus disease from Saudi Arabia: a descriptive study. *The Lancet Infectious Diseases*. **2013**, 13(9): 752-761.

Axfors, C.; Schmitt, A. M.; Janiaud, P.; Van't Hooft, J.; Abd-Elsalam, S.; Abdo, E. F.; Abella, B. S.; Akram, J.; Amaravadi, R. K.; Angus, D. C.; Arabi, Y. M.; Azhar, S.; Baden, L. R.; Baker, A. W.; Belkhir, L.; Benfield, T.; Berrevoets, M. A. H.; Chen, C-P.; Chen, T-C.; Cheng, S-H.; Cheng, C-Y.; Chung, W-S.; Cohen, Y. Z.; Cowan, L. N.; Dalgard, O.; de Almeida, F. F.; de Lacerda, M. V. G.; de Melo, G. C.; Derde, L.; Dubee, V.; Elfakir, A.; Gordon, A. C.; Hernandez-Cardenas, C. M.; Hills, T.; Hoepelman, A. I. M.; Huang, Y. W.; Igau, B.; Jin, R.; Jurado-Camacho, F.; Khan, K. S.; Kremsner, P. G.; Kreuels, B.; Kuo, C.-Y.; Le, T.; Lin, Y.-C.; Lin, W.-P.; Lin, T-H.; Lyngbakken, M. N.; McArthur, C.; McVerry, B. J.; Meza-Meneses, P.; Monteiro,

W. M.; Morpeth, S. C.; Mourad, A.; Mulligan, M. J.; Murthy, S.; Naggie, S.; Narayanasamy, S.; Nichol, A.; Novack, L. A.; O'Brien, S. M.; Okeke, N. L.; Perez, L.; Perez-Padilla, R.; Perrin, L.; Remigio-Luna, A.; Rivera-Martinez, . E.; Rockhold, F. W.; Rodriguez-Llamazares, S.; Rolfe, R.; Rosa, R.; Røsjø, H.; Sampaio, V. S.; Seto, T. B.; Shahzad, M.; Soliman, S.; Stout, J. E.; Thirion-Romero, I.; Troxel, A. B.; Tseng, T.-Y.; Turner, N. A.; Ulrich, R. J.; Walsh, S. R.; Webb, S. A.; Weehuizen, J. M.; Velinova, M.; Wong, H. L.; Wrenn, R.; Zampieri, F. G.; Zhong, W.; Moher, D.; Goodman, S. N.; Ioannidis J. P. A.; Hemkens, L. G.; Mortality outcomes with hydroxychloroquine and chloroquine in COVID-19 from an international collaborative meta-analysis of randomized trials. *Nature Communications*. **2021**, 12: 2349.

Basavarajappa, D.; Wan, M.; Lukic, A.; Rådmark, O. Roles of coactosin-like protein (CLP) and 5-lipoxygenase-activating protein (FLAP) in cellular leukotriene biosynthesis. *PNAS*. **2014**, 111(31): 11371–11376.

Bazinet, R. P.; Layé, S. Polyunsaturated fatty acids and their metabolites in brain function and disease. *Nature Reviews Neuroscience*. **2014**, 15: 771–785.

Beetham, J. K.; Tian, T. G.; Hammock, B. D. cDNA Cloning and Expression of a Soluble Epoxide Hydrolase from Human Liver. *Archives of Biochemistry and Biophysics*. **1993**, 305: 197–201.

Beigel, J. H.; Tomashek, K. M.; Dodd, L. E.; Mehta, A. K.; Zingman, B.S.; Kalil, A.C.; Hohmann. E.; Chu, H. Y.; Luetkemeyer, A.; Kline, S.; Lopez de Castilla, D.; Finberg, R.W.; Dierberg, K.; Tapson, V.; Hsieh, L.; Patterson, T.F.; Paredes, R.; Sweeney, D.A.; Short, W.R.; Touloumi, G.; Lye, D. C.; Ohmagari, N.; Oh, M.D.; Ruiz-Palacios, G. M.; Benfield, T.; Fätkenheuer, G.; Kortepeter, M. G.; Atmar, R. L.;

Creech, C. B.; Lundgren, J.; Babiker, A. G.; Pett, S.; Neaton, J. D.; Burgess, T. H.; Bonnett, T.; Green, M.; Makowski, M.; Osinusi, A.; Nayak, S.; Lane, H. C.; ACTT-1 Study Group Members. Remdesivir for the Treatment of Covid-19 - Final Report. *The New England Journal of Medicine*. **2020**, 383 (19): 1813-1826.

Belkner, J.; Wiesner, R.; Kuhn, H.; Lankin, V.Z. The oxygenation of cholesterol esters by the reticulocyte lipoxygenase, *FEBS Letters*. **1991**, 279: 110–114.

Bertamino, A.; Iraci, N.; Ostacolo, C.; Ambrosino, P.; Musella, S.; Di Sarno, V.; Ciaglia, T.; Pepe, G.; Sala, M.; Soldovieri, M. V.; Mosca, I.; Gonzalez-Rodriguez, S.; Fernandez-Carvajal, A.; Ferrer-Montiel, A.; Novellino, E.; Taglialatela, M.; Campiglia, P.; Gomez-Monterrey, I. Identification of a Potent Tryptophan-Based TRPM8 Antagonist With in Vivo Analgesic Activity. *Journal of Medicinal Chemistry*. **2018**, 61: 6140−6152.

Bertamino, A.; Soprano, M.; Musella, S.; Rusciano, M. R.; Sala, M.; Vernieri, E.; Di Sarno, V.; Limatola, A.; Carotenuto, A.; Cosconati, S.; Grieco, P.; Novellino, E.; Illario, M.; Campiglia, P.; Gomez-Monterrey, I. Synthesis, in Vitro, and in Cell Studies of a New Series of [Indoline-3,2′ -thiazolidine]-Based p53 Modulators. *Journal of Medicinal Chemistry.* **2013**, 56: 5407−5421.

Bettaieb, A.; Chahed, S.; Bachaalany, S.; Griffey, S.; Hammock, B. D.; Haj, F. G. Soluble Epoxide Hydrolase Pharmacological Inhibition Ameliorates Experimental Acute Pancreatitis in Mice. *Molecular Pharmacology.* **2015**, 88(2): 281–290.

Biancolella, M.; Colona, V. L.; Mehrian-Shai, R.; Lee Watt, J.; Luzzatto, L.; Novelli G.; Reichardt, J. K. V. COVID-19 2022 update: transition of the pandemic to the endemic phase. *Human Genomics*. **2022**, 16, 19.

Biava, M.; Porretta, G. C.; Poce, G.; Battilocchio, C.; Alfonso, S.; Rovini, M.; Valenti, S.; Giorgi, G.; Calderone, V.; Martelli, A.; Testai, L.; Sautebin, L.; Rossi, A.; Papa, G.; Ghelardini, C.; Di Cesare Mannelli, L.; Giordani, A.; Anzellotti, P.; Bruno, A.; Patrignani, P.; Anzini, M. Novel Analgesic/Anti-Inflammatory Agents: Diarylpyrrole Acetic Esters Endowed with Nitric Oxide Releasing Properties. *Journal of Medicinal Chemistry*. **2011**, 54: 7759−7771.

Boeglin, W. E.; Kim, R. B.; Brash, A. R.. A 12R-lipoxygenase in human skin: mechanistic evidence, molecular cloning, and expression. *Proceedings of the National Academy of Sciences of the United States of America*. **1998**, 95: 6744–6749.

Brash, A. R.; Boeglin, W. E.; Chang, M. S. Discovery of a second 15S-lipoxygenase in humans. *Proceedings of the National Academy of Sciences of the United States of America*. **1997**, 6148–6152.

Buckley, C. D.; Gilroy, D.W.; Serhan, C. N. Proresolving lipid mediators and mechanisms in the resolution of acute inflammation. *Immunity.* **2014**, 40(3): 315-327.

Burrage, D. R.; Koushesh, S.; Sofat, N. mmunomodulatory Drugs in the Management of SARS-CoV-2. *Frontiers in immunology*. **2020**, 11: 1844.

Bystrom, J; Wray, J.A.; Sugden, M.C.; Holness, M.J.; Swales, K.E.; Warner, T.D.; Edin, M.L.; Zeldin, D.C.; Gilroy, D.W.; Bishop-Bailey, D. Endogenous Epoxygenases Are Modulators of Monocyte/Macrophage Activity. *PLoS ONE*. **2011**, 6: e26591.

Celotti, F. and Laufer, S. Anti-inflammatory drugs: new multitarget compounds to face an old problem. The dual inhibition concept. *Pharmacological Research*. **2001**, 43(5): 429-36.

Chan, J. F. W.; Kok, K. H.; Zhu, Z.; Chu, H.; To, K. K.; Yuan, S.; Yuen, K. Y. Genomic characterization of the 2019 novel human-pathogenic coronavirus isolated from a patient with atypical pneumonia after visiting Wuhan. *Emerging Microbes & Infections*. **2020**, 9 (1): 221-236.

Chavda, V. P.; Prajapati, R.; Lathigara, D.; Nagar, B.; Kukadiya, J.; Redwan, E M.; Uversky, V. N.; Kher, M. N.; Patel, R. Therapeutic monoclonal antibodies for COVID-19 management: an update. *Expert Opinion on Biological Therapy*. **2022**, 22 (6): 763-780.

Chen, L.; Deng, H.; Cui, H.; Fang, J.; Zuo, Z.; Deng, J.; Li, Y.; Wang, X.; Zhao, L. Inflammatory responses and inflammation-associated diseases in organs. *Oncotarget*. **2018**, 9 (6): 7204-7218.

Cheng, C. V.; Lau, S. K.; Woo, P. C.; Yuen, K. Y. Severe acute respiratory syndrome coronavirus as an agent of emerging and reemerging infection. *Clinical Microbiology Reviews*. **2007**, 20 (4): 660-694.

Choi, J.; Azmat, C. E. Leukotriene Receptor Antagonist. *StatPearls*. **2022**.

Citarella, A.; Scala, A.; Piperno, A.; Micale, N. SARS-CoV-2 $M^{pro}$: A Potential Target for Peptidomimetics and Small-Molecule Inhibitors. *Biomolecules*. **2021**, 11 (4): 607.

Conrad, D. J.; Kuhn, H.; Mulkins, M.; Highland, E.; Sigal, E. Specific inflammatory cytokines regulate the expression of human monocyte 15-lipoxygenase. *Proceedings of the National Academy of Sciences of the United States of America*. **1992**, 89: 217–221.

Da Silva, J. C.; Barbosa Fèlix, V.; Barbosa Fèlix Leao, S. A.; Trindade-Filho, E. M.; Scorza, F. A. New Brazilian variant of the SARS-CoV-2 (P1/Gamma) of COVID-19 in Alagoas state. *The Brazilian Journal of infectious diseases*. **2021**, 25 (3): 101588.

Dai, W.; Zhang, B.; Jiang, X.M.; Su, H.; Li, J.; Zhao, Y.; Xie, X.; Jin, Z.; Peng, J.; Liu, F.; Li, C.; Li, Y.; Bai, F.; Wang, H.; Cheng, X.; Cen, X.; Hu, S.; Yang, X.; Wang, J.; Liu, X.; Xiao, G.; Jiang, H.; Rao, Z.; Zhang, L.K.; Xu, Y.; Yang, H.; Liu, H. Structure-based design of antiviral drug candidates targeting the SARS-CoV-2 main protease. *Science*. **2020**, 368 (6497): 1331-1335.

Deng, Y.; Edin, M. L.; Theken, K. N.; Schuck, R. N.; Flake, G. P.; Kannon, M. A.; DeGraff, L. M.; Lih, F. B.; Foley, J.; Bradbury, A.; Graves, J. P.; Tomer, K. B.; Falck, J. R.; Zeldin, D. C.; Lee, C. R. Endothelial CYP epoxygenase overexpression and soluble epoxide hydrolase disruption attenuate acute vascular inflammatory responses in mice. *Faseb Journal*. **2011,** 25(2): 703-13.

Di Micco, S.; Terracciano, S.; Cantone, V.; Fischer, K.; Koeberle, A.; Foglia, A.; Riccio, R.; Werz, O.; Bruno, I.; Bifulco, G. Discovery of new potent molecular entities able to inhibit mPGES-1. *European Journal of Medicinal Chemistry*. **2018**, 143: 1419−1427.

Dixon, R. A. F.; Diehl, R. E.; Opas, E.; Rands, E.; Vickers, P. J.; Evans, J. F.; Gillard, J. W.; Miller, D. K.; Requirement of a 5-lipoxygenase-activating protein for leukotriene synthesis. *Nature*. **1990**, 343: 282–284.

Domingues, M. F.; Callai-Silva, N.; Piovesan , A. R.; Carlini, C. R. Soluble Epoxide Hydrolase and Brain Cholesterol Metabolism. *Frontiers in Molecular Neuroscience*. **2020**, 12: 325.

Du Toit, A. Outbreak of a novel coronavirus. *Nature Review Microbiology.* **2020**, 18 (3): 123.

Duroudier, N. P.; Tulah, A. S.; Sayers, I. Leukotriene pathway genetics and pharmacogenetics in allergy. *The Authors Journal compilation*. **2009**, 64: 823-839

Eldrup, A. B.; Soleymanzadeh, F.; Taylor, S. J.; Muegge, I.; Farrow, N. A.; Joseph, D.; McKellop, K.; Man, C. C.; Kukulka, A.; De Lombaert, S. Structure-Based Optimization of Arylamides as Inhibitors of Soluble Epoxide Hydrolase. *Journal of Medicinal Chemistry*. **2009**, 52: 5880−5895.

Eldrup, A. B.; Soleymanzadeh, F.; Taylor, S. J.; Muegge, I.; Farrow, N. A.; Joseph, D.; McKellop, K.; Man, C. C.; Kukulka, A.; De Lombaert, S. Structure-Based Optimization of Arylamides as Inhibitors of Soluble Epoxide Hydrolase. *Journal of Medicinal Chemistry*. **2009**, 52: 5880−5895.

Enayetallah, A. E.; French, R. A.; Thibodeau, M. S.; Grant, D. F. Distribution of soluble epoxide hydrolase and of cytochrome P450 2C8, 2C9, and 2J2 in human tissues. *Journal of Histochemistry & Cytochemistry*. **2004**; 52: 447–454.

Farid, R.; Day, T.; Friesner, R. A.; Pearlstein, R. A. New insights about HERG blockade obtained from protein modeling, potential energy mapping, and docking studies. *Bioorganic & Medicinal Chemistry*. **2006**, 14: 3160−3173.

Fischer, L.; Szellas, D.; Radmark, O.; Steinhilber, D.; Werz, O. Phosphorylation- and stimulus-dependent inhibition of cellular 5-lipoxygenase activity by nonredox-type inhibitors. *FASEB Journal*. **2003**, 17: 1−24.

Friesner, R. A.; Banks, J. L.; Murphy, R. B.; Halgren, T. A.; Klicic, J. J.; Mainz, D. T.; Repasky, M. P.; Knoll, E. H.; Shaw, D. E.; Shelley, M.; Perry, J. K.; Francis, P.;

Shenkin, P. S. Glide: A New Approach for Rapid, Accurate Docking and Scoring. 1. Method and Assessment of Docking Accuracy. *Journal of Medicinal Chemistry*. **2004**, 47: 1739–1749.

Friesner, R. A.; Murphy, R. B.; Repasky, M. P.; Frye, L. L.; Greenwood, J. R.; Halgren, T. A.; Sanschagrin, P. C.; Mainz, D. T. Extra Precision Glide: Docking and Scoring Incorporating a Model of Hydrophobic Enclosure for Protein−Ligand Complexes. *Journal of Medicinal Chemistry*. **2006**, 49: 6177−6196.

Funk, C. D. and Fitzgerald, G. A. COX-2 inhibitors and cardiovascular risk. *Journal of Cardiovascucar Pharmacology*. **2007**, 50(5): 470–479.

Funk, C. D.; Chen, X. S.; Johnson, E. N.; Zhao, L. Lipoxygenase genes and their targeted disruption, *Prostaglandins & Other Lipid Mediators*. **2002**, 68–69: 303–312.

Funk, C. D.; Furci, L; FitzGerald, G. A. Molecular cloning, primary structure, and expression of the human platelet/erythroleukemia cell 12-lipoxygenase. *Proceedings of the National Academy of Sciences of the United States of America*. **1990**, 87: 5638–5642.

Funk, C. D.; Hoshiko, S.; Matsumoto, T.; Rådmark, O.; Samuelsson. B.; Characterization of the human 5-lipoxygenase gene. *Proceedings of the National Academy of Sciences of the United States of America*. **1989**, 86: 2587–2591.

Gilbert, K. G.; Maule, H. G.; Rudolph, B.; Lewis, M.; Vandenburg, H.; Sales, E.; Tozzi, S.; Cooke, D. T. Quantitative analysis of indigo and indigo precursors in leaves of Isatis and Polygonum tinctorium. *Biotechnology Progress*. **2004**, 20 (4): 1289-1292.

Gilbert, N. C.; Bartlett, S. G.; Waight, M. T.; Neau, D. B.; Boeglin, W. E.; Brash, A. R.; Newcomer, M. E. The Structure of Human 5-Lipoxygenase. *Science*, **2011**, 331: 217−219.

Giles, B.; Meredith, P.; Robson, S.; Smith, G.; Chauhan, A. The SARS-CoV-2 B.1.1.7 variant and increased clinical severity—the jury is out. *The Lancet, Infectious Diseases*. **2021**, 21 (9): 1213-1214.

Giordano, A.; Del Gaudio, F.; Johansson, C.; Riccio, R.; Oppermann, U.; Di Micco, S. Virtual Fragment Screening Identification of a Quinoline-5,8-dicarboxylic Acid Derivative as a Selective JMJD3 Inhibitor. *ChemMedChem*. **2018**, 13: 1160−1164.

Giordano, A.; Forte, G.; Terracciano, S.; Russo, A.; Sala, M.; Scala, M. C.; Johansson, C.; Oppermann, U.; Riccio, R.; Bruno, I.; Di Micco, S. Identification of the 2-Benzoxazol-2-yl-phenol Scaffold as New Hit for JMJD3 Inhibition. *ACS Medicinal Chemistry Letters*. **2019**, 10: 601−605.

Golden, M. P. Cell Biology of the 5-Lipoxygenase Pathway. *American Journal of Respiratory and Critical Care Medicine.* **1998**, 157: S227–S232.

Gomez, G. A.; Morisseau, C.; Hammock, B. D.; Christianson, D. W. Human soluble epoxide hydrolase: structural basis of inhibition by 4-(3-cyclohexylureido)-carboxylic acids. *Protein Science*. **2006**, 15: 58−64.

Gorbalenya, A. E.; Baker, S. C.; Baric, R. S.; de Groot, R. J.; Drosten, C.; Gulyaeva A. A.; Haagmans, B. L.; Lauber, C.; Leontovich, A. M.; Neuman, B. W.; Penzar, D.; Perlman, S.; Poon, L. L. M.; Samborskiy, D.; Sidorov, I. A.; Sola, I.; Ziebuhr, J. The species Severe acute respiratory syndrome-related coronavirus: classifying 2019-nCoV and naming it SARS- CoV-2. *Nature Microbiology.* **2020**, 5 (4): 536-544.

Gounari, F.; Chang, R.; Cowan, J.; Guo, Z.; Dose, M.; Gounaris, E.; Khazaie, K. Loss of adenomatous polyposis coli gene function disrupts thymic development. *Nature Immunology*. **2005**, 6: 800-809.

Haeggstrom, J. Z.; Funk, C. D. Lipoxygenase and leukotriene pathways: biochemistry, biology, and roles in disease. *Chemical Reviews*. **2011**, 111: 5866–5898.

Hammaberg, T.; Provost, P.; Persson, B. ; radmark, O. The N-terminal domain of 5-lipoxygenase binds calcium and mediates calcium stimulation of enzyme activity. *Journal of Biological Chemistry*. **2000**, 275(49): 38787-93.

Hammarberg, T.; Kuprin, s.; Rådmark, O.; Holmgren, A. EPR investigation of the active site of recombinant human 5-lipoxygenase: inhibition by selenide. *Biochemistry*. **2001**, 40: 6371–6378.

Hammond, J. Targeting endosomal acidification by chloroquine analogs as a promising strategy for the treatment of emerging viral diseases. *Pharmacology Research e Perspectives*. **2017**, 5 (1): e00293.

Harder, E.; Damm, W.; Maple, J.; Wu, C.; Reboul, M.; Xiang, J. Y.; Wang, L.; Lupyan, D.; Dahlgren, M. K.; Knight, J. L.; Kaus, J. W.; Cerutti, D. S.; Krilov, G.; Jorgensen, W. L.; Abel, R.; Friesner, R. A. OPLS3: A Force Field Providing Broad Coverage of Drug-like Small Molecules and Proteins. *Journal of Chemical Theory and Computation.* **2016**, 12: 281−296.

Harris, T. R.; Hammock, B. D. Soluble epoxide hydrolase: Gene structure, expression and deletion. *Gene*. **2013**, 526(2): 61–74.

He, J.; Wang, C.; Zhu, Y.; Ai, D. Soluble epoxide hydrolase: A potential target for metabolic diseases. *Journal of Diabetes.* **2016**, 8(3): 305–313.

Hegg, E. L.; Que, L. Jr. The 2-His-1-carboxylate facial triad–an emerging structural motif in mononuclear non-heme iron(II) enzymes. *European Journal of Biochemistry*. **1997**, 250: 625–629.

Heise, . E.; O'Dowd, B. F.; Figueroa, D. J.; Sawyer, N.; Nguyen, T.; Im, D. S.; Stocco, R.; Bellefeuille, J. N.; Abramovitz, M.; Cheng, R.; Williams Jr, D. L.; Zeng, Z.; Liu, Q.; Ma, L.; Clements, M. K.; Coulombe, N.; Liu, Y.; Austin, C. P.; George, S. R.; O'Neill, G. P.; Metters, K. M.; Lynch, K. R.; Evans J. F. Characterization of the human cysteinyl leukotriene 2 receptor. *Journal of Biological Chemistry*. **2000**, 275(39): 30531-6.

Hiesinger, K.; Wagner, K. M.; Hammocl, B. D.; Proschak, E.; Hwang, S. E. Development of Multitarget Agents Possessing Soluble Epoxide Hydrolase Inhibitory Activity. *HSS Public Access*. **2020**, 140: 31-39.

Hoffmann, M.; Kleine-Weber, H.; Schroeder, S.; Kruger, N.; Herrler, T.; Erichsen, S.; Schiergens, T. S.; Herrler, G.; Wu, N. H.; Nitsche, A.; Muller, M. A.; Drosten, C.; Pohlmann, S. SARS-CoV-2 cell entry depends on ACE2 and TMPRSS2 and is blocked by a clinically proven protease inhibitor. *Cell.* **2020**, 181 (2): 271-280.

Horby, P.; Lim, W. S.; Emberson, J.; Mafham, M.; Bell, J. L.; Linsell, L.; Staplin, N.; Brightling, C.; Ustianowski, A.; Elmahi, E.; Prudon, B.; Green, C.; Felton, T.; Chadwick, D.; Rege, K.; Fegan, C.; Chappell, L. C.; Faust, S. N.; Jaki, T.; Jeffery, K.; Montgomery, A.; Rowan, K.; Juszczak, E.; Baillie, J. K.; Haynes, R.; Landray, M. J. Effect of Dexamethasone in Hospitalized Patients with COVID-19. *The New England Journal of Medicine*. **2021**, 384: 693-704.

Hou, Y., J.; Chiba, S.; Halfmann, P.; Here, C.; Kuroda, M.; Dinnon, K. H.; Leist, S. R.; Schafer, A.; Nakajima, N.; Takahashi, K.; Lee, R. E.; Mascenik, T. M.; Graham, R.; Edwards, C. E.; Tse, L. V.; Okuda, K.; Markmann, A. J.; Bartelt, L.; De Silva, A.; Margolis, D. M.; Boucher, R. C.; Randell, S. H.; Suzuki, T.; Gralinski, L. E.; Kawaoka, Y.; Baric, R. S. SARS-CoV-2 D614G variant exhibits efficient replication ex vivo and transmission in vivo. *Science*. **2020**, 370 (6523): 1464-1468.

Huang, C.; Wang, Y.; Li, X.; Ren, L.; Zhao, J.; Hu, Y. Zhang, L.; Fan, G.; Xu, J.; Gu, X.; Cheng, Z.; Yu, T.; Xia, J.; Wei, Y.; Wu, W.; Xie. X.; Yin, W.; Li, H.; Liu, M.; Xiao, Y.; Gao, H.; Guo, L.; Xie, J.; Wang, G.; Jiang, R.; Gao, Z.; Jin, Q.; Wang, J.; Cao, B. Clinical features of patients infected with 2019 novel coronavirus in Wuhan, China. *The Lancet.* **2020**, 395 (10223): 497-506.

Iliff, J. J.; Wang, R.; Zeldin, D. C.; Alkayed, N. J. Epoxyeicosanoids as mediators of neurogenic vasodilation in cerebral vessels. *American Journal of Physiology-Heart and Circulatory Physiology*. **2009**, 296: H1352–1363.

Irvin, C. G.; Tu, Y. P. ; Sheller, J. R. ; Funk, C. D. 5-Lipoxygenase products are necessary for ovalbumin-induced airway responsiveness in mice. *American Journal of Physiology-Lung Cellular and Molecular Physiology*. **1997**, 272(6): L1053.

Ivanov, I.; Heydeck, D.; Hofheinz, K.; Roffeis, J.; O'Donnell, V. B.; Kuhn, H.; Walther, M. Molecular enzymology of lipoxygenases. *Archives of Biochemistry and Biophysics*. **2010**, 503: 161-174.

Jankiewicz, W. K.; Barnett, S. D.; Stavniichuk, A.; Hwang, S. H.; Hammock, B. D.; Belayet, J. B.; Khan, A. H.; Imig, J. D. Dual sEH/COX-2 Inhibition Using PTUPB-

A Promising Approach to Antiangiogenesis-Induced Nephrotoxicity. *Frontiers in Pharmacology*. **2021**, 12: 744776.

Jin, Z.; Du, X.; Xu, Y.; Deng, Y.; Liu, M.; Zhao, Y.; Zhang, B.; Li, X.; Zhang, L.; Peng, C.; Duan, Y.; Yu, J.; Wang, L.; Yang, K.; Liu, F.; Jiang, R.; Yang, X.; You, T.; Liu, X.; Yang, X.; Bai, F.; Liu, H.; Liu, X.; Guddat, L.W.; Xu, W.; Xiao, G.; Qin, C.; Shi, Z.; Jiang, H.; Rao, Z.; Yang, H. Structure of Mpro from SARS-CoV-2 and discovery of its inhibitors. *Nature*. **2020**, 582 (7811): 289-293.

Jisaka, M.; Kim, R. B.; Boeglin, W. E.; Nanney, L. B.; Brash, A. R. Molecular cloning and functional expression of a phorbol ester-inducible 8S-lipoxygenase from mouse skin. *Journal of Biological Chemistry*. **1997**, 272: 24410–24416.

Joshi, E. M.; Heasley, B. H.; Chordia, M. D.; McDonald, T. L. In Vitro Metabolism of 2-Acetylbenzothiophene: Relevance to Zileuton Hepatotoxicity. *Chemical Research in Toxicology*. **2004**, 17: 137-143.

Joshi, Y. B.; Pratico, D. The 5-lipoxygenase pathway: oxidative and inflammatory contributions to the Alzheimer's disease phenotype. *Frontiers in Cellular Neuroscience*. **2014**, 8: 436.

Jump, D. B. The biochemistry of n-3 polyunsaturated fatty acids. *Journal of Biological Chemistry*. **2002**, 277: 8755–8758.

Kim, H.; Hwang, Y. S.; Kim, M.; Park, S. B. Recent advances in the development of covalent inhibitors. *RSC Medicinal Chemistry*. **2021**, 12: 1037-1045.

Kinzig, A.; Heidt, M; Furstenberger, G.; Marks, F.; Krieg, P. cDNA cloning, genomic structure, and chromosomal localization of a novel murine epidermis-type lipoxygenase. *Genomics*. **1999**, 58: 158–164.

Kitamura, N.; Dominic Sacco, M.; Ma, C.; Hu, Y.; Townsend, J. A.; Meng, X.; Zhang, F.; Zhang, X.; Ba, M.; Szeto, T.; Kukuljac, A.; Marty, M. T.; Schultz, D.; Cherry, S.; Xiang, Y.; Chen, Y.; Wang, J. Expedited Approach toward the Rational Design of Noncovalent SARS-CoV-2 Main Protease Inhibitors. *Journal of Medicinal Chemistry*. **2022**, 65(4): 2848-2865.

Krieg, P.; Furstenberger, G. The role of lipoxygenases in epidermis. *Biochimica et Biophysica Acta*. **2014**, 1841: 390–400.

Kroetz, D. L.; Zeldin, D. C. Cytochrome P450 pathways of arachidonic acid metabolism. *Current Opinion in Lipidology*. **2022**, 13(3): 273-83.

Lacourciere, G. M.; Armstrong, R. N. The catalytic mechanism of microsomal epoxide hydrolase involves an ester intermediate. *Journal of the American Chemical Society*. **1993**, 115: 10466–67.

Lee, J. S., Bukhari, S. N. A., Fauzi, N. M. Effects of chalcone derivatives on players of the immune system. *Drug Design, Development and Therapy*. **2015**, 9: 4761-4778.

Lee, N.; Hui, D.; Wu, A.; Chan, P.; Cameron, P.; Joynt, G. M.; Ahuja, A.; Yung, M. Y.; Leung, C. B.; To, K. F.; Lui, S. F.; Szeto, C. C.; Chung, S.; Sung, J. J. A major outbreak of severe acute respiratory syndrome in Hong Kong. *New England Journal of Medicine*. **2003**, 348 (20): 1986-1994.

Leister-Tebbe, H.; Gardner, A.; Abreu, P.; Bao, W.; Wisemandle, W.; Baniecki, M.; Hendrick, V. M.; Damle, B.; Simón-Campos, A.; Pypstra, R.; Rusnak, J. M. Oral Nirmatrelvir for High-Risk, Nonhospitalized Adults with Covid-19. *The New England Journal of Medicine*. **2022**, 386: 1397-1408.

Letko, M.; Marzi, A.; Munster, V. Functional assessment of cell entry and receptor usage for SARS-CoV-2 and other lineage B betacoronaviruses. *Nature Microbiology*. **2020**, 5 (4): 562-569.

Li, Q.; Guan, X.; Wu, P.; Wang, X.; Zhou, L.; Tong, Y.; Ren, R.; Leung, K.S.M.; Lau, E.H.Y.; Wong, J.Y.; Xing, X.; Xiang, N.; Wu, Y.; Li, C.; Chen, Q.; Li, D.; Liu, T.; Zhao, J.; Liu, M.; Tu, W.; Chen, C.; Jin, L.; Yang, R.; Wang, Q.; Zhou, S.; Wang, R.; Liu, H.; Luo, Y.; Liu, Y.; Shao, G.; Li, H.; Tao, Z.; Yang, Y.; Deng, Z.; Liu, B.; Ma, Z.; Zhang, Y.; Shi, G.; Lam, T.T.Y.; Wu, J.T.; Gao, G.F.; Cowling, B.J.; Yang, B.; Leung, G.M.; Feng, Z. Early transmission dynamics in Wuhan, China, of novel coronavirus-infected pneumonia. *New England Journal of Medicine.* **2020**, 382 (13): 1199-1207.

Li, W.; Moore, M. J.; Vasilieva, N.; Sui, J.; Wong, S. K.; Berne, M. A.; Somasundaran, M.; Sullivan, J. L.; Luzuriaga, K.; Greenough, T. C.; Choe, H.; Farzan, M. Angiotensin-converting enzyme 2 is a functional receptor for the SARS coronavirus. *Nature*. **2003**, 426 (6965): 450-454.

Liao, T. T.; Wang, L.; Jia, R. W.; Fu, X. H.; Chua, H. Lipophilic organic pollutants induce changes in phospholipid and membrane protein composition leading to Vero cell morphological change. *Journal of Environmental Science and Health, Part B.* **2014**, 49(10): 760-768.

Lipiński, P.F.J.; Zaborniak, J.; Garnuszek, P.; Szurmak, P. Virtual screening for small molecular non-covalent binders of the SARS-CoV-2 main protease. *Archives of Medical Science*. **2021**, 17(3): 838-842.

Liu, H.; Ye, F.; Sun, Q.; Liang, H.; Li, C.; Li, S.; Lu, R.; Huang, B.; Tan, W.; Lai, L. Scutellaria baicalensis extract and baicalein inhibit replication of SARS-CoV-2 and its 3C-like protease in vitro. *Journal of Enzyme Inhibition and Medicinal Chemistry*. **2021**, 36(1): 497-503.

Liu, J. Y.; Yang, J.; Inceoglu, B.; Qiu, H.; Ulu, A.; Hwang, S. H.; Chiamvimonvat, N.; Hammock, B.D. Inhibition of soluble epoxide hydrolase enhances the anti-inflammatory effects of aspirin and 5-lipoxygenase activation protein inhibitor in a murine model. *Biochemical Pharmacology*. **2010**, 79(6): 880–887.

Liu, J.Y.; Yang, J.; Inceoglu, B.; Qiu, H.; Ulu, A.; Hwang, S.H.; Chiamvimonvat, N.; Hammock, B.D. Inhibition of soluble epoxide hydrolase enhances the anti-inflammatory effects of aspirin and 5-lipoxygenase activation protein inhibitor in a murine model. *Biochemical Pharmacology*. **2010**, 79: 880–887.

Liu, Y.; Zhang, Y.; Schmelzer, K.; Lee, T.S.; Fang, X.; Zhu, Y.; Spector, A. A.; Gill, S., Morisseau, C.; Hammock, B. D.; Shyy, J. Y. The antiinflammatory effect of laminar flow: the role of PPARgamma, epoxyeicosatrienoic acids, and soluble epoxide hydrolase. *Proceedings of the National Academy of Sciences of the United States of America*. **2005**, 102: 16747–16752.

Locatelli, C.; Rosso, R.; Santos-Silva, M. C.; de Souz, C. A.; Licínio, M. A.; Leal, P.; Bazzo, M. L.; Yunes, R. A.; Creczynski–Pasa, T. B.; Ester derivatives of gallic acid with potential toxicity toward L1210 leukemia cells. *Bioorganic & Medicinal Chemistry*. **2008**, 16(7): 3791-3799.

Lu, H.; Stratton, C. W.; Tang, Y. W. Outbreak of pneumonia of unknown etiology in Wuhan, China: the mystery and the miracle. *Journal of Medical Virology*. **2020**, 92 (4): 401-402.

Lynch, K. R.; O'Neill, G. P.; Liu Q, Im D. S.; Sawyer, N.; Metters, K. M.; Coulombe, N.; Abramovitz, M.; Figueroa, D.J.; Zeng, Z.; Connolly, B. M.; Bai, C.; Austin, C. P.; Chateauneuf, A.; Stocco, R.; Greig, G. M.; Kargman, S.; Hooks, S. B.; Hosfield, E.; Williams Jr, D. L.; Ford-Hutchinson, A. W.; Caskey, C. T.; Evans, J. F.; Characterization of the human cysteinyl leukotriene CysLT1 receptor. *Nature*. **1999**, 399: 789–793.

Madhavi Sastry, G.; Adzhigirey, M.; Day, T.; Annabhimoju, R.; Sherman, W. Protein and ligand preparation: parameters, protocols, and influence on virtual screening enrichments. *Journal of Computer-Aided Molecular Design*. **2013**, 27: 221−234.

Mahase, E. Covid-19: Pfizer's paxlovid is 89% effective in patients at risk of serious illness, company reports. *British Medical Journal*. **2021**, 375: 2713.

Markov, P. V.; Katzourakis, A.; Stilianakis, N. I. Antigenic evolution will lead to new SARS-CoV-2 variants with unpredictable severity. **2022**, 20: 251–252.

Marowsky, A.; Burgener, J.; Falck, J. R.; Fritschy, J. M.; Arand, M. Distribution of soluble and microsomal epoxide hydrolase in the mouse brain and its contribution to cerebral epoxyeicosatrienoic acid metabolism. *Neuroscience*. **2009**, 163: 646–661.

McGill, K. A.; Busse, W. M. Zileuton. *The Lancet*. **1996**. 348, 9026: 519-524.

Medzhitov, R. Origin and physiological roles of inflammation. *Nature*. **2008**, 454(7203): 428-35

Mehrabian, M.; Allayee, H. 5-Lipoxygenases and atherosclerosis. *Current Opinion in Lipidology*. **2003**, 14: 447-457.

Mehrabian, M.; Allayee, H.; Womg, J.; Shi, W.; Wang, X. P.; Shaposhnik, Z.; Funk, C. D.; Lusis, A. J. Identification of 5-lipoxygenase as a major gene contributing to atherosclerosis susceptibility in mice. *Circulation Research*. **2002**, 91: 120-126.

Meirer, K.; Glatzel, D.; Kretschmer, S.; Wittmann, S. K.; Hartmann, M.; Blöcher, R.; Angioni, C.; Geisslinger, G.; Steinhilber, D.; Hofmann, B.; Fürst, R.; Proschak, E.; Design, synthesis and cellular characterization of a dual inhibitor of 5-Lypoxygenase and Soluble Epoxide Hydrolase. *Molecules*. **2017**, 22(1): 45.

Mody, V.; Ho, J.; Wills, S.; Mawri, A.; Lawson, L.; Ebert, M. C. C. J. C.; Fortin, G. M.; Rayalam, S.; Taval, S. Identification of 3-chymotrypsin like protease (3CLPro) inhibitors as potential anti-SARS-CoV-2 agents. *Communications Biology*. **2021**, 93.

Meirer, K.; Rödl, C. B.; Wisniewska, J. M.; Sven, G.; Häfner, A. K.; Buscató, E.; Klingler, F. M.; Hahn, S.; Berressem, D.; Wittmann, S. K.; Steinhilber, D.; Hofmann, B.; Proschak, E. Synthesis and structure-activity relationship studies of novel dual inhibitors of soluble epoxide hydrolase and 5-lipoxygenase. *Journal of Medicinal Chemistry*. **2013**, 56(4): 1777-1781.

Meirer, K.; Steinhilber, D.; Proschak, E. Inhibitors of the Arachidonic Acid Cascade: Interfering with Multiple Pathways. *Basic & Clinical Pharmacology & Toxicology*. **2014**, 114: 83-91.

Mons, E.; Jansen, I. D. C.; Loboda, J.; Van Doodewaerd, B. R.; Hermans, J.; Verdoes, M.; Van Boeckel, C. A. A.; Van Veelen, P. A.; Turk, B.; Turk, D.; Ovaa, H. The alkyne moiety as a latent electrophile in irreversible covalent small molecule

inhibitors of cathepsin K. *Journal of the American Chemical Society*. **2019**, 141: 3507-3514.

Morisseau, C. Role of epoxide hydrolases in lipid metabolism. *Biochimie*. **2013**, 95: 91-95.

Morisseau, C.; Hammock, B. D. Epoxide hydrolases: mechanisms, inhibitor designs, and biological roles. *Annual Review of Pharmacology and Toxicology*. **2005**, 45: 311–33.

Morphy, R. and Rankovic, Z. Designing multiple ligands - medicinal chemistry strategies and challenge. *Current Pharmaceutical Design*. **2009**, 15(6): 587-600.

Morse, J. S.; Lalonde, T.; Xu, S.; Liu, W. R. Learning from the Past: Possible Urgent Prevention and Treatment Options for Severe Acute Respiratory Infections Caused by 2019-nCoV. *ChemBioChem*. **2020**, 21 (5): 730-738.

Nandha, B.; Ramareddy, S. A.; Kuntal, H.; Synthesis of substituted fluorobenzimidazoles as inhibitors of 5-lipoxygenase and soluble epoxide hydrolase for anti-inflammatory activity. *Archiv der Pharmazie Chemistry in Life Sciences*. **2018**, 351: 1800030.

Narayanan, A.; Narwal, M.; Majowicz, S. A.; Varricchio, C.; Toner, S. A.; Ballatore, C.; Brancale, A.; Murakami, K. S.; Jose, J. Identification of SARS-CoV-2 inhibitors targeting Mpro and PLpro using in-cell-protease assay. *Communications Biology*. **2022**, 5(1): 169.

National Institutes of Health. Coronavirus Disease 2019 (COVID-19) Treatment Guidelines. **2021**.

Node, K.; Huo, Y.; Ruan, X.; Yang, B.; Spiecker, M.; Ley, K.; Zeldin, D. C.; Liao, J. K. Anti-inflammatory properties of cytochrome P450 epoxygenase-derived eicosanoids. *Science*. **1999**, 285: 1276–1279.

Oguro, A.; Imaoka, S.; Lysophosphatidic acids are new substrates for the phosphatase domain of soluble epoxide hydrolase. *Journal of Lipid Research*. **2012**, 53: 505–512.

Osipiuk, J., Azizi, S. A., Dvorkin, S., Endres, M., Jedrzejczak, R., Jones, K. A., Kang, S., Kathayat, R. S., Kim, Y., Lisnyak, V. G., Maki, S. L., Nicolaescu, V., Taylor, C. A., Tesar, C., Zhang, Y. A., Zhou, Z., Randall, G., Michalska, K., Snyder, S. A., Dickinson, B. C., Joachimiak, A. Structure of papain-like protease from SARS-CoV-2 and its complexes with non-covalent inhibitors. *Nature Communications*. **2021**, 12: 743.

Ostacolo, C.; Miceli, F.; Di Sarno, V.; Nappi, P.; Iraci, N.; Soldovieri, M. V.; Ciaglia, T.; Ambrosino, P.; Vestuto, V.; Lauritano, A.; Musella, S.; Pepe, G.; Basilicata, M. G.; Manfra, M.; Perinelli, D. R.; Novellino, E.; Bertamino, A.; Gomez-Monterrey, I. M.; Campiglia, P.; Taglialatela, M. Synthesis and Pharmacological Characterization of Conformationally Restricted Retigabine Analogues as Novel Neuronal Kv7 Channel Activators. *Journal of Medicinal Chemistry*. **2020**, 63: 163−185.

Pace, S.; Rossi, A.; Krauth, V.; Dehm, F.; Troisi, F.; Bilancia, R.; Weinigel, C.; Rummler, S.; Werz, O.; Sautebin, L. Sex differences in prostaglandin biosynthesis in neutrophils during acute inflammation. *Scientific Reports*. **2017**, 7: 3759.

Pahwa, R.; Goyal, A.; Jialal, I. Chronic Inflammation. *StatPearls*. **2022.**

Payne, S. Family Coronaviridae. *Viruses*. **2017**, 149-158.

Pein, H.; Ville, A.; Pace, S.; Temml, V.; Garscha, U.; Raasch, M.; Alsabil, K.; Viault, G.; Dinh, C. P.; Guilet, D.; Troisi, F.; Neukirch, K.; Konig, S.; Bilancia, R.; Waltenberger, B.; Stuppner, H.; Wallert, M.; Lorkowski, S.; Weinigel, C.; Rummler, S.; Birringer, M.; Roviezzo, F.; Sautebin, L.; Helesbeux, J. J.; Seraphin, D.; Mosig, A. S.; Schuster, D.; Rossi, A.; Richomme, P.; Werz, O.; Koeberle, A. Endogenous metabolites of vitamin E limit inflammation by targeting 5-lipoxygenase. *Nature Communications*. **2018**, 9: 3834.

Petrovszki, D.; Walter, F. R.; Vigh, J. P.; Kocsis, A.; Valkai, S.; Deli, M. A.; Dér, A. Penetration of the SARS-CoV-2 Spike Protein across the Blood–Brain Barrier, as Revealed by a Combination of a Human Cell Culture Model System and Optical Biosensing. *Biomedicines*. **2022**, 10: 188.

Planas, D.; Bruel, T.; Grzelak, L.; Guivel-Benhassine, F.; Staropoli, I.; Porrot, F.; Planchais, C.; Buchrieser, J.; Rajah, M. M.; Bishop, E.; Albert, M.; Donati, F.; Prot, M.; Behillil, S.; Enouf, V.; Maquart, M.; Smati-Lafarge, M.; Varon, E.; Schortgen, F.; Yahyaoui, L.; Gonzalez, M.; De Sèze, J.; Péré, H.; Veyer, D.; Sève, A.; Simon-Lorière, E.; Fafi-Kremer, S.; Stefic, K.; Mouquet, H.; Hocqueloux, L.; Van der Werf, S.; Prazuck, T.; Schwartz, O. Sensitivity of infectious SARS-CoV-2 B.1.1.7 and B.1.351 variants to neutralizing antibodies. *Nature Medicine*. **2021**, 27: 917-924.

Plante, H.; Piacrd, S.; Mancini, J.; Borgeat, P. 5-Lipoxygenase-activating protein homodimer in human neutrophils: evidence for a role in leukotriene biosynthesis. *Biochemical Journal*. **2006**, 393: 211–218.

Radmark, O.; Werz, O.; Steinhilber, D.; Samuelsson, B. 5-Lipoxygenase: regulation of expression and enzyme activity. *TRENDS in Biochemical Sciences.* **2007**, 32(7).

Ren, Q.; Ma, M.; Ishima, T.; Morisseau, C.; Yang, J.; Wagner, K. M.; Zhang, J. C.; Yang, C.; Yao, W.; Dong, C.; Han, M.; Hammock, B. D.; Hashimoto, K. Gene deficiency and pharmacological inhibition of soluble epoxide hydrolase confers resilience to repeated social defeat stress. *Proceedings of the National Academy of Sciences of the United States of America*. **2016**, 113: E1944–1952.

Ritter, J. M.; Harding, I.; Warren, J. B. Precaution, cyclooxygenase inhibition, and cardiovascular risk. *Trends in Pharmacological Sciences*. **2009**, 30(10): 503–508.

Rossi, A.; Ligresti, A.; Longo, R.; Russo, A.; Borrelli, F.; Sautebin, L. The inhibitory effect of propolis and caffeic acid phenethyl ester on cyclooxygenase activity in J774 macrophages. *Phytomedicine*. **2002**, 9: 530−535.

Rut, W., Lv, Z., Zmudzinski, M., Patchett, S., Nayak, D., Snipas, S. J., El Oualid, F., Huang, T. T., Bekes, M., Drag, M., Olsen, S. K. Activity profiling and crystal structures of inhibitor-bound SARS-CoV-2 papain-like protease: A framework for anti-COVID-19 drug design. *Science Advances*. **2020**, 6(42).

Sadik, C. D.; Sezin, T.; Kim, N. D. Leukotrienes orchestrating allergic skin inflammation. *Experimental dermatology*. **2013**, 705-709.

Salehi-Vaziri, M.; Fazlalipour, M.; Khorrami, S. M. S.; Azadmanesh, K.; Pouriayevali, M. H.; Jalali, T.; Shoja, Z.; Maleki, A. The ins and outs of SARS-CoV-2 variants of concern (VOCs). *Archives of Virology*. **2022**, 167: 327-344.

Samuelsson, B.; Dahlen, S. E.; Lindgren, J. A.; Rouzer, C A.; Serhan, C. N. Leukotrienes and lipoxins: structures, biosynthesis, and biological effects. *Science*. **1987**, 237: 1171–1176.

Schewe, T.; Halangk, W.; Hiebsch, C.; Rapoport, S. M. A lipoxygenase in rabbit reticulocytes which attacks phospholipids and intact mitochondria, *FEBS Letters*. **1975**, 60: 149–152.

Schmelzer, K. R.; Kubala, L.; Newman, J. W.; Kim, I. H.; Eiserich, J. P.; Hammock, B. D. Soluble epoxide hydrolase is a therapeutic target for acute inflammation. *Proceedings of the National Academy of Sciences*. **2005**, 102(28): 9772-7.

Schmelzer, K. R.; Inceoglu, B.; Kubala, L.; Kim, I..; Jinks, S.L.; Eiserich, J. P.; Hammock, B. D. Enhancement of antinociception by coadministration of nonsteroidal anti-inflammatory drugs and soluble epoxide hydrolase inhibitors. *Proceedings of the National Academy of Sciences of the United States of America*. **2006**, 103: 13646–13651.

Schmelzer, K. R.; Inceoglu, B.; Kubala, L.; Kim, I. H.; Jinks, S. L.; Eiserich, J. P.; Hammock, B. D. Enhancement of antinociception by coadministration of nonsteroidal anti-inflammatory drugs and soluble epoxide hydrolase inhibitors. *Proceedings of the National Academy of Sciences of the United States of America*. **2006**, 103: 13646–13651.

Shen, H. C. Soluble epoxide hydrolase inhibitors: a patent review. *Expert Opinion on Therapeutic Patents*. **2010**, 20(7): 941-56.

Shen, H. C.; Hammock, B. D. Discovery of Inhibitors of Soluble Epoxide Hydrolase: A Target with Multiple Potential Therapeutic Indications. *Journal of Medicinal Chemistry*. **2012**, 55(5): 1789–1808.

Sherman, W.; Beard, H. S.; Farid, R. Use of an Induced Fit Receptor Structure in Virtual Screening. *Chemical Biology & Drug Design*. **2006**, 67: 83−84.

Sigal, E.; Dicharry, S.; Highland, E.; Finkbeiner, W. E. Cloning of human airway 15-lipoxygenase: identity to the reticulocyte enzyme and expression in epithelium. *American Journal of Physiology*. **1992**, 262: L392–L398.

Sigal, E.; Grunberger, D.; Cashman, J. R.; Craik,C. S.; Caughey, G. H.; Nadel, J. A. Arachidonate 15-lipoxygenase from human eosinophil-enriched leukocytes: partial purification and properties. *Biochemical and Biophysical Research Communications*. **1988**, 150: 376–383.

Singh, A. K.; Singh, A.; Singh, R.; Misra, A. Molnupiravir in COVID-19: A systematic review of literature. *Diabetology & Metabolic Syndrome*. **2021**, 15 (6): 102329.

Singh, M.; De Wit, E. Antiviral agents for the treatment of COVID-19: Progress and challenges. *Cell Reports Medicine.* **2022**, 3: 100549.

Sommer, S.; Weikart, N. D.; Linne, U.; Mootz, H. D. Covalent inhibition of SUMO and ubiquitin-specific cysteine proteases by an in situ thiol-alkyne addition. *Bioorganic & Medicinal Chemistry*. **2013**, 21: 2511-2517.

Spector, A. A. Arachidonic acid cytochrome 450 epoxygenase pathway. *Journal of Lipid Research*. **2009**; 50: S52–56.

Still, W. C.; Tempczyk, A.; Hawley, R. C.; Hendrickson, T. Semianalytical treatment of solvation for molecular mechanics and dynamics. *Journal of the American Chemical Society*. **1990**, 112: 6127−6129.

Sun, C. P.; Zhang, X. Y.; Morisseau, C.; Hwang, S. H.; Zhang, Z. J.; Hammock, B. D.; Ma, X.C. Discovery of Soluble Epoxide Hydrolase Inhibitors from Chemical Synthesis and Natural Products. *Journal of Medicinal Chemistry*. **2020**, 64(1): 184–215.

Sun, C. P.; Zhang, X. Y.; Morisseau, C.; Hwang, S. H.; Zhang, Z. J.; Hammock, B. D.; Ma, X. C. Discovery of Soluble Epoxide Hydrolase Inhibitors from Chemical Synthesis and Natural Products. *Journal of Medicinal Chemistry*. **2021**, 64: 184−215.

Temml, V.; Garscha, U.; Romp, E.; Schubert, G.; Gerstmeier, J.; Kutil, Z.; Matuszczak.; Waltenberger, B.; Stuppner, H.; Werz, O.; Schuster, D. Discovery of the first dual inhibitor of the 5-lipoxygenase-activating protein and soluble epoxide hydrolase using pharmacophore-based virtual screening. *Scientific Reports*. **2017**, 42751.

Tortorici, M. A.; Veesler, D. Structural insights into coronavirus entry. *Advances in Virus Research.* **2019**, 105: 93-116.

Tsai, Y. C.; Lee, C. L.; Yen, H. R.; Chang, Y. S.; Lin, Y. P.; Huang, S. H.; Lin, C. W. Antiviral Action of Tryptanthrin Isolated from Strobilanthes cusia Leaf against Human Coronavirus NL63. *Biomolecules*. **2020**, 10 (3): 366.

Tu, X.; Xiao, B.; Xiong, J.; Chen, X. A simple miniaturised photometrical method for rapid determination of nitrate and nitrite in freshwater. *Talanta*. **2010**, 82: 976−983.

Uhl, J.; Klan, N.; Rose, M.; Entian, K. D.; Werz, O.; Steinhilber, D. The 5-lipoxygenase promoter is regulated by DNA methylation. *Journal of Biological Chemistry*. **2002**, 277: 4374–4379.

Ullrich, S.; Nitsche, C. The SARS-CoV-2 main protease as drug target. *Bioorganic & Medicinal Chemistry Letters*. **2020**, 30 (17): 127377.

Violette, S. H.; Ebtisam Abdel, A. H. Synopsis of arachidonic acid metabolism: A review. *Journal of Advanced Research.* **2018**, 11: 23-32.

Virchow, J. C.; Bachert, C. Efficacy and safety of montelukast in adults with asthma and allergic rhinitis. *Respiratory Medicine*. **2006**, 100: 1952-1959.

V'kovski, P.; Gerber, M.; Kelly, J.; Pfaender, S.; Ebert, N.; Braga Lagache, S.; Simillion, C.; Portmann, J.; Stalder, H.; Gaschen, V.; Bruggmann, R.; Stoffel, M. H.; Heller, M.; Dijkman, R.; Thiel, V. Determination of host proteins composing the microenvironment of coronavirus replicase complexes by proximity-labeling. *Elife*. **2019**, 8: e42037.

V'kovski, P.; Kratzel, A.; Steiner, S.; Stalder H.; Thiel, V. Coronavirus biology and replication: implications for SARS-CoV-2. *Nature Reviews Microbiology*. **2021**, 19: 155–170.

Wagner, K. M.; McReynolds, C. B.; Schmidt, W. K.; Hammock, B. D. Soluble epoxide hydrolase as a therapeutic target for pain, inflammatory and neurodegenerative diseases. *Pharmacology & Therapeutics*. **2017**, 180: 62–76.

Wang, M.; Cao, R.; Zhang, L.; Yang, X.; Liu, J.; Xu, M.; Shi, Z.; Hu, Z.; Zhong, W.; Xiao, G. Remdesivir and chloroquine effectively inhibit the recently emerged novel coronavirus (2019-nCoV) in vitro. *Cell Research*. **2020**, 30 (3): 269-271.

Wang, Q.; Zhang, Y.; Wu, L.; Niu, S.; Song, C.; Zhang, Z.; Lu, G.; Qiao, C.; Hu, Y.; Yuen, K. Y.; Wang, Q.; Zhou, H.; Yan, J.; Qi, J. Structural and Functional Basis of SARS-CoV-2 Entry by Using Human ACE2. *Cell*. **2020**, 181(4): 894-904.

Wang, Y.; Armando, A. M.; Quehenberger, O.; Yan, C.; Dennis, E. A. Comprehensive ultra-performance liquid chromatographic separation and mass spectrometric analysis of eicosanoid metabolites in human samples. *Journal of Chromatography A*. **2014**, 1359: 60−69.

Ward, P. A.; Lentsch, A. B. The Acute Inflammatory Response and Its Regulation. *Archives of Surgery*. **1999**, 134(6): 666-9

Werz, O.; Steinbhilber, D. Development of 5-lipoxygenase inhibitors-lessons from cellular enzyme regulation. *Biochemical Pharmacology*. **2005**, 327-333.

WHO Director-General's remarks at the media briefing on 2019-nCoV. 11 February **2020**.

WHO Director-General's opening remarks at the media briefing on COVID-19. 11 March **2020**.

Williams, L.; Bradley, L.; Smith, A.; Foxwell, B. Signal Transducer and Activator of Transcription 3 Is the Dominant Mediator of the Anti-Inflammatory Effects of IL-10 in Human Macrophages. *The Journal of Immunology*. **2004**, 172: 567–576.

Wisniewska, J. M.; Rödl, C. B.; Kahnt, A. S.; La Buscató, E.; Ulrich, S.; Tanrikulu, Y.; Achenbach, J.; Rörsch, F.; Grösch, S.; Schneider, G.; Cinatl Jr, J.; Proschak, E.; Steinhilber, D.; Hofmann, B. Molecular characterization of EP6--a novel imidazo[1,2-a]pyridine based direct 5-lipoxygenase inhibitor. *Biochemical Pharmacology*. **2012**, 83(2): 228-40.

Word Health Organization. Global Surveillance for human infection with novel coronavirus (2019-nCoV): interim guidance. 31 January **2020**.

World Health Organization. Laboratory testing for coronavirus disease (COVID-19) in suspected human cases: interim guidance. 19 March **2020**.

Wu, F.; Zhao, S.; Yu, B.; Chen, Y. M.; Wang, W.; Song, Z. G.; Hu, Y.; Tao, Z. W.; Tian, J. H.; Pei, Y. Y.; Yuan, M. L.; Zhang, Y. L.; Dai, F. H.; Liu, Y.; Wang, Q. M.; Zheng, J. J.; Xu, L.; Holmes, E. C.; Zhang, Y. Z. A new coronavirus associated with human respiratory disease in China. *Nature*. **2020,** 579 (7798): 265-269.

You, D.; Lyn-Cook, L. E.; Gatti, D. M.; Bell, N.; Mayeux, P. R.; James, L. P.; Mattes, W. B.; Larson, G. J. and Harrill, A. H. Nitrosative stress and lipid homeostasis as a mechanism for zileuton hepatotoxicity and resistance in genetically sensitive mice. *Toxicological Sciences.* **2020**, 175(2): 220–235.

Young, J. L.; Chang-Kneum, K. Montelukast use over the past 20 years: monitoring of its effects and safety issues. *Clinical and Experimental Pediatrics*. **2020**, 63(10): 376-381.

Zhan, Y.; Yin, H.; Yin, J. Y. B.1.617.2 (Delta) Variant of SARS-CoV-2: features, transmission and potential strategies. *International Journal of Biological Sciences*. **2022**, 18 (5): 1844–1851.

Zhang, C. H.; Stone, E. A.; Deshmukh, M.; Ippolito, J. A.; Ghahremanpour, M. M.; Tirado-Rives, J.; Spasov, K. A.; Zhang, S.; Takeo, Y.; Kudalkar, S. N.; Liang, Z.; Isaacs, F.; Lindenbach, B.; Miller, S. J.; Anderson, K. S.; Jorgensen, W. L. Potent noncovalent inhibitors of the main protease of SARS-CoV-2 from molecular sculpting

of the drug perampanel guided by free energy perturbation calculations. *ACS Central Science*. **2021**, 7(3): 467-475.

Zhang, L.; Lin, D.; Sun, X.; Curth, U.; Drosten, D.; Sauerhering, L.; Becker, S.; Rox, K.; Hilgenfeld, R. Crystal structure of SARS-CoV-2 main protease provides a basis for design of improved α-ketoamide inhibitors. *Science*. **2020**, 368: 6489.

Zhang, W.; Yang, A. L.; Liao, J.; Li, H.; Dong, H.; Chung, Y. T.; Bai, H.; Matkowskyj, K. A.; Hammock, B. D.; Yang, G. Y. Soluble Epoxide Hydrolase Gene Deficiency or Inhibition Attenuates Chronic Active Inflammatory Bowel Disease in IL-10(-/-) Mice. *Digestive Diseases and Sciences*. **2012**, 57: 2580–91.

Zhou, P.; Yang, X.; Wang, X.; Hu, B.; Zhang, W; Si, H. R.; Zhu, Y.; Li, B.; Huang, C. L.; Chen, H. D.; Chen, J.; Luo, Y.; Guo, H.; Jiang, R. D.; Liu, M. Q.; Chen, Y.; Shen, X. R.; Wang, X.; Zheng, X. S.; Zhao, K.; Chen, Q. J.; Deng, F.; Liu, L. L.; Yan, B.; Zhan, F. X.; Wang, Y. Y.; Xiao, G. F.; Shi, Z. L. A pneumonia outbreak associated with a new coronavirus of probable bat origin. *Nature*. **2020**, 579 (7798): 270-273.

Zhu, J.; Ji, P.; Pang, J.; Zhong, Z.; Li, H.; He, C.; Zhang, J.; Zhao, C. Clinical characteristics of 3062 COVID-19 patients: A meta-analysis. *Journal of Medical Virology*. **2020**, 92 (10): 1902-1914.